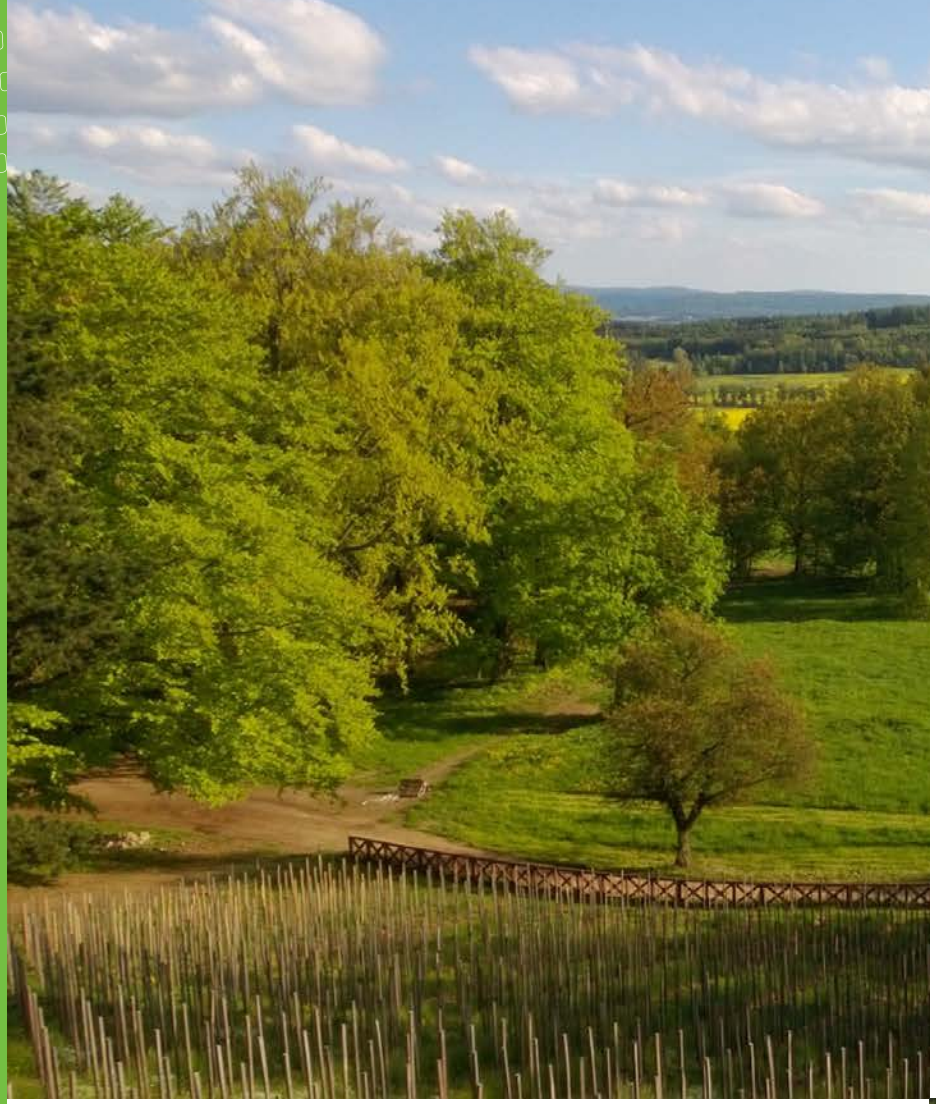

SCIENCE • TECHNOLOGY • RESEARCH HIGHLIGHTS • VISIONS

Dissertation
74

Nickel- and iron-based HVOF thermal spray coatings for high temperature corrosion protection in biomass-fired power plant boilers

Maria Oksa

VTT

VTT SCIENCE 74

Nickel- and iron-based HVOF thermal spray coatings for high temperature corrosion protection in biomass-fired power plant boilers

Maria Oksa

VTT Technical Research Centre of Finland Ltd

Doctoral dissertation for the degree of Doctor of Science (Tech.) to be presented with due permission of the School of Chemical Technology for public examination and debate in Auditorium V1, at the Aalto University School of Chemical Technology (Espoo, Finland), on the 23 January at 12 o'clock noon.

ISBN 978-951-38-8206-8 (Soft back ed.)
ISBN 978-951-38-8207-5 (URL: http://www.vtt.fi/publications/index.jsp)

VTT Science 74

ISSN-L 2242-119X
ISSN 2242-119X (Print)
ISSN 2242-1203 (Online)

JULKAISIJA – UTGIVARE – PUBLISHER

VTT
PL 1000 (Tekniikantie 4 A, Espoo)
02044 VTT
Puh. 020 722 111, faksi 020 722 7001

VTT
PB 1000 (Teknikvägen 4 A, Esbo)
FI-02044 VTT
Tfn +358 20 722 111, telefax +358 20 722 7001

VTT Technical Research Centre of Finland
P.O. Box 1000 (Tekniikantie 4 A, Espoo)
FI-02044 VTT, Finland
Tel. +358 20 722 111, fax +358 20 722 7001

Grano Oy, Kuopio 2015

Preface

The research work was performed between the years of September 2010 – September 2014 at VTT Technical Research Centre of Finland. The related studies were carried out at Aalto University, formerly known as Helsinki University of Technology, at the School of Chemical Technology, Department of Materials Science and Engineering. Main part of this work was carried out under the EU FP7 project NextGen-Power – Meeting the Materials and Manufacturing Challenge for Ultra High Efficiency PF Power Plants with CCS. The financial support via European Commission and VTT Technical Research Centre of Finland are gratefully acknowledged. The opportunity to conduct on-site testing at the Alholmens Kraft Ab, Pietarsaari, Finland, and Turku Energia, Turku, Finland, power plants is also greatly appreciated.

Professor Simo-Pekka Hannula, Aalto University, is greatly acknowledged for his valuable guidance during my doctoral studies. I warmly thank Simo-Pekka and his wife Leena for their hospitality during the lovely dinner parties at their home. Professor Erja Turunen is also acknowledged for acting as thesis advisor at VTT.

I would like to thank my co-authors for their valuable support. My sincere thanks go to my colleagues at VTT for their contribution and support. Thank you, Tommi Varis, Jarkko Metsäjoki, Tomi Suhonen, Janne Kärki, Satu Tuurna, Sini Metsä-Kortelainen, Outi Härkki, Henriikka Brandt and other colleagues in Otaniemi. Special thanks are reserved for Seija Kivi, who performed the sample preparation, hardness and elastic modulus testing; Mika Jokipii and Markku Lindberg, who performed the HVOF coating; and the colleagues in Jyväskylä, who carried out the probe measurements. Warm thanks also to the doctoral students at Aalto University for generously sharing their experiences and support. I would also like to give many thanks to my friends for their interest in my studies and the thesis work.

Finally, I would like to express my warmest gratitude to my mother Sanni Oksa and my father Raimo Oksa, for their support, and my husband Pete for taking care of our two small, lovely daughters during the long years of the work. Pyry the Sheltie is also praised for taking me out in the woods to clear my thoughts and keep me in shape. I would also like to remember my sister Leena. My warmest thoughts go where ever you are. My deepest thanks are reserved for Sofia and Helmi, my wonderful daughters. Thank you, dear Sofia, for being the break impulse for starting the studies, and dearest Helmi, for attending the lectures at Aalto University before you were even born and since. Thank you for being my sunshine and thank you for being patient when I have not been able to be there for you.

Espoo, December 2014
Maria Max Oksa

Academic dissertation

Supervising professor	Professor Simo-Pekka Hannula Department of Materials Science and Engineering School of Chemical Technology Aalto University Espoo, Finland
Thesis advisor	Professor Erja Turunen VTT Technical Research Centre of Finland Espoo, Finland
Pre-examiners	Professor Petri Vuoristo Department of Materials Science Tampere University of Technology Tampere, Finland
	Docent Dr. Michael Spiegel Salzgitter Mannesmann Forschung GmbH Duisburg, Germany
Opponent	Ph.D. David Baxter Joint Research Centre, European Commission Petten, the Netherlands

List of publications

This thesis is based on the following original publications which are referred to in the text as I–VI. The thesis consists of a summary of the author's work on thermal spray coatings for high temperature corrosion protection in biomass boiler conditions, optimization and spraying HVOF coatings, characterization of materials, testing and validation of the corrosion performance of the coatings in laboratory and on-site conditions, post-exposure analysis of samples, and comparison to reference bulk materials. The publications are reproduced with kind permission from the publishers.

I M. Oksa, E. Turunen, T. Suhonen, T. Varis, S.-P. Hannula, Optimization and characterization of high velocity oxy-fuel sprayed coatings: techniques, materials, and applications. *Coatings* 1 (2011) 17–52

II Oksa, M., J. Metsäjoki, Optimizing NiCr and FeCr HVOF coating structure for high temperature corrosion protection applications. *Journal of Thermal Spray Technology* (2014), published online 20.11.2014

III Oksa, M., Metsäjoki, J., Kärki, J., Thermal spray coatings for high temperature corrosion protection in biomass co-fired boilers. *Journal of Thermal Spray Technology* 24 (2015) 194-205

IV Oksa, M., Auerkari, P., Salonen, J., Varis, T., Nickel-based HVOF coatings promoting high temperature corrosion resistance of biomass-fired power plant boilers. *Fuel Processing Technology* 125 (2014) 236–245

V Oksa, M., Varis, T., Ruusuvuori, K., Performance testing of iron based thermally sprayed HVOF coatings in a biomass-fired fluidized bed boiler. *Surface & Coatings Technology* 251 (2014) 191–200

VI M. Oksa, S. Tuurna, T. Varis, Increased lifetime for biomass and waste to energy power plant boilers with HVOF coatings: High temperature corrosion testing under chlorine-containing molten salt. *Journal of Thermal Spray Technology* 22 (2013) 783–796

Author's contributions

The author of this thesis is the responsible author for the publications (I-VI) presented in this thesis.

Publication I Writing the optimization of the HVOF process and applications of the coatings.

Publication II Designing and supervising the coating manufacturing and application of the process diagnostics, coating characterization and corrosion testing, analysing the results and writing the manuscript.

Publication III Planning and supervising the corrosion testing, HVOF coating and coating characterization, interpreting the results and preparing the manuscript.

Publication IV Characterizing the coating and reference materials with SEM/EDX, analysing the results and writing the manuscript.

Publication V Characterizing the coating and reference materials with SEM/EDX, interpreting the results and preparing the manuscript.

Publication VI Planning the testing, supervising the coating process, performing the post-exposure characterization with SEM/EDX, performing the analysis and writing the manuscript.

The contributions of the co-authors to the experimental work and preparation of the manuscripts are listed below:

- Professor Erja Turunen provided the original idea for the thesis and contributed for Publication I by the introduction part.
- Senior Scientist Tomi Suhonen contributed for Publication I for the characterization part.
- Senior Scientist Tommi Varis provided valuable support through his expertise on thermal spraying, which was applied to Publications I, IV, V and VI for parameter selection, coating process and analysis of diagnostic data.
- Professor Simo-Pekka Hannula supervised the thesis work and contributed for Publication I by writing the coating characterization and properties part.
- Research Scientist Jarkko Metsäjoki performed gas permeability testing of the coatings for Publications II and III, diagnostic data analysis for Publication

II, post-exposure characterization with SEM/EDX for Publication III and thermodynamic calculations for Publications III and IV.

- Senior Scientist Janne Kärki was responsible for the on-site probe measurement for Publications II and III.
- Senior Principal Scientist Pertti Auerkari performed the tube failure analysis for Publication IV.
- Senior Scientist Jorma Salonen performed the tube failure analysis for Publication IV.
- Mr. Kimmo Ruusuvuori was responsible for thermal spray coating process for Publication V.
- Senior Scientist Satu Tuurna supervised the high temperature corrosion testing for Publication VI.

Contents

List of symbols and abbreviations

CFB	circulating fluidized bed
CJS	carbide jet spray
Cr_2O_3	chromium oxide
CTE	coefficient of thermal expansion
$CuCl_2$	copper chloride
CuO	copper oxide
DJ	Diamond Jet Hybrid
EDX	energy dispersive X-ray spectrometry
Fe_2O_3	hematite (iron oxide)
Fe_3O_4	magnetite (iron oxide)
F/O	fuel-oxygen ratio
FeCr	iron-chromium
HAZ	heat affected zone
HCl	hydrochloric acid
HVOF	high velocity oxy-fuel
HVOFGF	high velocity oxy-fuel, gas fuelled
HVOFLF	high velocity oxy-fuel, liquid fuelled
ICP	in-situ coating property measurement
KCl	potassium chloride
K_2FeO_4	potassium ferrate
K_2SO_4	potasssium sulfate
$K_2S_2O_7$	potassium pyrosulfate

MW_{th}	megawatt (thermal output)
NaCl	sodium chloride
Na_2SO_4	sodium sulfate
$Na_2S_2O_7$	sodium pyrosulfate
$NiCl_2$	nickel chloride
NiCr	nickel-chromium
SEM	scanning electron microscope
SO_2	sulfur dioxide
SO_3	sulfur trioxide
SRF	solid recovered fuel
T	temperature
TS	thermal spray
v	velocity
XRD	X-ray diffraction
$ZnCl_2$	zinc chloride

1. Introduction

The use of biomass as fuel has been increasing due to legislation in Europe. Growing awareness of environmental problems has led to strict restrictions on greenhouse emissions in the energy sector, and increased demand for higher use of renewable energy sources and carbon-neutral fuels, such as biomass. The EU has committed to cutting its emissions to 20% below 1990 levels by the year 2020. This commitment is one of the headline targets of the Europe 2020 growth strategy and is being implemented through a package of binding legislation. This includes raising the share of needed energy produced by renewable energy sources, such as wind, solar and biomass, to 20% by 2020 (Ref 1).

There are over 1,000 biomass boilers in Europe, and the number is increasing (Ref 2, 3). Biomass boilers can utilize different kinds of fuels, such as wood, forest residues, recycled wood, and agricultural crops, such as straw. These plants often face serious problems due to fouling, slagging, and severe high temperature corrosion of metallic heat exchanger surfaces, such as superheaters. Fouling and corrosion in biomass boilers originate from burnt fuels, which contain alkali metals, chlorine and other corrosive elements, and can lead to material wastage, tube failures, tube leakages, unplanned shutdowns of the boiler and shortened lifetime of the boiler tubing; these are harmful and expensive consequences of corrosion. In addition, demand for higher efficiency of electricity and heat generation requires an increase in steam temperatures, which in turn raises the material temperatures of boiler tubes, and may result in more severe corrosion problems. To overcome material wastage and potential tube failure in boilers, commonly used carbon or low-alloy steels are being replaced by higher-alloyed tube materials. However, the high price and sometimes difficult machinability of these materials hinders their adoption.

Thermal spray coatings offer an attractive solution for the corrosion protection of boiler tubing. They can be applied to load-carrying carbon steel or low-alloy steel tubes to increase the corrosion resistance and lifetime of boiler tubes, e.g. in superheaters and waterwalls. The material selection for coatings is wide and spraying can be optimized to produce well-adhered and dense coatings. This enables both the coating structure and composition to be tailored for specific conditions.

This work was performed in order to increase the lifetime of the heat exchanger surfaces of power plant boilers consuming biomass as fuel. The high temperature corrosion mechanisms of metallic tube materials have been studied widely both in laboratory and boiler exposures. However, optimizing and testing the high temperature corrosion properties of HVOF (high velocity oxy-fuel) thermal spray coatings in actual biomass power plant boiler conditions has not been reported previously.

The aim of this work was to manufacture thermal spray coatings of sufficient quality for high temperature corrosion protection in biomass boilers. This involved optimizing the thermal spray process to produce an optimal coating structure by applying a process-structure-properties-performance methodology with the help of diagnostic tools. The expected outcome of the study was demonstration and confirmation of the applicability of thermal spray coatings for high temperature corrosion protection in actual power plant conditions.

The research focused on improving the high temperature corrosion resistance of nickel- and iron-based HVOF coatings by optimizing their structure and verification of their corrosion resistance. The corrosion performance of the selected coatings was validated both in laboratory conditions and real biomass boiler conditions. Focus was also placed on determining the corrosion mechanisms of thermal spray coatings based on iron and nickel and beneficial alloying elements. The results of the present study will help to optimize the coating process for high temperature corrosion applications and, especially, the adoption of thermal spray coatings for the protection of the heat exchanger surfaces of biomass boilers prone to severe corrosion failure.

The research was based on the following hypotheses:

1) The high temperature corrosion performance of the manufactured Fe and Ni based HVOF sprayed coatings is adequate for corrosion protection of boiler tubes in biomass boiler conditions.
2) Diagnostic tools can be applied for HVOF coating process optimization in order to attain an optimal coating structure for corrosion protection in high temperature applications.

The study begins with a review of power plant boilers utilizing biomass fuels and the high temperature corrosion taking place in them. Currently applied tube materials, advanced materials and weld-overlays are presented in brief. Requirements for thermal spray coatings in boiler coatings are declared. In the experimental section, two HVOF spray systems were employed to enable comparison of the effect of different coating structures on high temperature corrosion performance. The coatings were characterized and their chemical and mechanical properties were analysed. The corrosion testing was performed for the coatings and reference materials both in controlled laboratory conditions and actual biomass power plant exposures. Special attention was paid to chlorine-induced corrosion and molten salt attack. Post-analysis of the exposed samples was performed by optical microscope and scanning electron microscope (SEM) with energy dispersive X-ray spectroscope (EDX). Finally, the main results and conclusions of **Publications I–VI** are presented and discussed in detail.

2. High temperature corrosion in biomass-fuelled power plant boilers

The aim of decreasing the carbon dioxide emissions from fossil fuels in electricity and heat production has increased the use of biomass and waste as a partial replacement for coal in co-combustion boilers (Ref 4). Biomass boilers can utilize different kinds of fuels, such as wood, forest residues, recycled wood, and agricultural crops, such as straw. The operating conditions of different boilers (temperature, flue gas composition, fly ash, etc.) depend on the fuels and the process parameters, and may vary inside the boiler. The burning of difficult fuels, such as biomass and solid recovered fuel (SRF), leads to very harsh conditions and may cause fouling, slagging, and high temperature corrosion of the metallic heat exchanger surfaces (Ref 5–9). Corrosion can cause severe material damage and tube leakage, leading to severe operational problems and expensive consequences such as unplanned plant shutdowns, high maintenance costs, reduced availability of the plant and shortened lifetime of the boiler tubing (Ref 10). In addition, the demand for higher efficiency of electricity and heat generation requires an increase in steam temperatures, which in turn raises the material temperatures of boiler tubes, and may lead to even more severe corrosion problems especially in economizer and/or superheater areas. The material temperatures are planned to raise up to 750...800 °C in advanced ultra super-critical power plant boilers in future. Schematic images of biomass-fuelled circulating fluidized bed (CFB) boilers are presented in **Figure 1**.

The operating conditions of different boilers (e.g. temperature, flue gas composition, fly ash) depend on fuels and process parameters, and may vary inside the boiler. There are several high temperature corrosion mechanisms that can occur in power plant boilers operating on chlorine-containing fuels, including biomass and waste-to-energy boilers. In the superheater area, corrosion derives from the reactions between fly ash, gaseous components, and cooler metal surfaces, on which a deposit is formed. The corrosion reactions derive from combustion gas containing HCl or deposited ash containing low-melting-point salts such as chlorides. Chlorine-induced active corrosion is detrimental to steels, and the corrosion starts almost immediately after introduction of chlorine-containing contamination into the environment (Ref 11). Chlorine is able to penetrate and destroy the metal oxide layer, probably through cracks in the scale, and at the metal-scale interface

the chlorine reacts with chromium and iron to form volatile metal chlorides (Ref 12). Severe corrosion of the boiler tubes occurs especially due to molten phases (Ref 13–15), and one of the extremely damaging corrosion mechanisms in biomass and waste-to-energy boilers is molten salt attack due to low melting temperature compounds such as alkali metal chlorides (NaCl, KCl) and zinc, copper or lead chlorides (Ref 16–20).

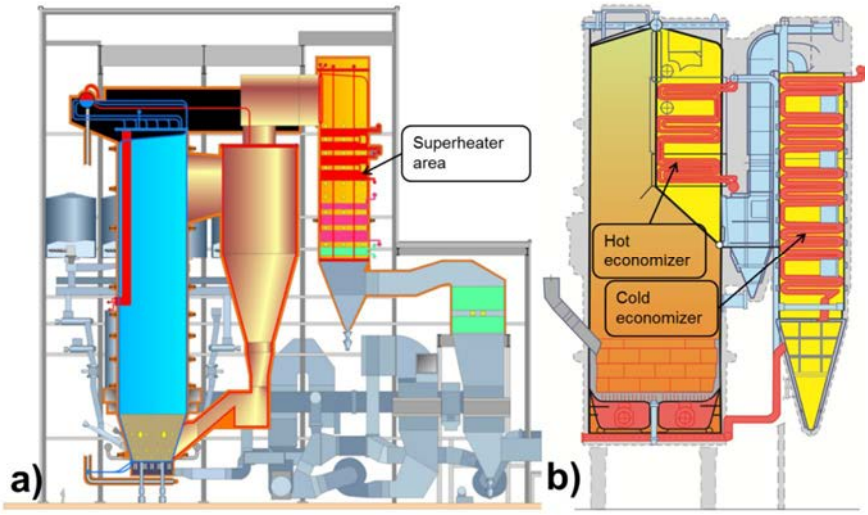

Figure 1 Schematic illustrations of circulating fluidized bed boilers. a) 550 MW_{th} co-firing biomass boiler (Publication III) and b) 40 MW_{th} district heating unit (Publication V).

Wood-derived fuels are the most utilized biomass type in Finland. Even though the Cl content of wood can be low, combustion of wood-based fuel, mainly recycled wood, may accelerate corrosion rates in power plants (Ref 21–23). **Table 1** presents the chemical composition of detrimental elements in some wood-based fuels and ashes (Ref 24). Typically fly ash and deposits in biomass combustion contain high amounts of potassium and chlorine. Other harmful elements are e.g. sodium, sulfur, lead, zinc, copper and bromine, which condensate and deposit on metallic tubes causing very severe material deterioration and tube failure (Ref 8, 19, 25–27). Particularly detrimental are compounds with low melting points.

Table 1 Elemental analysis of detrimental elements in fly ash and bottom ash (dry solids content) and the wood-derived fuels in mg/kg (Ref 24) (Publication V).

Element [mg/kg]	Fly ash	Bottom ash	Forest residue	Bark	Recycled wood
Organic carbon, TOC	21000	< 1000	51.7*	52.5*	49.4*
Fluoride, F^-	< 100	< 100	...	...	...
Chloride, Cl^-	4400	200	0.031*	0.019*	0.09*
Sulfate, SO_4^{2-}	44000	300	0.01**	0.03**	0.07**
Arsenic, As	< 15	< 15	0.11	0.11	69
Barium, Ba	5300	3700	67	120	583
Cadmium, Cd	6.8	< 0.1	0.26	0.38	1.8
Chromium, Cr	52	15	21	35	90
Copper, Cu	160	43	2.4	3.9	50
Mercury, Hg	0.47	< 0.03	0.022	0.033	0.11
Molybdenum, Mo	6.9	2.7	0.74	1.3	0.41
Nickel, Ni	71	11	6	11	1.2
Lead, Pb	100	11	0.64	1	213
Antimony, Sb	< 10	< 10	...	...	...
Selenium, Se	17	< 15	...	...	...
Zinc, Zn	1500	650	85	150	1950

* Percentage of dry fuel weight. ** Elemental S, percentage of dry fuel weight.

Several high temperature corrosion mechanisms prevail in power plant boilers utilizing chlorine-containing fuels including chlorine-induced active oxidation, selective chlorine corrosion, hot corrosion by eutectic melts and sulfidation (Ref 6, 8, 28). Type II hot corrosion is caused by gas phase acid fluxing or sulfidation and occurs typically at 600-800 °C. Sulfur dioxide and sulfates cause accelerated corrosion as a gaseous reaction as well as in deposits. Type II hot corrosion forms typically pitting, which results from the formation of mixtures of e.g. Na_2SO_4 and $NiSO_4$, which may have low melting temperature. For the Type II corrosion reactions to occur, a high partial pressure of SO_3 is required. Deposit formation and factors influencing corrosion rate are described in **Figure 2** (Ref 29). In the superheater area, corrosion derives from the reactions between fly ash, gaseous components, and cooler metal surface, on which a deposit is formed. The corrosion reactions are due to combustion gas containing HCl or deposited ash containing low-melting-point salts such as chlorides.

The corrosion problems related to biomass combustion have been reported mainly be caused especially by chlorine as stated earlier. Sulfidation has not been reported to be that serious a problem in boiler conditions. In some cases, additional sulfur has been added to combustion with fuels with high chlorine content, e.g. biomass or recovered fuel, in order to prevent chlorine induced corrosion. Sulfur addition to decrease chlorine corrosion into the combustion process has been studied and made also commercially available (Ref 21, 22). The main focus in this work was to study corrosion resistance by chromium alloyed coatings, and

therefore sulfidation was not considered as relevant as chlorine induced corrosion and corrosion caused by low melting compounds. However, at higher temperatures, Type II hot corrosion may be very important corrosion mechanism with nickel-based materials in particular.

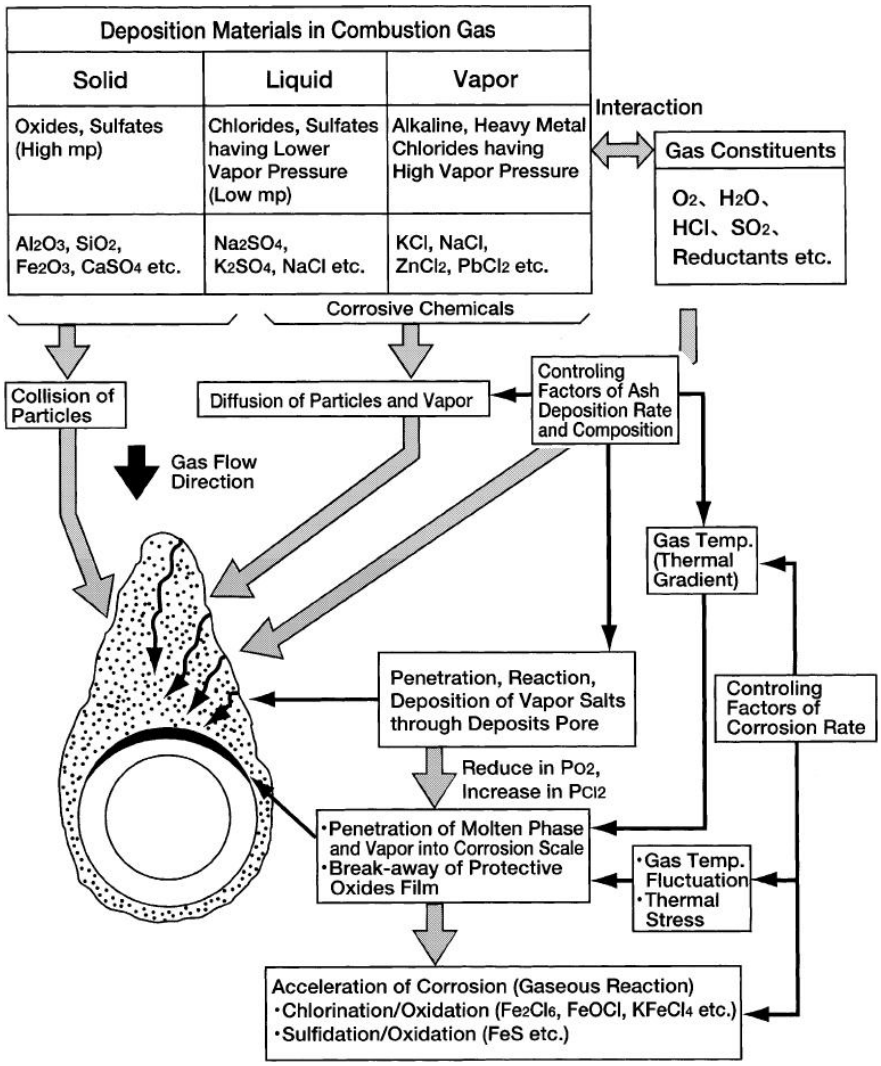

Figure 2 Main factors of ash deposition and corrosion rate (Kawahara, Ref 29).

2.1 Chlorine-induced corrosion

Chlorine and chlorides are especially detrimental to iron and low-alloy steels as they prevent the formation of protective oxide layers or degrade already formed layers. Corrosion starts almost immediately after introduction of chlorine-containing contamination into the environment (Ref 30). Chlorine contamination may be relatively low; e.g. Bramhoff et al. (Ref 31) have shown that an addition of 250-3000 vppm HCl(g) into oxidizing atmosphere leads to accelerated catastrophic corrosion of a low-alloy steel.

Active oxidation occurs in the presence of alkali chlorides in deposits and hydrogen chloride in the atmosphere (Ref 11). Chlorine gas or chloride ions penetrate the oxide-metal interface, where they react with the alloy components, typically forming $FeCl_2$. The metal chloride evaporates and, during its diffusion to the scale surface, is oxidized in the area with higher oxygen vapour pressure forming a non-protective oxide scale. The chlorine released in the reaction is able to participate again in the corrosion reaction, thus enhancing it. The active oxidation reaction circuit induced by chlorine is depicted schematically in **Figure 3**. Outward diffusion of $FeCl_2$(g) through the oxide scale is the rate controlling mechanism for the active oxidation process (Ref 11). The reactions are similar for high-chromium alloys. Chlorine reacts with $FeCr_2O_4$ or Cr_2O_3. However, mainly $FeCl_2$ is formed due to the of lower Gibbs free energy of $FeCl_2$ compared to $CrCl_2$ (Ref 11).

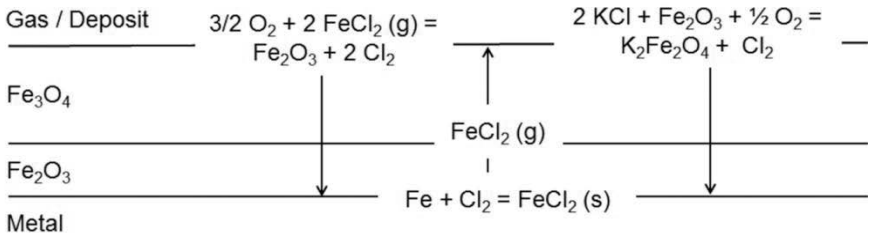

Figure 3 Schematic illustration of the active oxidation reaction circuit caused by chlorine. The reactions are similar for NaCl. Adapted from (Ref 11) (Publication IV).

2.2 High temperature corrosion due to molten phases

Chlorine is especially detrimental to heat exchanger surfaces because it forms compounds with low melting point and high volatility in boiler conditions. One important corrosion mechanism in biomass and waste-to-energy boilers is molten salt attack due to low-melting compounds such as alkali metal chlorides (NaCl and KCl); calcium, potassium, and sodium sulfates; and zinc, copper or lead chlorides (Ref 5, 14–17, 19, 32). Molten phases in the deposits may result in oxide scale fluxing and, hence, strong corrosion when the protective oxide scale is damaged and formation of new scale is hindered. Copper in the presence of chlorine has

been reported to act detrimentally in boiler conditions, strongly accelerating the corrosion of iron- and nickel-based alloys (Ref 33). Some reactions that may occur in the presence of chlorine, heavy metals and sulfates are presented in approximate Equation 1 adapted from (Ref 15), Equation 2 (Ref 33) and Equation 3 (Ref 11).

$$ZnCl_2(l) + 2\ Fe_2O_3 = (Zn,Fe)O + Fe_3O_4 + Cl_2 + ½\ O_2 \quad (1)$$

$$2\ CuCl_2 + O_2 \rightarrow 2\ CuO + 2\ Cl_2 \quad (2)$$

$$(Na,K)_2SO_4 + SO_2 + ½\ O_2 = (Na,K)_2S_2O_7 \quad (3)$$

Chlorine also plays an important role in the formation of fine particles and deposits (Ref 34). Alkali metal chlorides of biomass combustion have high vapour pressures and therefore condensate at low temperatures in the flue gas. On the other hand, sulfur reacts with alkali metal (sodium or potassium) chlorides and hydroxides by sulfation reactions (Ref 35), as presented in Equations 4-5 (Ref 36). In the sulfation reaction, chlorine of the metallic chloride is released as HCl, which has been found to significantly reduce deposit formation and corrosion in power plants operating with chlorine-rich fuels (Ref 37).

$$2\ (Na/K)OH + SO_2 + \frac{1}{2}\ O_2 \leftrightarrow (Na/K)_2SO_4 + H_2O \quad (4)$$

$$2\ (Na/K)Cl + H_2O + SO_2 + \frac{1}{2}\ O_2 \leftrightarrow (Na/K)_2SO_4 + 2\ HCl \quad (5)$$

Zinc has high influence on the corrosion mechanism, especially when waste wood is used for combustion (Ref 6). When burning biomass or waste, for instance the following low-melting compounds are formed $ZnCl_2$, $FeCl_2$ and $FeCl_3$, with melting points of 318 °C, 676 °C and 303 °C, respectively (Ref 15, 30). Lead and copper have the same detrimental effect on the corrosion behaviour of stainless steels (Ref 17). According to thermodynamic equilibrium calculations by Otsuka (Ref 38), vapour condensation of KCl, NaCl, Na_2SO_4, as well as lead and zinc salts takes place on the tube surfaces below 350 °C. Montgomery (Ref 39) has reported on the occurrence of pitting corrosion at low temperatures (300 °C) due to chlorides and sulfates present as heavy metal salts in a melt or semi-melt phase. Catastrophic corrosion rates can occur in the presence of molten chlorides on heat exchanger surfaces even at 250 °C (Ref 40). Skrivfars et al. (Ref 41) have shown that enhanced corrosion can occur even below the first melting point of alkali sulfate and alkali chloride salts. It is assumed that water vapour accelerates the breakdown of the protective layer. Ehlers et al. (Ref 42) have shown that under the conditions of high $H_2O(g)/O_2$ ratios the penetration of water vapour molecules triggers enhanced oxidation and sustains high growth rates of the poorly protective Fe-rich oxide scale formed in the atmospheres.

2.3 Conventional boiler tube materials

Boiler components are traditionally manufactured from low-alloy steels (Ref 43). However, due to increasingly aggressive conditions in present boilers, high- alloyed materials have been considered for the critical parts of boilers, e.g. superheaters and lower furnace walls. The main alloying element used for increasing corrosion resistance is chromium. Material properties influencing boiler lifetime are, e.g., creep rupture, yield strength, corrosion and erosion resistance and mechanical stability. Other material requirements for boiler materials are weldability and machinability, which are dependent on the size and shape of the part (Ref 44). The tube materials need to endure thermal stresses in order to withstand shutdown/start-up cycles and temperature variations. Therefore, in large and thick-walled parts the coefficient of thermal expansion (CTE) is kept small and the thermal conductivity as high as possible. Ferritic steels perform better than austenitic steels in large parts, mainly due to the huge differences in CTE. The CTE of low-alloy or ferritic steels is typically about $10...12 \cdot 10^{-6}$/°C compared to $16...18 \cdot 10^{-6}$/°C for austenitic steels, depending on the alloy and the temperature (Ref 45). In very demanding high temperature conditions the creep properties of ferritic or austenitic stainless steels are not adequate, and nickel super alloys should be applied. However, the high price and sometimes difficult machinability and joining of high-alloyed materials hinders their use. The CTE for nickel super alloys is around $13...17 \cdot 10^{-6}$/°C (Ref 45). Some generally applied materials in different boiler parts and the average operating temperatures of these critical components are listed in **Table 2**.

Table 2 Conventional and high-end materials used for boiler components, including low-alloy steels, stainless steels, high-alloy steels and nickel-based alloys and their operation temperatures. (Ref 44, 46–51).

Boiler part	Temperature range	Applied materials
Superheaters	450–750 °C	DIN X20CrMoV121, 13CrMo44 (T12), T91, HCM 12 (P122, SUS410J3TB), Super 304H, Sanicro 25, HR3C, TP347H(FG), Alloy 617, AC66, Inconel 625, A263
Reheaters	290–500 °C	10CrMo910 (T22, SA213), 13CrMo44 (T12), HCM 12, Super304H, TP347H, Alloy 617
Economizers	150–300 °C	ST35.8, DIN 15Mo3, SA201-Gr.A1
Furnace walls	~500 °C at the end	13CrMo44 (T12), DIN 15Mo3, T22, T23, T24, HCM 12, Alloy 617
Steam pipes	500–620 C°	P91, P92 (NF616), P122, DIN X20CrMoV121, HCM 12, SAVE121, NF121, Alloy 617, A263

Recent trends in fuel technology aimed at increasing the production of electricity using renewable fuels have led to major changes in operating conditions inside boilers. Specifically, there is an increased risk of significant alkali chloride deposition in the superheater area of biomass-fuelled boilers due to the chlorine content of the fuels. Depending on the alkali metal volatilization in the boiler and the sulfur and chlorine content of the fuel, condensation of vaporized alkali chlorides on flue gas particles or directly on heat transfer surfaces may cause accelerated corrosion in the superheater area. Hence, even high-alloy steels may experience severe corrosion in biomass boiler conditions. An example of a molten salt corrosion test of steels is presented in **Figure 4**. Half-immersion test of metallic materials in a molten NaCl-KCl-Na_2SO_4 salt at 525 °C under atmospheric conditions was performed for low-alloy (10CrMo910), stainless (AISI 304) and high-alloyed steels (HR11N) and a nickel alloy (IN625) (Ref 52). Low-alloy steels were damaged mainly by intergranular corrosion and rapid oxide growth. High-alloyed stainless steels and the high-nickel alloy suffered from severe pitting.

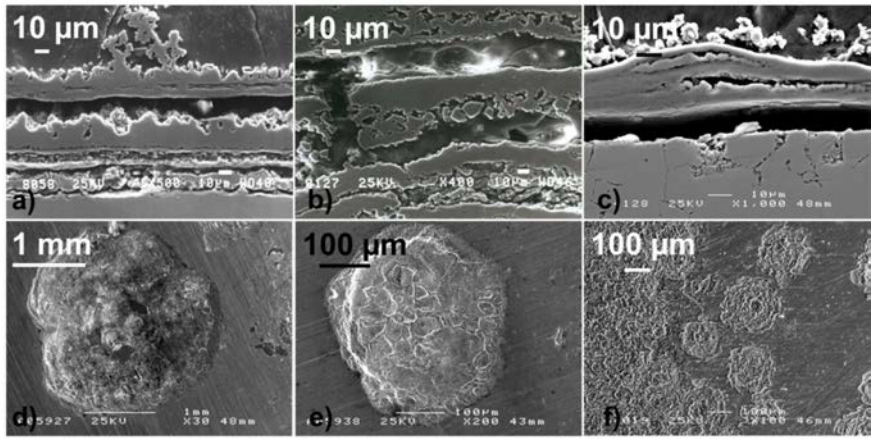

Figure 4 Steels after exposure in molten salt at 525 °C. a) Cross-section of 10CrMo (duration of exposure 44 hours), b) as reference, cross-section of 10CrMo after exposure in actual recovery boiler, c) cross-section of AISI 304 (65 h), d) corrosion pit on the surface of SAN28 (65 h), e) corrosion pit on the surface of HR11N (65 h) and f) pitting on the surface of IN625 (65 h) (Ref 52).

High-alloyed alloys can be applied on economical low-alloy steels as weld overlays (Ref 53, 54) or laser claddings (Ref 55). Weld overlays are thick, typically 2 mm, and dense (Ref 56). Problems associated with the weld overlay coatings include varying corrosion resistance of beads due to heat affected zone (HAZ), increased risk of stress corrosion cracking and mismatch in coefficients of thermal expansion. In laser cladding, a laser beam fuses a consumable onto the substrate surface producing a dense, uniform and crack-free coating with low porosity (Ref 55, 57). During deposition, the top layer of the substrate is melted to give metal-

lurgical bonding with some dilution of the coating to the substrate. Compared to weld overlays, laser cladding gives lower dilution and lower component heating and the laser beam can more rapidly treat larger surface areas. The biggest drawback in claddings, both weld overlays and laser cladding, is the metallurgical bonding mechanism of coating to the substrate material, which may have a negative influence on the mechanical properties of boiler tubes under high pressure.

3. Thermal spray coatings

Thermal spraying is a general term describing a coating method in which typically a metallic or ceramic raw material is heated and sprayed in molten or semi-molten form onto a substrate. Different spraying methods include flame, arc, plasma, high velocity oxy-fuel (HVOF), detonation and cold spray techniques. Common to all thermally sprayed coatings is a lamellar structure although there are vast differences, e.g., in the nature of lamellae (splat) boundaries, porosity and residual stress state. In particular, splat boundaries, interconnected voids and pores can act as fast diffusion paths for corrosive species (Ref 55). For high temperature corrosion applications HVOF spraying is a potential coating method, as it produces dense and well-adhering protective coatings (Ref 58–60). However, optimization of the composition and structure of thermal spray coatings are especially important in the case of corrosion protection in extreme conditions, such as power plant boilers. Several diagnostic tools can be employed for thermal spray process optimization.

3.1 Requirements for thermal spray coatings in boiler conditions

The composition and structure of the coatings should be tailored to endure general conditions as well as harsh corrosion conditions to in order protect the low-alloy steel tubes. The coefficient of thermal expansion (CTE) of the coating should match with the substrate material in order to endure the thermal variations during start-ups, shutdowns and the boiler process itself without cracking (Publication VI). The CTE for NiCr is about $14 \cdot 10^{-6}$/°C, for NiCrAlY $12 \cdot 10^{-6}$/°C, for IN625 $13...16 \cdot 10^{-6}$/°C and for Fe19Cr around $10 \cdot 10^{-6}$/°C (Ref 61, 62).

Dense coating structure and high adherence to the substrate are of utmost importance for coatings in high temperature conditions, where corrosive gaseous and molten phases may be present. HVOF spraying is widely used for depositing metallic materials due to its very high particle velocities, which produce dense and well-adhered coatings. The ability to produce dense coatings with low degradation, low oxidation of metallic materials, and minimal phase transformation are the main advantages of the HVOF process (Publication I), making it ideal for the manufacture of corrosion-resistant coatings. This is due to the short dwell time of the parti-

cles in a relatively cold flame. In the HVOF process, fuel and oxygen are introduced to the combustion chamber together with the spray powder. Combustion of the gases produces high temperature and high pressure in the chamber, which causes supersonic flow of the gases through the nozzle. In the HVOF process the particles melt completely or only partially, depending on the flame temperature, particle dwell time, material melting point and thermal conductivity.

3.2 HVOF process parameters

HVOF technology is applied for materials synthesis and fabrication of protective and multi-layered coatings. It is a versatile process with complex process-materials interactions. Coating performance is not only related to the inherent properties of material but also to the process-induced degradation of material properties resulting from the thermal exposure (Ref 63). Thermal spray deposit formation dynamics is highly complicated phenomenon involving droplet impact, spreading, rapid solidification and layered assembly of different sized impact droplets called splats (Ref 64). The particle impact and stacking have an important effect on the coating properties, as the microstructure exhibits many defects associated with droplet based assembly. During the spray process, particle flame interactions, inflight metal oxidation, evaporation in low conductivity oxides and decomposition processes of thermally sensitive materials may occur, and cause variations in coating composition and structure. The substrate condition and spray environment have influence on the coating characteristics, as well. The stresses and strain introduced by the defected structure are important for the properties, behaviour and lifetime of a thermal spray coating. Therefore, the knowledge of stress evolution and residual stresses associated with coating formation and cooling is of particular importance.

The main factors influencing the formation of HVOF thermal spray coatings are the spray system used, raw material properties (composition, particle size distribution, etc.), nozzle type and fuels, and process parameters such as oxygen to fuel ratio, spray distance, and powder feed rate. Different spray guns, nozzles, and fuels can be used to alter the temperature and velocity of the spray particles. Higher temperature produces more molten particles and thus a denser coating structure. By increasing the particle velocity and keeping the particles at lower temperature, the particles maintain their original structure and composition better (e.g., nanostructure, volatile elements). Furthermore, the oxidation of metallic particles can be lower due to the shielding effect of the flame, the chemistry of the flame, shorter dwell time and lower particle temperature (Ref 65).

Particle velocity (v) and particle temperature (T) together with substrate characteristics are the main parameters affecting deposit formation that can be measured (Ref 66). They determine the deposit build-up process and deposit properties. Particle velocity and temperature affect the deposit efficiency as well as the microstructure. The trend in HVOF process development has been towards higher gas pressures, faster particle velocities and lower particle temperatures as shown

schematically in **Figure 5**. This development has a clear influence on the coating microstructure, with the amount of oxidation in the lamellar boundary decreasing and the flattening rate increasing, resulting in improved coating density generation by generation.

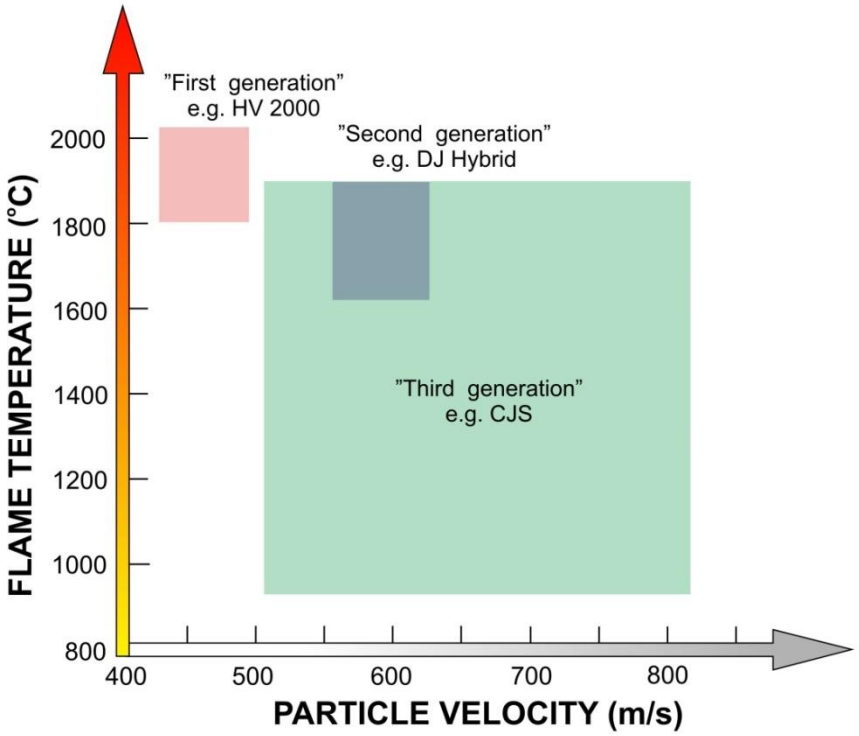

Figure 5 Trend in HVOF process development towards higher gas pressures, faster particle velocities and lower particle temperatures (Publication I).

3.3 Process-structure-properties-performance relationship

For advanced material design, deeper understanding of the relationship between the process, coating structure, properties and performance is needed. This relationship is presented in **Figure 6**. The coating process can be monitored to measure characteristics of the spray stream and to analyse the effect of changes in selected process parameters. By comparing the formed microstructure and the properties of the coatings with the spray characteristics, a deeper understanding of the spray process could be achieved and the link between process parameters and deposit formation possibly determined.

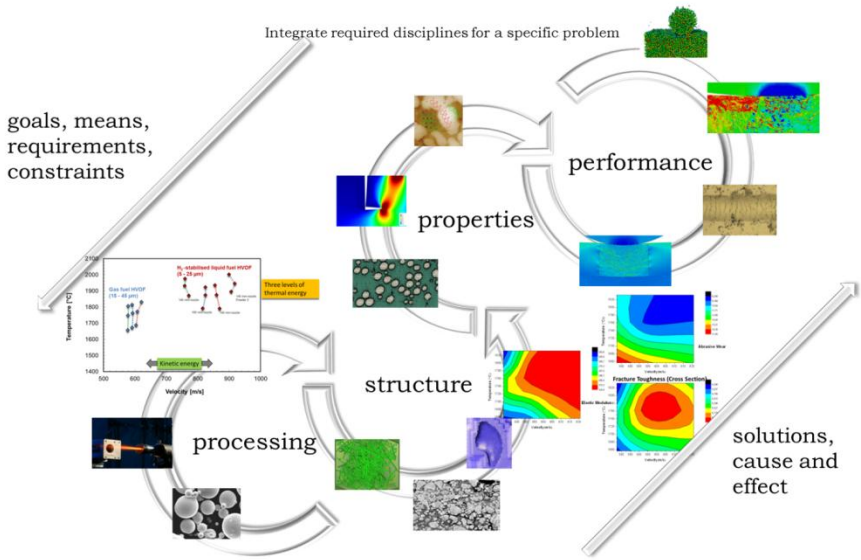

Figure 6 In the PSPP approach to material design, the processing parameters are linked to material structures, the structures are linked to properties and the properties to material performance (Ref 67).

3.4 HVOF process optimization

Factors influencing the control of the HVOF process include the gases/liquid fuels used, total volume flow of gases/liquid fuels, fuel-oxygen (F/O) ratio, choice of nozzle and its geometry, spray distance, powder feed rate, robot speed, etc. Kinetic and thermal energy transferred to the particles is dependent on the flame energy (enthalpy of the used fuel, fuel density, and ratio of fuel to oxygen). Higher energy levels of the flame yield higher kinetic and thermal energies in the particles. Powder feedstock properties have a very important effect on the formed coating, as the particle characteristics are very different in the spray process (e.g., temperature and velocity). Powder properties and characteristics (e.g., particle shape, structure and size, powder density and flow ability, purity, phase content, agglomeration) depend on the specific powder manufacturing method, i.e., crushing and milling, water and gas atomization, spray drying, agglomeration and sintering (Ref 58). Examples of different powder morphologies are presented in **Figure 7** (Publication I).

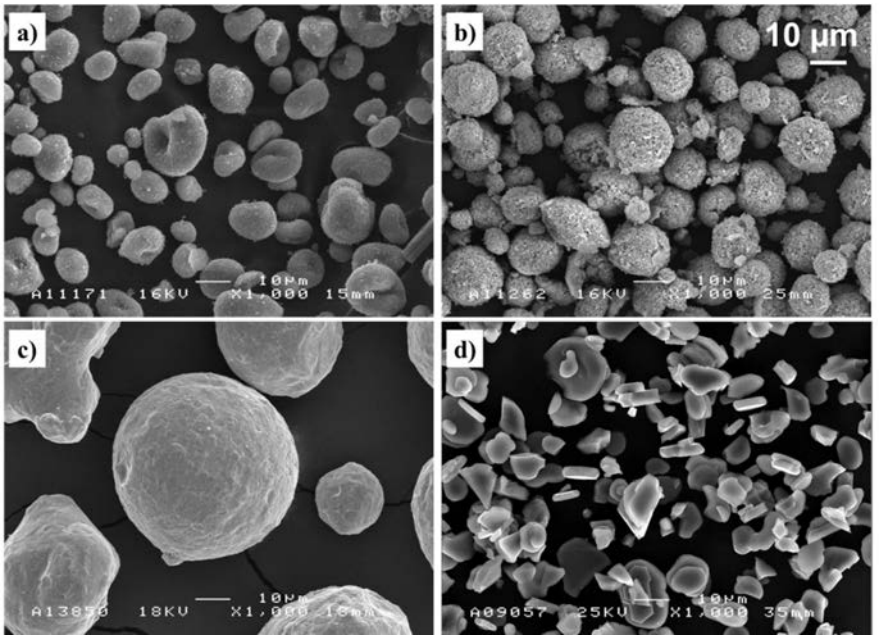

Figure 7 SEM images of thermal spray powders representing different morphologies. a) Ball mill mixed, agglomerated and sintered Al_2O_3/SiC; b) spray dried Cr_2O_3; c) gas atomized Ni20Cr; and d) fused and crushed Al_2O_3 powder by Praxair (Publication I).

Thermal spray process monitoring and optimization tools have developed strongly in recent decades due to improved on-line diagnostic techniques. Optimization of the coating process has consequently progressed from trial and error based evaluation to systematic process control (Ref 68, 69). Several systems have been developed for monitoring the effects of conventional spray parameters (e.g. gas flow rate, nozzle diameter, particle size distribution) on in-flight particle conditions, i.e. particle temperature and velocity (Ref 68). These diagnostic tools have markedly improved the reproducibility and reliability of thermal spray coatings. In parallel, stress formation during the spray process can be measured with an in-situ coating property sensor (ICP) (Ref 70). Characteristics of the coatings, such as adherence to the substrate, are strongly influenced by the residual stresses generated during the coating deposition process (Ref 71).

Sampath et al. (Ref 72) introduced a Process Map methodology, in which diagnostic tools are used for understanding the fundamental relationships in the thermal spray process from powder feedstock, thermal spraying and deposit formation, to coating characteristics and to coating performance. Predictable quality and properties of a manufactured coating may be achieved by combining on-line diagnostics and the process map methodology with the process-structure-properties concept. The process map methodology was developed for process

control and optimization of coating properties. Benefits of the methodology include, e.g., improved coating manufacturing and quality, process reliability, advanced coating design, predictable operating life of coatings, and enhanced process and deposition efficiency (Ref 65, 73-76).

A first-order process map expresses the relationship between torch parameters and particles in the spray stream, which are measured by diagnostics. A second-order process map represents the relationship between the spray stream measured responses and coating properties. Systematic evaluation of the processes, leading to optimization of coating properties for specified performance and assessment of process reliability, can be performed using process map method. The process map concept for HVOF spraying is presented in Figure 8 below.

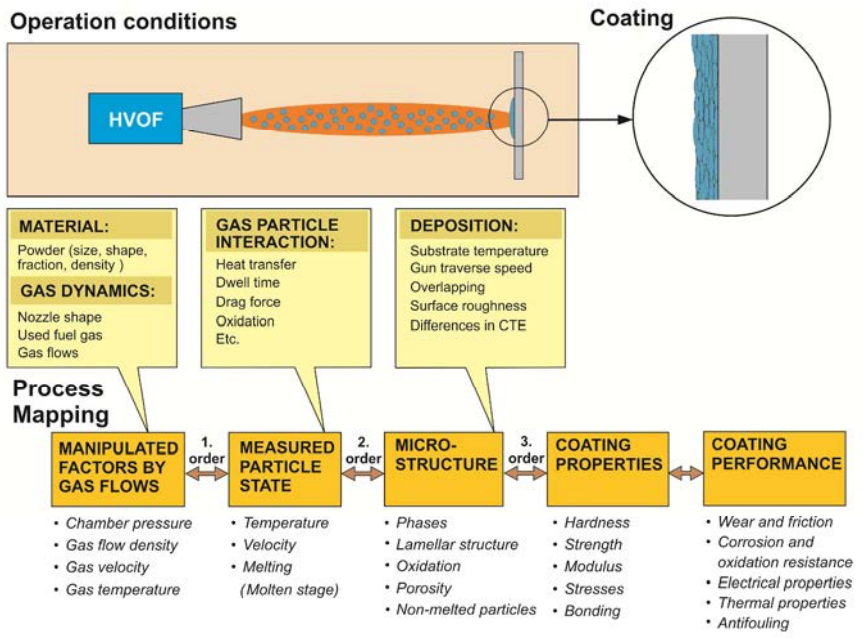

Figure 8 Process Map concept for the HVOF process. The goal of process mapping is to understand the thermal spray process and coating structure and properties (process-structure-properties) in order to enhance the coating design (Publication I).

Principle objectives of diagnostic tools are to measure the variables of particles within the spray stream, i.e., velocity, temperature, flux, trajectory, and size distribution, which all influence the microstructure and properties of sprayed coatings (Ref 75). The sensors are mainly based on two-wavelength pyrometry and time triggered measurement of velocity. Example sensors for thermal spraying include the Tecnar DPV2000, Oseir SprayWatch, Tecnar Accuraspray, Inflight Particle Pyrometer, and Spray Position Trajectory sensors. These are based on either

individual particle (DPV2000) or ensemble (group of particles) measurement (SprayWatch, Accuraspray). Ensemble measurement is the faster of the two, at a few seconds versus a few minutes (Ref 68). The diagnostic tools differ in how they measure the spray stream, including the spray volume, number of particles, and ability to scan the stream. These differences between single particle and ensemble sensors may lead to different results when measuring temperature and velocity. Comparison between single and ensemble sensors has shown good correlation for ceramic and metallic coatings when velocity was measured, but with average particle temperature measurement no correlation was shown for metallic materials (Ref 72). The reason for these differences might be that high-temperature ceramic materials have higher total radiated intensity due to higher temperature and higher emissivity, whereas metals are influenced by oxidation and change in emissivity (Ref 72). Therefore, the results of diagnostic tools require careful consideration (Publication I).

3.5 Sealing methods

Thermal spray coatings consist of a complex structure that typically features some porosity, non-melted particles, cracks, and oxides in the splat boundaries. This type of structure might lower the coating resistance in aggressive environments where corrosive agents are present and able to penetrate the coating-substrate interface more easily due to the open structure (Ref 77). Splat boundaries, interconnected voids and pores can act as fast diffusion paths for corrosive species (Ref 55, 78). Therefore, post-treatment methods have been developed for thermal spray coatings, including sealing by (i) impregnation of some material to fill the pores and cracks and (ii) partial melting or sintering of the coating layer to reduce the amount of open porosity and increase adhesion between splats. Inorganic sealants are mainly aimed at high temperature applications where the coatings are exposed to corrosive gases and molten salts. Inorganic sealants include aluminium phosphates, chromic acid, sodium and ethyl silicates and sol–gel type solutions (Ref 77, 79). Several studies have also reported reduced porosity and enhanced erosion corrosion resistance of thermal sprayed coatings by laser glazing (Ref 80, 81). However, it is expected that due to current advanced thermal spray technologies dense coatings without the need for post-treatment can be manufactured.

4. Beyond state-of-art

Several high temperature corrosion tests simulating biomass and waste incineration conditions on bulk materials and the corrosion mechanisms involved have been reported in the literature (Ref 11, 14, 15, 25, 29, 82–88). These tests have included e.g. ferritic and austenitic steels, pure metals, oxides and nickel alloys in oxidizing conditions, under chlorine attack, or under salt deposits. Coatings such as HVOF sprayed Ni20Cr, Ni50Cr, Ni21Cr9Mo, NiCrBSiFe, Cr_3C_2-NiCr, Alloy 625, Stellite-6, Fe_3Al and WC-Co have also been tested in similar laboratory conditions (Ref 55, 89–92). Testing of bulk materials has been carried out in actual power plant conditions and some testing of coatings (e.g. Ni20Cr, NiCrBSi, Stellite-6 and TiO_2-50% Alloy 625) in coal-fired boilers at 900 °C and in waste incinerators (Ref 53, 93). However, relevant research results on thermal spray coatings in actual biomass boiler conditions in the economizer (about 200 °C) or superheater (about 550 °C) area have not been reported. The testing and validation of HVOF coatings at 750 °C in actual biomass boiler conditions in the present study sheds new light on the corrosion performance of HVOF coatings. Optimization and comparison of the structures of HVOF thermal spray coatings with respect to corrosion performance in actual biomass conditions and under severe molten phase exposure are reported here for the first time.

5. Experimental

5.1 Coating Materials

The following nickel- and iron-based coating materials were employed in this work (*code in parenthesis*): NI-980-1/1260F (*NiCr*) of Praxair Surface Technologies, Indianapolis, IN, USA; 1260F/Diamalloy 1005 (*Ni22Cr*) and 4006 (*Ni21Cr*) of Sulzer Metco Europe GmbH, Hattersheim, Germany; AI-1625-TG (*NiCr9Mo*) of Plasmalloy, Baytown, TX, USA; Alloy 59 (*NiCr16Mo*) of MBC Metal Powders Ltd., UK; Amperit 413 (*NiCr10Al*) of H.C.Starck, Goslar, Germany; SHS9172HV1 (*Fe19Cr*) of The Nanosteel Company, Providence, RI, USA and Durmat 580 (*Fe27Cr*) of Durum Verschleiss-Schutz GmbH, Willich, Germany. Diamalloy 1005 and AI-1625-TG are similar in chemical composition to the IN625 material. These alloys were selected because they are designed for high temperature corrosion protection especially in harsh boiler conditions. The chemical compositions of the coating powders are presented in **Table 3**. Hereafter, the coating materials will be denoted by their code names.

Table 3. Chemical compositions [wt.%] of the coating powders as obtained from the manufacturer or by EDX analysis (Publications II–VI).

Code	Ni	Fe	Cr	Mo	Nb	W	C	B	Mn	Si	Cu	Al	Y	Ti
NiCr	Bal.	1.1	46	-	-	-	0.1	-	-	2.1	-	-	-	-
Ni22Cr	Bal.	2.5	21.5	9.0	3.7	-	-	-	0.1	0.2	-	-	-	-
Ni21Cr	Bal.	<1.0	20.5	9.0	-	10.0	0.8	0.8	-	-	4.0			
NiCr9Mo	Bal.	2.2	22.5	9.1	3.6	-	-	-	0.3	-	-	0.5	-	0.1
NiCr16Mo	Bal.	1.5	24	16.5	-	-	-	-	-	-	-	0.5	-	
NiCr10Al	Bal.	-	21.4	-	-	-	-	-	-	-	-	9.4	0.8	
Fe19Cr	-	Bal.	18.6	3.6	7.1	8.6	2.1	<5*	1.1	1.6	-	-	-	-
Fe27Cr	10.7	Bal.	27.2	3.9	-	-	2	-	-	1.4	-	-	-	-

* According to the manufacturer; could not be analysed by EDX.

5.2 Reference tube materials

Thermal spraying was performed on steel alloys. Reference coatings for microstructural and mechanical testing were sprayed either on X10CrMoVNb9-1 (X10) or X20CrMoV11-1 (X20) steels by SFS-EN 10216-2:2014 and coatings for residual stress measurements were sprayed on structural steel S355 by SFS-EN 10025-2. These steels have similar thermal properties (e.g. coefficient of thermal expansion) and therefore the coatings are comparable irrespective of the substrate. Tube materials P235GH by SFS-EN 10216-2:2014 (St35.8 by DIN 17175), X10CrWMoVNb9-2 by SFS-EN 10216-2:2014 (T92; SA-213 T92 by ASTM), X20, Sanicro 25 (SAN25) and Nimonic® alloy 263 (A263) were applied as reference materials in the high temperature corrosion testing. St35.8 is a carbon steel with low corrosion properties. Ferritic (martensite) stainless steels T92 and X20 show sufficient creep resistance at high operating temperatures and moderately higher corrosion resistance than carbon and low-alloy steels. A263 is a precipitation hardening alloy with high strength and corrosion resistance properties. SAN25 (Sanicro 25) by Sandvik (Sandviken, Sweden) is a recently developed iron-based alloy with excellent high temperature properties, designed for use in advanced pulverized coal fired steam boilers. The chemical composition of the reference materials is presented in **Table 4**.

Table 4 Main elements of the reference materials [wt.%].

Mater.	Fe	Ni	Cr	Mo	Co	W	Mn	Cu
St35.8	Fe.	-	-	-	-	-	0.4-0.8	-
T92	Bal.	0.2	9.3	0.5	-	2	0.7	-
X20	Bal.	0.3-0.8	10-12.5	0.8-1.2	-	-	<1	-
A263	0.3	Bal.	19.9	5.8	19.6	-	0.3	0.2
SAN25	Bal.	25	22.5	-	1.5	3.6	0.5	3

5.3 Thermal spray coating

Coatings were manufactured by thermal spraying using the high velocity oxy-fuel (HVOF) technique. Two HVOF spray systems were used: gas-fuelled Diamond Jet Hybrid 2600 (later: DJ) (Sulzer-Metco, Westbury, NY, USA) and liquid-fuelled Carbide Jet System (later: CJS) (Thermico GmbH & Co KG, Dortmund, Germany). The DJ was fuelled with propane (C_3H_8) and the CJS with kerosene and hydrogen. The spray process was optimized particularly for two coating powders, NiCr and Fe-19Cr, in order to determine the optimal coating structure for high temperature corrosion protection (Publication II). Optimization was performed by varying the spray system (DJ vs. CJS), nozzles and selected process parameters (amount

and ratio of fuels). Spray distance was kept constant at 250 mm, as well as powder feed rate at 50 g/min for the CJS and 40 g/min for the DJ. The spray parameters for different coating materials are presented in detail in Publications II–VI.

5.4 Process monitoring and optimization by diagnostic tools

In order to achieve a dense, well-adhered coating structure, the thermal spray coating process was monitored using diagnostic tools. Monitoring of HVOF spraying was performed with the on-line diagnostics device SprayWatch 2i (Oseir Ltd., Tampere, Finland) and an in-situ coating property (ICP) sensor (ReliaCoat Technologies, East Setauket, NY, USA) (Publication II). SprayWatch, an ensemble monitoring system, measures particle temperature by measuring the radiation intensity of the particle flow in two wavelength ranges, while the in-flight particle velocity in the spray stream is calculated using the time-of-flight method. The nozzle types and lengths and the amount of fuels were varied, and the effect on the spray jet and formed coatings were monitored and analysed. Spray distance and powder feed rate were kept constant during spraying. The ICP sensor enables measurement of the curvature of the coated substrate materials during spraying and cooling. Stress formation during the spraying and resulting residual stresses after the cooling stage can be calculated from this curvature. The evolution of residual stresses is described in detail in Ref 63.

Deposition efficiency was calculated according to standard SFS-EN ISO 17836:2004, where the substrate is weighed before and after spraying, and the spray time on the substrate [s] and powder feed per minute [g/min] are measured (Publication II). Based on that information, the deposition efficiency can be calculated as accumulated powder [g] / used powder [g] * 100%.

5.5 Characterization of coating microstructure

The coated specimens were prepared as metallographic cross-sections and characterized with an optical microscope and scanning electron microscope (SEM). Metallographic sample preparation was performed by mounting the samples into resin, cutting the samples with a diamond cutter, and grinding and polishing the samples to 1 µm diamond paste fineness. The samples exposed to high temperature corrosion tests were prepared with ethanol and glycerol to prevent the loss of water-soluble elements and compounds from the corrosion products. The following mechanical, chemical and structural analyses were then performed on the samples.

5.5.1 Microscopy

The microstructure of the coatings was studied with an optical microscope. The cross-sections were examined with an optical microscope and a scanning electron microscope (SEM; Philips XL30ESEM) equipped with energy-dispersive X-ray

spectroscope (EDX; Thermo Fisher Scientific Inc. UltraDry EDS Detector) for elemental analysis and mapping.

5.5.2 Porosity by permeability testing

Viscous gas permeability was measured using a GPT-02 testing cell (Kermetico Inc.) with N_2 gas. The tester is able to measure up to 7 bar N_2 pressure and a minimum flow rate of 0.10 ml/min. Standard porous discs of 25.4 mm diameter are used as substrates on which the coatings are deposited. The discs do not notably hinder gas flow, yet are strong and solid enough to allow good quality coatings to be deposited on them. In the test, a coated porous disc is inserted into the testing cell facing an O-ring that seals the chamber. Then, N_2 pressure is increased stepwise and the flow rate through the specimen is recorded at each step. Knowing the coating thickness and tested surface area, the viscous gas permeability coefficient (m^2) can be calculated from the measured data. The coefficient represents the surface area of through pores in a single m^2 sample.

5.5.3 X-ray diffraction

The powders and coatings were analysed with an X-ray diffractometer (XRD; Panalytical X´Pert^3 Powder) using Cu-Kα activation.

5.5.4 Measurement of oxygen content

Elemental analysis of oxygen was performed with a TC-436 LECO instrument applying the inert gas fusion principle.

5.5.5 Hardness and elastic modulus

Hardness and elastic modulus of the cross-sections were measured with an instrumented Zwick ZHU 0.2 hardness tester. Elastic modulus values were calculated from the load-displacement data taken from indentations on the coating surface following the procedure proposed by Oliver and Pharr (Ref 63, 94).

5.5.6 Adhesion

Adhesion was tested according to modified SFS-EN 13144:2003, using the materials tester 1185 by Instron Ltd. The testing differed from the standard by the measured area; the measurement was performed using square samples, which were not cut into a circular shape in order to avoid cracking before the testing. The coating area was therefore larger than the standard counterpart (625 mm^2 vs. 1963 mm^2).

5.6 High temperature corrosion testing

High temperature corrosion testing was performed both in controlled laboratory conditions (Publication VI) and in actual biomass power plant exposures (Publications III-V). Special attention was paid to chlorine and salt melt induced high temperature corrosion. After exposure, the specimens were removed from the probe and embedded in cold-setting resin on site. The embedded specimens were cross-sectioned by grinding in ethanol followed by polishing. Post-analysis of the exposed samples was performed by optical microscopy, SEM and EDX spectroscopy.

5.6.1 On-site boiler exposure in superheater area

The corrosion performance of the coatings and the reference materials was tested in real boiler conditions with a probe exposure (Publication III). The probe with coated and uncoated ring specimens was installed in the superheater area after the cyclones for up to 5900 hours. The flue gas temperature in that area varies typically from 750 to 900 °C. The advanced air- and water-cooled probe with separate controllable cooling unit is approximately two meters in length and can accommodate two sections with six test rings in each. One section is water and air cooled and exposed to metal temperatures of approximately 550 °C, the other section is air-cooled and exposed to metal temperatures of about 750 °C (**Figure 9**).

Figure 9 Test probe before exposure in a biomass co-fired boiler. On the left, section with specimens exposed to 550 °C; on the right specimens exposed to 750 °C (Ref 95).

The on-site exposure was conducted at the Alholmens Kraft power plant in Pietarsaari, Finland. The 550 MW_{th} circulating fluidized bed boiler is one of the largest biomass-fuelled power plants in the world producing electricity, district heating and process steam and heat for a pulp and paper mill. The live steam parameters of the boiler are 194 kg/s, 165 bar and 545 °C. A schematic diagram of the power plant boiler is presented in Figure 1a. During the measurements the boiler was fired on average with 15% peat, 30% coal, 46% biomass (forest residues, industrial wood and bark, etc.) and 9% solid recovered fuel (SRF). Chemical analyses of

the fuels were not available, but Sandberg et al. (Ref 24) have presented the chemical composition of similar fuels in their study. Gas composition was gathered from the plant's reporting systems. SO_2 and HCl levels showed high variation due to fluctuating production rates of the boiler as well as varying fuel shares. SO_2 level was 150 mg/Nm^3 on average (50-200 mg/Nm^3) and HCl 80 mg/Nm^3 (35-115 mg/Nm^3).

5.6.2 On-site boiler exposure in economizer area

Coating testing in the economizer area took place in a 40 MW_{th} circulating fluidized bed (CFB) boiler fired by solid biomass (Publications IV-V). Coatings were thermally sprayed on two-metre-long boiler tube sections, which were then welded onto actual boiler tubes for a two-year period of in-situ exposure. The district heating power plant had encountered severe problems with corrosion, and the economizer tubes had to be replaced every two years. The test coatings were installed on the hot and cold economizer, where strong corrosion and tube failure had occurred. The boiler design is presented in Figure 1b. The boiler was fired mainly by wood-based fuels, including recycled wood, mixed with small amounts of peat. The moisture content of the wood was high, at over 50%. The water inlet temperature to the economizers was about 102–115 °C, and the maximum water temperature in the hot economizer was about 200 °C. The temperature of the flue gas was about 360–400 °C before the cold economizer and about 520…800 °C before the hot economizer according to the boiler operator.

5.6.3 Laboratory testing

Two high temperature salt deposit corrosion tests were carried out in a high temperature corrosion test furnace under controlled conditions. The test layout is presented in **Figure 10**. The deposit tests were performed to simulate the actual situation in boilers, where molten salt deposits may form on the tubes and cause severe corrosion. The tests were made using salt deposit and a controlled atmosphere consisting of synthetic air and 10% H_2O. The gas flow was controlled by mass flow controllers. The composition of the gas phase is not representative for actual biomass boiler conditions as e.g. HCl and SO_2 were not present in the tests. The duration of each test was 168 h in total, and it was run at a constant temperature of either 575 °C or 625 °C. The applied deposit was an alkali chloride – alkali sulfate salt mixture of eutectic composition (6.5 wt.% NaCl; 59 wt.% Na_2SO_4; and 34.5 wt.% KCl), which transforms in molten state at 520–530 °C. The test conditions are presented in **Table 5**. The water-soluble deposits were sprayed onto preheated (150-200 °C) samples following the TESTCORR recommended procedures (Ref 96). The deposit was applied on one side of the samples.

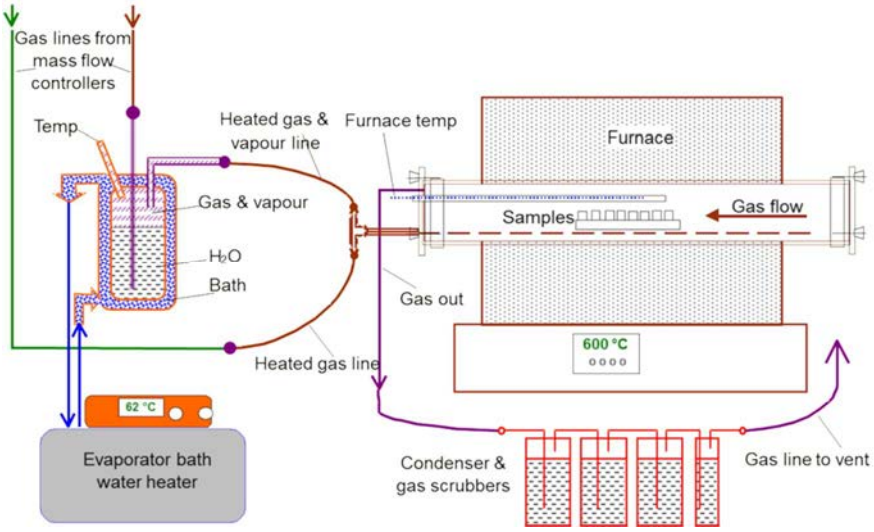

Figure 10 Furnace layout for high temperature corrosion testing in laboratory (Publication VI).

Table 5 Conditions applied for the laboratory corrosion tests (Publication VI).

Test	Temperature	Salt	Gas	Duration
1	575 °C	NaCl, Na_2SO_4, KCl	Synthetic air + 10% H_2O	168 h
2	625 °C	NaCl, Na_2SO_4, KCl	Synthetic air + 10% H_2O	168 h

5.7 Thermodynamic calculations

Thermodynamic calculations were performed using the FactSage 6.4 Phase Diagram module with FactPS database (Publications III, IV).

6. Summary of results

This chapter summarizes the major findings. Detailed results are presented in the attached Publications I–VI.

6.1 HVOF process optimization

Optimization of the HVOF coating process was performed by applying diagnostic tools together with careful characterization of the coatings for NiCr in particular. The optimization was aimed at attaining dense coating structures suitable for high temperature corrosion resistance.

Particle velocity (v) and particle temperature (T) together with substrate characteristics are the main parameters affecting the deposit formation that can be measured (Ref 66). They determine the deposit build-up process and deposit properties. Particle velocity and temperature affect the deposit efficiency as well as the microstructure (Publication I). The trend in HVOF process development towards higher gas pressures, faster particle velocities and lower particle temperatures has had a clear influence on the coating microstructure, with amount of oxidation in the lamellar boundary decreasing and the flattening rate increasing, resulting in continuous generation by generation coating density improvement (Publication I), as presented in **Figure 11**.

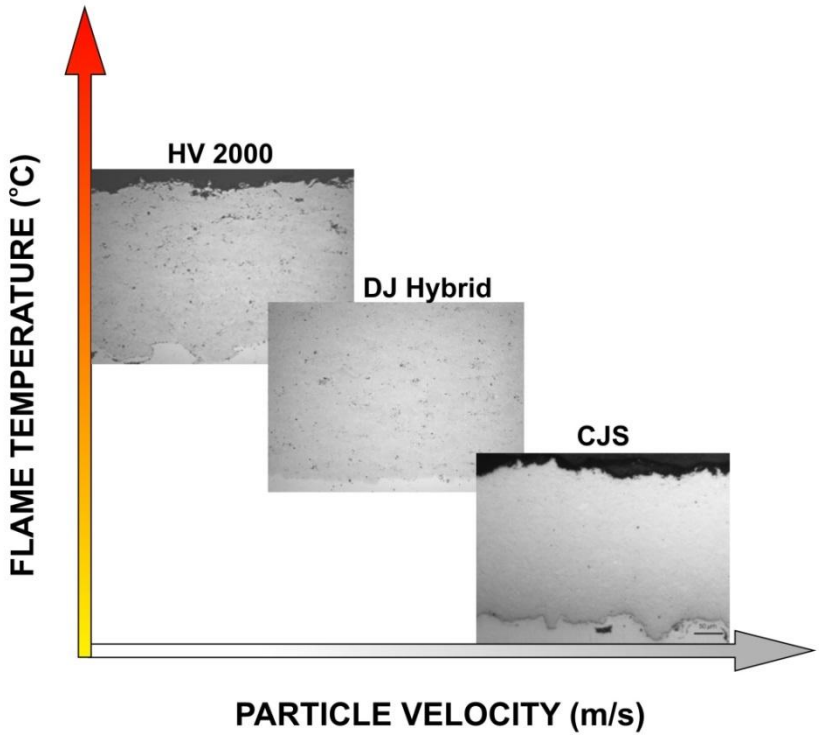

Figure 11 The trend in HVOF process development towards higher gas pressures, faster particle velocities and lower particle temperatures has had a clear influence on coating microstructure (Publication I).

6.2 Process optimization for NiCr coating

Thermal spray coatings were prepared using the HVOF spray technique. For NiCr coating, several process parameter combinations were applied in order to achieve a dense structure with sufficient adhesion to the substrate (Publication II). The process parameters used for NiCr coating are presented in **Table 6**. Spray optimization was performed with the DJ and CJS spray systems by using two nozzles for the DJ and three nozzles for the CJS. The amount of fuel and oxygen feed was alternated. The spray distance was 250 mm and the powder feed rate was 40 g/min for the DJ and 50 g/min for the CJS. The spray parameters for other coating materials are presented in detail in Publications I–VI.

Table 6 HVOF process parameters for NiCr coating. Fuel feed is shown in [l/min]. Spray distance was 250 mm and powder feed rate was 50 g/min for CJS and 40 g/min for DJ (Publication II).

Gun	Spray	Nozzle	C_3H_8	O_2	Air	N_2	Total flow	F/O
DJ	**A1**	2702	45	179	390	12.5	626.5	0.17
DJ	**A2**	2702	59	165	390	12.5	626.5	0.24
DJ	**A3**	2702	78	146	390	12.5	626.5	0.28
DJ	**A4**	2702	69	166	390	12.5	637.5	0.34
DJ	**A5**	2701	56	252	400	12.5	720.5	0.17
DJ	**A6**	2701	62	290	400	12.5	764.5	0.17
DJ	**A7**	2701	85	222	400	12.5	712.5	0.28
DJ	**A8**	2701	77	195	400	12.5	684.5	0.28
Gun	**Spray**	**Nozzle**	**Keros.**	H_2	O_2	N_2		
CJS	**B1**	5.2/100	16	100	850	20		
CJS	**B2**	5.2/100	16	100	1000	20		
CJS	**B3**	5.2/100	20	100	850	20		
CJS	**B4**	5.2/100	20	100	1000	20		
CJS	**B5**	5.2/100	21	100	900	12		
CJS	**B6**	5.2/140	16	100	850	12		
CJS	**B7**	5.2/140	16	100	1000	12		

6.2.1 On-line diagnostics: T - v measurement

Temperature (T) and velocity (v) values were measured for NiCr coating with the DJ and CJS systems (Publication II). The diagnostics data for selected spray process parameters are presented in a temperature-velocity chart in **Figure 12**. For DJ spray gun 2702, the highest particle temperatures (average 2110 °C) were achieved with A1 spray parameters and lowest (1867 °C) with A4 spray parameters. With the 2701 spray gun, the highest temperature values were achieved with A6 (2078 °C) and lowest with A7 (1924 °C) spray parameters. With the 2702 spray gun, the highest measured particle velocities were for spray A3 (average 645 m/s) and the lowest for spray A1 (563 m/s). Higher velocities were produced by the 2701 spray gun: the highest value being for the A8 (703 m/s) and the lowest for A5 (633 m/s) spray. Dependency of F/O ratio on temperature and of total flow on velocity could be detected, **Figure 13**. The highest temperature was achieved with the smallest F/O ratio (0.17) and the highest velocity with the highest total fuel flow (765 l/min).

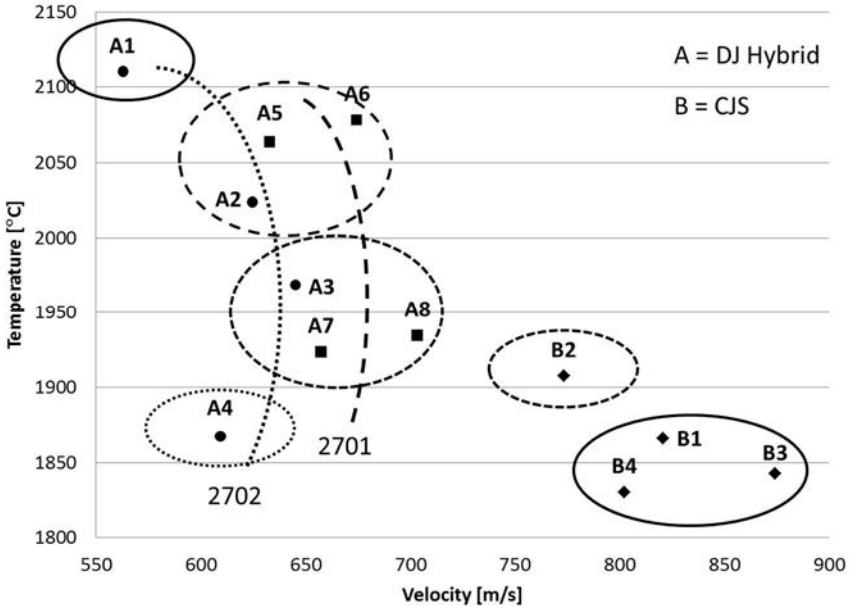

Figure 12 Temperature-velocity chart for NiCr coatings sprayed with HVOF DJ and CJS (Publication II).

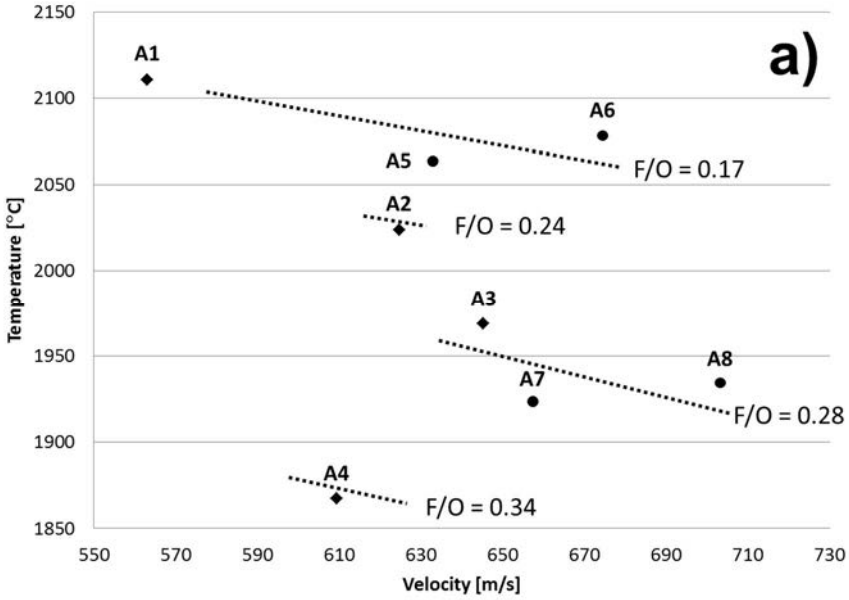

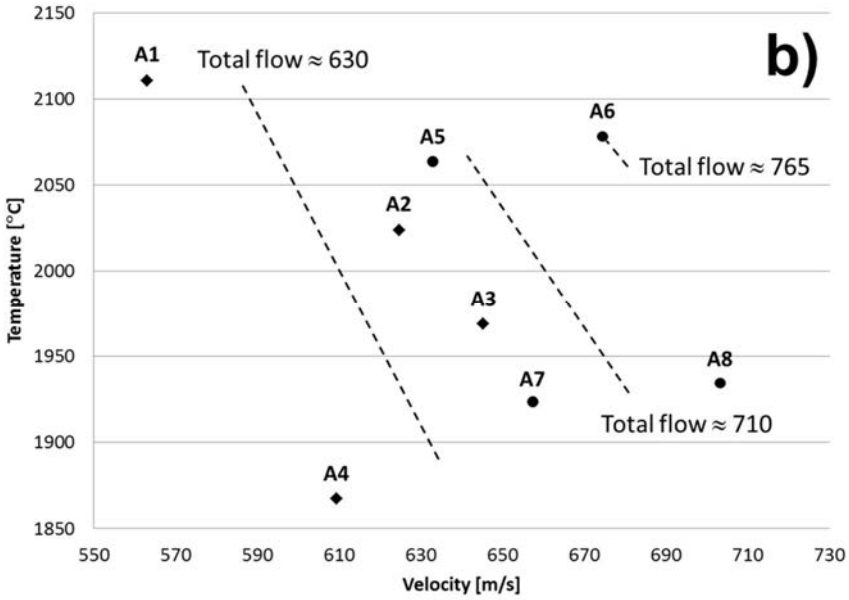

Figure 13 Dependencies of a) F/O ratio and b) total flow [l/min] on particle temperature and velocity for NiCr coating by HVOF DJ spraying (Publication II).

The particle temperatures for CJS spraying varied between 1830 °C (for B4 spray) and 1908 °C (for B2 spray). For the CJS, velocities were distinctly higher than with the DJ system. The highest value was produced with the B3 spray (average 874 m/s) and the lowest with the B2 spray (773 m/s). However, the reliability of measurement of CJS spraying is not high, as only a few measurement points were possible to detect due to limitations of the device to detect lower particle temperatures.

6.2.2 Deposition efficiency for NiCr coatings

Calculated relative deposition efficiencies for NiCr coating spraying varied between 53–67% (Table 7) (Publication II). Best efficiency value was achieved by the A8 spray (67%) with the DJ 2701 spray gun. With the 2702 spray gun, the best efficiency was given by the A4 spray (64%) and with the CJS by the B4 spray (62%).

Table 7. Relative deposition efficiency DE [%] for NiCr coating sprays with DJ Hybrid (2702 A1–4 and 2701 A5–8) and CJS (B1–4) (Publication II).

	DJ 2702				**DJ** 2701				**CJS**			
Spray	**A1**	**A2**	**A3**	**A4**	**A5**	**A6**	**A7**	**A8**	**B1**	**B2**	**B3**	**B4**
[%]	58	61	62	64	58	49	62	67	53	54	59	62

6.2.3 Microstructure of NiCr coatings

There was a clear difference between the microstructures of DJ and CJS sprayed coatings. The DJ sprayed coatings exhibited a higher melting state and stronger oxidation behaviour than the CJS sprayed coatings. Melting state varied between different DJ sprays. The A6 spray parameters produced the highest melting state and flattest lamellar structure, whereas A4 coating showed a lower melting state and a clear lamellar structure with perceivable round particle form. The CJS spray produced quite similar coatings with all the applied spray parameters. With the CJS, the peening effect of previous passes was distinctive, as the appearance of the coating structure was much denser near the substrate, and the lamellar boundaries were more prominent in the surface layers of the coating.

In the temperature-velocity diagram (**Figure 12**), six different T-v ranges can be distinguished. For example, A1 coating represents a combination of high temperature and moderate velocity and B1 coating a combination of low temperature and high velocity. These six coating microstructures are presented in detail in **Figure 14**, where evident differences in melting state, lamellar structure and oxidation could be detected visually. The A4 DJ coating resembles CJS sprayed coatings, with lower oxidation and a circular lamella form. High oxidation on lamellar boundaries can be detected in the A6 coating compared to the A4 coating with a lower particle temperature during spraying.

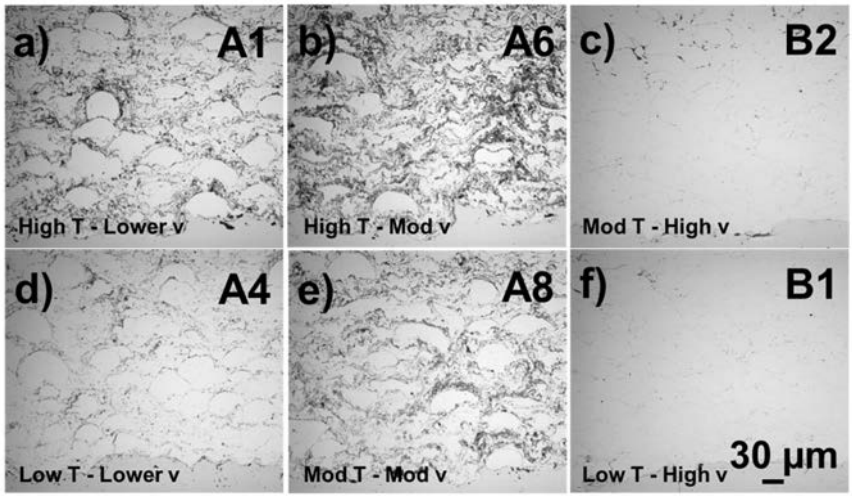

Figure 14 Comparison of HVOF NiCr coating microstructures by optical microscope with different temperature–velocity values: a,b,d,e) DJ and c,f) CJS (Publication II).

6.2.4 Stress formation in NiCr coatings

In-situ coating property (ICP) measurement was carried out for selected samples (Publication II). With the DJ system, both tensile and compressive stresses were formed in the NiCr and Fe19Cr coatings. The highest tensile stress state was built with A1 spray parameters for NiCr (123 MPa). The highest compressive stress state was developed with A6 spray parameters for NiCr coating (-54 MPa). High compressive stress values were formed in all the CJS sprayed NiCr coatings. The highest compressive stress values were built with sprays B3 and B8 (residual stress -396 MPa). A typical curvature evolution and substrate temperature history for the DJ and CJS coatings during spraying are presented in **Figure 15**. With an almost identical temperature history, the stress development between the A1 and B1 sprays were significantly different. For the DJ, the quenching stresses are dominant (positive curvature during spraying) producing tensile residual stress in the coating, and for CJS spraying the peening stresses dominate (negative curvature) resulting in compressive residual stresses in the coating.

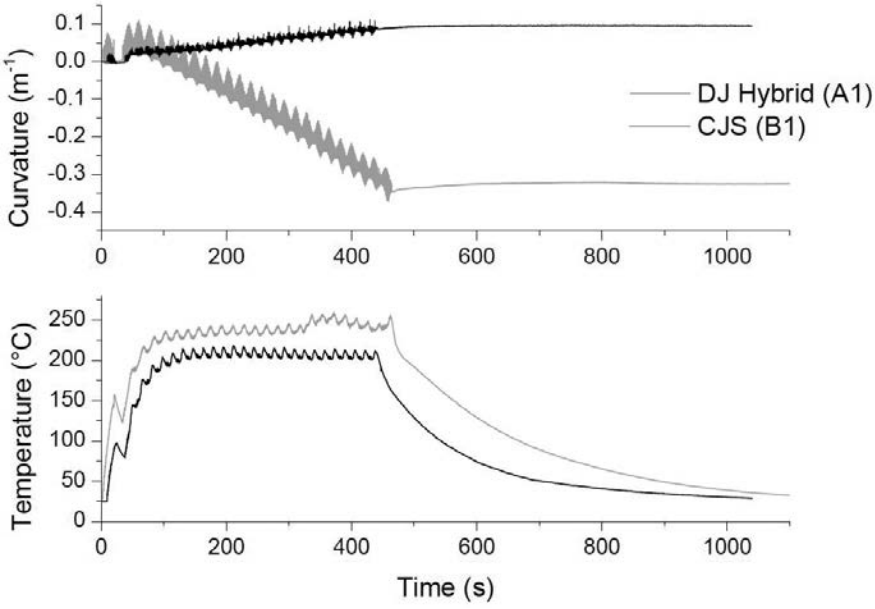

Figure 15 Typical curvature evolution (up) and substrate temperature history (below) for DJ Hybrid and CJS coatings during spraying. With an almost identical temperature history, the stress development between A1 and B1 sprays are significantly different (Publication II).

6.2.5 Characteristics of NiCr coatings

Mechanical and chemical properties were measured for NiCr coatings A1-A8 (DJ) and B1-B4 (CJS) (Publication II). According to XRD analysis, NiCr coating was composed of chromium, silicon and iron in a nickel matrix (**Figure 16**) (Publication II). The crystal structure of the coatings remained similar to the crystal structure of the feed material independent of the HVOF spray system (DJ or CJS). Heat treatment of the coatings in air (168 h, 700 °C) caused a slight shift in the peaks and a few peaks of chromium appeared. Hardness of the samples varied between 395-454 HV0.3 for DJ sprayed NiCr coatings. The highest hardness value was obtained with A8 spray parameters. Young's modulus varied between 146-187 GPa with coating A8 again showing the highest value. For CJS, the hardness of the coatings showed greater variation: HV0.3 was 341-492 depending on the spraying parameters, the highest being obtained with B3 coating. Young's modulus was 145-182 GPa, and the highest value was again achieved with B3 spray parameters. The values of the viscous gas permeability test measurement varied between 0.0-33.9 nm^2 for the NiCr coatings. Zero porosity was achieved in the A6 DJ and B4 CJS sprayed NiCr coatings. The test values are presented in **Table 8**.

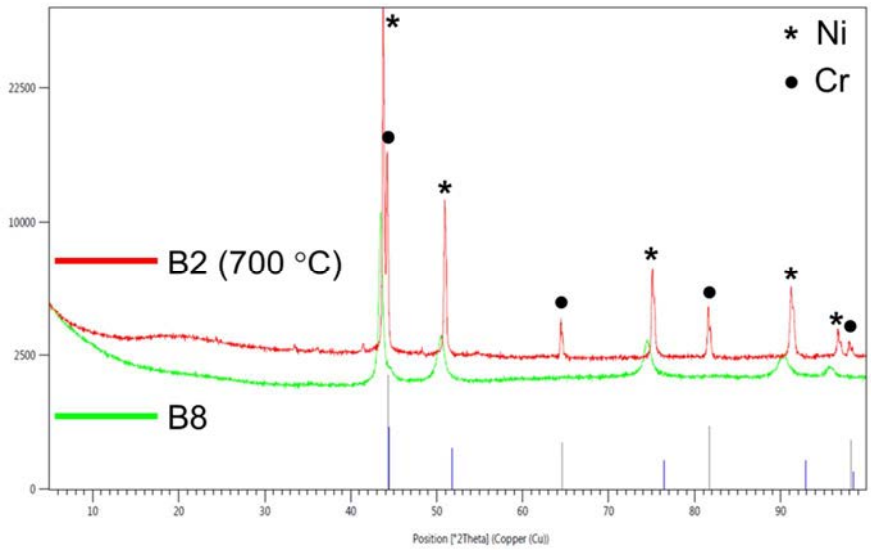

Figure 16 X-ray diffraction pattern presenting the phases of NiCr coating as sprayed (B8) and after heat treatment (B2) (168 h at 700 °C in air).

Table 8 Measured coating properties for NiCr: hardness, elastic modulus, viscous gas permeability coefficient, oxygen content and tensile bond strength. The bond strength was measured for five selected samples (Publication II).

Spray	HV0.3	E_{IT} [GPa]	κ [nm^2]*	O_2 [w.%]**	R_H [N/mm^2]*
A1	426 ± 30	152 ± 8	5.94	2.19 ± 0.07	-
A2	424 ± 33	152 ± 9	1.66	1.94 ± 0.03	-
A3	438 ± 30	157 ± 9	1.96	1.63 ± 0.09	-
A4	416 ± 36	177 ± 9	33.89	0.79 ± 0.03	78
A5	401 ± 33	157 ± 10	1.69	2.72 ± 0.08	-
A6	414 ± 44	146 ± 7	0.00	3.27 ± 0.04	81
A7	395 ± 67	164 ± 3	4.51	1.33 ± 0.01	-
A8	454 ± 23	187 ± 7	1.83	1.82 ± 0.02	-
B1	341 ± 60	145 ± 8	8.66	0.13 ± 0.00	55
B2	423 ± 16	158 ± 7	4.18	0.12 ± 0.00	-
B3	492 ± 33	182 ± 8	0.53	0.24 ± 0.01	70
B4	461 ± 26	165 ± 15	0.00	0.23 ± 0.00	77

κ*	B5	B6	B7	B8	B9	B10	B11
[nm^2]	1.76	5.12	9.78	0.88	4.01	8.11	3.26

* One measurement performed for each sample

** Two measurements performed for each sample

All of the NiCr samples contained small amounts of oxygen (Publication II). The amount of oxygen in coatings sprayed with DJ varied between 0.79 wt.% and 3.27 wt.%. CJS sprayed coatings contained much less oxygen: 0.12–0.24 wt.%. The highest oxygen content was formed in the A6 coating and the lowest in the A4 coating with the DJ. Lowest oxygen content was in the CJS sprayed B2 coating. The oxygen content equates well with visual examination of the optical micrographs, the dark areas between lamellas being oxidized areas. The measured relative bond strengths for the selected specimens were 55–81 N/mm^2. Most of the coatings showed very high bond strength values, the highest being with the DJ sprayed A6 coating. The oxygen values and bond strengths are shown in Table 8.

6.3 Coating structure of Fe19Cr coating

X-ray diffraction analysis of the FeCr powder and coatings showed that the material was partly amorphous with some of the iron-based matrix crystallized (Publica-

tion II). The DJ sprayed coating contained less distinct peaks of iron-based alloy with some Fe_3C crystalline phase. With the CJS system, some other peaks presenting crystalline phases, such as WC and Cr_2C, were detected. Heat treatment at 700 °C for 168 hours in air increased the number of crystalline phases in the coating. In EDX analysis, FeCr coating contained several phases with different chemical compositions as presented in **Figure 17**. The stress state formed in the FeCr coating was tensile with the DJ spray system (288 MPa residual stresses for C1) and with the CJS the measured coatings were all in compressive state from -88 MPa to -750 MPa.

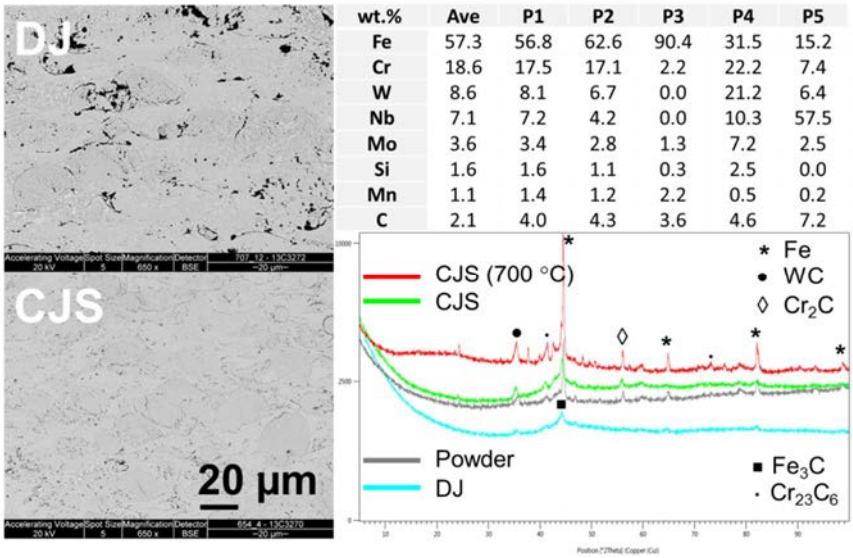

wt.%	Ave	P1	P2	P3	P4	P5
Fe	57.3	56.8	62.6	90.4	31.5	15.2
Cr	18.6	17.5	17.1	2.2	22.2	7.4
W	8.6	8.1	6.7	0.0	21.2	6.4
Nb	7.1	7.2	4.2	0.0	10.3	57.5
Mo	3.6	3.4	2.8	1.3	7.2	2.5
Si	1.6	1.6	1.1	0.3	2.5	0.0
Mn	1.1	1.4	1.2	2.2	0.5	0.2
C	2.1	4.0	4.3	3.6	4.6	7.2

Figure 17 SEM (BSE) images, EDX analyses and X-ray diffraction patterns presenting the chemical composition and phases of FeCr coating. Boron was not included in the EDX analysis (Publication II).

6.4 High temperature corrosion performance

6.4.1 Corrosion resistance in the superheater area of a biomass boiler

NiCr (DJ and CJS), Ni22Cr and Fe19Cr coatings were tested in the superheater area of a biomass co-fired circulating fluidized bed boiler as a probe measurement for 5900 hours (Publication III). The microstructure of the coatings presented typical features of the applied spray methods (**Figure 18**). The CJS sprayed NiCr and Fe19Cr coatings were dense with round lamellae showing lower melting state and minor oxidation. The DJ sprayed NiCr and Ni22Cr coatings were also dense, having a higher melting state with flat and oxidized layered structure. Ferritic steel T92

was applied as a reference material at 550 °C, and nickel-based super alloy A263 at 750 °C.

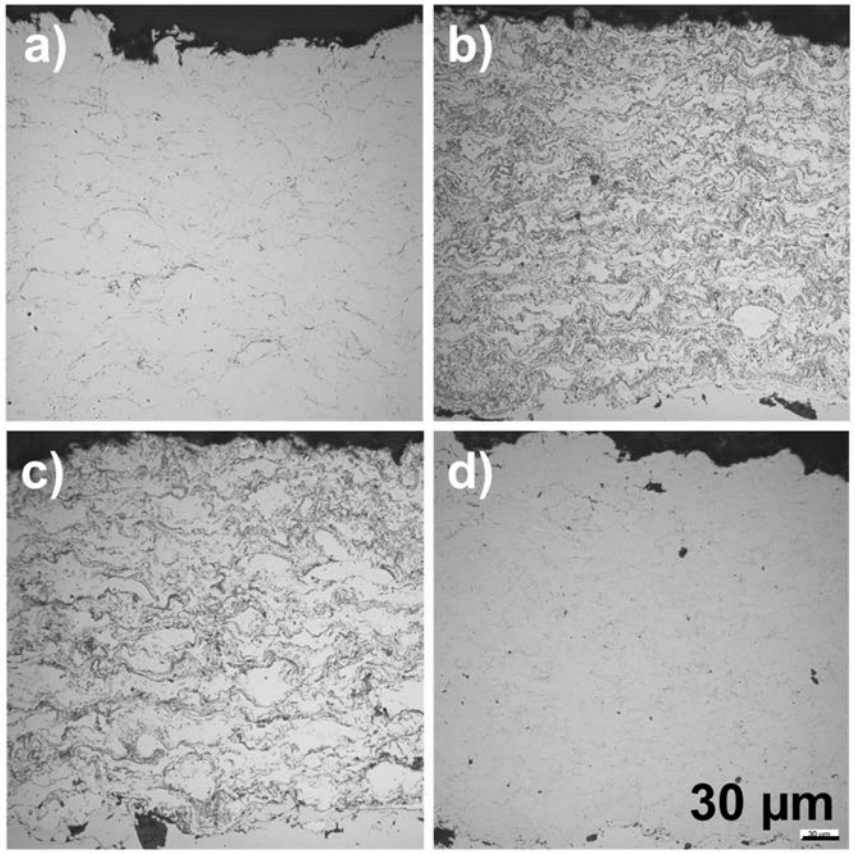

Figure 18 Optical micrographs of the as-sprayed coatings: a) NiCr_CJS, b) NiCr_DJ, c) Ni22Cr_DJ and d) Fe19Cr_CJS (Publication III).

The probe with the specimens was covered with a thick light-brown deposit after the 5900 h exposure. The appearance of the probe before and after is presented in **Figure 19**. The deposit consisted mainly of oxygen (43 wt.%), calcium (13 wt.%), silicon (12 wt.%), sulfur (11 wt.%), aluminium (7 wt.%), potassium (6 wt.%), iron (3 wt.%) and sodium (1 wt.%). Small amounts (< 1% each) of titanium, phosphorus, magnesium, zinc, lead, chromium, barium, copper, manganese and chlorine were also present in the deposits.

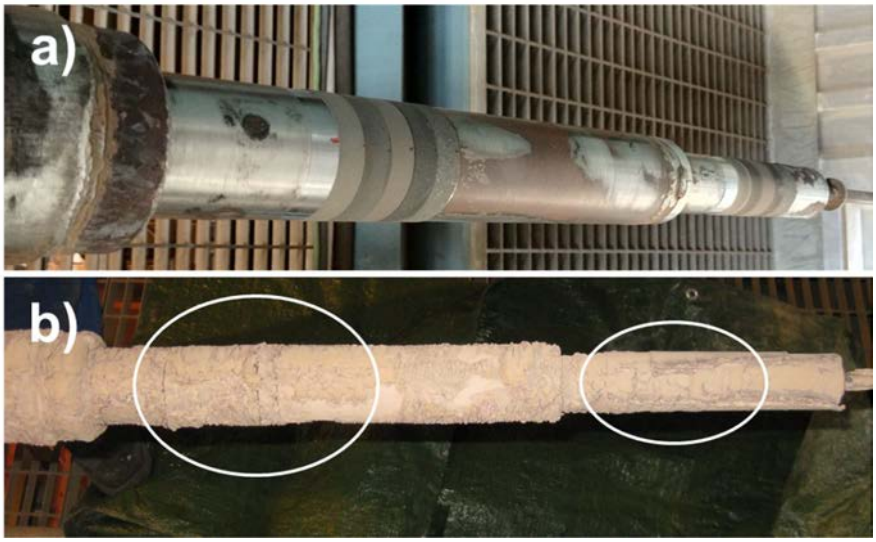

Figure 19 Probe a) before exposure and b) after 5900 h exposure in the biomass co-fired boiler. Left: specimens exposed at 550 °C. Right: specimens exposed at 750 °C.

Corrosion performance at 550 °C

The coatings showed excellent corrosion resistance in the experiment at 550 °C compared to the uncoated ferritic steel T92 (Publication III). The steel tube was covered with an approximately 600 µm thick partly loose oxide scale consisting of several iron and chromium oxide layers. The layers contained e.g. potassium (5 wt.%), sulfur (3 wt.%), sodium (2 wt.%), copper (2 wt.%) and small amounts (< 1 wt.%) of chlorine and zinc. All of the tested thermal spray coatings protected the ferritic substrate material against high temperature corrosion during the exposure. The Ni-based HVOF coatings NiCr and Ni22Cr had mainly a thin, 4–5 µm chromium oxide layer. Propagation of sulfur through lamellar boundaries down to 50 µm was detected with the NiCr_CJS coating on the windward side (about 0.2 wt.% in total). Images of the T92, CJS sprayed NiCr coating and DJ sprayed Ni22Cr and NiCr coatings after the exposure are presented in **Figure 20**.

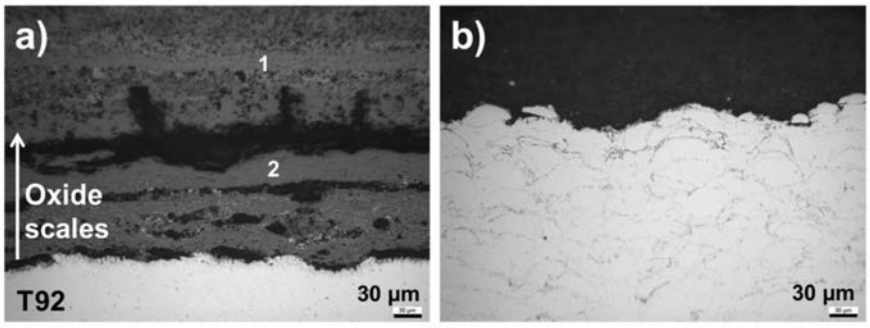

#	O	Fe	Cr	K	S	Na	Cu	Ni	Si	Al	Cl
1	28.9	39.6	16.5	5.3	3.5	2.3	1.3	1.0	1.1	0.4	0.2
2	25.2	73.8	0.5							0.6	

Figure 20 Optical micrographs of the coatings and the T92 reference material after exposure at 550 °C. a) T92, b) NiCr_CJS, c) Ni22Cr_DJ and d) NiCr_DJ. EDX analyses of the corrosion scales of T92 (# 1-2) are presented below the images [wt.%] (Publication III).

A 7–20 µm thick chlorine containing iron-chromium oxide was detected on the surface of the Fe19Cr coating on the windward side (against the flue gas stream) after the 5900 h exposure (Publication III). Furthermore, a thin chlorine-containing layer was detected below the chromium oxide. A thicker, about 80 µm corrosion layer with chromium and iron oxide had formed on the leeward side (opposite to the flue gas stream) (**Figure 21**). The scales consisted of e.g. sulfur (< 5 wt.%), copper (< 6.0 wt.%), chlorine (< 3 wt.%), potassium (0.5 wt.%), lead (0.6 wt.%) and zinc (0.6 wt.%). The corrosion layer exhibited a typical oxide structure with an outer porous iron oxide layer and a denser inner chromium oxide layer.

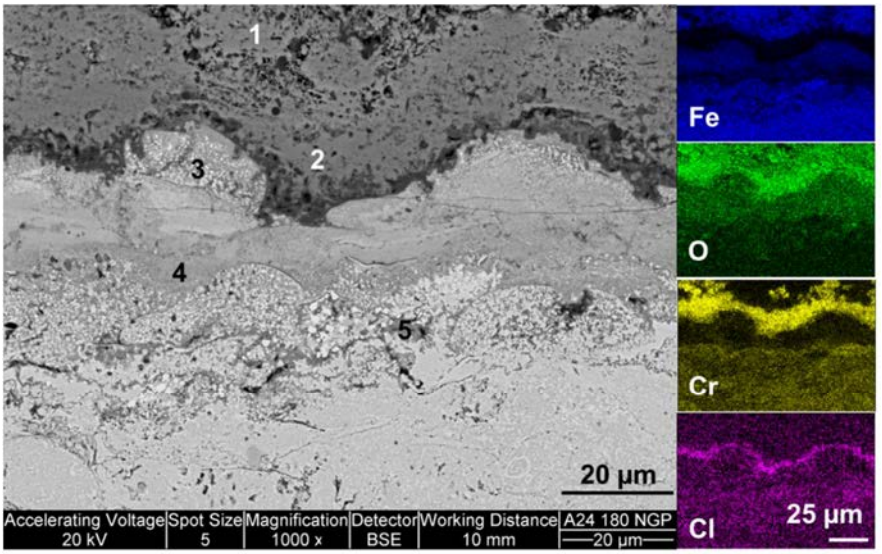

#	O	Fe	Cr	W	Nb	Mo	Si	S	Mn	Cu	Al	K	Pb	Cl	Zn
1	24.5	72.6	0.6		0.2	0.2	0.1	0.1	0.4	0.2	0.3	0.1	0.4		
2	28.4	12.7	49.1	0.5	0.1	0.3	0.8	0.2	3.0	1.5	0.8	0.5	0.6	0.1	0.6
3	23.7	25.0	3.5	15.5	11.2	6.0	2.3	4.9	0.5	6.0	0.2		0.1	0.3	0.2
4	29.4	22.7	5.5	17.2	13.1	6.8	1.3	1.8	0.6	0.1	0.2	0.3	0.3	0.5	
5	17.2	32.7	10.5	14.8	10.4	6.4	0.9	0.2	0.6	0.1	0.2	0.1		2.7	

Figure 21 SEM (BSE) image of the Fe19Cr coating after 5900 h exposure at 550 °C. Elemental maps and EDX point analyses of the corrosion scales (1-5) are presented [wt.%] (Publication III).

Corrosion performance at 750 °C

In the exposure at 750 °C, the uncoated nickel-based alloy A263 as well as most of the coatings showed high corrosion resistance in the boiler conditions (Publication III). Maximum corrosion rates of the reference and coating materials after the superheater area exposure of 5900 hours in a co-firing biomass boiler are presented in **Table 9** (Publication III). The A263 developed a thin (about 15 µm thick) chromium oxide layer, which also contained titanium. Internal grain boundary attack of roughly 15 µm was detected in the alloy, and sulfur was detected at these boundaries. The NiCr coating performance was similar to that of the lower 550 °C test temperature (**Figure 22**). A thin chromium oxide layer was formed on the coating surface. The oxide scale thickness was about five micrometres with NiCr-CJS and 20 µm with NiCr_DJ in most areas. Stronger reaction was detected with NiCr_DJ as pitting corrosion with a maximum corrosion layer thickness of 65 µm. Increased porosity at lamellar boundaries down to 60 µm from the coating surface was noticed in the NiCr_DJ coating.

Table 9 Maximum thickness of corrosion layers (including oxide layer and internal attack) and maximum corrosion rates of the materials in the 5900 h co-firing biomass boiler exposure. WW = windward, against the flue gas stream and LW = leeward, the opposite side (Publication III).

	Max. corrosion layer [µm]				Max. corr. rate [µm/1000h]			
	550°C		750°C		550°C		750°C	
Material	ww	lw	ww	lw	ww	lw	ww	lw
T92	613	484	-	-	103.9	82.0	-	-
A263	-	-	29	12	-	-	4.9	2.0
NiCr_CJS	3*	6	31	6	0.5	1.0	5.3	1.0
NiCr_DJ	4	8	65	20	0.7	1.4	11.0	2.7
Ni22Cr_DJ	18	6	434**	323	3.1	1.0	73.6	54.7
Fe19Cr_CJS	23	80	111	55	3.9	13.6	18.8	8.6

* Additionally corrosion through lamellar boundaries down to 50 µm

** Total coating failure including 50 µm of substrate corrosion

As in the exposure at 550 °C, an outer un-protective iron oxide layer of thickness about 50 µm and an inner chromium-rich mixed oxide layer of equal thickness were formed on the windward side on the Fe19Cr coating (Publication III). Niobium (9 wt.%), tungsten (6 wt.%) and small amounts of e.g. sulfur (2 wt.%), potassium (2 wt.%), and sodium (1 wt.%) were also present in the chromium-rich (28 wt.%) oxide layer. Zinc (2 wt.%), copper (1 wt.%) and lead (1 wt.%) were also detected in the mixed oxide layer.

Ni22Cr coating was consumed totally on the windward side of the tube at 750 °C (Publication III). The strong corrosion had progressed down to the substrate material A263, which showed grain boundary corrosion with sulfur penetration down to 50 µm. Some of the Ni22Cr coating remained in the side area and opposite area (the leeward side) with the corrosion layers containing chromium oxide and sulfur and nickel oxide. Corrosion of Ni22Cr was initiated as localized pitting corrosion on the windward side, as shown in **Figure 23**. Corrosion products consisted mainly of chromium (4–69 wt.%), oxygen (5–20 wt.%), nickel (3–78 wt.%) and sulfur (4 wt.%). One of the oxide layers contained potassium (4 wt.%) and small amounts (< 1 wt.%) of Na, Zn, Pb, Cu and Cl.

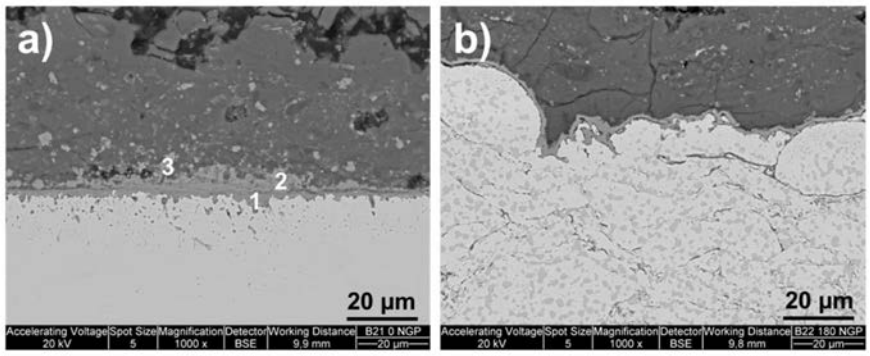

#	O	Cr	Ni	Mo	Nb	Co	Ti	Fe	S	K	Ca	Mn	Cu	Zn
1	27.7	56.6	2.8	2.4		2.1	5.7			0.3				
2	28.4	15.0	16.3			13.5	4.6		2.2	1.3	1.2	10.2	1.4	1.3
3	34.0	7.0	12.3			7.0	0.8	15.7	4.5	2.9	2.6	6.9		1.1
4	24.5	37.6	18.1	10.0	8.7	0.8								
5	3.5	10.0	67.9	15.0		3.2								

Figure 22 SEM (BSE) images of the reference material A263 and the HVOF coatings after exposure at 750 °C. a) A263, b) NiCr-F_CJS, c) Ni22Cr_DJ and d) Fe19Cr_CJS. EDX analyses of the corrosion scales are presented below the images [wt.%] (Publication III).

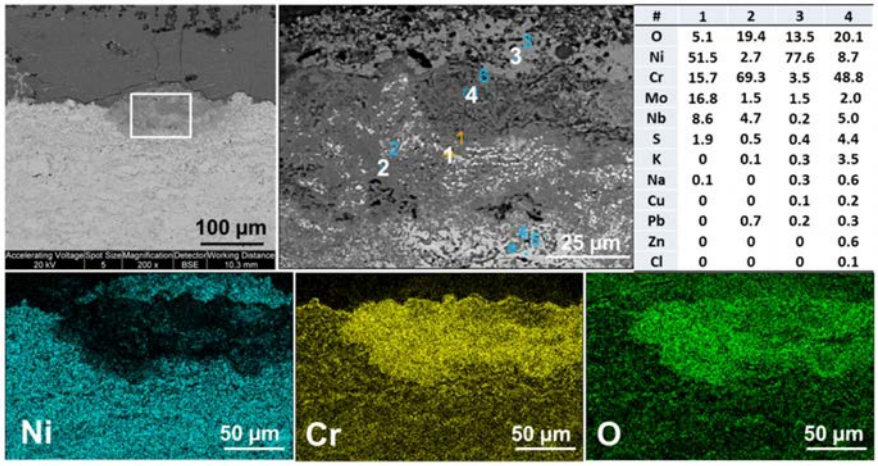

#	1	2	3	4
O	5.1	19.4	13.5	20.1
Ni	51.5	2.7	77.6	8.7
Cr	15.7	69.3	3.5	48.8
Mo	16.8	1.5	1.5	2.0
Nb	8.6	4.7	0.2	5.0
S	1.9	0.5	0.4	4.4
K	0	0.1	0.3	3.5
Na	0.1	0	0.3	0.6
Cu	0	0	0.1	0.2
Pb	0	0.7	0.2	0.3
Zn	0	0	0	0.6
Cl	0	0	0	0.1

Figure 23 SEM (BSE) image of corrosion initiation in Ni22Cr coating at 750 °C. EDX mapping of the corrosion pit is presented with elemental maps of nickel, chromium and oxygen. Main compositions of the corrosion layers are presented in the EDX point analyses (1–4) (Publication III).

6.4.2 High temperature performance in field test in economizer area

HVOF coated tubes were installed in the water circulation tubes of a biomass boiler in the hot and cold economizer area, where maximum water temperature was about 200 °C. After two years of exposure, the coatings were covered partly with ash deposit. The resistance of the Ni-based (NiCr16Mo, NiCr9Mo and NiCr10Al) and Fe-based (Fe27Cr and Fe19Cr) coatings to corrosion in the biomass boiler exposure appeared superior compared to the uncoated tubes (Publications IV, V). Considerable material wastage associated with formation of deep cavities had occurred in carbon steel St35.8 during the two-year exposure in the biomass boiler. Chemical composition of the deposits on the coatings and carbon steel is presented in **Table 10**. Barium (0.2–0.3 wt.%) and molybdenum (1.0–1.3 wt.%) were also detected in deposits of the Fe-based coatings.

The NiCr16Mo coating was dense with minimal porosity and a lamellar structure typical of a thermal spray coating. Corrosion resistance of the NiCr16Mo coating was excellent in the two-year biomass boiler testing in the cold economizer (Publication IV). The coating showed no sign of corrosion after the exposure. The outer layer of the coating consisted of nickel, chromium, molybdenum, oxygen and a small amount of aluminium. A cross-section of the NiCr16Mo coating before and after exposure is presented in **Figure 24** a and d.

Table 10 EDX analyses of the deposits on the coatings and carbon steel after two-year exposure in a biomass boiler [wt.%] (Publications IV, V).

Element	O	Ca	S	K	Si	Fe	Mg	Al	P	Na	Mn	Zn	Cl	Ti	Pb
NiCr16Mo[a]	46.2	21.3	15.1	6.1	3.3	1.4	0.8	1.4	1.9	0.6	0.8	0.5	0.5	...	0.2
NiCr9Mo[a]	44.4	21.9	11.9	1.8	6.1	3.3	1.5	2.9	2.6	0.6	1.0	0.8	0.4	0.4	0.5
NiCr10Al[b]	36.2	25.1	13.6	8.5	4.9	1.9	2.1	1.8	2.3	0.6	1.3	0.7	0.5	0.3	0.3
Fe27Cr[b]	33.7	23.9	13.8	7.0	6.8	2.8	2.2	2.5	2.1	0.8	1.3	0.6	0.6	0.4	0.3
Fe19Cr[b]	37.3	24.5	16.5	4.1	4.1	2.3	1.6	1.4	2.0	0.9	1.3	0.6	0.7	...	0.1
St35.8[a]	36.5	24.6	8.3	7.3	4.5	4.2	4.3	2.4	3.3	0.7	1.9	1.0	0.5	0.4	0.2
St35.8[b]	40.2	20.8	6.3	3.9	8.1	6.2	3.5	4.5	3.0	0.8	1.5	0.4	0.4	0.3	0.2

a Cold economizer, b Hot economizer

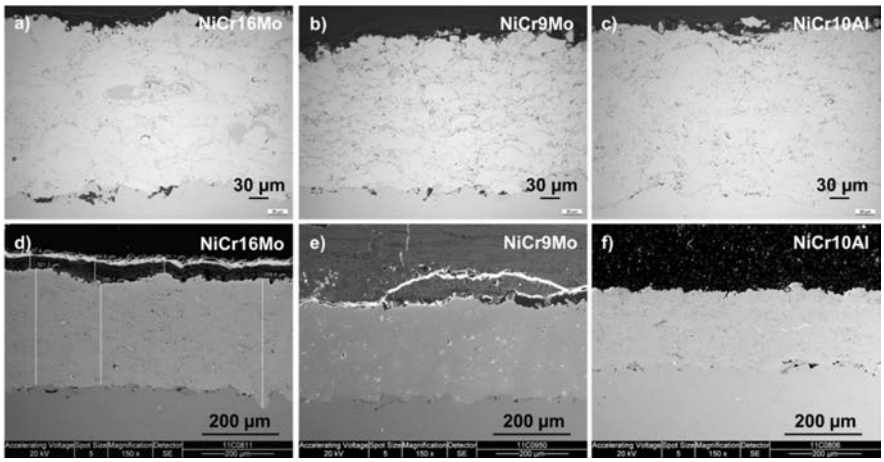

Figure 24 Optical images of the coating cross-sections before exposure: HVOF sprayed a) NiCr16Mo, b) NiCr9Mo and c) NiCr10Al. SEM images of the coating cross-sections after two-year exposure: d) NiCr16Mo, e) NiCr9Mo and f) NiCr10Al (Publication IV).

The NiCr9Mo coating exposed in the cold economizer had similar coating quality to NiCr16Mo, with a dense structure and sufficient adherence to the substrate and some closed porosity (Publication IV). The structure of the coating is presented in **Figure 24** before (b) and after (e) the exposure. The corrosion resistance of the NiCr9Mo coating was highly satisfactory. Only traces of chlorine and potassium were detected in the outer surface of the coating down to some tens of micrometres.

The NiCr10Al coating had high corrosion performance in the biomass boiler conditions in the hot economizer and protected the underlying carbon steel tube excellently (Publication IV). The coating was sufficiently dense with low porosity. The structure of the coating is presented in **Figure 24** before (c) and after (f) the exposure.

The Fe27Cr and Fe19Cr coatings were dense and well-adhered to the substrate. However, the outer surface of the coatings showed weak cohesion and detachment of lamellas. Both coatings had a lamellar structure typical of thermal spray coatings, with some porosity and non-molten particles present. Corrosion resistance of the coatings was excellent in the boiler exposure compared to the uncoated steel tubes (Publication V). Corrosion products were not detected in the Fe27Cr coating. SEM images of the coatings before and after the exposure are presented in **Figure 25**. Only some thin surface areas of the Fe19Cr coating, about 10 µm deep, contained corrosion products, such as small amounts of chlorine (0.6 wt.%) and potassium (0.4 wt.%). However, in the Fe19Cr coating some perpendicular cracks extending to the substrate material were present. This had led to some corrosion at the coating-substrate interface in these areas (**Figure 26**). Iron oxide containing sodium, sulfur, chlorine and small amounts of potassium and zinc was detected on the coating-substrate interface. The nature of the corrosion scale indicated that it had been molten during the exposure (Publication V).

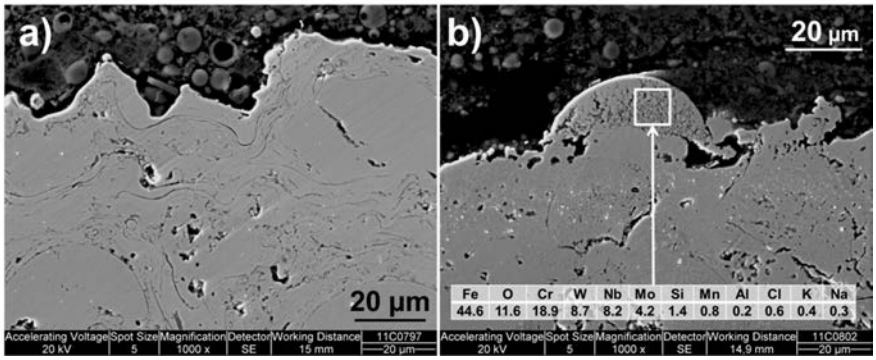

Figure 25 a) SEM image of the Fe27Cr coating after two-year biomass boiler exposure. The coating shows no signs of corrosion. b) SEM figure and EDX analysis [wt.%] of the Fe19Cr coating surface shows minor amounts of corrosion products in the outer lamella (Publication V).

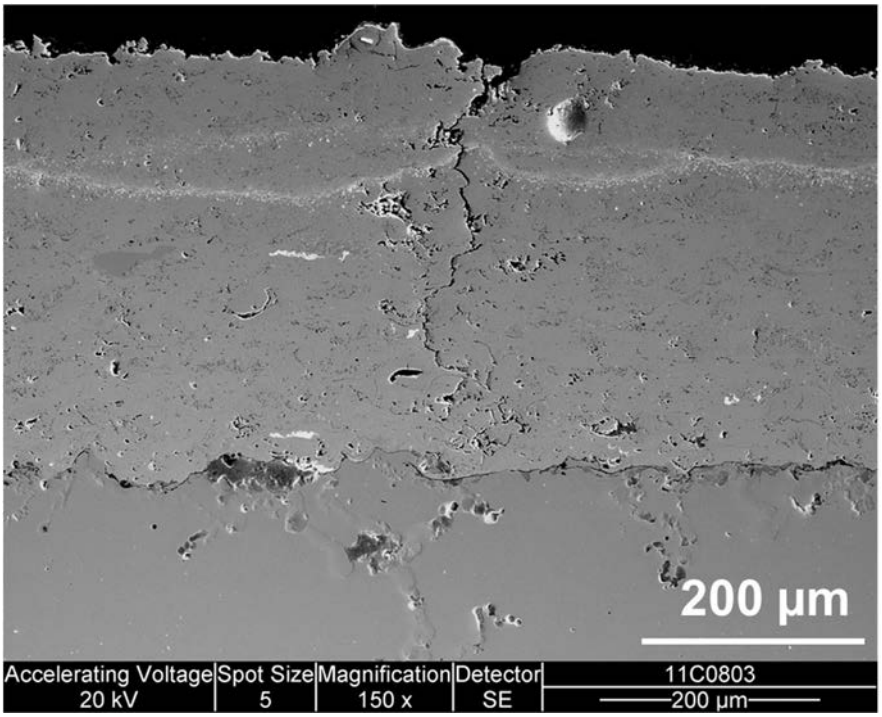

Figure 26 SEM image of the Fe19Cr coating cross-section showing the perpendicular cracking that propagated to the substrate. Corrosion products were detected in the coating-substrate interface after the two-year biomass boiler exposure due to cracks.

In comparison to the excellent high temperature corrosion performance of the coatings, severe deterioration of the uncoated carbon steel St35.8 tubes had taken place in the biomass boiler in both the cold and hot economizer. In the worst cases, several millimetres of tube wall thickness were consumed within two years, with a maximum corrosion rate of 2.3 mm/y in both the hot and cold economizer (Publication IV). An example of deep corrosion cavities formed on the steel is presented in **Figure 27** (Publication IV). Both even and pitting types of corrosion were detected on the samples. Chlorine was detected in some of the corrosion layers (Publication V).

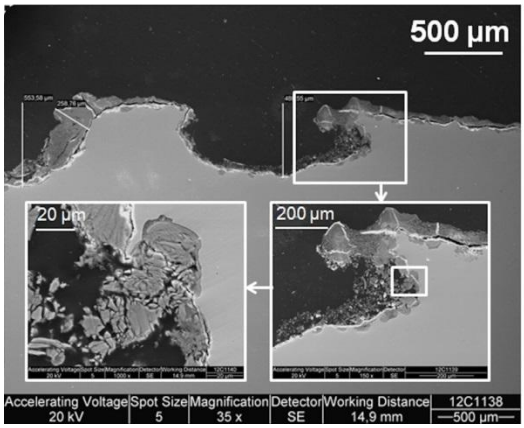

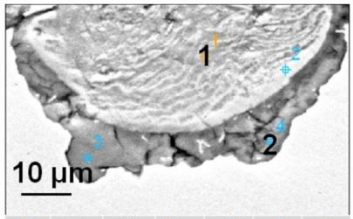

#	Fe	O	Mg	Al	Si	S
1	69.2	27.5	0.5	0.3	0.3	0.3
2	58.7	33.2	0.8	0.2	0.3	0.9
#	Cl	K	Ca	Cr	Mn	Cu
1	0.3	0.4	0.5	0.2	0.4	...
2	0.2	2.2	2.1	...	0.6	0.8

Figure 27 Deep corrosion cavities on the St35.8 tube in the cold economizer. Both chlorine and copper were detected in the oxide-metal interface in EDX analysis [wt.%].

6.4.3 High temperature corrosion performance in laboratory tests

High temperature corrosion testing was carried out in controlled laboratory conditions simulating alkali chloride – alkali sulfate molten salt attack in a biomass boiler (Publication VI). Test temperatures were 575 °C and 625 °C and test duration 168 hours. Tested HVOF coatings were NiCr, Ni21Cr, Ni22Cr and Fe19Cr, sprayed both with DJ and CJS systems. The microstructure of the coatings prior to the testing is presented in **Figure 28**.

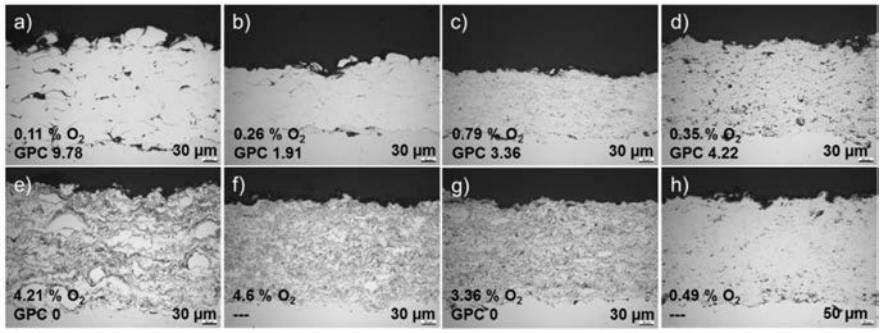

Figure 28 Optical images of the coatings before testing. (a) NiCr_CJS, (b) Ni22Cr_CJS, (c) Ni21Cr_CJS, (d) Fe19Cr_CJS, (e) NiCr_DJ, (f) Ni22Cr_DJ, (g) Ni21Cr_DJ, and (h) Fe19Cr_DJ. Oxygen content [wt.%] and viscous gas permeability coefficients (GPC) are presented in the images (f and h not measured) (Publication VI).

The coatings exhibited superior high temperature corrosion performance compared to reference steels X20 and SAN25, but nickel-based alloy A263 had the highest corrosion resistance in the tests (Publication VI). Ni21Cr_DJ and Fe19Cr_CJS showed the best high temperature corrosion performance of the coatings. Maximum corrosion layer thicknesses are presented in **Figure 29**.

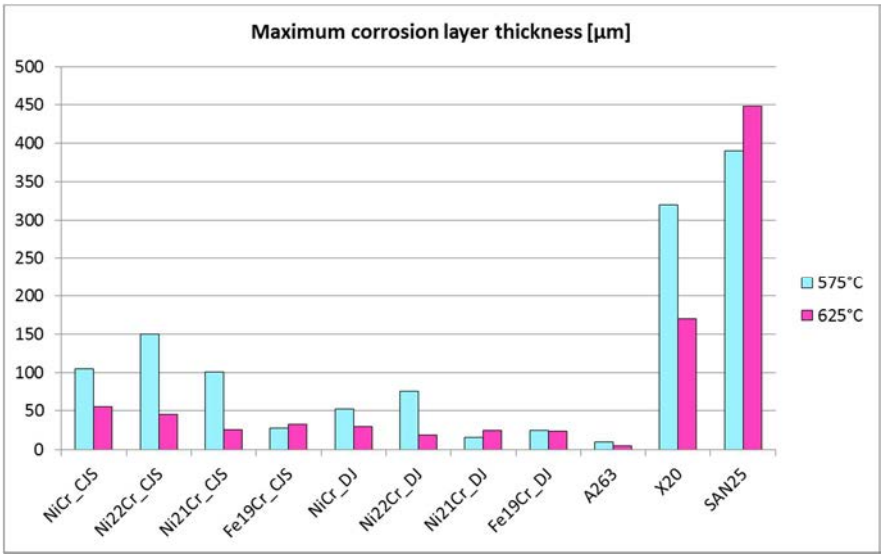

Figure 29 Maximum thickness values of the oxide/corrosion layers formed during the tests. Coatings performed better than X20 or SAN25 steels, and nickel-based alloy A263 had the best corrosion resistance. Ni21Cr_DJ and Fe19Cr_CJS had the best corrosion performance of the coatings (Publication VI).

Corrosion resistance of NiCr coatings

The NiCr coatings showed considerably better corrosion resistance than the reference iron-based tube materials (Publication VI). The maximum corrosion layer thickness was about 1/10...1/3 of the X20 or SAN25 steel. The NiCr_DJ coatings with higher density performed better. The NiCr_CJS coatings suffered from the exposure, especially at 575 °C (**Figure 30**). The better corrosion at higher temperatures may have two reasons. At higher temperatures, the growth kinetics of the protective scale is faster. The other reason is the dissociation pressure of Na_2SO_4, as it is not stabilized by some gaseous SO_2. At lower temperature, SO_3 is more stable than SO_2 and because SO_3 is more corrosive, the corrosion rate is increased. The oxide layer on NiCr_CJS consisted mainly of chromium oxide and contained a small amount of chlorine and sulfur. The layer formed on NiCr_DJ was composed of chromium oxide together with potassium, sodium and sulfur. The coating beneath the layer seemed dense. However, in the EDX analysis it was observed that chlorine had penetrated deeper into the coating (about 120 µm), and depletion of chromium from the coating was observed (**Figure 31**).

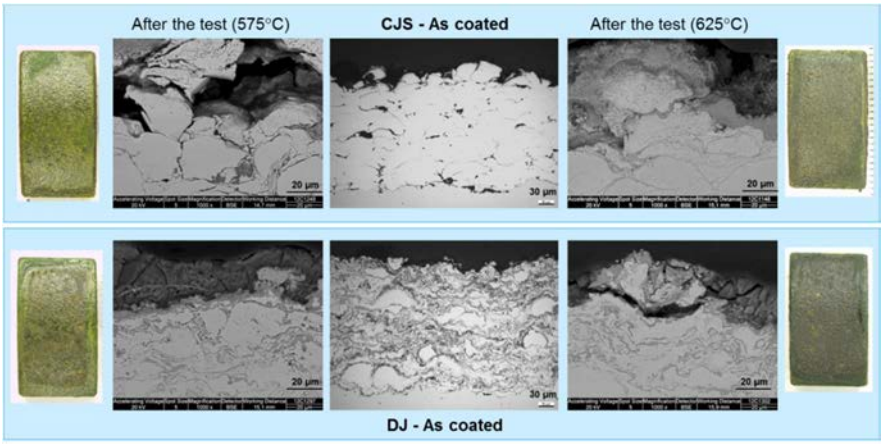

Figure 30 Performance of NiCr coating in molten salt attack in laboratory high temperature corrosion testing (168 h).

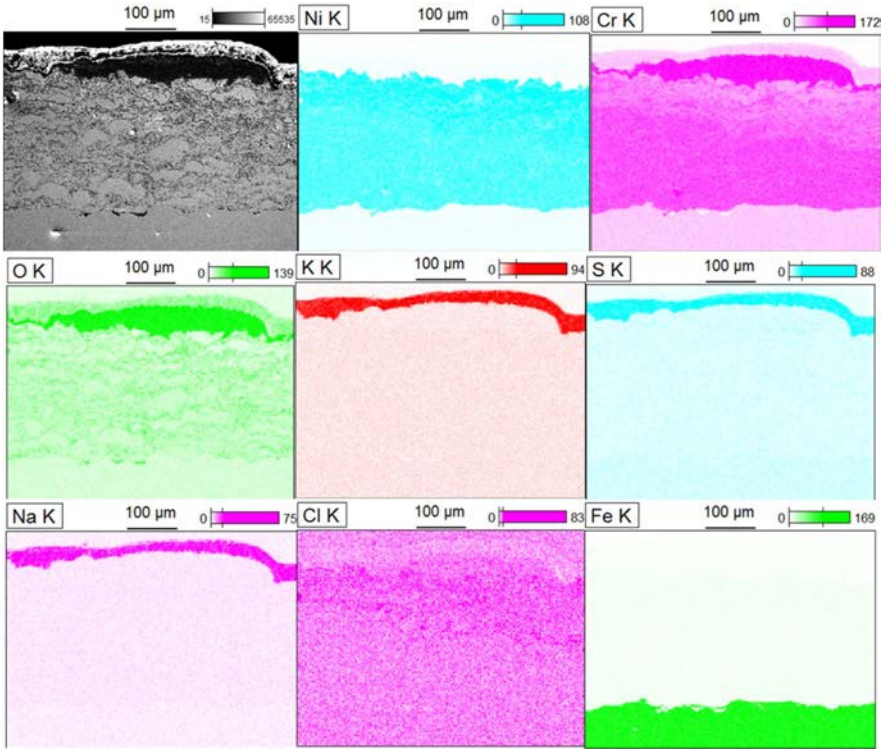

Figure 31 EDX mapping of NiCr_DJ coating after the test at 575 °C. Chromium had diffused from the coating to form oxide in the surface and chlorine had penetrated into the coating (Publication VI).

Corrosion behaviour of Ni22Cr coatings

Ni22Cr coatings showed similar corrosion resistance to NiCr coatings, and the corrosion layer thicknesses were 1/2...1/20 of the values of X20 and SAN25 (Publication VI). However, Ni22Cr_CJS had a detached, thick corrosion layer, and some detachment of the outer lamellas had occurred (**Figure 32**). The oxide layer consisted mainly of chromium and iron oxide, with a very small amount of chlorine. Ni22Cr_DJ had an oxide layer, which was Cr-rich near the coating and Fe-rich further to the layer surface. A small amount of chlorine was detected in the oxide layer, as well as at the lamellar boundary near the surface. Test temperature had a strong effect on the corrosion behaviour of the Ni22Cr_DJ coating. At lower temperature, the oxide layer was thicker and consisted mainly of iron oxide. At higher temperature, a thinner chromium oxide layer had formed. The Ni22Cr coating surface was rich in nickel and depleted of chromium. At higher temperature, only a chromium layer formed on the surface. The DJ produced higher density for the Ni22Cr coating than the CJS, but in spite of that chlorine had penetrated into the coating at lower test temperature.

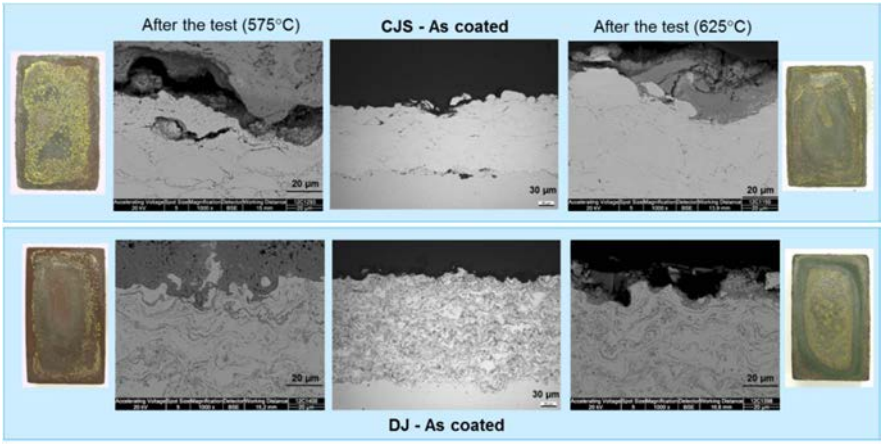

Figure 32 Performance of Ni22Cr coating in molten salt attack in laboratory high temperature corrosion testing (168 h).

Corrosion performance of Ni21Cr coatings

The corrosion behaviour of Ni21Cr coatings differed strongly depending on the spray system used, in similar way as with the NiCr and Ni22Cr coatings (Publication VI). Ni21Cr showed excellent corrosion resistance compared to the reference materials X20 and SAN25. However, with CJS the Ni21Cr coating experienced strong corrosion with an approximately 100 µm thick corrosion layer consisting mainly of iron, chromium and oxygen, with small amounts of e.g. chlorine, potassium and sulfur (**Figure 33**). Ni21Cr_DJ endured the test well with only a 15 µm thick oxide layer containing nickel, chromium, tungsten and molybdenum. Chlorine

was, however, observed in a lamellar boundary near the surface. At lower temperature, a thin oxide-containing layer of nickel, chromium, molybdenum and tungsten was formed. At higher temperature, a slightly thicker oxide layer with nickel, chromium, copper and niobium was formed on the coating. The outer surface of the coating was depleted of Ni and enriched with Mo and W. Outermost was a detached copper-rich oxide layer, as with the Ni21Cr_DJ coating. The oxide layer contained an iron-rich area further from the coating surface, and a chromium-rich area close to the coating, and the innermost oxide consisted of Ni, Cr, Fe and chlorine.

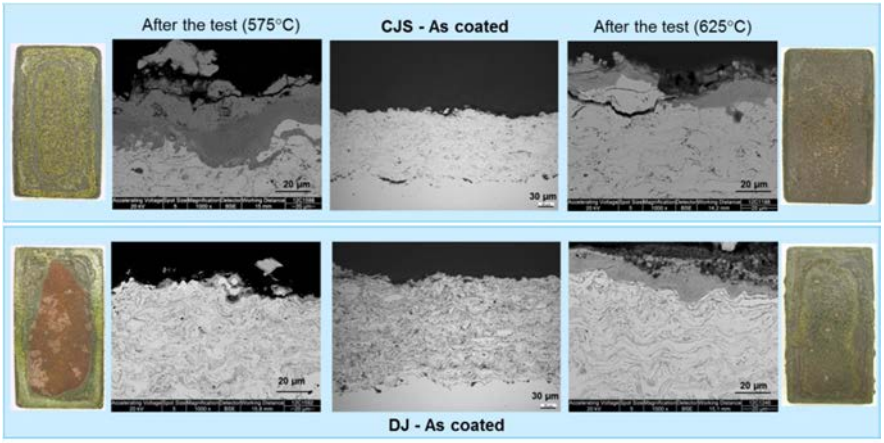

Figure 33 Performance of Ni21Cr coating in the molten salt attack in laboratory high temperature corrosion testing (168 h).

Corrosion performance of Fe19Cr coatings

The Fe19Cr_DJ and Fe19Cr_CJS coatings both performed well against corrosion attack compared to X20 and SAN25, with corrosion layer thicknesses of 1/20...1/5 of the values of the reference materials (Publication VI). The coatings were dense and had corrosion layers of about 25-30 µm and only slight detachment of the lamellas was found (**Figure 34**). The oxide layer consisted mainly of iron and chromium oxide with a small amount of sodium. The iron oxide on Fe19Cr_CJS was rich in niobium near the coating surface. Chlorine was detected only on the lamellar boundary of Fe19Cr_CJS (625°C), not in the oxide layers. At lower temperature, a small amount of chlorine was present in the oxide and on the outer surface of the coating. The Fe19Cr_DJ coating showed very good corrosion resistance at both test temperatures.

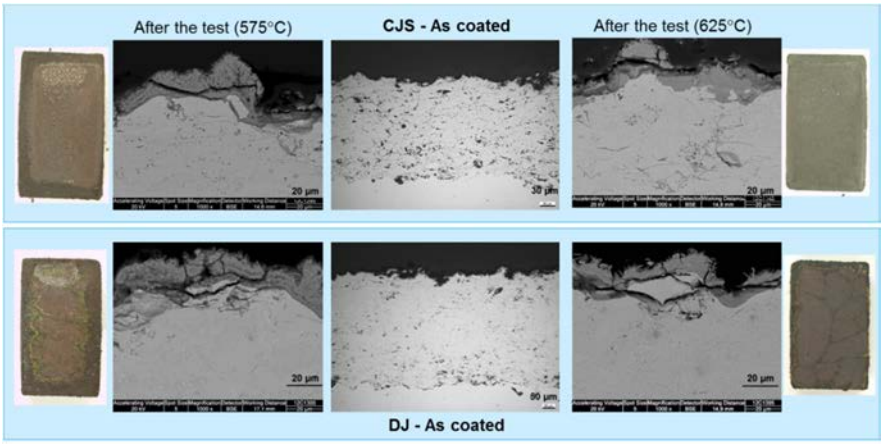

Figure 34 Performance of Fe19Cr coating in molten salt attack in laboratory high temperature corrosion testing (168 h).

Corrosion resistance of the reference materials

Corrosion resistance of the reference nickel alloy A263 proved excellent in the tests (Publication VI). The oxide layer formed at 575 °C consisted of nickel, chromium, cobalt, titanium, molybdenum, and small amounts of sulfur, potassium, and chlorine. The reference material, X20 steel, experienced severe corrosion at both test temperatures (**Figure 35**). The corrosion layers were porous and detached with multilayer oxides, mainly consisting of Fe_2O_3, with some sulfur, chlorine and potassium. A Ni-rich oxide was present at the metal surface of the X20 after both tests.

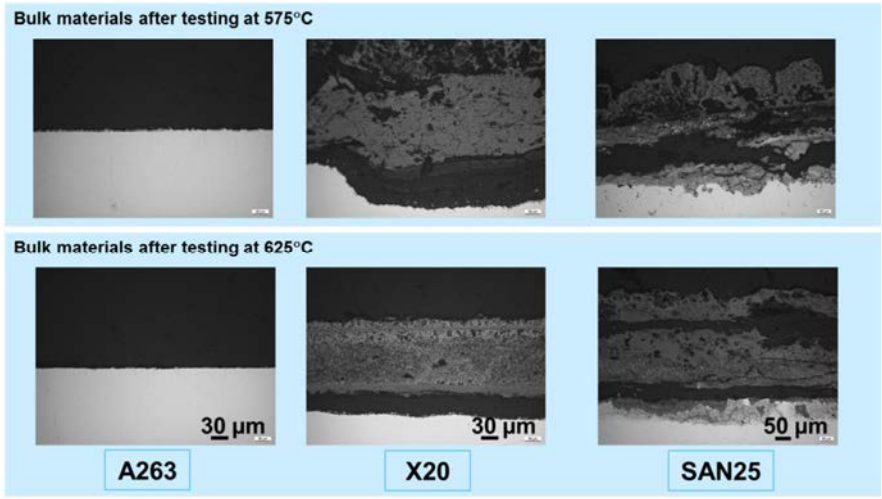

Figure 35 Corrosion performance of the reference alloys in molten salt attack laboratory testing (168 h).

Austenitic alloy SAN25 suffered extreme corrosion during the tests. The oxides were thick, detached and contained chlorine. The outermost layer consisted of iron oxide with a thin Cu-Na-O overlay. This was followed by a chromium oxide layer. The innermost layer consisted of Ni, Cu, O, and small amounts of sodium, sulfur, chlorine and potassium. Corrosion had progressed through the grain boundaries beneath the oxide layer to a depth of about 100 µm. The grain boundary attack was induced by chlorine, and the corrosion area was depleted of chromium and contained chlorine. SEM images with EDX mapping of SAN25 are presented in **Figure 36**.

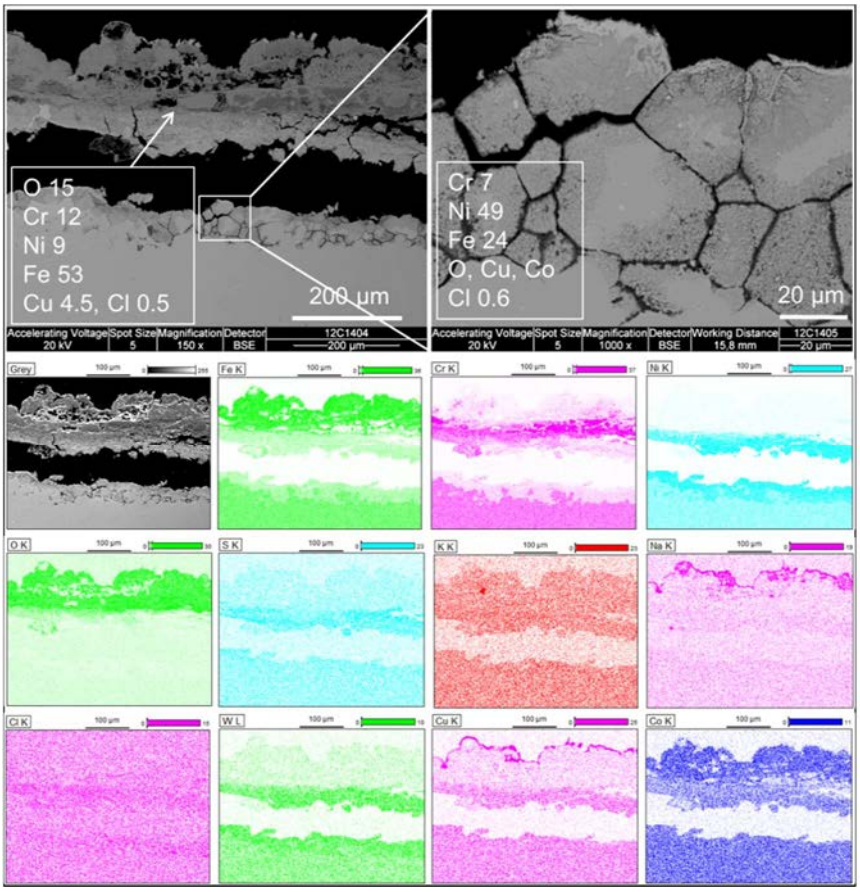

Figure 36 SEM images (BSE) of the SAN25 material after the test at 575 °C, and EDX mapping of the corrosion layer elements. Chlorine was detected in the corrosion layer and on the metal surface with intergranular corrosion (Publication VI).

6.4.4 Comparison of NiCr coating performance in corrosion tests

The high temperature laboratory testing in molten salt was very harsh and resulted in high corrosion rates, 1.56-5.48 mm/y for the selected NiCr coatings (**Table 11**) (Publication II). However, the reference ferritic and austenitic steels suffered even stronger corrosion (8.86 mm/y for X20CrMoV121 and 23.36 mm/y for Sanicro 25) (Publication II). In this short exposure (168 h), corrosion initiation is underway as opposed to actual steady-state corrosion. In the biomass boiler exposures with longer duration, the corrosion performance of the NiCr coatings in particular was excellent. The corrosion rates were between 0.01-0.50 mm/y.

Table 11 High temperature corrosion testing results for NiCr (A6-B8) and Fe19Cr (C1-D4) coatings presented as maximum corrosion rate [mm/y] (Publication II).

[mm/y]	550°C Boiler	575° C Lab	625°C Lab	750°C Boiler
A6	0.01	2.71	1.56	0.10
B7	0.01	5.48	2.87	0.04
B8	0.02	...	...	0.05
C1	0.19	1.30	1.25	0.19
D1	0.27	1.46	1.72	0.40
D4	0.19	…	…	0.50

Corrosion of the DJ sprayed NiCr occurred mainly via formation of a thick chromium oxide layer, which protected the coating from further, severe corrosion. At the higher test temperature (750 °C), the formation of pores could be detected in the outer layer of the coating. With the CJS sprayed coatings, cohesion between lamellas was insufficient and the corrosion proceeded through the lamellar boundaries and detached the outer lamellas at 575 °C in the laboratory test. However, at higher test temperature and with longer exposure the structure of the CJS sprayed coating had densified and a thin, coherent and protective chromium oxide layer had prevented further corrosion. With NiCr, the CJS spray system produced better corrosion performance at a higher test temperature compared to the DJ sprayed coating. At lower test temperature, the coating suffered from low cohesion and corrosion propagation through the lamellar boundaries. However, in boiler exposures the corrosion rate was independent of the spray system. SEM images of NiCr coatings tested in laboratory and in boiler are presented in **Figure 37**.

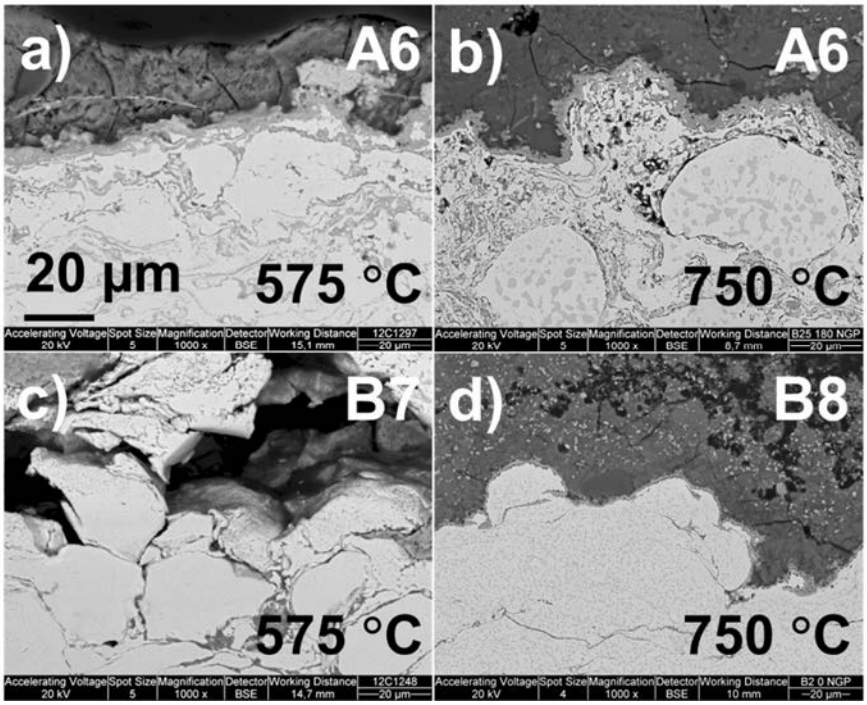

Figure 37 SEM (BSE) images of high temperature corrosion tested NiCr coatings: a) DJ sprayed coating tested in laboratory for 168 hours and b) in boiler for 5900 hours, c) CJS sprayed coating tested in laboratory for 168 h and d) in boiler for 1300 h (Publication II).

7. Discussion

The corrosion performance of the HVOF coatings exposed in actual biomass boiler conditions and in laboratory tests was analysed and evaluated against the reference bulk materials.

7.1 Corrosion performance of the HVOF coatings

The HVOF coatings were exposed to biomass combustion conditions in economizer (material temperature about 200 °C) and superheater region (550 °C and 750 °C) and molten salt attack in laboratory tests (575 °C and 625 °C). The corrosion performance, corrosion mechanisms and the ability of the coatings to offer high temperature corrosion protection are discussed in the following.

Chlorine induced corrosion was observed as main corrosion mechanism in the boiler and laboratory exposures. Chlorine was detected in small amounts in deposits of the specimens after the boiler exposures, on metal surface of the damaged tubes and in the corrosion products of some of the coatings. The amount of chlorine compared to sulfur was typically lower in the analysed specimens. Similar observations of chlorine corrosion have been reported, even though the amount of chlorine has been low (e.g. Ref 5, 7, 11). This is due to volatilization of chlorine from the corrosion products during the corrosion reactions. Sulfur may have played a role in suppressing the corrosion process by reacting with alkali metal chlorides and releasing chlorine as HCl especially at higher temperatures.

7.1.1 On-site exposure in economizer region in biomass boiler

The tested Ni- and Fe-based HVOF coatings showed very high corrosion resistance at a temperature of about 200 C° in the economizer area of the biomass boiler (Publications IV, V). Carbon steel St35.8 experienced extremely severe corrosion in the presence of chlorine and low melting phases of potassium, copper and zinc. Catastrophic corrosion rates of heat exchanger tubes have been reported, even at relatively low temperatures of 250 °C, in the presence of eutectic melts such as KCl-$ZnCl_2$ or $PbCl_2$ (Ref 40). Due to its low condensation temperature, zinc chlorine $ZnCl_2$ (144–302 °C) may have condensed on the tube surfaces in the upper part of the cold economizer (Ref 97), leading to severe corrosion and further to leakage of the St35.8 boiler tube. Iron and its oxides have been reported to be

completely unable to withstand chlorine (HCl) attack in test conditions starting from 400 °C, whereas both chromium and nickel can resist corrosion against chlorine (Ref 98). Strong corrosion of carbon steel compared to the coating materials can be explained also by the higher solubility of iron chloride in the $ZnCl_2$-KCl melt compared to nickel chloride and chromium (III) chlorine (Ref 99). According to thermodynamic stability calculations, iron forms a liquid phase with chlorine at 310 °C, whereas reactions with chromium produce solid reaction products (**Figure 38**a). Copper and zinc can form liquid phases at 430 °C and 320 °C, respectively (**Figure 38**b). It has been shown that with sufficient oxygen partial pressures chromium can form a protective oxide layer on the coating surface, which prevents reaction with chlorine and, hence, detrimental active oxidation (Ref 13). Molybdenum is also known to act favourably for corrosion resistance in oxidizing–chloridizing environments by reacting slowly and behaving rather inertly (Ref 82). The severe corrosion of carbon steel St35.8 compared to the excellent performance of HVOF Ni- and Fe-based coatings with high chromium content are in line with these findings.

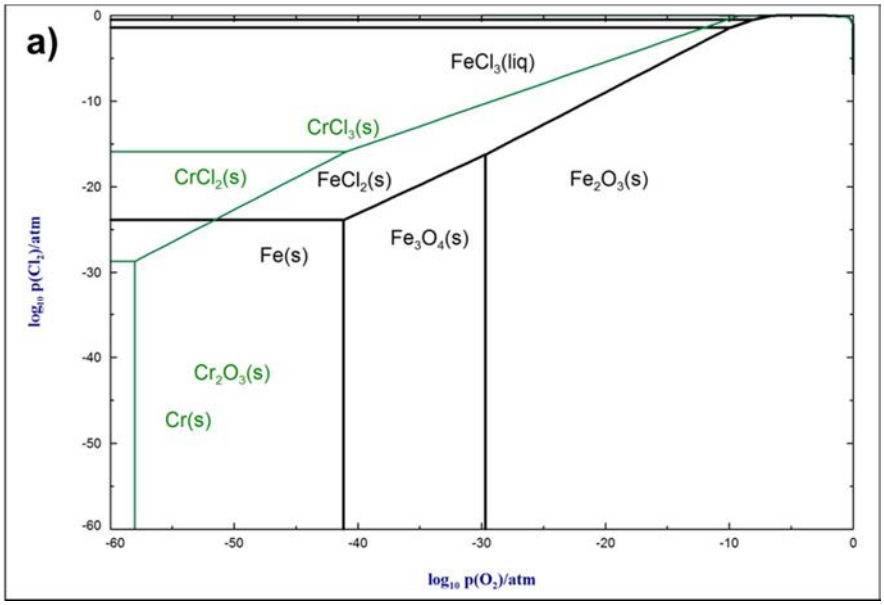

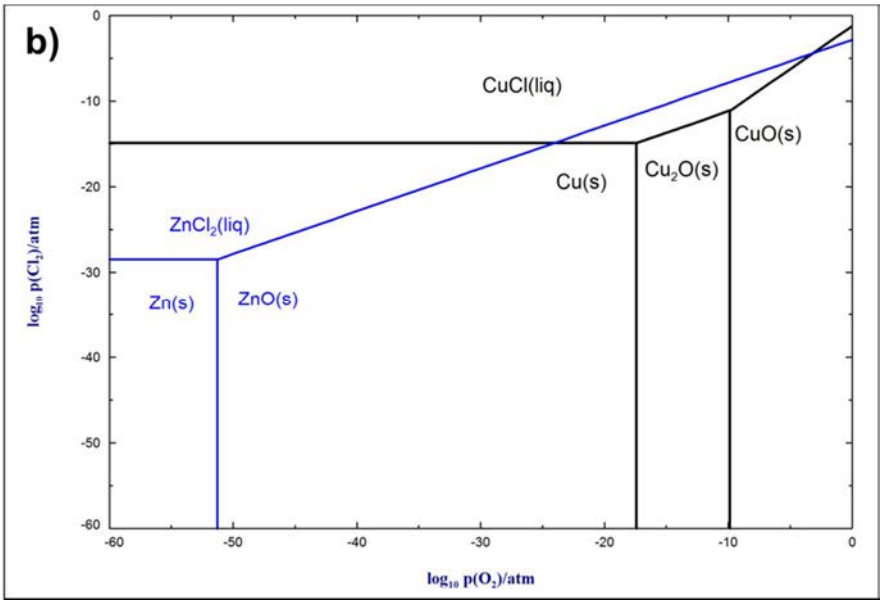

Figure 38 a) Thermodynamic stability of iron and chromium at 310 °C in the presence of chlorine and oxygen. b) Phase diagram of Cu-Cl_2-O_2 and Zn-Cl_2-O_2 systems at 430 °C and at 320 °C, respectively. (Publication VI).

7.1.2 On-site testing in the superheater region of biomass boiler

NiCr coatings showed high corrosion resistance in the boiler testing in the superheater area, which is due to the formation of a protective chromium oxide layer on the surface of the NiCr coatings during exposure. Contrary to the high performance of the coatings, chlorine-induced corrosion was detected in the ferritic steel T92 and resulted in a corrosion rate of 0.9 mm/y at 550 °C. Typically, Fe-Cr steels have high corrosion rates in conditions containing chlorine, and especially in molten chlorides due to fluxing (dissolution) and destruction of the oxide (Ref 15). As the formation of a protective oxide layer is not possible in the present conditions, the corrosion rate is increased. Ni-base alloys are expected to resist chloride attack because the vapour pressure of $NiCl_2$ is much lower than that of Fe and Cr chlorides at the same Cl activity and gas temperature (Ref 100). Instead, internal grain boundary attack (about 10 µm thick) caused by sulfidation was detected on the A263 material at 750 °C exposure. According to the thermodynamic calculation (FactSage 6.4), chromium oxide is expected to form even at very low vapour pressure of oxygen both at 550 °C and 750 °C (**Figure 39**).

The Fe19Cr coating showed sufficient corrosion protection, although chlorine reactions and zinc compounds enhanced the corrosion compared to the NiCr coatings. Niobium alloying may have been beneficial for the FeCr coating corrosion resistance, as niobium did not react during exposure and was enriched in the coating surface below the oxide scales (Ref 82).

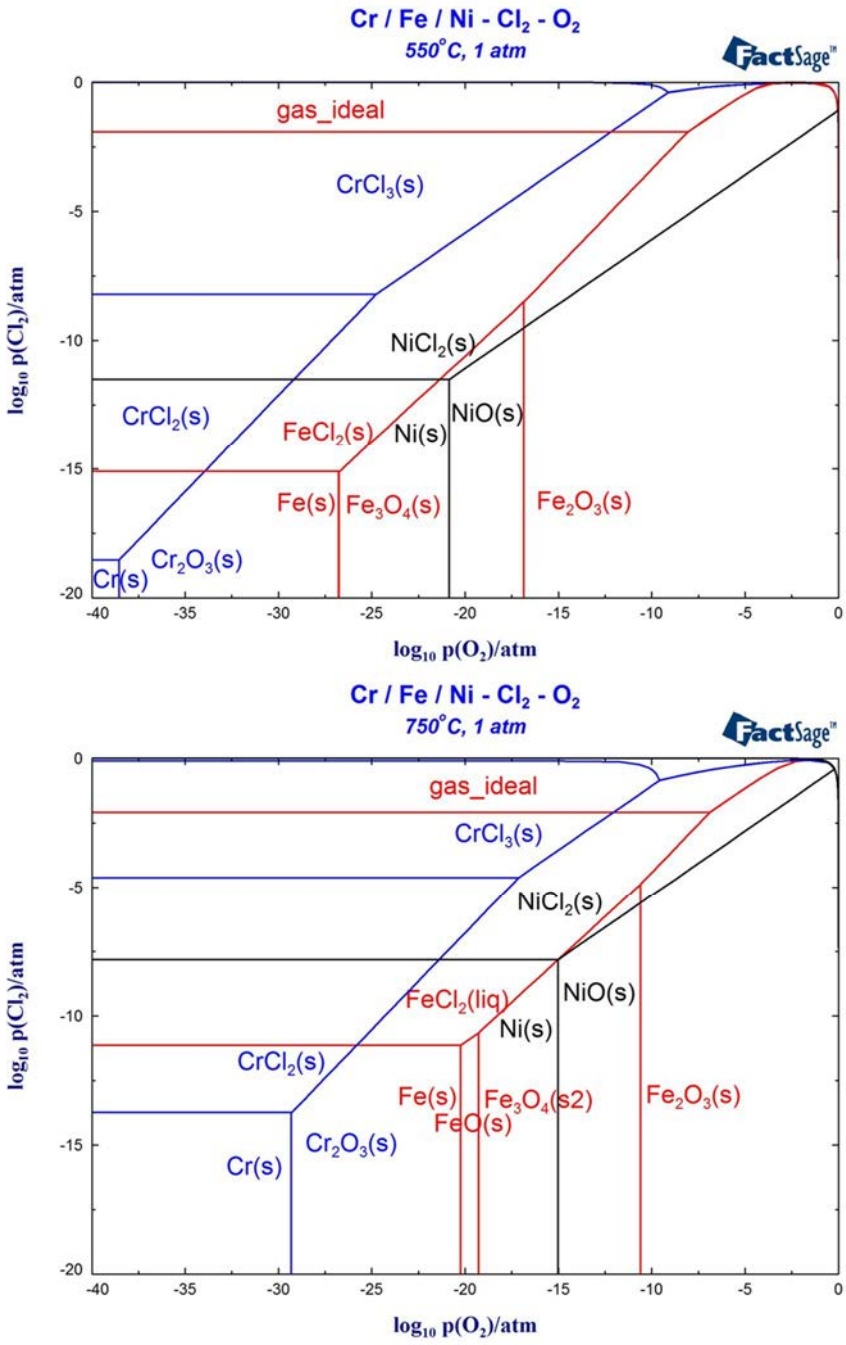

Figure 39 Thermodynamic calculation for Fe, Cr, Ni, O and Cl at a) 550 °C and b) 750 °C. (Publication III)

The Ni22Cr coating failed completely at 750 °C despite its dense structure. Chromium had diffused from the coating to form chromium oxide and was depleted in the nickel matrix. Segregated areas with high molybdenum content were detected. Due to the enhanced corrosion rate, the amount of chromium was not high enough to protect the material. IN625 weld overlay has been reported to suffer from pitting and selective dendritic corrosion due to chlorides and sulfates together with heavy metals in biomass and waste incineration plants (Ref 39); corrosion was also claimed to occur in sites where potassium chloride was condensed. Those results are in line with Montgomery et al. (Ref 101), who reported IN625, which has a similar composition to Ni22Cr, to form a galvanic pair within the material due to difference in molybdenum content between the core and the interdendritic zone.

7.1.3 Effect of molten salt attack on corrosion resistance

The purpose of the accelerated laboratory corrosion test was in particular to screen the corrosion resistance of the thermal spray coatings in comparison to bulk materials under molten salt attack in oxidizing conditions. Typically, HCl and SO_2 are present in the gas phase in actual boiler conditions. Consequently, the laboratory conditions do not fully represent real conditions, but allow comparison of the materials in these conditions. The exposure time (168 h) is too short to make reliable lifetime estimation of the corrosion resistance in biomass boiler exposure. However, as the test was very harsh, distinct differences in the corrosion behaviour of the materials were detected.

Ni22Cr coating sprayed with the CJS system showed signs of chlorine-induced active oxidation, which was enhanced by interconnected porosity. The lamellar boundaries acted as easy paths for chlorine penetration through the coating. Below the scale, chromium was selectively attacked by chlorine, which has been reported to increase the corrosion rate significantly above 520 °C (Ref 16). Iron was detected in the coating, which indicates formation of volatile iron chlorides at the coating/substrate interface (Ref 55). With high-alloy steels, mainly $FeCl_2$ is formed due to its higher thermodynamic stability compared to $NiCl_2$, $CoCl_2$ and $CrCl_2$ (Ref 11). At the higher test temperature of 625 °C the corrosion mechanism of Ni22Cr indicated the reaction of chromia with the melt.

The most important factors regarding the corrosion resistance of alloys against molten salt corrosion proved to be suitable alloying and an optimized dense coating structure (Publication VI). The corrosion protection of any alloy against salt melt attack depends on the chemical stability of both the kinds of metal and their compounds, such as oxides and chlorides (Ref 84). Chromium has been found to be the most beneficial alloying component against corrosion in atmospheres containing chlorine (Ref 102, 103). According to results of the present studies, even though chromia has high solubility in NaCl-KCl melts (Ref 14), a sufficient amount of chromium (i.e. more than 22 wt.%) was required to form a protective chromium oxide layer on the surface to achieve high corrosion resistance. Advantageous alloying elements against molten chloride salt corrosion in the Ni21Cr and Fe19Cr coating materials were both molybdenum and niobium. The free energy of $MoCl_2$ /

$NbCl_2$ formation is considerably less negative than that for $FeCl_2$ and $CrCl_2$ (Ref 29, 82). Silicon and aluminium have been observed to increase the high temperature corrosion resistance of Fe-Cr and Ni-Al alloys (Ref 82), and these were found in the oxides of the well-performing Fe19Cr coating.

The reference material, high-alloy steel SAN25, failed in the molten salt phase attack laboratory testing (Publication VI). The material was not tested in boiler conditions in the present study, so its performance in real conditions is not known. A probable cause for the catastrophic corrosion of SAN was the reaction of the Cr_2O_3 with the melt, leading to depletion of chromium in the alloy and formation of nickel-rich spinels and nickel oxides (Ref 15). Because NiO scale is highly porous, volatile salts diffused into the scale/melt interface and condensed as solid or molten phases, and the corrosive attack continued. Presence of copper compounds has been reported to increase corrosion rate significantly (the Deacon reaction) (Ref 17, 33). Therefore, copper alloying can be detrimental in chlorine-containing atmospheres (Publication VI). SAN25 is designed for ultra-supercritical coal-fired boilers (Ref 104) in which the molten salt conditions that cause catastrophic corrosion are not likely to occur. However, SAN25 cannot be recommended for severe conditions with any risk of molten phase attack by chlorine.

7.2 Process optimization and effect of coating structure

Because a dense and homogenous structure is essential for HVOF coatings against corrosion, special attention was paid to the optimization of spray parameters. When such a coating structure is achieved, the need for post-treatments such as laser re-melting as well as unwanted coating breakdown during usage can be avoided (Ref 81, 105). Diagnostic tools were applied to monitor the HVOF coating process in order to detect the influence of process conditions on coating properties and high temperature corrosion performance. The process optimization was performed in particular for the NiCr coatings, which were sprayed with CJS (HVOFLF) and DJ (HVOFGF) systems. In general, both the DJ and CJS spray systems can produce dense coatings with good adhesion to the substrate due to the high velocities of the sprayed particles.

Coatings sprayed by the CJS system showed a distinct lamellar structure and low oxygen content. However, with the applied process parameters lamellar cohesion was not sufficient close to the coating surface, resulting in the lamellar boundaries acting as corrosion paths. Nevertheless, the peening effect clearly promoted a denser structure in the inner layers of the coating and corrosion did not proceed into the substrate in neither laboratory nor boiler testing. The lack of cohesion may have resulted from insufficient splat deformation (Ref 60, 106). As the particle temperature increases, spray particles become more ductile and more prone to oxidation. Splats are strongly deformed at higher particle temperature, which generally causes less coating porosity. If particle velocities are not high enough, cavities are not filled and fully dense coatings are not attained from cold, hard spray particles. Thus, fully dense coatings require both sufficient particle

velocity and particle ductility. Particle melting state and oxidation is affected by the dwell time, heat transfer and interactions of the particles in the upstream (with the flame chemistry) and downstream (with the ambient air) (Ref 76). The oxidation levels and intersplat/interpass bonding between the splats have influence on the coating performance (Ref 65). The currently available CJS spray gun can generate much higher velocities than detected in the study by Hanson et al. (Ref 106), with particle velocities up to 550 m/s, so high density can be achieved. However, the low particle temperature may have a negative influence on the cohesive strength of the coating, and despite the low oxygen content the coating may not provide maximal corrosion resistance (Ref 107, 108).

Compared to the CJS sprayed coatings, DJ sprayed coatings exhibited a higher melting state, flatter lamellar structure and stronger oxidation. With both systems, gas-tight coatings were attained according to the viscous gas permeability measurement. High compressive residual stresses were formed in the CJS sprayed coatings, whereas both compressive and tensile stresses were formed in DJ sprayed coatings, and at lower total flow (< 700 l/min) these coatings were fully under tensile stress. With higher propane and total flow of the fuels, compressive stresses were formed for also in DJ sprayed coatings due to higher particle velocities, which induced a strong peening effect in the coatings.

The microstructure of the coatings was in good correlation with the measured T-v values, especially with the DJ system. The measured temperature and velocity values could be attributed to the lamellar structure (flatness, individual round semi-molten particles) and oxidation of lamellar boundaries (dark areas) in the micrographs. The oxygen content measurement confirmed the visual result. With the DJ system, the oxygen content of the coatings increased with decreasing F/O ratio due to more oxidizing spray conditions. The results on oxygen content corresponded well with the results by Valarezo et al. (Ref 76), who presented the correlation between F/O ratio and oxygen content in the coating.

Selected coatings were tested in high temperature corrosion tests in actual power plant boilers as well as in controlled laboratory conditions. The selection of candidate coatings for high temperature corrosion testing was based on the following specific coating properties: low porosity, high adhesion and compressive stress state in addition to mechanical properties. Different oxygen contents were also chosen, DJ sprayed coatings representing a higher and CJS sprayed coatings a lower amount of oxygen. The test matrix also included materials other than optimized variations of NiCr and FeCr coatings and therefore there was a limited possibility for testing of these coatings. NiCr coating sprayed with A6 parameters had high density (zero through-porosity according to the gas permeability test), high adhesion and compressive residual stresses, but also high oxygen content. The CJS sprayed B8 coating with low viscous gas permeability coefficient and high compressive residual stresses was selected to compare the effect of oxygen content on corrosion resistance compared to the DJ sprayed coating. In order to compare the DJ and CJS spray systems with the FeCr coating, the DJ sprayed C1 coating with dense structure and the CJS sprayed D4 coating, which showed zero

in the gas permeability test, high elastic modulus, and compressive residual stresses, were selected for the tests.

Due to the limited number of tests, no detailed conclusions regarding the association between process parameters and coating structure, coating properties and high temperature corrosion performance could be made (Publication II). Nevertheless, the selected specimens showed excellent corrosion performance in the tests. In general, the DJ spray system resulted in better corrosion performance of the coatings compared to CJS sprayed coating. With the CJS spray system the coatings suffered from inadequate lamellar cohesion and related corrosion propagation through lamellar boundaries. This was especially the case in molten salt exposure. In the boiler exposures, the corrosion rate was somewhat independent of the spray system.

Interconnected porosity and oxides in the splat boundaries have been reported to be detrimental to the corrosion resistance of coatings because corrosive elements, such as gases or molten salt, can percolate through the coating and attack the splat boundaries (Ref 80). Conversely, Sidhu et al. (Ref 90) have claimed that the formation of oxides along the splat boundaries may have a positive influence on corrosion resistance as the oxides may act as a diffusion barrier to the inward diffusion of corrosive species. Because low porosity is critical for corrosion resistance, sufficient particle oxidation during the spray process may be required for high corrosion resistance (Ref 80, 103, 107). However, due to high particle velocities, CJS spray can produce coatings with zero through-porosity according to the gas permeability measurement (coating parameters B4). These coatings should be tested in future with close examination of the potential beneficial or detrimental effects of oxides in the lamellar boundaries on corrosion resistance.

The diagnostic tools used enabled monitoring of the spray process and linking of some of the coating characteristics and properties with the process parameters. However, as previously stated, it was detected that temperature and velocity measurement alone do not indicate the melting state of the particles and impinging of the particles on the substrate material and, hence, the deposit build-up process (Ref 75, 109, 110). The structure and quality of the coating, such as residual stress formation, adhesion, cohesion, density, interconnecting porosity, and amorphous phases, can be influenced by optimization of the thermal spray process parameters. Coating structure plays a crucial role in determining the corrosion resistance of thermal spray coatings by preventing the transport of corrosive elements towards the substrate (Publication V).

8. Summary and conclusions

This study reported for the first time results of HVOF coating spray process optimization and testing in economizer (about 200 °C) and superheater (550 °C and 750 °C) regions in actual biomass power plant conditions. It was shown that several nickel- and iron-based HVOF thermal spray coatings with high chromium content exhibited sufficient or excellent corrosion performance in biomass boiler exposures. The corrosion rates were much lower compared to typically applied boiler tube materials (Ref 5, 6, 21). The coatings also exhibited high corrosion resistance in simulated biomass boiler conditions in laboratory tests. On the basis of the results presented in this thesis and attached publications, the following specific conclusions on the corrosion performance of the coatings can be drawn:

- NiCr16Mo, NiCr9Mo, NiCr10Al and Fe27Cr HVOF sprayed coatings showed excellent corrosion resistance in the economizer of a power plant firing wood-based biomass due to sufficient alloying against corrosion and dense structure. In comparison, St35.8 carbon steel tubes experienced severe corrosion in the circulating fluidized bed. Several millimetres of tube wall thickness were corroded within two years. Corrosion mechanism of St35.8 carbon steel was chlorine-induced corrosion with influence of low melting phases of potassium, copper, zinc and lead.
- NiCr coatings had high corrosion resistance in biomass boiler conditions in the superheater area. Best corrosion performance in actual biomass boiler exposure at 750 °C was shown by NiCr coating sprayed with CJS, the HVOFLF system, due to formation of a very thin protective chromium oxide layer on the coating surface.
- Ni22Cr exhibited high corrosion resistance at 550 °C in the biomass boiler exposure but failed completely at 750 °C despite the dense structure. In laboratory conditions, corrosion mechanisms of Ni22Cr coating under molten salt attack included chlorine-induced active oxidation at 575 °C and reaction of chromia (Cr_2O_3) with the melt at 625 °C. Ni22Cr cannot be recommended for biomass combustion above 700 °C if there is a risk of chlorine or molten salt attack. The results confirm that thorough testing in relevant conditions prior to application in actual conditions is essential.

Process-structure-properties-performance methodology together with diagnostic tools and careful characterization of the coatings were applied for optimization of the coating structure. Two HVOF spray systems (gas-fuelled DJ and liquid-fuelled CJS) were used for coating to study the influence of different coating structures on high temperature corrosion resistance. Based on this comparison, the following distinct conclusions can be drawn:

- High quality NiCr coatings with dense coating structure can be produced both by high total fuel flow DJ spray and high kerosene flow CJS spray. In general, DJ sprayed coatings showed better corrosion performance compared to CJS sprayed coatings. With the CJS spray system the coatings suffered from inadequate lamellar cohesion and related corrosion propagation through lamellar boundaries. This was most markedly evident in molten salt exposure.
- NiCr coatings with low oxygen content can be produced with CJS spraying. Lamellar cohesion is important in high temperature corrosion environments and hence sufficient melting state and oxidation level of powder particles together with high kinetic energy are required for formation of a dense coating structure.
- Dense structure is essential to the corrosion resistance of thermal spray coatings in order to prevent the transport of corrosive elements towards the substrate. Structure and quality of the coating, such as adhesion, cohesion and porosity can be influenced by optimization of TS process parameters.
- DJ sprayed Fe19Cr suffered perpendicular cracking. With CJS, cracking was avoided due to higher kinetic energy and lower thermal energy, which resulted in compressive residual stresses in the coating.

In conclusion, HVOF thermal spray coatings can be recommended for corrosion protection and, hence, for increasing the lifetime of carbon steel or low-alloy steel substrates in biomass-fired boilers where chlorine and low melting compounds can cause severe corrosion. Particularly at the higher temperatures, sulfur may play a more important role than chlorine due to Type II hot corrosion mechanism. Therefore it is important to analyse the corrosion conditions properly, as some elements are beneficial for chlorine, but harmful for sulfur induced corrosion effects. The key challenges are thus correct material selection for specific conditions and application of the coatings at large scale with high coating quality. Careful attention should be paid to joint areas of coated and uncoated tubes.

In future, an extensive corrosion testing matrix should be included in order to establish clear relations between process parameters, coating structure, coating properties and corrosion performance. Due to the limited number of tests, no systematic relations could be derived in the present work. However, some qualitative correlations were drawn. Process diagnostics can be used to monitor, in particular, stress formation in the coatings and for quality assurance during the spraying process. To exploit their full benefits, diagnostic tools should be applied systematically in thermal spray coating together with careful characterization and testing.

References

1. http://ec.europa.eu/clima/policies/brief/eu/index_en.htm (Accessed 9.10.2014)

2. Döing, M., Siebertz, M., Loenicker, J., Schneider, K., Küpper, L., Ersoy, S.R. and Shi, W., Biomass to energy. The world market for biomass power plants 2012/2013. EcoProg GmbH, Cologne, October 2012. 770 p.

3. European waste to energy plant market – Stricter waste management legislation is diverting waste from landfills to waste to energy plants. M8EE-15 March 2013. Frost & Sullivan.

4. Baxter, L., Biomass-coal co-combustion: Opportunity for affordable renewable energy, Fuel 84 (2005) 1295–1302.

5. Nielsen, H.P., Frandsen, F.J., Dam-Johansen, K. and Baxter, L.L., The implications of chlorine-associated corrosion on the operation of biomass-fired boilers. Progress in Energy and Combustion Science 26 (2000) 283–298

6. Frandsen, F.J., Utilizing biomass and waste for power production—a decade of contributing to the understanding, interpretation and analysis of deposits and corrosion products. Fuel 84 (2005) 1277–1294.

7. Persson, K., Broström, M., Carlsson, J., Nordin, A. and Backman, R., High temperature corrosion in a 65 MW waste to energy plant. Fuel Processing Technology 88 (2007) 1178–1182.

8. Montgomery, M., Vilhelmsen, T. and Jensen, S.A., Potential high temperature corrosion problems due to co-firing of biomass and fossil fuels. Materials and Corrosion 59 (2008) 783–793.

9. Otsuka, N., Chemistry and melting characteristics of fireside deposits taken from boiler tubes in waste incinerators. Corrosion Science 53 (2011) 2269–2276.

10. Schofield, M.J., Corrosion, in Plant Engineer's Reference Book, 2nd Edition, D.A. Snow, Elsevier, 2002, 9 p.

11. Grabke, H.J., Reese, E. and Spiegel, M., The effect of chlorides, hydrogen chloride and sulphur dioxide in the oxidation of steels below deposits. Corrosion Science 37 (1995) 1023–1043.

12. Zahs, A., Spiegel, M. and Grabke, H.J., Chloridation and oxidation of iron, chromium, nickel and their alloys in chloridizing and oxidizing atmospheres at 400–700°C. Corrosion Science 42 (2000) 1093–1122.

13. Nielsen, H.P., Frandsen, F.J. and Dam-Johansen, K., Lab-scale investigations of high-temperature corrosion phenomena in straw-fired boilers. Energy & Fuels 13 (1999) 1114–1121.

14. Ishitsuka, T. and Nose, K., Stability of protective oxide films in waste incineration environment—solubility measurements of oxides in molten chlorides. Corrosion Science 44(2) (2002) 247–263.

15. Spiegel, M., Salt melt induced corrosion of metallic materials in waste incineration plants. Materials and Corrosion 50 (1999) 373–393.

16. Michelsen, H.P., Frandsen, F., Dam-Johansen, K. and Larsen, O.H., Deposition and high temperature corrosion in a 10 MW straw fired boiler. Fuel Processing Technology 54 (1998) 95–108.

17. Nakagawa, K. and Matsunaga, Y., The effect of chemical composition of ash deposit on the corrosion of boiler tubes in waste incinerators. Materials Science Forum 251-254 (1997) 535–542.

18. Åmand, L.-E., Leckner, B., Eskilsson, D. and Tullin, C., Deposits on heat transfer tubes during co-combustion of biofuels and sewage sludge. Fuel 85 (2006) 1313–1322.

19. Vainikka, P., Bankiewicz, D., Frantsi, A., Silvennoinen, J., Hannula, J., Yrjas, P. and Hupa, M., High temperature corrosion of boiler waterwalls induced by chlorides and bromides. Part 1: Occurrence of the corrosive ash forming elements in a fluidised bed boiler co-firing solid recovered fuel. Fuel 90 (2011) 2055–2063.

20. Enestam, S., Bankiewicz, D., Tuiremo, J., Mäkelä, K., Hupa, M., Are NaCl and KCl equally corrosive on superheater materials of steam boilers?, Fuel 104 (2013) 294–306.

21. Henderson, P., Szakálos, P., Pettersson, R. and Andersson, C. and Högberg, J., Reducing superheater corrosion in wood-fired boilers. Materials and Corrosion 57 (2006) 128–134.

22. Aho, M., Yrjas, P., Taipale, R., Hupa, M. and Silvennoinen, J., Reduction of superheater corrosion by co-firing risky biomass with sewage sludge. Fuel 89 (2010) 2376–2386.

23. Hupa, M., Ash-related issues in fluidized-bed combustion of biomasses: Recent research highlights. Energy Fuels 26 (2012) 4–14.

24. Sandberg, J., Karlsson, C. and Bel Fdhila, R., A 7 year long measurement period investigating the correlation of corrosion, deposit and fuel in a bi-

omass fired circulated fluidized bed boiler. Applied Energy 88 (2011) 99–110.

25. van Lith, S.C., Frandsen, F.J., Montgomery, M., Vilhelmsen, T. and Jensen, S.A., Lab-scale investigation of deposit-induced chlorine corrosion of superheater materials under simulated biomass-firing conditions. Part 1: Exposure at 560 °C. Energy Fuels 23 (2009) 3457–3468.

26. Chandra, K., Kain V. and Dey, G.K., Failure of 2.25Cr–1Mo steel superheater tubes in a fluidized bed combustor due to fireside corrosion. Materials Characterization 62 (2011) 62–69.

27. Enestam, S., Boman, C., Niemi, J., Boström, D., Backman, B., Mäkelä, K. and M. Hupa, M., Occurrence of zinc and lead in aerosols and deposits in the fluidized-bed combustion of recovered waste wood. Part 1: Samples from boilers. Energy Fuels 25 (2011) 1396–1404.

28. Antunes R.A. and Lopes de Oliveira, M.C., Corrosion in biomass combustion: A materials selection analysis and its interaction with corrosion mechanisms and mitigation strategies. Corrosion Science 76 (2013) 6–26.

29. Kawahara, Y., High temperature corrosion mechanisms and effect of alloying elements for materials used in waste incineration environment. Corrosion Science 44 (2002) 223–245.

30. Grabke, H.J., Proceedings of the International Conference on Fireside problems while incinerating municipal and industrial waste, 8-12.10.1989, FL, USA, 1989, 161–176.

31. Bramhoff, D., Grabke, H.J., Reese, E. and Schmidt , H.P., Einfluss von HCl und Cl_2 auf die Hochtemperaturkorrosion des 2 1/4Cr1Mo-Stahls in Atmosphären mit hohen Sauerstoffdrücken. Werkstoffe und Korrosion 41 (1990) 303–310. (in German)

32. Salonen, J. and Heikinheimo, L., Korkean hyötysuhteen höyryvoimalaitoksen materiaalit, VTT tutkimusraportti BTUO74031180, Espoo 2003. (in Finnish)

33. Galetz, M.C., Bauer, J.T., Schütze, M., Noguchi, M., Takato, C. and Cho, H., The influence of copper in ash deposits on the corrosion of boiler tube alloys for waste-to-energy plants. Materials and Corrosion 63 (2012) 1–8.

34. Lind, T., Kauppinen, E. Hokkinen, J., Jokiniemi, J.K., Orjala, M., Aurela, M. and Hillamo, R., Effect of chlorine and sulfur on fine particle formation in pilot-scale CFBC of biomass. Energy & Fuels 20 (2006) 61–68.

35. Hansen, L.A., Nielsen, H.P., Frandsen, F.J., Dam-Johansen, K., Hørlyck, S. and Karlsson. A., Influence of deposit formation on corrosion at a straw-fired boiler. Fuel Processing Technology 64 (2000) 189–209.

36. Sippula, O., Lind, T. and Jokiniemi, J., Effects of chlorine and sulphur on particle formation in wood combustion performed in a laboratory scale reactor. Fuel 87 (2008) 2425–2436.

37. Liu, K., Xie, W., LI, D., Pan, W.P., Riley, J.T. and Riga, A., The effect of chlorine and sulfur on the composition of ash deposits in a fluidized bed combustion system. Energy & Fuels 14 (2000) 963–972

38. Otsuka, N., A thermodynamic approach on vapor-condensation of corrosive salts from flue gas on boiler tubes in waste incinerators. Corrosion Science 50 (2008) 1627–1636.

39. Montgomery, M., Biede, O. and Larsen, O.H., Experiences with Inconel 625 in biomass and waste incineration plants. Materials Science Forum 522-523 (2006) 523–530.

40. Spiegel, M., Zahs, A. and Grabke, H.J., Fundamental aspects of chlorine induced corrosion in power plants. Materials at high temperatures 20 (2003) 153–159.

41. Skrifvars, B.-J., Westén-Karlsson, M., Hupa, M. and Salmenoja, K., Corrosion of super-heater steel materials under alkali salt deposits. Part 2: SEM analyses of different steel materials. Corrosion Science 52 (2010) 1011–1019.

42. Ehlers, J., Young, D.J., Smaardijk, E.J., Tyagi, A.K., Penkalla, H.J., Singheiser, L. and Quadakkers, W.J., Enhanced oxidation of the 9%Cr steel P91 in water vapour containing environments. Corrosion Science 48 (2006) 3428–3454.

43. ASME Boiler & Pressure Vessel Code (BPVC), The American Society of Mechanical Engineers, 2013.

44. Salonen, J. and Heikinheimo, L., Korkean hyötysuhteen höyryvoimalaitoksen materiaalit, VTT tutkimusraportti BTUO74031180, Espoo 2003. (in Finnish)

45. Metals Handbook Ninth Edition. Vol 3 Properties and Selection: Stainless Steels, Tool Materials and Special-Purpose Metals. ASM, Ohio, USA, 1980, 882 p.

46. Sroda S., Mäkipää M., The corrosion resistance of boiler steels in simulated combustion atmospheres with various CO_2 content, Proceedings of BALTICA VI, VTT Symposium 233, vol 2 (2004), 553–565.

47. Srikanth S., Ravikumar B., Swapan K. Das, Gopalakrishna K., Nandakumar K. and Vijayan P., Analysis of failures in boiler tubes due to fireside corrosion in a waste heat recovery boiler. Engineering Failure Analysis 10 (2003) 59–66.

48. Makkonen P. and Mäkipää M., Materials for fluidized bed heat exchangers, Proceedings of BALTICA VI, VTT Symposium 233, vol 1 (2004), 197–208.

49. Venäläinen, I., Supercritical circulating fluidized bed technology for Lagisza 460 MWe power plant, Proceedings of BALTICA VI, VTT Symposium 233, vol 1 (2004), pp. 115–129.

50. Henderson P., Andersson C., Kassman, H., Högberg J., Reducing superheater corrosion in wood-fired power plant, Proceedings of BALTICA VI , VTT Symposium 233, vol 1 (2004), 143–154.

51. Mäkipää M., Baxter D., Turunen E. and Oksa M., Sulfidation attack of the heat transfer surfaces in boilers: Materials performance and views on future prospects, Proceedings of BALTICA VI, VTT Symposium 233, vol 1 (2004), 209–221.

52. Oksa, M. and Mäkipää, M., Comparative laboratory testing of molten salt attack of superheater tube materials. Proceedings of 10th International Symposium on Corrosion in the Pulp and Paper Industry. Helsinki,21 - 24 August 2001. Helsinki (2001), Hakkarainen, Tero (ed.),523–537.

53. Kawahara, Y., Application of high temperature corrosion-resistant materials and coatings under severe corrosive environment in waste-to-energy boilers. Journal of Thermal Spray Technology 16 (2007) 202–213.

54. Pettersson, R.F.A., Storesund, J. and Nordling, M., Corrosion of overlay weld cladding in waterwalls of a waste-fired CFB boiler. In proceedings: EUROCORR 2008 European Corrosion Congress - Managing Corrosion for Sustainability, p. 12, 07–11 Sep 2008, Edinburgh, UK, 2008.

55. Uusitalo, M.A., Vuoristo, P.M.J. Mäntylä, T.A., High temperature corrosion of coatings and boiler steels below chlorine-containing salt deposits. Corrosion Science 46 (2004) 1311–1331.

56. Paul, L., Clark, G., Ossenberg-Engels, A. and Hansen, T., Alloy 33 weld overlay extends boiler tube life and saves money. Power Engineering 111 (2007) 64–69.

57. Suutala, J., Tuominen, J. and Vuoristo, P., Laser-assisted spraying and laser treatment of thermally sprayed coatings. Surface & Coatings Technology 201 (2006) 1981–1987.

58. Davis, J.R., (Ed.), Handbook on Thermal Spray Technology, ASM International, Materials Park, Ohio 2004. 338 p.

59. Sidhu, T.S., Agrawal, R.D. and Prakash, S., Hot corrosion of some superalloys and role of high-velocity oxy-fuel spray coatings—a review. Surface & Coatings Technology 198 (2005) 441–446.

60. Deshpande, S., Sampath, S. and Zhang, H., Mechanisms of oxidation and its role in microstructural evolution of metallic thermal spray coatings—Case study for Ni–Al. Surface & Coatings Technology 200 (2006) 5395–-5406.

61. Taylor, T.A. and Walsh, P.N., Thermal expansion of MCrAlY alloys. Surface and Coatings Technology 177-178 (2004) 24–31.

62. Lima, C.R.C. and Guilemany, J.M., Adhesion improvements of Thermal Barrier Coatings with HVOF thermally sprayed bond coats. Surface & Coatings Technology 201 (2007) 4694–4701.

63. Varis, T., Suhonen, T., Ghabchi, A., Valarezo, A., Sampath, S., Liu, X. and Hannula, S.P., Formation mechanisms, structure, and properties of HVOF-sprayed WC-CoCr coatings: An approach toward process maps. Journal of Thermal Spray Technology 23(6) (2014) 1009–1018.

64. Sampath, S., Dwivedi, G., Valarezo, A. and Choi, B., Partnership for accelerated insertion of new technology: case study for thermal spray technology. Integrating Materials and Manufacturing Innovation 2 (2013) 1–35

65. Valarezo, A., Choi, W.B., Chi, W., Gouldstone, A. and Sampath, S., Process control and characterization of NiCr coatings by HVOF-DJ2700 system: A process map approach. Journal of Thermal Spray Technology 19 (2010) 852–865.

66. Ghabchi, A., Sampath, S., Holmberg, K. and Varis, T., Damage mechanisms and cracking behaviour of thermal sprayed WC–CoCr coating under scratch testing. Wear 313 (2014) 97–105.

67. Holmberg, K., Laukkanen, A., Turunen, E. and Laitinen T., Wear resistance optimisation of composite coatings by computational microstructural modelling. Surface & Coatings Technology 247 (2014) 1–13.

68. Fauchais P. and Vardelle A., Sensors in spray processes. Journal of Thermal Spray Technology 19(4) (2010) 668–694.

69. Sampath, S., Jiang, X., Kulakarni, A., Matejicek, J., Gilmore, D.L. and Neiser, R.A., Development of process maps for plasma spray: case study for molybdenum. Materials Science and Engineering A 348 (2003) 54–66.

70. Matejicek, J. and Sampath, S., In-situ measurements of residual stresses and elastic moduli in thermal sprayed coatings: Part 1: Apparatus and analysis. Acta Materialia 51 (2003) 863–872.

71. Bansal, P., Shipway, P.H. and Leen, S.B. Residual stresses in high-velocity oxy-fuel thermally sprayed coatings – Modelling the effect of particle velocity and temperature during the spraying process. Acta Materialia 55 (2007) 5089–5101.

72. Sampath, S., Srinivasan, V., Valarezo, A., Vaidya A. and Streibl, T., Sensing, control, and in situ measurement of coating properties: An integrated approach toward establishing process-property correlations. Journal of Thermal Spray Technology 18(2) (2009) 243–255.

73. Vaidya, A., Srinivasan, V., Streibl, T., Friis, M., Chi W. and Sampath, S., Process maps for plasma spraying of yttria-stabilized zirconia: An integrated approach to design, optimization and reliability. Materials Science Engineering A 497(1-2) (2008) 239–253.

74. Dwivedi, G., Wentz, T., Sampath, S. and Nakamura, T., Assessing process and coating reliability through monitoring of process and design relevant coating properties. Journal of Thermal Spray Technology 19 (2010) 695–712.

75. Zhang, W. and Sampath, S. A., Universal method for representation of in-flight particle characteristics in thermal spray processes. Journal of Thermal Spray Technology 18 (2009) 23–34.

76. Valarezo, A. and Sampath, S., An integrated assessment of process-microstructure-property relationships for thermal-sprayed NiCr coatings, Journal of Thermal Spray Technology 20(6) (2011) 1244–1258.

77. Oksa, M., Turunen E. and Varis, T., Sealing of thermally sprayed coatings. Surface Engineering 20 (2004) 251–254.

78. Gil, L. and Staia, M.H., Influence of HVOF parameters on the corrosion resistance of NiWCrBSi coatings. Thin Solid Films 420-421 (2002) 446–454.

79. Formanek, B., Szymanski, K., Szczucka-Lasota, B. and Włodarczyk, A., New generation of protective coatings intended for the power industry. Journal of Materials Processing Technology 164-165 (2005) 850–855.

80. Uusitalo, M.A., Vuoristo, P.M.J. Mäntylä, T.A., High temperature corrosion of coatings and boiler steels in oxidizing chlorine-containing atmosphere. Materials Science and Engineering A346 (2003) 168–177.

81. Sidhu, B.S., Puri D. and Prakash, S., Mechanical and metallurgical properties of plasma sprayed and laser remelted Ni–20Cr and Stellite-6 coatings. Journal of Materials Processing Technology 159 (2005) 347–355.

82. Grabke, H.J., Spiegel, M. and Zahs, A., Role of alloying elements and carbides in the chlorine-induced corrosion of steels and alloys. Materials Research 7(1) (2004) 89–95.

83. Regina, J. R., DuPont, J.N. and Marder, A.R., The effect of water vapor on passive-layer stability and corrosion behavior of Fe-Al-Cr base alloys. Oxidation of Metals 61 (2004) 69–90.

84. Li, Y.S., Spiegel, M. and Shimada, S., Corrosion behaviour of various model alloys with NaCl–KCl coating. Materials Chemistry and Physics 93 (2005) 217–223.

85. Skrifvars, B.J., Backman, R., Hupa, M., Salmenoja, K. and Vakkilainen, E., Corrosion of superheater steel materials under alkali salt deposits, Part 1, The effect of salt deposit composition and temperature. Corrosion Science 50 (2008) 1274–1282.

86. Ma, H.T., Zhou, C.H. and Wang, L., High temperature corrosion of pure Fe, Cr and Fe–Cr binary alloys in O_2 containing trace KCl vapour at 750 °C. Corrosion Science 51 (2009) 1861–1867.

87. Pettersson, J., Svensson, J.-E. and Johansson, L.-G., KCl-induced corrosion of a 304-type austenitic stainless steel in O_2 and in O_2 + H_2O environment: The influence of temperature. Oxidation of Metals 72 (2009) 159–77.

88. Kaur, M., Singh, H. and Prakash, S., Surface engineering analysis of detonation-gun sprayed Cr_3C_2–NiCr coating under high-temperature oxidation and oxidation–erosion environments. Surface & Coatings Technology 206(2-3) (2011) 530–541.

89. Sidhu, H.S., Sidhu, B.S. and Prakash, S., The role of HVOF coatings in improving hot corrosion resistance of ASTM-SA210 GrA1 steel in the presence of Na_2SO_4–V_2O_5 salt deposits Surface & Coatings Technology 200 (2006) 5386–5394.

90. Sidhu, T.S., Prakash, S. and Agrawal, R.D., Evaluation of hot corrosion resistance of HVOF coatings on a Ni-based superalloy in molten salt environment. Materials Science and Engineering A 430 (2006) 64–78.

91. Chatha, S.S., Sidhu, H.S. and Sidhu, B.S., High temperature hot corrosion behaviour of NiCr and Cr_3C_2-NiCr coatings on T91 boiler steel in an aggressive environment at 750 °C. Surface & Coatings Technology 206(19–20) (2012) 3839–3850.

92. Paul, S. and Harvey, M.D.F., Corrosion testing of Ni alloy HVOF coatings in high temperature environments for biomass applications. Journal of Thermal Spray Technology 22 (2013) 316–327.

93. Sidhu, T.S., Prakash S. and Agrawal, R.D., Hot corrosion studies of HVOF NiCrBSi and Stellite-6 coatings on a Ni-based superalloy in an actual industrial environment of a coal fired boiler. Surface & Coatings Technology 201 (2006) 1602-1612.

94. Oliver, W.C. and Pharr, G.M., An improved technique for determining hardness and elastic modulus using load and displacement sensing indentation experiments. Journal of Materials Research 7(6) (1992) 1564–1583.

95. Oksa, M., Kärki J. and Metsäjoki, J., Coating solutions against high temperature corrosion – performance validation and feasibility at biomass fired boilers, In: Baltica IX. International conference on Life management and maintenance for power plants. Pertti Auerkari & Juha Veivo (eds.). VTT Technology 106. VTT. Espoo (2013) 656–670.

96. Tomkings, A.B. Nicholls, J.R. Robertson, D.G., EC Report, EUR 19479 EN, Discontinuous Corrosion testing in high temperature gaseous atmospheres (TESTCORR), London, Directorate-General for Research, 2001.

97. Enestam, S., Corrosivity of hot flue gases in the fluidized bed combustion of recovered waste wood. Academic Dissertation, Åbo, Finland 2011, 86 p.

98. Asteman, H. and Spiegel, M., Investigation of the HCl (g) attack on preoxidized pure Fe, Cr, Ni and commercial 304 steel at 400 °C. Corrosion Science 49 (2007) 3626–3637.

99. Ruh, A. and Spiegel, M., Thermodynamic and kinetic consideration on the corrosion of Fe, Ni and Cr beneath a molten KCl–$ZnCl_2$ mixture. Corrosion Science 48 (2006) 679–695.

100. Natesan, K. and Park, J.H., Fireside and steamside corrosion of alloys for USC plants. International Journal of Hydrogen Energy 32 (2007) 3689–3697.

101. Montgomery, M., Hansson, A.N., Jensen, S.A., Vilhelmsen, T. and Nielsen, N.H., In situ corrosion testing of various nickel alloys at Måbjerg waste incineration plant. Materials and Corrosion 64 (2013) 14–25.

102. Gagliano, M.S., Hack H. and Stanko, G., Update on the fireside corrosion resistance of proposed advanced ultrasupercritical superheater and reheater materials: laboratory and field test results. The 2009 Clearwater Coal Conference, Clearwater, FL, USA, 31.5.-4.6.2009, 12 p.

103. Hussain, T., Dudziak, T., Simms, N.J. and Nicholls, J.R., Fireside corrosion behavior of HVOF and plasma-sprayed coatings in advanced coal/biomass co-fired power plants. Journal of Thermal Spray Technology 22(5) (2013) 797–807.

104. Intiso, L., Johansson, L.-G., Canovic, S., Bellini, S., Svensson, J.-E. and Halvarsson, M., Oxidation behaviour of Sanicro 25 (42Fe22Cr25NiWCuNbN) in O_2/H_2O mixture at 600 °C. Oxidation of Metals 77 (2012) 209–235.

105. Schütze, M., Malessa, M., Rohr, V. and Weber, T., Development of coatings for protection in specific high temperature environments. Surface & Coatings Technology 201 (2006) 3872–3879.

106. Hanson T.C. and Settles, G.S., Particle temperature and velocity effects on the porosity and oxidation of an HVOF corrosion-control coating. Journal of Thermal Spray Technology 12(3) (2003) 403–415.

107. Dobler, K., Kreye, H. and Schwetzke, R., Oxidation of stainless steel in the high velocity oxy-fuel process. Journal of Thermal Spray Technology, 9(3) (2000) 407–413.

108. Zhang, D., Harris, S.J. and McCartney, D.G., Microstructure formation and corrosion behaviour in HVOF-sprayed Inconel 625 coatings. Materials Science and Engineering A 344 (2003) 45–56.

109. Vaidya, A., Bancke, G., Sampath, S. and Herman, H., Influence of process variables on the plasma sprayed coatings – an integrated study. International Thermal Spray Conference, May 28-30, 2001 (Singapore), 1345–1349.

110. Turunen, E., Varis, T., Hannula, S.-P., Vaidya, A., Kulkarni, A., Gutleber, J., Sampath, S. and Herman, H., On the role of particle state and deposition procedure on mechanical, tribological and dielectric response of high velocity oxy-fuel sprayed alumina coatings. Materials Science and Engineering A 415 (2006) 1–11.

Errata

Publication IV

On page 4 (239), in Fig. 5. caption, the b) NiCr16Mo, and c) NiCr16Mo should be written as b) NiCr9Mo, and c) NiCr10Al; and the e) NiCr16Mo, and f) NiCr16Mo should be written as e) NiCr9Mo, and f) NiCr10Al.

Publication VI

On page 15 (795), line 1, the (Ref 14, 15) should be written as (Ref 16, 17).

On page 15 (795), line 6, the (Ref 14) should be written as (Ref 16).

PUBLICATION I

Optimization and characterization of high velocity oxy-fuel sprayed coatings: techniques, materials, and applications

In: Coatings 1 (2011) 17–52.

Coatings **2011**, *1*, 17-52; doi:10.3390/coatings1010017

OPEN ACCESS

coatings

ISSN 2079-6412
www.mdpi.com/journal/coatings/

Article

Optimization and Characterization of High Velocity Oxy-fuel Sprayed Coatings: Techniques, Materials, and Applications

Maria Oksa [1,*], Erja Turunen [1], Tomi Suhonen [1], Tommi Varis [1] and Simo-Pekka Hannula [2]

[1] VTT Technical Research Centre of Finland, POB 1000, VTT 02044, Finland;
E-Mails: erja.turunen@vtt.fi (E.T.); tomi.suhonen@vtt.fi (T.S.); tommi.varis@vtt.fi (T.V.)

[2] Department of Materials Science and Engineering, Aalto University School of Chemical Technology, POB 16200, Aalto 00076, Finland; E-Mail: simo-pekka.hannula@aalto.fi

* Author to whom correspondence should be addressed; E-Mail: maria.oksa@vtt.fi;
Tel.: +358-20-722-5412; Fax: +358-20-722-7069.

Received: 28 July 2011; in revised form: 19 August 2011 / Accepted: 19 August 2011 / Published: 2 September 2011

Abstract: In this work High Velocity Oxy-fuel (HVOF) thermal spray techniques, spraying process optimization, and characterization of coatings are reviewed. Different variants of the technology are described and the main differences in spray conditions in terms of particle kinetics and thermal energy are rationalized. Methods and tools for controlling the spray process are presented as well as their use in optimizing the coating process. It will be shown how the differences from the starting powder to the final coating formation affect the coating microstructure and performance. Typical properties of HVOF sprayed coatings and coating performance is described. Also development of testing methods used for the evaluation of coating properties and current status of standardization is presented. Short discussion of typical applications is done.

Keywords: thermal spray; coating; HVOF; optimization; characterization; standardization

1. Introduction to Thermal Spray Processes

Thermal spraying is a general term to describe all methods in which the coating is formed from melted or semi-melted droplets. In thermal spraying the material is in the form of powder, wire or rod

and is fed into the flame produced by a spray gun, where it melts and the formed droplets are accelerated towards the substrate to be coated. The thermal and kinetic energy of the flame can be produced either with burning mixtures of fuel gas and oxygen, or by using an electrical power source. Based on the energy source, thermal spray methods can be divided into a few main groups: plasma spray methods (atmospheric plasma APS, vacuum plasma VPS, and low pressure plasma LPPS), combustion flame spray methods (flame spray), high velocity oxy/air-fuel methods (HVOF/HVAF), electrical arc methods (wire arc), detonation method (D-Gun), and, as the latest technology, cold gas methods (CGS).

Since coating is built up from flattened, fast solidified droplets the velocity plays an important role for the obtained density of the lamella structured coating. Temperature of the flame has a strong effect on the suitable materials to be sprayed. Ceramic coatings are mainly manufactured by using atmospheric plasma spray method, while temperature sensitive materials, such as cermets, are more preferably sprayed by methods with a lower flame temperature. In **Figure 1** the typical operation ranges for various spray systems are presented.

Figure 1. Typical flame temperature and particle velocity operation ranges for various thermal spray systems.

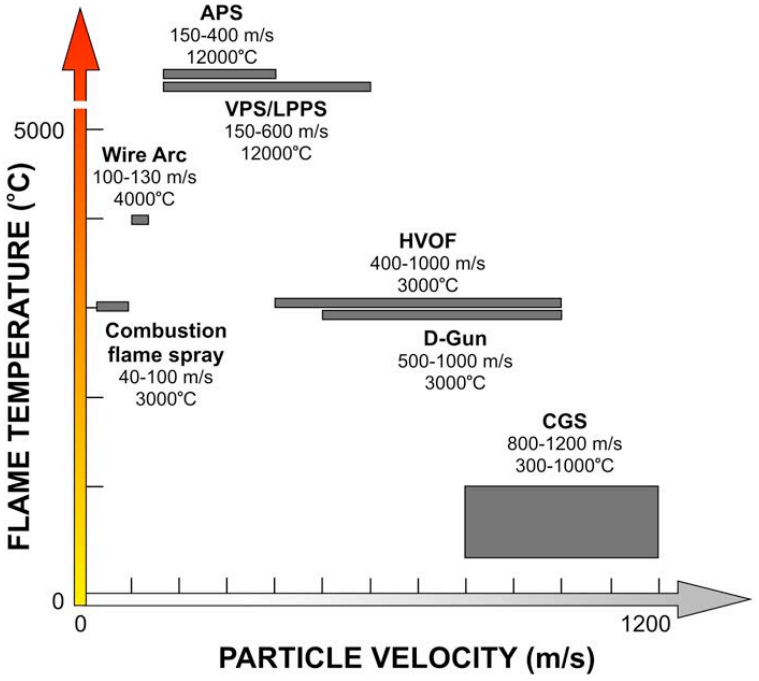

Thermal spray coatings are often applied for better corrosion and wear resistance. Therefore, low porosity and good adhesion are desired properties for the coating. High velocity processes—especially HVOF (High velocity oxy-fuel) spraying—are the preferred methods for producing coating with low porosity and high adhesion. In HVOF spraying, heat is produced by burning mixture of oxygen and

fuel such as hydrogen, kerosene, propane, propylene, natural gas, ethylene, or acetylene. Due to the special nozzle design, a jet with supersonic speed is produced.

The ability to produce dense coatings with low amount of degradation, oxidation of metallic materials, and phase transformations is the main feature of the HVOF process. This is due to the short dwell time of the particles in a relatively cold flame. It is widely used to produce cermet and metal coatings, but the HVOF process has also been demonstrated to be able to deposit dense ceramic coatings.

In the HVOF process, fuel and oxygen are introduced to the combustion chamber together with the spray powder. The combustion of the gases produces a high temperature and high pressure in the chamber, which causes the supersonic flow of the gases through the nozzle. The powder particles melt or partially melt in the combustion chamber and during the flight through the nozzle. The flame temperature varies in the range of 2500 °C–3200 °C, depending on the fuel, the fuel gas/oxygen ratio and the gas pressure. In the HVOF process the particles melt completely or only partially, depending on the flame temperature, particle dwell time, material melting point and thermal conductivity.

A few different HVOF spray systems exist with partly different gun designs and capacities. Each one has differences in design, but all are based on the same fundamental principles. The combination of high pressure (over 3 bar) and gas flow rates of several hundred liters per minute generate supersonic gas velocities. These systems can be roughly divided into the first, second and third generation. In all first and second generation guns, the pressurized burning of gaseous fuel with oxygen is used to produce an exhaust jet traveling at a speed of about 2000 m/s. The main fundamental difference between first and second generation is the design of the nozzle. In the first generation HVOF systems there is typically relatively large combustion chamber and a straight nozzle. With this design maximum of 1 Mach (gas velocity related to the sonic speed) velocities can be produced. The second generation is based on the de Laval nozzle, which enables over 1 Mach velocities at the diverging part of the nozzle. Under standard spray conditions the systems are operated at a power level of about 100 kW and are capable of spraying about 2–3 kg/h of WC-Co. The third generation systems are for power levels ranging from 100 to 300 kW and for higher chamber pressures ranging from 8 bar up to as far as 25 bars, being capable of spray rates up to about 10 kg/h. **Table 1** summarizes the key differences between generations.

Table 1. The differences between three generations of HVOF systems.

	Nozzle type	**Power level (kW)***	**Chamber pressure (bar)**	**Kg/h** (WC-Co)
1st generation	straight	80	3 to 5	2 to 6
2nd generation	De laval	80 to120	5 to 10	2 to 10
3rd generation	De laval	100 to 300	8 to 12 (up to 25)	10 to 12

*Total Heat Output

From a scientific point of view, particle velocity (v) and particle temperature (T) together with substrate characteristics are the main parameters affecting the deposit formation. They determine the deposit build-up process and deposit properties. Particle velocity and temperature affect the deposit efficiency as well as the microstructure. Trend in HVOF process development has been towards higher

gas pressures, faster particle velocities and lower particle temperatures as shown schematically in Figure 2. This has a clear influence on the coating microstructure, where amount of oxidation in the lamella boundary is decreased and flattening rate is increased, and due to this the coating density is improved generation by generation, as presented in the Figure 3.

Figure 2. The trend in HVOF process development has been towards higher gas pressures, faster particle velocities and lower particle temperatures.

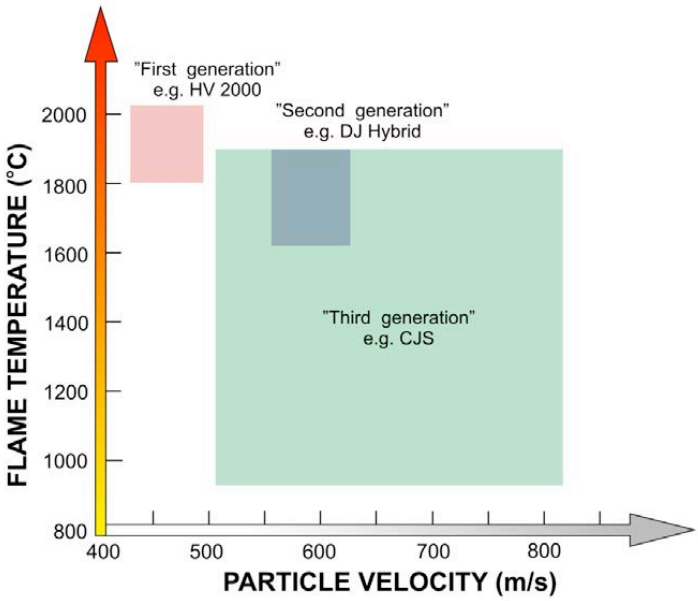

Figure 3. Faster particle velocities and lower particle temperatures in HVOF process have a clear influence on the coating microstructure, where amount of oxidation in the lamella boundary is lowered, the flattening rate increased, and due to this the coating density is improved.

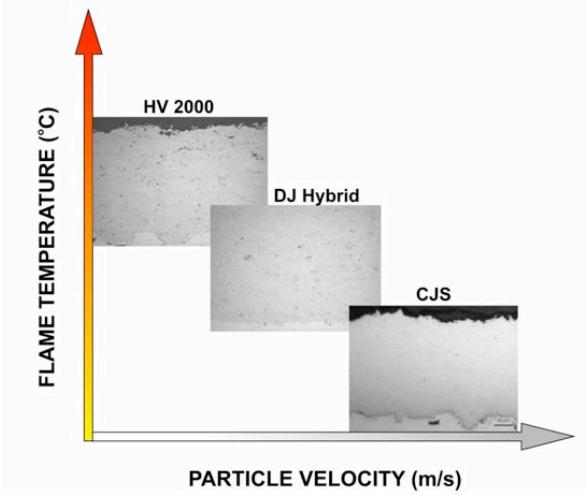

2. HVOF Process Optimization

HVOF spraying is a very complex process, which has a large variety of variables affecting the deposit formation and hence coating properties. These variables include hardware characteristics (e.g., nozzle geometry and spraying distance) and process parameters, e.g., fuel gas, gas flow density, and powder feedstock. In the spray process, the powder particles experience very high speed combined with fast heating up to its melting point or above. This high temperature may cause evaporation of the powder or some components of it, dissolution, and phase transformations. Due to this complex nature of HVOF technique, the control and optimization of the process in order to achieve coating with desired properties is a highly challenging task. There are different ways of optimizing and analyzing the thermal spray processes and deposit formation. These include statistical methods such as Taguchi and design of experiments (DoE), numerical modeling and simulation, and FE methodology [1-5]. In the Taguchi method, for example, the test matrix can be significantly reduced and the relative importance between variables can be determined sufficiently. The result in Taguchi is dependent on the design and selection of variables and their levels and the result may therefore be misleading. Determining the importance and weight of a large number of variables is very difficult with the HVOF process. This applies to different modeling procedures as well.

Good coating quality with suitable properties and required performance for specific applications is the goal in producing thermal spray coatings. In order to reach this goal, a deeper understanding of the spray process as a whole is needed. Starting material, spray process and particle-substrate interactions all affect the formation of coating with different microstructure and hence the coating properties and eventually the coating performance. Use of submicron and nanostructured powders sets demands for the coating process in order to maintain the fine-scaled structures and enhance the coating properties. For better control of thermal spraying, different sensing devices have been developed during the last decade. These diagnostic tools have enabled better investigation and measuring of the spray process, and helped to understand the impact of different process variables on in-flight particle state (flux, temperature and velocity). In tandem with the diagnostic tool development, a novel comprehensive optimization tool has been developed for thermal spray processes. The process mapping concept was first introduced by Professor Sanjay Sampath [6], and its use has increased since introduction [7-10]. In this chapter the diagnostic equipments are introduced, as well as the process mapping tool and factors related to it. Examples of applying the process maps for process control and coating design are presented.

2.1. Diagnostic Tools for Process Optimization

For the last fifteen years active development of spray process sensing systems has taken place. These diagnostic tools are nowadays robust, user-friendly and cost-effective, and therefore their use has increased strongly. Principle objectives of diagnostic tools are to measure the variables of particles within the spray stream, *i.e.*, velocity, temperature, flux, trajectory, and size distribution, which all have influence on the microstructure and properties of sprayed coatings [9]. The sensors are mainly based on two-wavelength pyrometry and time triggered measurement of velocity. Examples of sensors for thermal spraying are Tecnar DPV2000, Oseir SprayWatch, Tecnar Accuraspray, Inflight Particle

Pyrometer, and Spray Position Trajectory sensor. These are based on either individual particle (DPV2000) or ensemble (group of particles) measurement (SprayWatch, Accuraspray). In its simplest form, the sensors are used for measuring the temperature and velocity of the powder particles in the spray stream. The placing of the sensors can either be fixed on the spray torch or on the side of it. With the former sensors, it is possible to monitor the process continuously, and any variation can be instantly detected. Ensemble measurement is the faster of the two, a few seconds against a few minutes [11]. The diagnostic tools have differences in measuring the spray stream, including volume, number of particles and the ability to scan the spray stream. These differences with single particle and ensemble sensors may lead to different results when measuring temperature and velocity. Comparison with single and ensemble sensors has shown good relation for ceramic and metallic coatings when velocity was measured [12]. However, average particle temperature measured by single and ensemble sensors did not correlate for metallic materials. The reason for this might be that high-temperature ceramic materials have higher total radiated intensity due to higher temperature and higher emissivity, but metals are influenced by oxidation and change of emissivity [12]. Therefore the results of diagnostic tools need careful consideration.

2.2. Process Optimization Procedures

The spraying process is monitored with diagnostic sensors, which measure the particle surface temperature and velocity in the spray stream. It is very important to place the equipment correctly in-line with the spray stream. By controlling the gas flow, the fuel/oxygen ratio, or back-pressure of the chamber, different particle states are formed. In order to examine coating formation in detail, individual splats can be sprayed in parallel with using diagnostic tools. By splat studies on the polished substrate, the particle melting state can be analyzed, and hence it is possible to get more information of the diverse coating build-up process. With splat analysis, it has been shown e.g., that small NiCr particles suffer more oxidation when particle temperatures are high [10]. It is common that high speed particles form air pockets when deposited on the substrate, especially when particles are not fully melted. Fully molten NiCr particles have formed smaller grain sized splats compared to feedstock material [10]. Examples of splats of Al_2O_3 are presented in Figure 4, showing different melting states of sprayed particles resulting from different spray parameters. Characterization of the formed coating by microscopic means and testing the coating after spraying, thickness, porosity, lamellar structure with fully or partially molten particles, flattening ratio, oxidation level, bonding, hardness, elastic modulus *etc*. are revealed, and can be linked to process variables. When the linkages between process variables, coating microstructure and properties are done, the reverse deduction is also possible. When a certain property is the goal, it is possible to go backwards by process maps and identify the correct process parameters in order to achieve the desired property.

Figure 4. In the SEM figures of splats different melting, flattening and splashing behavior of HV2000 (Praxair) sprayed Al_2O_3 particles can be detected. The used spray parameters have been (**a**) 776 L/min H_2 / 272 L/min O_2 / 20 L/min N_2 (fuel ratio 2.85), 150 mm stand-off distance, (**b**) 776/272/20 (2.85) 200 mm, (**c**) 699/349/20 (2.00) 150 mm, and (**d**) 747/301/20 (2.48) 150 mm.

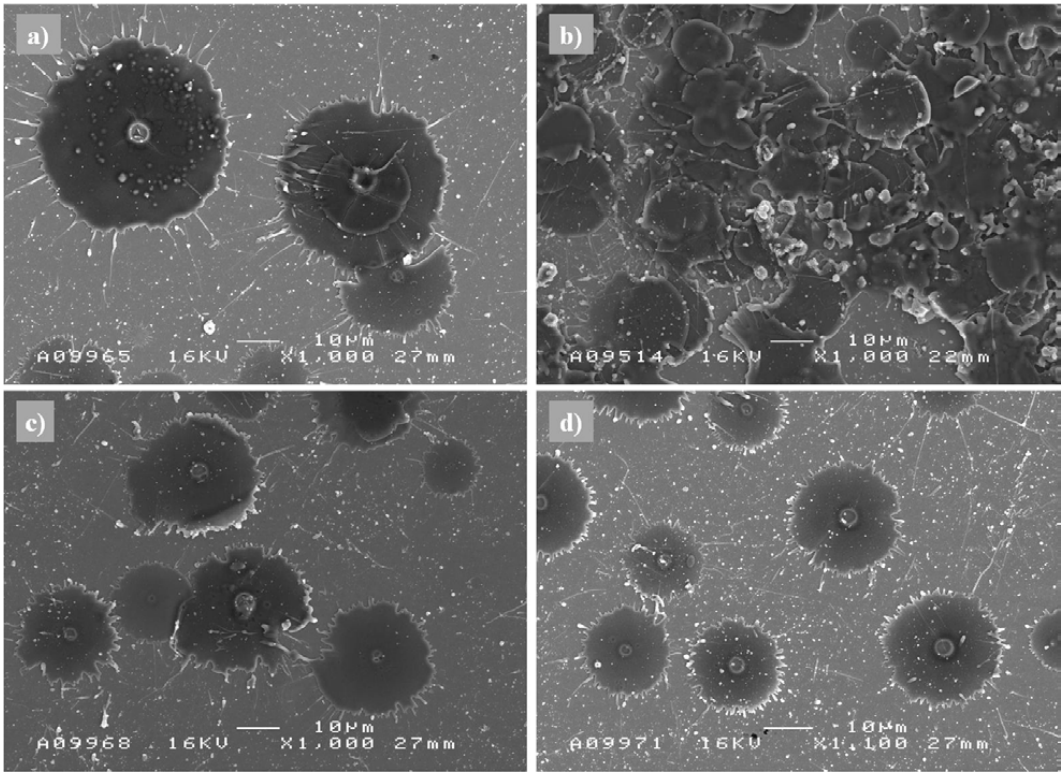

Three operational gas/liquid flow variables can be used for the control of HVOF process: (i) choice of used gases/liquids; (ii) total volume flow of gases/liquids; and (iii) the ratio between them (oxygen/fuel). All these have influence on particle velocity (backpressure of the chamber) and particle temperature. Independent operational parameters with HVOF can be oxygen, fuel, nitrogen and air flow. Other variables, which play an important role, include spray distance and deposition rates (combination of e.g., feed rate and robot speed). Gas flow control can be used as a tool for particle state measurements (T, v), as well as a tool for using different fuels, chamber and nozzle designs, which change the particle state significantly.

The spraying process must be calibrated, so that errors in the measurement can be prevented or estimated. Use of feedback control in the process enables this. Repeating a certain condition whilst performing the process map procedure indicates the data scatter and error, both to temperature and velocity measurement. Errors rise from input parameters (emissivity), instruments, control of gas flows and feed rate, and degradation effects of nozzle and injection wear [8]. These may have influence on the achieved temperature-velocity values during a long process time, and therefore calculation, re-calculation and re-adjusting of spraying parameters are needed throughout the spraying process.

An example of the HVOF spraying of NiCr powder has shown the influence of oxygen-rich flame, resulting in higher temperature and lower velocity [10]. When fuel-rich flame was used, the temperature decreased (as the flame energy decreased), and particle velocity increased. Kinetic and thermal energy transferred to the particles is dependent on the flame energy (enthalpy of the used fuel, fuel density, and ratio of fuel to oxygen). Higher energy levels of the flame yield higher kinetic and thermal energies to the particles. Increment of airflow to the flame decreases the temperature and increases the particle velocity slightly by increasing the drag force to the particles and shortening of their dwell time. Changes in fuel-oxygen mixture cause stronger effect. Feed rate plays also a role on the kinetic and thermal energy. A flame quenching effect has been observed when increasing the feed rate of NiCr powder [10]

The oxide content of the coatings is predominantly determined by the in-flight reactions. Longer flame protects the particles from oxidation by shortening the interaction with the surroundings, and by burning the oxygen within the flame, a so-called shielding effect. Therefore the fuel-rich conditions produce metallic coatings with less oxidation [10]. Higher particle speeds reduce particle overheating, thus preventing the oxidation and decarburization of carbides [13]. On the other hand, higher particle temperature leads to slightly higher oxide content [10].

2.3. Process Mapping

Particle state is influenced by fuel gas chemistry (fuel/oxygen ratio), total gas flow, and energy input, which affect the particle temperature, velocity and hence coating formation dynamics and properties. The process-structure-property relations can be presented by process maps, which can be used as design tool for coating processing. Process maps are interrelationships among the process variables and output responses [12]. The process mapping optimization tool has been widely applied for plasma spray process [12,14], but it can be successfully used for HVOF process as well [10,15].

2.3.1. Concept of Process Mapping

The process map methodology is developed for process control and coating properties optimization. In the process mapping concept, the diagnostic tools are used for understanding the fundamentals of relationships in the thermal spray process, starting from powder to thermal spraying process, to deposit formation, to coating characteristics, and finally to coating performance. In **Figure 5**, the process map concept for HVOF spraying is presented. A first order process map expresses the relationship between torch parameters and particles in the spray stream, which are measured by diagnostics. A second order process map represents relationship between the spray stream measured responses and coating properties. Systematic evaluation of the processes, eventually leading to optimization of coating properties for specified performance and an assessment of process reliability, can be performed by creating first and second order maps for certain material and thermal spray process. A third order process map, which links coating microstructure and properties to coating performance can also be constructed.

Figure 5. The process map concept for the HVOF process. The relationship between process parameters, measured particle state, coating microstructure and coating properties are described as process maps of different order. The goal of process mapping is to understand the process-structure-properties in order to be able to use the tool for coating design.

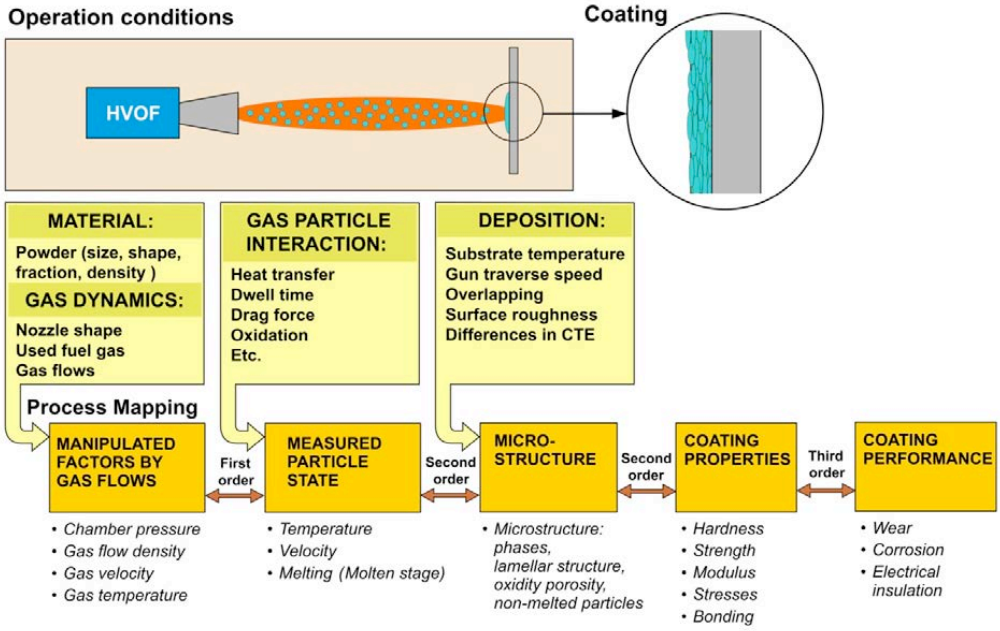

2.3.2. First-Order Process Map

A first order process map relates the process variables to particle state (temperature and velocity). The results acquired with diagnostic tools are plotted in a T-v diagram, which is called a first order process map. An example of first-order (T-v) process map is shown in Figure 6, which presents different temperature and velocity ranges for two different fuel mixtures for HVOF sprayed Al_2O_3 [15]. A generalized first-order process map in Figure 1 for different thermal spray processes, presenting the typical temperature and velocity ranges. In the figure it can be seen that HVOF process has moderate temperature and high velocity compared to other common thermal spray processes. First-order process map helps to understand how the particle state influences on the formation of the coating microstructure.

Figure 6. A first-order process map for HVOF alumina, showing particle temperature and velocity ranges for propylene-oxygen and hydrogen-oxygen fuel mixtures [15].

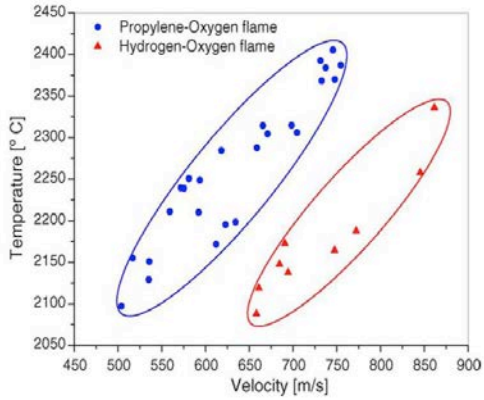

2.3.3. Second-Order Process Map

A second-order process map links the process and deposit interactions. It describes the influence of coating microstructure on the coating properties. In order to produce a second-order map, a certain T-v process window from the first-order map is selected. After the spraying, the coating properties, such as weight, elastic modulus and thermal conductivity, are measured, and thus linked to the process parameters (temperature, velocity). The purpose of the second order map is to provide a tool for designer to choose coatings of selected combination of properties and specify the values of T-v of the particle state. Actual operational parameters are specified from the first-order map. A second-order process map for HVOF sprayed NiCr is presented in Figure 7, showing values of elastic modulus and hardness reflected with different particle temperature and velocity values [10]. A schematic illustration of an idea of the second-order process map is presented in Figure 3, where different HVOF processes are compared in T-v diagram, linking the formed microstructure to the process parameters.

Figure 7. Second-order process maps for HVOF NiCr of elastic modulus and hardness with different particle temperatures and velocities [10].

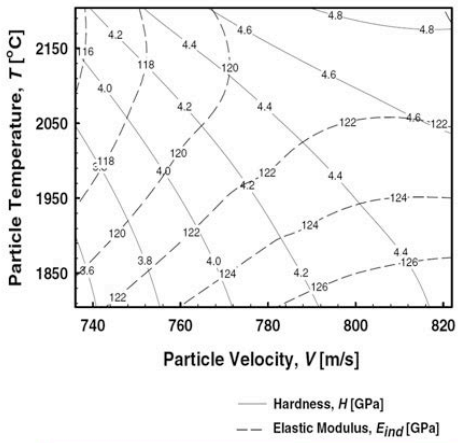

2.4. Reliability through Process Optimization

More stringent requirements for coatings in different applications enhance the use of process optimization, repeatability, reproducibility and reliability (3 R's) of the coating process as a goal [16]. However, reliance and manufacturing reproducibility is a complex task due to the multitude of interrelated parameters that influence spraying process and the deposit formation dynamics. The complexity of the process and material variables has made it difficult to understand the process-structure-property relationships as well as industry/application related attributes, such as coating design, property characterization and reliability [8]. Process optimization is used for process development by parameter improvement, tracking instabilities and examining reproducibility, and that way for improved coating manufacturing. A strategy for coating design can be obtained by careful use of process maps, because process parameters can be linked to coating characteristics and hence understanding of the process-microstructure-property relationships is possible [12]. Through process optimization it is possible to produce reliable and reproducible coatings with designed performance together with predictable life of operation [15]. Therefore the process map concept is an excellent tool for analyzing and controlling the effects of spraying parameters in production of coatings. The method can be applied for any thermal spray technology [10]. Also deposition efficiency (DE) can be improved, as well as process efficiency. Materials usage and the amount of defective coated components can be minimized, and that way it is possible to lower the coating production costs.

2.5. Case Studies of Process Optimization with Process Map Concept

Challenges arise when spraying nanoscale carbides, because with fine carbide sizes the dissolution of carbides and carbon loss becomes easier. The powder quality is important, as the size distribution, density, carbon and oxygen content have influence on the deposit formation. Choosing right spray process and optimizing control parameters are essential in generating good coating quality. Agglomerated and sintered WOKA 3652, −45+45 μm WC-10Co4Cr powder was sprayed with DJ Hybrid HVOF spray, with hydrogen as fuel gas. The goal was to increase both wear resistance and fracture toughness. As can be seen in the generalized second order process map for WC-CoCr in Figure 8, a small process window to achieve such characteristics combination was found. The goal of using WC-CoCr with nanoscale carbides was to achieve high hardness combined with good fracture toughness. Thermico CJS (carbide jet spray), a colder HVOF thermal spray process with broader process window, was applied for maintaining the nanoscale carbides within the matrix. With careful process optimization, both the characteristics were enhanced [17].

Figure 8. A generalized second order process map for WC-CoCr HVOF coating. Different coating properties are placed into the temperature-velocity diagram. This process map can be used as a design tool to optimize coating process conditions in order to achieve desired coating property or coating property combinations.

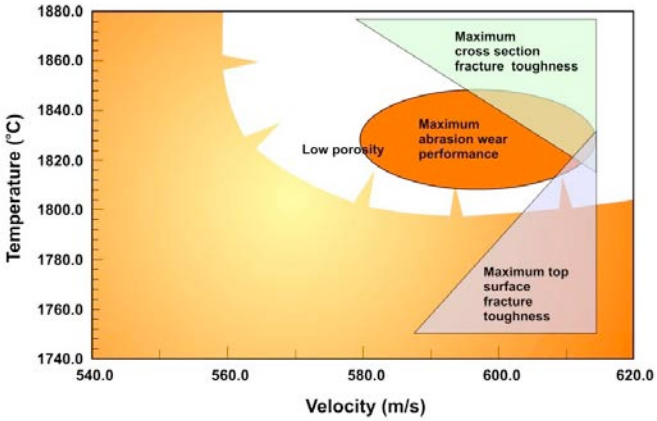

Process map methodology has been used for HVOF spraying of Ni-20%Cr coatings [10]. Design of experiments was used to prepare a first order process map. According to the map, different conditions were chosen to produce the coatings with a low feed rate, and to analyze them with an *in-situ* coating property sensor (ReliaCoat Technology ICP). It was noted that increase in the feed rate decreased both the particle temperature and velocity. In the same process optimization trials, an increment on airflow feeding was detected to result in lower particle temperature but higher velocity. When spraying distance was increased, the particle temperature was risen and the velocity was reduced. In order to enhance the thermal conductivity, high kinetic energy with high thermal energy of particles was required so as to deposit dense coatings with improved intersplat bonding (metallurgical, intimate mechanical contact), but oxide content must be kept relatively low. Electrical resistivity was enhanced with high thermal-kinetic energy as well. Stiffer coatings were formed with high particle velocity and sufficient melting state.

An example of plasma spray process optimization for yttrium stabilized zirconium (YSZ) plasma sprayed coating showed possibility of controlling the particle state within a small process window (±10 °C average temperature and ±2 m/s average velocity) by using a first order process map while varying process parameters (e.g., gas flow, current). However, different melting states were observed in the temperature distribution diagrams for various sprayings, as well as differences for deposition efficiencies, and modulus between the coatings. These results indicate that temperature and velocity measurement solely do not describe the melting state of the particles [15].

2.6. Thermal Energy and Kinetics of Particles in Spray Stream

In order to better understand the melting behavior of particles in the spray stream, another factor has been developed besides the use of temperature. Especially with ceramic materials, with low thermal conductivity, the particle surface temperature does not directly indicate the particle melting status due

to large temperature gradient within the particle [9,18]. The particle surface may even evaporate before the core melts. In the case of metallic materials, the oxidation of particles occurs in the spray stream. This phenomenon can have an effect on the measured temperature values and emissivity value. Melting index (MI) also takes into account the time particles stay under the influence of flame and particle size. It can be expressed as [12]:

$$MI = \frac{T\Delta t_{fly}}{D} \quad (1)$$

where T = measured particle surface temperature [K], D = particle size [m], and Δt_{fly} particle in-flight time assuming constant acceleration of particles [s]. In the MI formula the Δt_{fly} = 2L/v, where L = spray distance [m], and v = particle velocity [m/s]. MI can be defined as the ratio of particle residence time in the flame to the total time needed for particle to melt: MI = $\Delta t_{fly}/\Delta t_{melt}$ [9]. There is also more thorough description of melting index, which attaches thermal resistance and energy balance analysis to the formula [9]:

$$MI = \frac{\Delta t_{fly}}{\Delta t_{melt}} = \frac{24\mathrm{k}}{\rho h_{fg}} \cdot \frac{1}{1 + 4/_{Bi}} \cdot \frac{\left(T_f - T_m\right) \cdot \Delta t_{fly}}{D^2} \quad (2)$$

where k is the thermal conductivity [W/mK], ρ is the density of the material in liquid state [kg/m^3], h_{fg} is the enthalpy of fusion [J/kg], and T_f is the flame temperature near the in-flight particle [K], T_m is the melting point of the material [K], D is the particle size [m], and Bi is the Biot number [9].

With this approach MI is non-dimensional, which allows cross-comparison of melting state among a range of materials. From Equation 2, it can be detected that if the flame temperature is higher than the melting point of the material, a positive MI value will be obtained, which corresponds to fully molten particles. Otherwise, the material will be unmolten (MI < 0) or partially molten (0 ≤ MI < 1). Since it is difficult to monitor the real time flame temperature in the vicinity of the flying particles, for simplifications particle surface temperature, T, has been often used instead of T_f. Metallic particles oxidize during the spraying process, which has effect on the measured temperature by diagnostic sensors. Oxidation reactions are exothermic, which raises the particle temperature in-flight. Extent of oxidation taking place with the metallic particles is described by Oxidation index (OI) [9].

Like temperature, the velocity values alone do not give sufficient information of the particles impinging on the substrate material and hence the deposit build-up process. Therefore either kinetic energy (KE) or Reynolds number (Re) can be used for describing the kinetic behavior of the particles. Kinetic energy is related to particle mass (m) and velocity (v) [9]:

$$KE = ½mv^2 \quad (3)$$

Reynolds number can be described with factors such as particle size, material density and viscosity [17]:

$$Re = \frac{Dv\rho}{\mu} \quad (4)$$

where D = particle diameter [m], ρ = density of the material in liquid state [kg/m^3] and μ = dynamic viscosity [kg/ms]. Both the kinetic energy and Re are important factors describing the impact, extent of spreading and flattening, and hence the nature of splat-substrate and splat-splat contact [9]. Melting state, kinetic energy and local deposition temperature are likely the most important factors controlling the microstructure and properties of the coatings [10].

Other factors besides particle state correlations that strongly effect deposit formation dynamics (wetting, spreading-splashing, flattening, solidification, and interlocking/bonding dynamics) and hence deposit characteristics, are substrate temperature and roughness, deposit conditions (rate, spray angle), and deposit rate [12]. Another factor affecting particle behavior and temperature is exothermic reaction of oxide formation (e.g., Cr_2O_3), which generates additional heat during flight [10].

2.7. Monitoring Deposit Formation In-Situ

Analysis of coating characteristics is mainly performed after the actual coating process. However, the actual deposit formation process is difficult to monitor. An *in-situ* coating property sensor (ICP) has been developed to monitor coating curvature evolution and substrate temperature during the spraying process [12]. Measuring curvature is possible by monitoring the substrate displacement with non-contact lasers. Temperature measurement is performed with multiple thermocouples attached to the back of the substrate material during both deposition and cooling. With this information, it is possible to calculate residual stresses, CTE, and elastic modulus of the coatings. The technique and the measurement method are described in detail by Matejicek *et al*. [19].

The particle state influences stress build-up during spraying process and coating residual stresses have an effect on the coating properties. The residual stresses depend strongly on the particle velocity and on the particle temperature [12]. Compressive stresses are formed due to peening at high particle velocities. As an example, in curvature measurements of NiCr it has been noticed that in the first pass, the quenching stresses prevail due to limited plastic deformation of the substrate [10]. Following passes induce compressive stresses due to the peening effect. The higher the velocity, the higher is the buildup of the compressive stresses. Peening intensity of the impacting particles can be monitored during spraying through an *in-situ* curvature technique. Correlation of it can be made to the microstructure, splats, residual stress and hardness of deposits [10]. Difference in CTE's (coefficient of thermal expansion) between the coating and substrate material also causes stress in the coating. Evolving stress and substrate temperature are main factors when considering strain hardening of the coating, compaction, and residual stress development [10].

2.8. Effect of Feedstock Properties on Coating Formation

Powder properties and characteristics (e.g., particle shape, structure and size, powder density and flow ability, purity, phase content, agglomeration) depend on the detailed powder manufacturing method, *i.e.*, crushing and milling, water and gas atomization, spray drying, agglomeration and sintering [13]. Studies have shown implication of different feedstock for the formed coating, as the particle characteristics are very different in the spray process (e.g., temperature and velocity). When powders from the same material, but with different morphologies or different size distribution, have been sprayed with similar temperature and velocity range, the formed coatings have shown substantial

differences in several properties e.g., elastic modulus [12]. Examples of different spray powder morphologies are presented in Figure 9. The feedstock characteristics (particle form, size distribution, density and chemistry) have an effect on deposit evolution and process efficiency by change in thickness per pass, and to other properties, such as thermal conductivity.

Figure 9. SEM images of thermal spray powders representing different morphologies. **a**) Ball mill mixed, agglomerated and sintered Al_2O_3/SiC; **b**) spray dried Cr_2O_3; **c**) gas atomized Ni20Cr; and **d**) fused and crushed Al_2O_3 powder by Praxair.

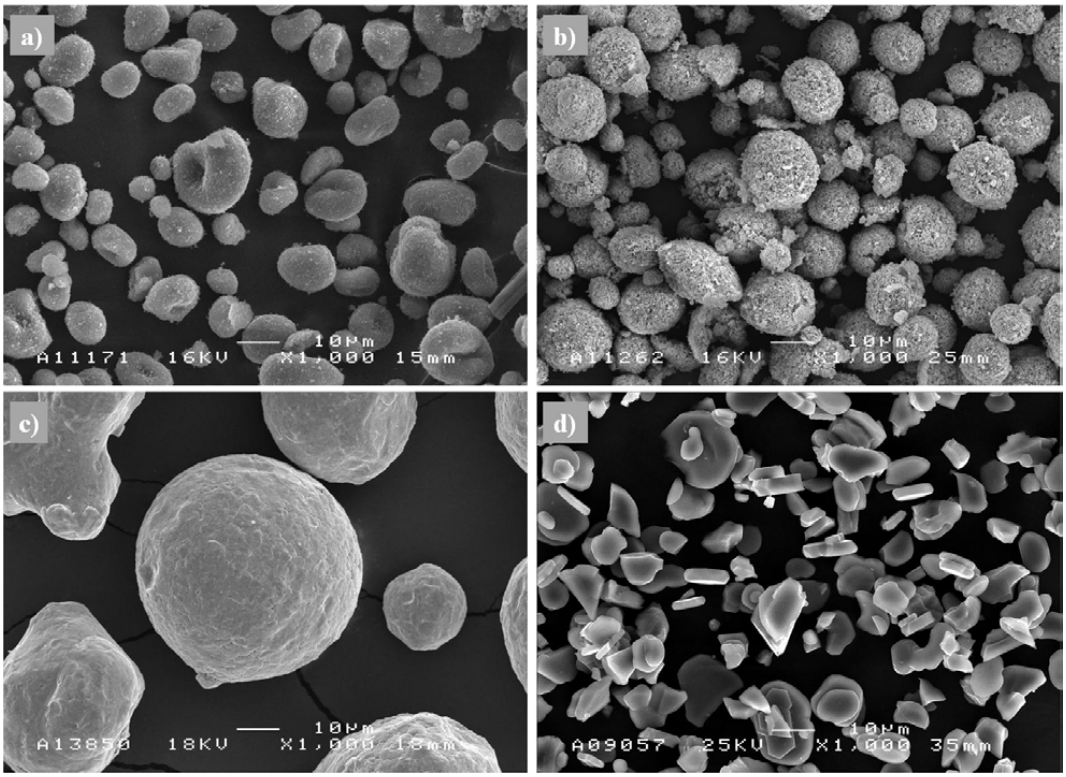

3. Characterization of HVOF Coatings and their Properties

The optimization of the coating microstructures and properties is a challenging task, not to mention the performance of the coating in a particular environment or application as presented in Figure 10. There are a number of influencing factors and interdependencies that influence the intrinsic coating properties as discussed above. These interdependencies are complicated and sometimes even impossible to handle although the systematic process optimization approach described in the previous chapter shows promise as an effective tool for such a task.

Figure 10. A typical optimization route of coating performance by controlling the intrinsic coating properties via optimization of coating microstructure and coating/substrate system interactions.

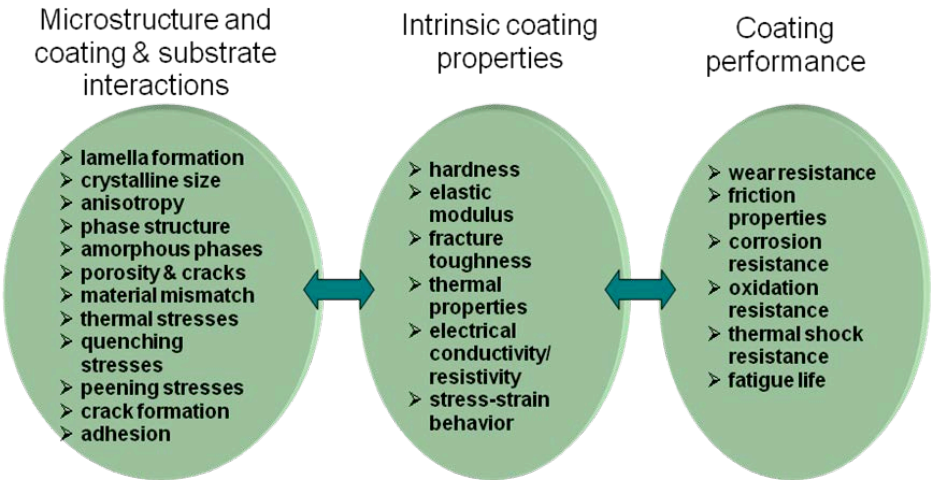

As described in previous chapters, the typical route for the optimization of coatings performance is via its intrinsic properties that in turn are controlled by the microstructure and coating/substrate—system interactions. For example, in wear applications such coating properties as hardness, elastic modulus and fracture toughness, along with porosity of the coating, are under focus. If the application requires environmental resistance, whether against corrosive media or oxidation, it is important to control the phase structure of the coating as well as its porosity. In both cases, also the system properties, *i.e.*, adhesion of the coating to the substrate and internal stresses must be under control to obtain a coating that has an optimal performance at the particular applications.

Before discussing the typical properties and the range of their variance in HVOF coatings we will introduce the most usual methods for characterizing the properties of HVOF coatings. It is important to acknowledge that although most of them are quite generally applied in materials characterization, thermal spray coatings bear many special features that must be taken into account when their properties are evaluated.

3.1. Characterization of Intrinsic Coating Properties: Special Features and Limitations

Characterization of coating microstructures and properties are usually carried out by methods developed for microstructural characterization in general. While most of these are directly applicable for HVOF coatings as well, there are certain precautions, which should be considered and taken into account. This concerns especially the preparation of samples for characterization of microstructural features of coatings.

3.1.1. Coating Hardness

Hardness of the coating is usually measured either from the cross section or the surface of the coating. Two types of methods are commonly used, *i.e.*, traditional hardness measurement preferably

carried out by Vickers' method or instrumented indentation techniques, where the hardness is evaluated from the load-displacement data.

When Vickers hardness is measured from the cross-section of thermal sprayed coating the applied loads should not lead to the formation of cracks. According to standard EN ISO 14923 the thickness of the coating should be at least three times the indentation diagonal *d*. This is observed to be the absolute minimum thickness required to make reliable measurements and, to be on the safe side, the upper corner of the indentation should be located at least at a distance of one diagonal from the surface of the coating, and the lower corner a similar distance away from the substrate. When Vickers hardness is measured from the top surface of the coating, the thickness is recommended to be ten times the plastic depth of the indentation to avoid any effect from the substrate on the measurement. Therefore, nanoindentation is currently used for a more detailed mechanical property characterization, such as for measuring hardness and elastic modulus of individual phases like carbides or matrix material of the coating or even from single splats [20-22].

3.1.2. Elastic Modulus

There are several methods to deduce the elastic modulus or Young´s modulus of the coating (E). Among them impulse excitation technique (IET), ICP sensor, and instrumented indentation test are most common. IET-standard procedures are described in ASTM E 1876-99 [23] and ENV 843-2 [24]. Elastic modulus can conveniently be determined by instrumented indentation. Values of E are calculated from the load-displacement data usually following the procedure proposed by Oliver and Pharr [25]. Because of the elastic field of the indentation is always larger than the plastic field, the boundary conditions of hardness measurement described above should be considered to be minimum requirements for elastic modulus measurements. Since elastic modulus is very sensitive to coating microstructure and especially to coating porosity and other faults, its value can also be used when estimating the uniformity and quality of the coating in comparison to other thermally sprayed coatings.

3.1.3. Coating Toughness

The toughness of a material describes its ability to absorb energy before and during fracture [26]. Because of the brittle nature of many thermal sprayed coatings, fracture mechanics play an important role in evaluation of the usability and performance of the coatings. Fracture mechanical theories, equations and measuring techniques of bulk ceramics, also possessing brittle nature, have been the starting point for studying the fracture behavior in the thermal sprayed coatings. Because of the required sample size in the methods developed for bulk materials, the indentation fracture toughness (IF) technique seems to be the only reasonable and suitable test for thermal sprayed coatings. The basic idea is to apply a large enough load with Vickers diamond pyramid tip to initiate cracks from the diagonal corners of the indentation mark. From the measured average crack length and applied indentation load, the fracture toughness (K_{IC}) can be calculated. It describes the critical stress intensity factor of mode I crack. Indentation fracture toughness K_{IC} can be measured from the cross-section or the surface of thermal sprayed coating. From the surface, one usually gets four corner cracks with the same length, and the boundary conditions described e.g., in JIS R 1668-2005 [27] can be used.

Because the applied loads needed for the initiation of cracks in the fracture toughness measurement are higher than those used in the hardness measurements, one must check that the maximum plastic depth of the indentation is less than one tenth of the coating thickness. When measuring fracture toughness from the cross-section of the coating, the obtained result describes the lamellar cohesion. Cracks in the coatings grow more easily in the direction parallel to the substrate—vertical cracks are usually produced only in the brittle ceramic coatings. The cracks parallel to the substrate will usually initiate and propagate in the lamella boundary. Because of this preferred crack growth direction, the equations and boundary conditions developed for homogenous bulk ceramics do not apply and some modifications are needed. If the cracks grow only in the parallel direction, the average crack length (l) should be calculated by dividing the total crack length (= sum of the cracks) by two, not by four as when measured from the surface. One requirement is that the cracks should initiate near the diagonal corners. If other major cracks than the corner cracks are developed, the measurement is not anymore valid. This prerequisite may lead to difficulties of finding valid measurements, especially if the coating possesses large residual stresses [22].

3.1.4. Coating Porosity

There are a number of different methods that can be used for determination of the coating porosity. Nondestructive methods such as water adsorption, mercury intrusion porosimetry, helium pycnometry, Archimedean method, and other more sophisticated and tedious methods such as small angle neutron scattering (SANS) or x-ray computed microtomography (CMT) [28] have all been employed for quantitative measurement of porosity. Accurate counts of porosity and its distribution can be obtained by the latter two methods, but they both require special instrumentation, which is not generally available for industrial use.

The most common practice to analyze the porosity of a coating is to prepare a metallographic cross-section sample of the coating and to determine its porosity from the micrographs taken with light microscope or a scanning electron microscope (SEM) e.g., by image analysis. Porosity within a microstructure can in principle be easily detected by image analysis because of the contrast difference between the dark pores (voids) and the more highly reflective coating material with sufficient resolution. Some reports claim that image analysis can reproducibly detect and measure microstructural features (pores, cracks, *etc*.) to a 95% confidence level within thermal spray coatings [29].

There is a lot of criticism presented on this procedure since the preparation of the samples has a large influence on the values obtained, *i.e.*, the preparation may result in formation of pores (in brittle coatings such as ceramics) or closure of pores (in ductile metallic coatings) resulting in erroneous values of porosity. In ISO/TC107/WG1, porosity measurement of thermal sprayed ceramic coatings by SEM cross-sectional photography and image analysis has been evaluated by a number of participating members. In a round robin test organized by the working group, five samples having a different ceramic coating were tested by each participant to obtain the respective porosity values. Further examinations have also been conducted by NIMS in Japan about the role of image analysis software, SEM and surface polishing procedures to rationalize the reasons for the observed differences. A preliminary and partial analysis of these results is given in ref. [30], and the final report is published as

an ISO Technical Report TR 26946. The findings can be summarized as follows. The differences in grinding/polishing conditions of the cross-sectional sample have a major influence on the porosity value obtained. Especially the pressure during polishing has an important role. It could be hypothesized that if the grinding pressure in the beginning of the polishing procedure is too low, the defects formed during the specimen cutting and preparation are not removed completely and too high value of porosity is obtained. If the pressure applied in the polishing is too high the sample preparation itself results in pull offs and too high porosity value. Furthermore, it is important to recognize that the imaging mode in SEM has an influence such that secondary electron image (SEI) typically yields lower values of porosity than the backscattered electron image (BEI) because the distinction of the coating matrix and the pores is more difficult in the SEI image, and the fraction of image judged to be a pore as a result has decreased. Based on this hypothesis an optimum pressure can be found, which results in a minimum value of porosity. Whether this is the actual porosity of the coating or higher than the real value depends on the mechanical properties of the particular coating.

An additional challenge is that the total percentage of porosity does not always give enough information on the quality of the coating even if determined correctly. A more detailed account of pores and cracks is actually needed if the coating properties and performance are to be judged or predicted in more detail. Therefore it would be advantageous to divide the net porosity into classes, such as coarse and fine globular pores and crack networks according to their process of formation [31]. Coarse pores refer to the size range of 3–10 μm pores, which are formed due to incomplete filling of interstices between impacting particles and previously deposited particles and typically formed, when the impacting particles are not completely molten. Fine pores are approximately 0.1–3 μm in size resulting from incomplete contact between lamellae during coating formation, and are therefore more or less oriented parallel to the substrate surface. The fine cracks approximately 0.01–0.5 μm in thickness result from relaxation of stresses generated within the splats during cooling and are thus oriented typically perpendicular to the lamellar plane.

3.2. Characterization of Coating Substrate System Properties: Challenges and Special Features

3.2.1. Coating Adhesion

Adhesion is one of the most important parameters, which influences the performance of thermal spray coatings—substrate system in practical applications of coatings. For many applications the adhesion of the coating is crucial to the performance of the coated part (e.g., [32]]. Since no metallurgical bonds are formed between the rapidly cooling deposit and the substrate, the surface finish and the deposition conditions during the first spray pass are of uttermost importance in obtaining good adhesion.

A standard method for the measurement of adhesion of thermal spray coatings is by tensile adhesive test [33]. This test is widely used although according to [34] more than 80 other methods are reported for the measurement of coating adhesion. However, in case of porous ceramic coatings tensile adhesion testing has an inherent problem of being prone to penetration of the adhesive used for gluing the tensile test holder through the coating. This may result in too high a value of adhesion in the test. Therefore, other types of tests have been proposed for the measurement of adhesion of thermal spray

ceramic coatings. Two of these are currently used or studied as an alternative for the tensile test, *i.e.*, shear test and scratch test.

Shear test developed in the frame of the EU-CRAFT-project "Shear Test for Thermally Sprayed Coatings" presents the main advantage of being possibly used in real time, *i.e.*, during the production process [34]. The small size of the substrate specimens allows them to be prepared in advance in large quantities, and no limitation of porosity or adhesive strength of the adhesive occurs. Therefore the shear test is more relevant to represent the real stress state acting on the mechanical parts during service. The main disadvantages are the samples characteristics (coating should be thicker than 150 μm) and the need of special equipment to perform the test.

Scratch test, which is widely used for testing adhesion of thin films to substrate, is with modifications currently considered also for determining the thermal spray coating adhesion. ISO TC 107 WG 1 is carrying out an international round robin test to study the feasibility of this test for the determination of the coating adhesion of ceramic thermal spray coatings. Preliminary results of this round robin test will be available by the end of 2011.

3.2.2. Evaluation of Internal Stresses

An important coating-substrate system property is the residual stress state of the coating after spraying. There are only few methods that can be used to measure the residual stresses of thermally sprayed coatings. The generally applied method for measuring the residual stresses in metallic materials is by XRD using standard *d vs.* $\sin^2 \Psi$ XRD techniques (see e.g., [35]]. In order to apply this method for the determination of residual stresses of thermally sprayed coating one needs to know the so-called X-ray elastic constants (XEC). XEC can be calculated using techniques based on the mechanical loading of the samples. However, the experimental behavior of the thermally sprayed coatings shows that the calculation of XEC is unreliable. Considering the characteristics of dense material to which the X-ray diffraction is sensitive, the use of XEC values calculated for the same phase of the bulk material can, according to [36], be used for the determination of stresses in the coatings with an engineering accuracy.

When internal stresses are measured during spraying using the so called *In-situ* Coating Property (ICP) sensor, it is possible to adjust the residual stresses to a large extent during spray by controlling the deposition parameters. In this way, the various stages of stress build-up can be monitored and the various stress contributions can be evaluated separately. The ICP sensor can also be used to extract in-plane elastic modulus of the coatings deposited. It is based on laser sensing of deflections in a strip during thermal spraying which is converted to sample curvature. A simultaneous measurement of temperature is achieved via multiple thermocouples. Elastic modulus and CTE of the coating can be calculated from the coating-substrate composite curvature change due to thermal mismatch [37].

3.2.3. Evaluation of Wear Resistance

Wear resistance of thermally sprayed coatings is of high interest for many applications. In general, wear resistance of a coating in a particular environment is a system property influenced by the coating and substrate material and in particular the type of wear environment. Therefore, it is impossible to quantify the wear resistance of the coating accurately without knowing these factors. However, for

particular types of wear environments there are tests, which give relative performance of different coatings quite accurately. One of the most used wear tests for thermally sprayed coating is the rubber wheel abrasion test (e.g., ASTM G-65), which is meant for testing material's resistance against abrasive type of wear. These tests are also extensively used for a wider screening of coatings, since the possible problems in coating microstructure (not so easily observed e.g., by metallographic means) are often manifested in the results of the abrasion test. Other tests exist for other types of wear situations, such as tests for adhesive wear (e.g., pin-on-disc types of test) and tests for erosive conditions (various modifications exists, e.g., slurry test depicted in standard ASTM G75-95 [38]).

3.2.4. Evaluation of Wet Corrosion Resistance

Corrosion resistance of thermally sprayed coating is always a system property. This is influenced first of all by the corrosive environment in question, but also by the coating properties (composition, phase structure and microstructure including the cracks and the pores) and the coating-substrate-environment interactions. It is very rarely possible to produce fully liquid or gas impenetrable coatings even by sealing the coatings afterwards. Therefore, it is not only the corrosion resistance of the coating, but of the substrate-coating system, which should be considered in each particular application where corrosion is a factor.

Measurement of the corrosion resistance of a coating-substrate system is typically carried out by immersion tests in actual conditions or by accelerated immersion tests in the laboratory. These tests in combination with metallographic and analytical studies help to identify the corroding parts of the system, whether this is corrosion of coating in general, selective corrosion of some specific phase of the coating, or corrosion of substrate via cracks or open porosity of the coating finally leading to coating detachment.

Electrochemical measurements may also be used to evaluate the response of coating—substrate system to corrosive environments. Typical measurement may include the determination of the free corrosion potential and the polarization behavior of the system. If the environment is selected such that the electrolyte causes corrosion only in the substrate, the corrosion current may yield information on the through porosity of the coating as well as on the possible passivation system while the pores of the coating are filled with corrosion products from the substrate.

4. Typical Properties of HVOF Coatings

Coatings prepared by various HVOF techniques have properties typically different from those produced by other thermal spray methods. As discussed in the previous chapter this results mainly from the characteristics of the HVOF process and in particular the combination of particle velocities and temperatures. Therefore, it is important to recognize that nominally similar coating compositions may have a wide variance in properties depending on the details of the processing. On the other hand, this also implies that properties of the coatings can be adjusted according to demands of the application at least to some extent.

4.1. Wear Resistant HVOF Coatings

Wear control is of uttermost importance for many applications of thermally sprayed coatings. These applications include various moving parts such as rotating rolls and axels e.g., for printing equipment, paper and pulp machinery, *etc*. Among different thermal spray methods high velocity oxy fuel (HVOF) spraying has proven to be especially suitable for deposition of carbide and metallic coatings because of relatively low flame temperature and supersonic particle velocities [16]. Under certain restrictions it can also be used to produce high quality ceramic coatings for wear protection.

4.1.1. Wear Resistant Cermets

Typical wear resistant coatings are based on cermet, *i.e.*, metal-ceramic composites, predominantly combining various mixtures of metal matrix including cobalt (Co), chromium (Cr) and nickel (Ni), and tungsten carbide (WC) or chromium carbide (Cr_3C_2). The most common combinations—WC-12 wt.% Co or WC-17 wt.% Co—are widely used in applications where high wear resistance is required. Theoretically the compositions correspond to 20% and 27% of cobalt in volume, but may slightly vary depending on spraying conditions and decomposition of WC during spraying.

For WC-Co-based material it is well known that during flight sprayed particles melt to different extents depending on their size, density and dwell times. Molten Co dissolves the WC grains whereas carbon loss occurs by diffusion through the liquid followed by reaction with the oxygen from the surroundings. There can be large amounts of carbon and tungsten dissolved in the matrix metal, especially in the outer regions of sprayed particles. During cooling, Co-rich liquid becomes supersaturated resulting from the formation of W_2C and other mixed carbides. High cooling rates can even be responsible for the formation of amorphous/nanocrystalline matrix phase. During cooling, precipitation of mixed carbides like *eta*-carbide [$(Co_6W_6)C$] phase may occur in the Co-rich material. All of these effects are most visible on the outer core of the particles. In the small size particles, the whole particle can be influenced by decarburization [39]. If cooling is fast enough, the matrix will stay amorphous and supersaturated of W and C. When the coating is heat-treated afterwards, precipitation of eta-carbide starts at temperatures above 600 °C resulting in marked increase of hardness and reduction of residual stresses in the coating [22,40].

In oxidizing atmospheres or at temperatures above approximately 450°C the resistance of Co-WC is not adequate, and alloying of cobalt binder e.g., with chromium or use of other type of cermet coatings such as Cr_3C_2-25 wt.% NiCr are frequently employed to protect against wear at such elevated temperatures [41]. However, in comparison to WC-Co coatings Cr_3C_2-NiCr coatings are less wear resistant in many cases. Likewise to WC powders Cr_3C_2 containing powders are susceptible to a range of decomposition reactions during thermal spraying and require careful optimization of the spraying process in order to obtain desired coating properties. This has prompted efforts to look for other type of cermet for high temperature applications. TiC and TiB_2 are potentially attractive alternatives to Cr_3C_2 for use in high temperature wear resistant cermet applications since it exhibits a high hardness, low density and good oxidation resistance. Wear properties of TiB_2-containing cermet coatings have been addressed e.g., in refs. [42,43]. HVOF spraying of Ni(Cr)-65 wt.% TiB_2 and Fe(Cr)-70 wt.% TiB_2 powders resulted in TiB_2-containing coatings that were found to perform better in abrasive wear with

alumina than conventional Cr_3C_2-NiCr deposits. Coatings having composition of Ni(Cr)-65 wt.% TiB_2, Ni(Cr)-40 wt.% TiB_2, and Ni(Cr)-40 wt.% TiB_2 with 5 at.% excess boron in order to promote matrix amorphization have also been studied [42]. The size of the TiB_2 particles within the cermet was found to depend critically on the initial composition; large particles were favored by low binder fractions and the presence of the excess boron. The presence of the larger boride particles was concluded to impart the wear resistance of these coatings in abrasion by alumina or silica abrades [43].

Other cermets studied for high temperature erosion include e.g., WC-CoCr, TiC-CoCr, NbC-CoCr [7]. In a study of the erosion-corrosion resistance of these coatings, Wang [44] noticed that peak wastage occurred at intermediate carbide contents at both shallow and steep impact angles for all of the HVOF carbide-cermet coatings tested. At shallow impact angles, this peak occurred on the side of lower carbide contents, while at steep impact angles the peak occurred on the side of higher carbide contents. At both shallow and steep impact angles, wastage in erosion-corrosion test decreased with decreasing carbide size of homogeneous distribution in the HVOF carbide-metal cermet coatings. It was concluded that the erosion-corrosion behavior of carbide/metal cermet coatings and the dependence of mass loss on carbide content are related to the morphology of the coatings and characteristics of erodent particles. Also Hawthorne *et al*. [45] noted that coating composition and microstructural integrity are the main factors determining the relative erosion resistance of the cermet coatings. They also noted that the WC-10Co-4Cr matrix coating was more resistant to erosion–corrosion damage in aqueous slurry testing than was the WC-12Co cermet coating. Similarly WC-10Co-5Cr coating has been found in simulative laboratory test to be a potential candidate for coating of hydro turbine components by Mann and Arya [46]. At low erosive conditions the erosion-corrosion resistance has been found to increase when increasing Cr-content from 5 to 8.5 wt.% [47].

An interesting development in the corrosion resistant HVOF coatings is being made with the amorphous coatings. Amorphous coatings with a composition of Fe48Cr15Mo14C15B6Y2 have been prepared by means of high velocity oxygen fuel (HVOF) thermal spraying under different conditions by Zhou *et al*. [48]. These coatings present dense layered structure and low porosity with some fraction of nanocrystals. The coatings are spontaneously passivated with wide passive region and low passive current density in chloride containing acidic solutions exhibiting excellent ability to resist localized corrosion.

4.1.2. Wear Resistant Ceramic Coatings by HVOF

HVOF spraying is applied mainly to cermet and metallic coatings because of the limited melting power of most of the HVOF spraying guns and systems. However, due to the higher kinetic energy, shorter dwell time of particles in the flame, and lower flame temperature compared to the plasma spray, HVOF offers an interesting combination to produce dense coatings with controlled phase transformations [49]. For high quality coatings particle melting state and possible phase transformations during particle flight in the thermal spray flame as well as coating build up mechanism including splat interface and stress stages must be controlled. Despite some limitations there are several reports on successful depositions of ceramic coatings by HVOF spraying techniques (e.g., [7,15,49-51]).

In order to produce high quality ceramic coatings by HVOF, the spraying system should have a high enough melting power to melt the powder particles during the short flight. It has been shown that the particle temperature and the melting state control the deposit efficiency and the build-up rate while the flattening behavior is dominated by particle kinetic energy [15]. The powders used for spraying must have a narrow size distribution and their average size should be somewhat smaller than for powders generally used for HVOF spraying. Selection of fuel gas is of high importance and the necessity of finding correct temperature-velocity combination is a must for successful deposition of high quality ceramic coatings. The coating density and mechanical properties are strongly affected by particle velocity when complete melting is achieved. The particle state in the case of HVOF is very sensitive to the standoff distance and is found to be an influential parameter controlling microstructure and properties. It has been noted that in HVOF the interpass interfaces play a dominant role in thermal, electrical and tribological properties [16].

4.1.3. Comparison of APS and HVOF Wear Resistant Coatings

It has been quite generally recognized that the wear resistance properties of HVOF coatings are superior to their APS counterparts. Li *et al*. [41] have compared the impact wear resistance of Cr_3C_2-25%NiCr coatings prepared by APS- and HVOF- spraying. They found that the wear resistance of Cr_3C_2-25%NiCr coatings under different impact conditions increases in the order of APS-Ar/H_2, APS-Ar/He and HVOF spraying. The HVOF sprayed Cr_3C_2-25%NiCr coatings showed the best impact wear resistance due to the denser structure and fewer defects since the wear mechanisms of Cr_3C_2-25%NiCr coatings under impact are influenced by the cohesive defects such as stratification, porosity and microcracks in the lamella, and therefore control of these factors has a large impact on the wear resistance of the coatings.

Similar findings have been made by the present authors on HVOF sprayed ceramic coatings. Although only a few HVOF spraying guns exist on the market that are suitable for depositing ceramic coatings, the coating properties obtained by the HVOF techniques have shown quite amazing improvements in comparison to coatings deposited by APS [52]. HVOF sprayed coatings show clearly improved density and less pores and cracks than the APS sprayed as depicted in Figure 11. The abrasion wear resistance of the coatings as measured in a standardized rubber wheel abrasion test is improved more than tenfold when the coating is made by HVOF spraying. The difference is more than 15 times with the alumina and chromia coatings where the spray parameters have been optimized. The HVOF zirconia coatings perform more than 20 times better than the corresponding APS coatings. It must be noted though that the reference value for comparison is for Thermal Barrier Coating (TBC), where maximum density is not aimed. However, the obtained results show that HVOF spraying of ceramics can be an effective method to produce dense, well-adhered ceramic coatings with good environmental protection capability. This can be attributed mainly to the lower porosity and improved cohesion of the ceramic coating structure when produced by HVOF techniques.

Figure 11. Comparison of abrasive wear resistance of plasma sprayed and HVOF sprayed oxide ceramic coating coatings: yttria-stabilized zirconia (YSZ), aluminia (Al_2O_3), and chromia (Cr_2O_3). Compiled based on [52].

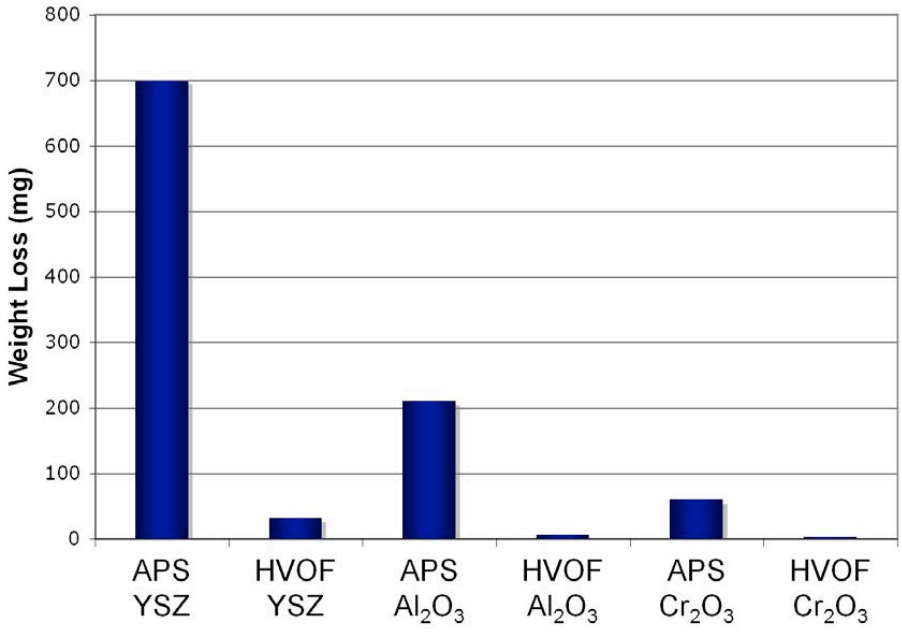

These findings were later confirmed by Bolelli *et al*. [53], who compared Al_2O_3 and Cr_2O_3 coatings deposited onto steel substrates by high velocity oxygen-fuel (HVOF) flame spraying using H_2 as fuel gas, and by conventional atmospheric plasma spraying (APS). In this study it was recognized that HVOF-sprayed coatings exhibited lower porosity and smaller average pore area than the APS ones. The HVOF-sprayed coatings possessed higher Vickers micro hardness, higher indentation fracture toughness and higher elastic modulus than the APS ones. During ball-on-disk tests against SiC, various wear mechanisms were observed. At room temperature and at low normal load, all of the coatings developed stable tribofilms under mild wear regime ($<10^{-6}$ mm^3/Nm) while at higher temperature and/or normal load, brittle fracture wear prevailed. Under these latter conditions, HVOF coatings become superior to APS ones, thanks to their higher toughness. Analogously, in dry particle abrasion, where brittle fracture prevails, the tougher HVOF coatings outperform APS ones.

Also in this study the HVOF ceramics were found to display lower overall porosity, and smaller and more rounded pores than the APS ones. Excellent interlamellar cohesion was noticed by FEG-SEM observations of fractured cross-sections. A large degree of melting of HVOF-sprayed nanostructured Al_2O_3 powder was found. While some glassy or poorly crystallized splats existed in Al_2O_3 coatings, the Cr_2O_3 ones were fully crystalline. In all cases, smaller and more equiaxed grains appeared in HVOF coatings, while grains were larger and mostly columnar in APS ones. In general, HVOF sprayed ceramics are harder and tougher than corresponding APS ones, and HVOF Al_2O_3 and n-Al_2O_3

are even tougher than APS Cr_2O_3 indicating the great influence of microstructure on coating mechanical properties [53].

As discussed in Chapter 3.1.4, the pore structure has a major impact on the mechanical properties of the coatings. Coarse pores in the size range of 3–10 μm are formed when the impacting particles are not completely molten because of incomplete filling of interstices between impacting particles and previously deposited particles. Fine pores approximately 0.1–3 μm in size result from incomplete contact between lamellae during coating formation being more or less oriented parallel to the substrate surface. The fine cracks approximately 0.01–0.5 μm in thickness result from relaxation of stresses generated within the splats during cooling and thus oriented typically perpendicular to the lamellar plane. It is the difference in the distribution of the latter two types of pores (fine pores and cracks), which probably can explain the huge difference in the wear properties of the plasma sprayed and HVOF sprayed ceramic coatings.

4.2. Corrosion and Oxidation Resistant HVOF Coatings

HVOF-spraying is a versatile technique that can yield high-density coatings with porosities less than 1% by optimization of the process variables. Because of these microstructural improvements of deposits produced by HVOF as compared with traditional spraying methods (including APS) the HVOF coatings have widely been studied for their corrosion resistance and consequently, there are a plethora of publications on the corrosion properties and performance of HVOF coatings. These can be divided into two categories, *i.e.*, those reporting oxidation resistance of HVOF coatings and the others regarding wet corrosion properties.

Resistance of MCrAlY coatings to oxidation in different oxidizing atmospheres has been studied and compared with that of VPS coatings by Brandl *et al*. [54]. Under the chosen oxidation conditions, which assured a high oxygen partial pressure, the oxidation kinetics of the HVOF and VPS coatings were very different, *i.e.*, the oxidation rate of the HVOF sprayed coating is considerably lower than that of the VPS coating. This observation was proposed to result from the formation of finely divided α-Al_20_3 during spraying hindering the grain boundary diffusion of the elements. As a consequence the oxide scale growth was very low.

Corrosion behavior of an HVOF Ni based self-fluxing alloy NiWCrBSi coatings in a chloride solution has been studied by Gil & Staia [55]. Since anticorrosion coatings must be impermeable to protect steel structures in corrosive environments optimization of deposition conditions must be determined. The optimization process indicated that especially the spraying distance, the fuel to oxygen ratio, and the powder feed rate have a significant effect on the porosity and consequently to the corrosion resistance of these coatings. Zhao *et al*. [56] noted that the corrosion of the NiCrBSi coating first occurs around the particles that have not melted during spraying and defects such as pores, inclusions and microcracks. Corrosion then proceeds along the paths formed by pores, microcracks and lamellar structure resulting in exfoliation or laminar peeling off the coating. Adjustment of the thermal spray parameters to reduce the electrochemical unevenness or sealing the pores can improve the corrosion resistance of the coating.

Hastelloy C coatings can offer corrosion protection in many aggressive environments. Similar to many other coatings aimed for corrosion resistance, the key question is whether the through porosity of

the coating in spraying can be controlled. Kawakita *et al*. [57] used quantitative analyses of dissolved substances derived from coated steel during immersion in HCl solution to evaluate the quality of Hastelloy C high-velocity oxyfuel (HVOF) sprayed coatings. This technique enables the detection of even small amounts of through-pores and separately calculates both coating through porosity and corrosion resistance. For Hastelloy C coatings, the number of pores extending through the coating was found to depend on the coating thickness and on the coating's stacking structure.

Electrochemical behavior of various HVOF-sprayed corrosion resistant coatings in acidic medium has been made by [58]. A total of eight different chromium-containing coatings with varying proportions of alloying elements (Ni, Mo, Si, Fe, Co, W, B and C) aiming for a corrosion behavior comparable to that of stainless steel AISI 316 were studied and compared with that of bulk AISI 316. The results indicate that HVOF-sprayed AISI 316 coating offers a lower corrosion resistance compared to bulk AISI 316 while high nickel- and chromium-containing coatings appear to offer a corrosion resistance comparable to bulk AISI 316. In addition, other alloying elements like molybdenum were proposed to be essential for obtaining higher corrosion protection. In extension of this study Chidambarama *et al*. [59] confirmed that HVOF sprayed nickel-chromium alloy coatings containing molybdenum were confirmed to exhibit corrosion resistance comparable to bulk AISI 316.

Hard chromium displacement by HVOF coatings has been a long-standing goal for spray industry and, consequently, there are several studies made on the corrosion resistance of HVOF coatings in comparison with hard chromium e.g., [60-65]. According to the studies, several HVOF coatings offer potential for replacing hard chrome at least from the corrosion point of view. For example according to Guilemany *et al*. [66] polarization curves of Cr_3C_2-NiCr recorded after immersion tests showed a lower current and higher corrosion potential for Cr_3C_2-NiCr coating than several other samples studied including hard chromium coatings.

High temperature corrosion resistance of HVOF coatings has also been studied intensively. For example Cr_3C_2-NiCr, NiCrBSi, Stellite-6 and Ni-20Cr are coatings of particular interest [e.g., 67]. The high temperature corrosion resistance of the coatings may generally be attributed to the formation of oxides and spinels of nickel, chromium or cobalt on the surface of the coating. The high temperature corrosion resistance of all the coatings was found superior to bare nickel-based superalloy. In the presence of Na_2SO_4-V_2O_5 salt deposits NiCr coating was found to be most protective followed by Cr_2C_3-NiCr coating. WC-Co coating was least effective to protect the substrate steel [68]. It was concluded that the formation of Cr_2O_3, NiO, $NiCr_2O_4$, and CoO may contribute to the development of high temperature corrosion resistance in the coatings. In cyclic oxidation [68] NiCrBSi coating was also found to be very effective in decreasing the corrosion rate in the Na_2SO_4-60% V_2O_5 molten salt environment at 900˚C. The high temperature corrosion resistance imparted by NiCrBSi coatings was attributed to the formation of oxides of silicon, chromium, nickel and spinels of nickel and chromium.

4.3. Nanocrystalline Powders and Coatings

During the last ten years considerable efforts have been made to develop thermally sprayed coatings having structural elements in the submicron or nanometer scale. Although the rapid cooling of melted particles during the coating deposition produces very fine structures—typical grain sizes being in submicron scale or even amorphous—the unmolten particle, e.g., carbides in cermets can controllably

be reduced in size only in powder processing. Because of the large influence of carbide size to the properties of cermets, this has prompted large efforts in producing powders having carbides in submicron and nanometer dimensions. Also, toughening of ceramic coating by nanosized metallic particles has aroused considerable interest and resulted in development of powders with nanosized metal particles. Finally, nanostructural powders produced by spray-drying and sintering offer several advantages via their melting behavior. It goes without saying that in order to take advantage of these powder technologies, optimization of the spraying process is a must.

The dissolution phenomenon of the carbides is more emphasized for WC-Co materials having sub-micron or nanosized carbides. Increasing the surface area of the carbides by reducing their size, the control of the spray conditions becomes more critical in order to avoid the overheating of the particles and fully benefit the positive effects from nanosized carbides for properties. For example, McCartney *et al*. [69] found that the nanocomposite had a poorer wear resistance than the conventional coating under the conditions examined. Wear was dominated by the loss of ductility in the Co-rich binder phase due to its amorphization. The differences in the wear behavior of the coatings could, thus, be explained in terms of differences in powder characteristics, the extent of reaction and decarburization during spraying, and the subsequent development of the microstructure in the coating during splat solidification at high cooling rates. In order to overcome this problem a shift towards the colder HVOF processes has taken place. For example in CJS HVOF process the process conditions can be adjusted more suitable for the deposition of nano or sub-micron sized carbides. In Figure 2 the relative difference in the particle temperature for the DJ Hybrid and CJS processes is demonstrated with some measurement points and from that the process window is estimated. The particle velocity and temperature measurements have been carried out for the same powder for both processes in order to demonstrate the difference. The process conditions effect on the carbide dissolution so that there is no W_2C formation in the coating sprayed with CJS. Powder size used for the CJS process was 5–25 micron and that for the DJ Hybrid process 15–36 micron.

Turunen *et al*. [7] studied the spraying of nanostructured Al_2O_3 and Al_2O_3-Ni HVOF powders and properties of coatings deposited thereof. It was found that by optimizing spray parameters high quality coatings with improved properties are obtained. Introduction of nanopowders to the coating process improved the hardness and wear resistance of the pure Al_2O_3-coating. Introduction of nickel alloying decreased the hardness and wear resistance of the coatings, but increased the toughness of the coatings via introduction of small nickel particles into alumina matrix and between the alumina splats. Addition of a small amount of nickel into alumina can thus be used to markedly modify the properties of the coating.

5. Applications of HVOF Coatings

Due to the excellent characteristics of HVOF coatings as mentioned in the previous chapter, there is a large variety of suitable materials, different HVOF sub-processes, such as CJS, and hence the possibility to tailor coatings for a large variety of applications; therefore, the use of HVOF is broad among several industries, and is increasing all the time. Examples of application areas include process industry, where the coatings are applied to ball and gate valves; pulp and paper industry with coatings to rolls and blades; aerospace industry, where coatings are used for turbine vanes as bond coats for

thermal barrier coatings, turbine sections, landing gears; and automotive industry, which applications include piston rings and cylinder bores [16]. Even some ceramic coatings, which have been previously sprayed by plasma process, are sometimes applied by HVOF spray method. Also raw materials with small-scale component, e.g., nanosized carbides, have enhanced the HVOF coating properties and potential applications as well. In the following, examples of HVOF coating applications and materials are briefly presented.

Typical HVOF coating materials are metals and cermets. Variety of materials is almost endless, and therefore the application areas are wide among different industries. At a very low porosity, below 1 %, HVOF coatings are suitable for protecting the substrate material against corrosion. Because of high hardness combined with high bond strength to the substrate and good inter-lamellar bonding, the use of HVOF coatings is extensive for wear protection applications, such as paper and pulp processing rolls and other wear-resistant parts in paper machines. Increased use of ceramics, and their dielectrical and thermal properties, has opened the door for HVOF coating use in electrical applications and as environmental barrier coatings (EBCs) in power and aerospace industry.

Applications, where coatings are used for protection from wear and friction, are very broad with HVOF technique. HVOF hardmetal coatings containing carbides and/or nitrides, such as WC-CoCr, WC-$(W,Cr)_2C$-Ni, and (Ti,Mo)(C,N)-Ni/Co, have very good hardness and tribological properties and hence are suitable for wear protection of machine parts [70]. HVOF sprayed WC-Co/NiCrFeSiB coating with high hardness values and low porosity has been studied for use in coal-fired power plant piping against erosion [71]. Due to brittle nature of the hard metal coating, the applications and conditions must be carefully chosen.

In the energy industry, especially power plant boilers experience both high temperature corrosion and erosion, and HVOF coatings can be applied to protect the tubing in the boilers, especially in the superheater area. HVOF sprayed NiCr and Cr_3C_2-20NiCr coatings have proven very good high temperature corrosion resistance in biomass fired boiler exposures [72]. NiCrBSi and Stellite-6 coatings tested in coal-fired boilers have shown good hot corrosion resistance [73]. HVOF coatings, such as NiCrSiB and Ni-Cr-Fe-Nb-Mo alloys, for high temperature erosion and corrosion protection have been widely used in waste-to-energy plants in order to [74]. Thermal barrier coatings (TBCs) are used for enhancing the service life of gas turbines and diesel engine components. The ceramic coatings are mainly manufactured with atmospheric plasma spraying (APS) due to high melting temperature of the materials, but the applied bond coats under the APS ceramic coatings to improve adhesion are increasingly made by HVOF technique, bond coat materials being e.g., CoNiCrAlY, NiCoCrAlTaY, NiCrAlY, or NiCr [75].

Different material forming techniques require use of coatings, as the components deteriorate easily in the processes. Deep-drawing is a widely used sheet metal forming process in the aircraft and automotive industries. High tribological demands of the forming tools can be fulfilled with HVOF cermet coatings, such as superfine structured WC-Co, which has high hardness enhancing sliding and abrasive wear [2]. HVOF coatings have been studied for the protection and upgrade of aluminum injection mould tooling, particularly for the low-cost and flexible manufacture of automotive components. Smooth, hard and very well bonded coatings with low porosity and homogeneous microstructure have been manufactured from WC-CoCr, and Cr_2C_3-NiCr through careful optimization of deposition [76]. Steel sheet continuous hot-dip galvanizing bath with molten metal is a very

detrimental process for the galvanizing components. Three different high temperature corrosion resistant HVOF coating types have been applied to galvanizing bath components. These include WC-Co, oxide-based, and quite recently developed MoB/CoCr coatings [77]. Optimization of the coating composition and microstructure is of utmost importance in order to extend the operating lifetime of the galvanizing hardware. Also bond coats may be used because of the mismatch between coating and substrate material. HVOF WC-CoCr cermet coatings on aluminum substrate could be used for plastic injection moulds due to high hardness, low sliding wear, low porosity, and good endurance against impacts [78]. MoCoB-Co/Cr cermet coating could be used for protection of glass sheet forming moulds because it has excellent high temperature properties, such as low friction coefficient to glass, oxidation resistance, and low mechanical abrasion [79].

Hard chromium plating has been an excellent and very widely used technique, but due to carcinogenic effect of hexavalent chrome ion (Cr^{6+}) in the manufacturing process, finding substituting solutions for the technique has been extensively studied during the last decade and possibilities of thermal spray coatings have been explored as replacer. HVOF Co-base alloy Tribaloy-800 coating has shown good friction and wear properties also in high temperature (500 °C) [1]. Due to good durability of the coating, it could be used for the protection of machine components vulnerable to frictional heat and wear, e.g., sliding surfaces such as high-speed spindle. To replace hard chromium coatings in applications under erosion-corrosion exposure, both HVOF sprayed WC-Ni and Cr_3C_2-NiCr have been tested to be promising alternatives for those conditions [80]. Cr_3C_2-NiCr HVOF coatings manufactured from fine-scale and nano-fractioned powders have proved to have very good mechanical, wear and corrosion properties, and could therefore be used as substitute to hard chromium coating in applications such as cylinders in earth moving machines and piston rings and valve stems applications in automotive industry [81,82]. HVOF coatings can be applied to landing gears in aircrafts to replace the hard chromium coatings. The HVOF process provides high hardness, good wear strength and better resistance to fatigue with WC-CrC-Ni coating compared to hard chromium coating [83].

Other versatile applications for HVOF coating include magnetic and biomedical use. HVOF sprayed ferromagnetic Fe-Si based deposits, which have been produced from nanostructured powder, can be used in several magnetic applications even at high temperatures [84]. HVOF hydroxyapatite (HAp) coatings are applied in various biomedical applications due to excellent biocompatibility of HAp [85]. Use of nanostructured Hap has been studied for biomedical use and the results are promising, as the coating exhibits high density and crystallinity, and good microstructural uniformity [86]. In the biomedical field, HVOF-sprayed nanostructured titania coatings could be used for prosthetic devices and other applications, where superior mechanical behavior is required [87].

6. Summary and Conclusions

In this work, HVOF thermal spray techniques have been reviewed. HVOF techniques have significantly developed over the last two decades and new modifications and improvements of the technology have been introduced on the market. The latest developments in spray technology also take advantage of the developments that have occurred in powder production, especially in nanostructured powders. However, in order to fully exploit the excellent properties of HVOF coatings, it is emphasized that optimization of the spraying process is a must. As compared to APS coatings, HVOF

coatings offer a number of advantages in terms of coating microstructure and properties resulting in improved performance in many applications. This holds especially true for metal and cermet coatings. For the deposition of ceramic coating, HVOF process offers improvements of coating quality in spraying of ceramics such as alumina. However, deposition efficiency of HVOF spray is typically lower than that of APS, and may hinder the wider use of the HVOF in many applications despite the clear improvement of properties.

HVOF coatings are nowadays applied in a variety of industries. Major application areas are within industries where coatings are used for protection from wear, friction and corrosion. Other applications for HVOF coatings include, e.g., magnetic and biomedical use.

Acknowledgments

The authors wish to express their gratitude to Sanjay Sampath and Stony Brook University for fruitful co-operation.

References

1. Cho, J.Y.; Zhang, S.H.; Cho, T.Y.; Yoon, J.H.; Joo, Y.K.; Hur, S.K. The processing optimization and property evaluations of HVOF Co-base alloy T800 coating. *J. Mater. Sci.* **2009**, *44*, 6348-6355.
2. Tillmann, W.; Vogli, E.; Baumann, I.; Kopp, G.; Weihs, C. Desirability-Based Multi-Criteria Optimization of HVOF Spray Experiments to Manufacture Fine Structured Wear-Resistant $75Cr_3C_2$-25(NiCr20) Coatings. *J. Therm. Spray Technol.* **2010**, *19*, 392-408.
3. Mostaghimi, J.; Chandra, S.; Ghafouri-Azar, R.; Dolatabadi, A. Modeling thermal spray coating processes: A powerful tool in design and optimization. *Surf. Coat. Technol.* **2003** *163-164*, 1-11.
4. Dongmo, E.; Wenzelburger, M.; Gadow, M. Analysis and optimization of the HVOF process by combined experimental and numerical approaches. *Surf. Coat. Technol.* **2008**, *202*, 4470-4478.
5. Bansal, P.; Shipway, P.H.; Leen, S.B. Residual stresses in high-velocity oxy-fuel thermally sprayed coatings—Modelling the effect of particle velocity and temperature during the spraying process. *Acta Mater.* **2007**, *55*, 5089-5101.
6. Sampath, S.; Jiang, X.; Kulakarni, A.; Matejicek, J.; Gilmore, D.L.; Neiser, R.A. Development of process maps for plasma spray: Case study for molybdenum. *Mater. Sci. Eng. A* **2003**, *348*, 54-66.
7. Turunen, E.; Varis, T.; Gustafsson, T.E.; Keskinen, J.; Fält, T.; Hannula, S.-P. Parameters optimization of HVOF sprayed nanostructured alumina and alumina-nickel composite coatings. *Surf. Coat. Technol.* **2006**, *200*, 4987-4994.
8. Vaidya, A.; Srinivasan, V.; Streibl, T.; Friis, M.; Chi, W.; Sampath, S. Process maps for plasma spraying of yttria-stabilized zirconia: An integrated approach to design, optimization and reliability. *Mater. Sci. Eng. A* **2008**, *497*, 239-253.
9. Zhang, W.; Sampath, S.A. Universal method for representation of in-flight particle characteristics in thermal spray processes. *J. Therm. Spray Technol.* **2009**, *18*, 23-34.
10. Valarezo, A.; Choi, W.B.; Chi, W.; Gouldstone, A.; Sampath, S. Process control and characterization of NiCr coatings by HVOF-DJ2700 system: A process map approach. *J. Therm. Spray Technol.* **2010**, *19*, 852-865.

11. Fauchais, P.; Vardelle, M. Sensors in spray processes. *J. Therm. Spray Technol.* **2010**, *19*, 668-694.
12. Sampath, S.; Srinivasan, V.; Valarezo, A.; Vaidya, A.; Streibl, T. Sensing, control, and *in situ* measurement of coating properties: An integrated approach toward establishing process-property correlations. *J. Therm. Spray Technol.* **2009**, *18*, 243-255.
13. *Handbook of Thermal Spray Technology*; Davis, J.R., Ed.; ASM International: Materials Park, OH, USA, 2004; pp. 338.
14. Vaidya, A.; Streibl, T.; Li, L.; Sampath, S.; Kovarik, O.; Greenlaw, R. An integrated study of thermal spray process-structure-property correlations: A case study for plasma sprayed molybdenum coatings. *Mater. Sci. Eng. A* **2005**, *403*, 191-204.
15. Turunen, E.; Varis, T.; Hannula, S.-P.; Vaidya, A.; Kulkarni, A.; Gutleber, J.; Sampath, S.; Herman, H. On the role of particle state and deposition procedure on mechanical, tribological and dielectric response of high velocity oxy-fuel sprayed alumina coatings. *Mater. Sci. Eng. A* **2006**, *415*, 1-11.
16. Dwivedi, G.; Wentz, T.; Sampath, S.; Nakamura, T. Assessing process and coating reliability through monitoring of process and design relevant coating properties. *J. Therm. Spray Technol.* **2010**, *19*, 695-712.
17. Hannula, S.-P.; Suhonen, T.; Varis, T.; Turunen, E. Challenges in processing and characterization of thermal sprayed coatings. In *Proceedings of "Product Property Prediction—P3" Conference*, Dortmund, Germany, 12–13 April 2010; p. 12.
18. Vaidya, A.; Bancke, G.; Sampath, S.; Herman, H. Influence of process variables on the plasma sprayed coatings—An integrated study. In *Proceedings of International Thermal Spray Conference*, Singapore, Singapore, 28–30 May 2001; pp. 1345-1349.
19. Matejicek, J.; Sampath, S. *In-situ* measurements of residual stresses and elastic moduli in thermal sprayed coatings: Part 1: Apparatus and analysis. *Acta Mater.* **2003**, *51*, 863-872.
20. Fisher-Cripps, A.C. *Nanoindentation*, 2nd edition, Mechanical Engineering Series; Springer: New York , NY, USA, 2004, p.263.
21. EN ISO 4516:2002. Metallic and other inorganic coatings. In *Vickers and Knoop Microhardness Tests?*; European Committee for Standardization: City, Country 2002.
22. Suhonen, T.; Varis, T.; Turunen, E.; Liu, X.; Yanling, G.; Söderberg, O.; Hannula, S.-P. Modelling the effect of microstructure on mechanical properties of HVOF sprayed WC-CoCr coatings. In *Proceedings of WMRIF Workshop for Young Scientists*, Tsukuba, Japan, 22–25 July 2008.
23. ASTM E 1876-09. *Standard Test Method for Dynamic Young's Modulus, Shear Modulus, and Poisson's Ratio by Impulse Excitation of Vibration*. American Society for Testing and Materials: West Conshohocken, PA, USA, 2009.
24. ENV 843-2:1997. *Advanced Technical Ceramics—Monolithic Ceramics, Mechanical Properties at Room Temperature—Part 2: Determination of Elastic Moduli*. European Committee for Standardization: City, Country1997.
25. Oliver, W.C.; Pharr, G.M. An improved technique for determining hardness and elastic modulus using load and displacement sensing indentation experiments. *J. Mater. Res.* **1992,** *7*, 1564-1583.

26. Griffith, A.A. The phenomena of rupture and flow in solids. *Phil. Trans. Roy. Soc. London* A **1920**, *221*, 163-198 (This article has been republished with additional commentary in Trans. ASM 61, 871, 1968).
27. JIS R 1688:2005. *Testing Method for Fracture Toughness of Porous Fine Ceramics*; Japanese Standards Association: Tokyo, Japan, 2005.
28. Deshpande, S.; Kulkarni, A.; Sampath, S.; Herman, H. Application of image analysis for characterization of porosity in thermal spray coatings and correlation with small angle neutron scattering. *Surf. Coat. Technol.* **2004**, *187*, 6-16.
29. Fowler, D.B.; Riggs, W.; Russ, J.C. Inspecting thermal sprayed coatings. *Adv. Mater. Proc.* **1990**, *11*, 41-52.
30. Komatsu, M.; Kuroda, S.; Sodeoka, S.; Sakoda, N.; Lee, S.W. Porosity measurement of thermal sprayed ceramic coatings by SEM cross sectional photography and image analysis—Round Robin test for ISO standardization. In *Proceedings of Asian Thermal Spray Conference*, Xi'an, China, 22–24 October 2009.
31. Mailhot, K.; Gitzhofer, F.; Boulos, M.I. Absolute coating porosity measurement using image analysis. In *Proceedings of the 15th ITSC*, Nice, France, 1998; Volume 1, pp. 917-922.
32. Final Report. *Aircraft Accident Investigation of Copterline Oy, Sikorsky S-76C+ in Tallinn Bay, Estonia on 10th August 2005*. Ministry of Economic Affairs and Communications, Estonia. 6 August 2008. Retrieved 11 August 2008.
33. EN 582:1993. *Determination of Tensile Adhesive Strength*; European Committee for Standardization: City, country1993.
34. Marot, G.; Lesage, J.; Démarécaux, P.H.; Hadad, M.; Siegmann, St.; Staia, M.H. Interfacial indentation and shear tests to determine the adhesion of thermal spray coatings. *Surf. Coat. Technol.* **2006**, *201*, 2080-2085.
35. Noyan, I.C.; Cohen, J.B. *Residual Stress—Measurement by Diffraction and Interpretation*; Springer-Verlag: New York, NY, USA, 1987; p. 626.
36. Pina, J.; Dias, A.; Lebrun, J.L. Mechanical stiffness of thermally sprayed coatings and elastic constants for stress evaluation by X-ray diffraction. *Mater. Sci. Eng. A* **1999**, *267*, 130-144.
37. Matejicek, J.; Sampath, S. *In-situ* measurements of residual stresses and elastic moduli in thermal sprayed coatings: Part 1: Apparatus and analysis, *Acta Mater.* **2003**, *51*, 863-872.
38. ASTM G75-95. *Standard Test Method for Determination of Slurry Abrasivity (Miller Number) and Slurry Abrasion Response of Materials (SAR Number)*; American Society for Testing and Materials: West Conshohocken, PA, USA, 1995.
39. Verdon, C.; Karimi, A.; Martin, J.-L. A study of high velocity oxy-fuel thermally sprayed tungsten carbide based coatings. Part 1: Microstructures. *Mater. Sci. Eng. A* **1998**, *246*, 11-24.
40. Stewart, D.A.; Shipway, P.H.; McCartney, D.G. Influence of heat treatment on the abrasive wear behavior of HVOF sprayed WC-Co coatings. *Surf. Coat. Technol.* **1998**, *105*, 13-24.
41. Li, X.M.; Yang, Y.Y.; Shao, T.M.; Jin, Y.S.; Barbezat, G. Impact wear performances of Cr_3C_2—NiCr coatings by plasma and HVOF spraying. *Wear* **1997**, *202*, 208-214.
42. Jones, M.; Horlock, A.J.; Shipway, P.H.; McCartney D.G.; Wood, J.V. A comparison of the abrasive wear behaviour of HVOF sprayed titanium carbide and titanium boride-based cermet coatings, *Wear* **2001,** *251*, 1009-1016.

43. Horlock, A.J.; McCartney, D.G.; Shipway, P.H.; Wood, J.V. Thermally sprayed Ni(Cr)-TiB2 coatings using powder produced by self-propagation high temperature synthesis: Microstructure and abrasive wear behaviour, *Mater. Sci. Eng. A* **2002**, *336*, 88-98.
44. Wang, B.-Q. The dependence of erosion—Corrosion wastage on carbide/metal binder proportion for HVOF carbide-metal cermet coatings, *Wear* **1996**, *196*,141-146.
45. Hawthorne, H.M.; Arsenault, B.; Immarigeon, J.P.; Legoux, J.G.; Parameswaran, V.R. Comparison of slurry and dry erosion behaviour of some HVOF thermal sprayed coatings, *Wear* **1999**, *225-229*, 825-834.
46. Mann, B.S.; Arya, V. Abrasive and erosive wear characteristics of plasma nitriding and HVOF coatings: Their application in hydro turbines. *Wear* **2001**, *249*, 354-360.
47. Berget, J.; Rogne, T.; Bardal, E. Erosion-corrosion properties of different WC-Co-Cr coatings deposited by the HVOF process—Influence of metallic matrix composition and spray powder size distribution. *Surf. Coat. Technol.* **2007**, *201*, 7619-7625.
48. Zhou, Z.; Wang, L.; Wang, F.C.; Zhang, H.F.; Liu, Y.B.; Xu, S.H. Formation and corrosion behavior of Fe-based amorphous metallic coatings by HVOF thermal spraying, *Surf. Coat. Technol.* **2009**, *204*, 563-570.
49. Lima, R.S.; Marple, B.R. From APS to HVOF spraying of conventional and nanostructured titania feedstock powders: A study on the enhancement of the mechanical properties, *Surf. Coat. Technol.* **2006**, *200*, 3428-3437.
50. Turunen, E.; Varis, T.; Gustafsson, T.; Keskinen, J.; Lintunen, P.; Fält, T.; Nowak, R.; Hannula, S.-P. Process optimization for nanostructured HVOF-sprayed Al_2O_3-based ceramic coatings, *Key. Eng. Mater.* **2006**, *317-318*, 545-554.
51. Turunen, E.; Varis, T.; Keskinen, J.; Fält, T.; Hannula, S.-P. Improved mechanical properties by nanoreinforced ceramic composite HVOF coatings, *Adv. Sci. Technol.* **2006**, *45*, 1240-1245.
52. Turunen, E.; Hirvonen, A.; Varis, T.; Fält, T.; Hannula, S.-P.; Sekino, T.; Niihara K. Application of HVOF techniques for spraying of ceramic coatings. *Adv. Technol. Mater.* **2007**, *9*, 63-68.
53. Bolelli, G.; Lusvarghi, L.; Manfredini, T.; Mantini, P.F.; Polini, R.; Turunen, E.; Varis, T.; Hannula, S.-P. Comparison between plasma- and HVOF-sprayed ceramic coatings. Part I: Microstructure and mechanical properties. *Int. J. Surf. Sci. Eng.* **2007**, *1*, 38-61.
54. Brandl, W.; Toma, D.; Krüger, J.; Grabke, H.J.; Matthäus, G. The oxidation behaviour of HVOF thermal-sprayed MCrAlY coatings. *Surf. Coat. Technol.* **1997**, *93-95*, 21-26.
55. Gil, L.; Staia, M.H. Influence of HVOF parameters on the corrosion resistance of NiWCrBSi coatings. *Thin Solid Films* **2002**, *420-421*, 446-454.
56. Zhao, W.-M.; Wang, Y.; Dong, L.-X.; Wu, K.-Y.; Xue, J. Corrosion mechanism of NiCrBSi coatings deposited by HVOF. *Surf. Coat. Technol.* **2005**, *190*, 293-298.
57. Kawakita, J.; Kuroda, S.; Kodama, T. Evaluation of through-porosity of HVOF sprayed coating. *Surf. Coat. Technol.* **2003**, *166*, 17-23.
58. Chidambarama, D.; Clayton, C.; Dorfman, M. Evaluation of the electrochemical behavior of HVOF-sprayed alloy coatings. *Surf. Coat. Technol.* **2004**, *176*, 307-317.
59. Chidambarama, D.; Claytona, C.R.; Dorfman, M.R. Evaluation of the electrochemical behavior of HVOF-sprayed alloy coatings—II. *Surf. Coat. Technol.* **2005**, *192*, 278-283.

60. Rastegar, F.; Richardson, D.E. Alternative to chrome: HVOF cermet coatings for high horse power diesel engines. *Surf. Coat. Technol.* **1997**, *90*, 156-163.
61. Nascimento, M.P.; Souza, R.C.; Miguel, I.M.; Pigatin, W.L.; Voorwald, H.J.C. Effects of tungsten carbide thermal spray coating by HP/HVOF and hard chromium electroplating on AISI 4340 high strength steel. *Surf. Coat. Technol.* **2001**, *138*, 113-124.
62. Sahraoui, T.; Fenineche, N.-E.; Montavon, G.; Coddet, C. Alternative to chromium: Characteristics and wear behavior of HVOF coatings for gas turbine shafts repair (heavy-duty), *J. Mater. Processing Technol.* **2004**, *152*, 43-55.
63. Guilemany, J.M.; Espallargas, N.; Suegama, P.H.; Benedetti, A.V. Comparative study of Cr_3C_2-NiCr coatings obtained by HVOF and hard chromium coatings. *Corros. Sci.* **2006**, *48*, 2998-3001?.
64. Bolelli, G.; Cannillo, V.; Lusvarghi, L.; Ricco, S. Mechanical and tribological properties of electrolytic hard chrome and HVOF-sprayed coatings. *Surf. Coat. Technol.* **2006**, *200*, 2995-3009.
65. Bolelli, G.; Lusvarghi, L.; Manfredini, T.; Mantini, P.F.; Turunen, E.; Varis, T.; Hannula, S.-P. Comparison between plasma- and HVOF-sprayed ceramic coatings. Part II: Tribological behaviour. *Int. J. Surf. Sci. Engin.* **2007**, *1*, 62-79.
66. Guilemany, J.M.; Espallargas, N.; Suegama, P.H.; Benedetti, A.V. Comparative study of Cr3C2-NiCr coatings obtained by HVOF and hard chromium coatings. *Corros. Sci.* **2006**, *48*, 2998-3013.
67. Sidhu, T.S.; Prakash, S.; Agrawal, R.D. Evaluation of hot corrosion resistance of HVOF coatings on a Ni-based superalloy in molten salt *environment, Mater. Sci. Eng. A* **2006**, *430*, 64-78.
68. Sidhu, H.S.; Sidhu, B.S.; Prakash, S. The role of HVOF coatings in improving hot corrosion resistance of ASTM-SA210 GrA1 steel in the presence of Na_2SO_4-V_2O_5 salt deposits. *Surf. Coat. Technol.* **2006**, *200*, 5386-5394.
69. Stewart, D.A.; Shipway, P.H.; McCartney, D.G. Abrasive wear behaviour of conventional and nanocomposite HVOF-sprayed WC–Co coatings. *Wear* **1999**, *225-229*, 789-798.
70. Berger, L.M.; Woydt, M.; Saaro, S. Comparison of self-mated hardmetal coatings under dry sliding conditions up to 600 °C. *Wear* **2009**, *266*, 406-416.
71. Ramesh, M.R.; Prakash, S.; Nath, S.K.; Sapra, P.K.; Venkataraman, B. Solid particle erosion of HVOF sprayed WC-Co/NiCrFeSiB coatings. *Wear* **2010**, *269*, 197-205.
72. Oksa, M.; Kärki, J.; Varis, T.; Turunen, E. Corrosion resistance of HVOF coatings in a biofuel boiler plant. In *Proceedings of EUROCORR 2005 The European Corrosion Congress*, Lissabon, Country,4–8 September 2005; p. 9.
73. Sidhu, T.S.; Prakash, S.; Agrawal, R.D. Studies of the metallurgical and mechanical properties of high velocity oxy-fuel sprayed stellite—6 coatings on Ni- and Fe-based superalloys. *Surf. Coat. Technol.* **2006**, *201*, 273-281.
74. Kawahara, Y. Application of high temperature corrosion-resistant materials and coatings under severe corrosive environment in waste-to-energy boilers. *J. Therm. Spray Technol.* **2007**, *16*, 202-213.
75. Lima, C.R.C.; Guilemany, J.M. Adhesion improvements of thermal barrier coatings with HVOF thermally sprayed bond coats. *Surf. Coat. Technol.* **2007**, *201*, 4694-4701.
76. Gibbons, G.J.; Hansell, R.G. Thermal-sprayed coatings on aluminium for mould tool protection and upgrade. *J. Mater. Process. Technol.* **2008**, *204*, 184-191.

77. Matthews, S.; James, B. Review of thermal spray coating applications in the steel industry: Part 2—Zinc pot hardware in the continuous galvanizing line. *J. Therm. Spray Technol.* **2010**, *19*, 1277-1286.
78. Bolelli, G.; Lusvarghi, L.; Barletta, M. HVOF-sprayed WC-CoCr coatings on Al alloy: Effect of the coating thickness on the tribological properties. *Wear* **2009**, *267*, 944-953.
79. Hamashima, K. Application of new boride cermet coating to forming of glass sheets. *J. Therm. Spray Technol*. **2007**, *16*, 32-33.
80. Espallargas, N.; Berget, J.; Guilemany, J.M.; Benedetti, A.V.; Suegama, P.H. Cr_3C_2-NiCr and WC-Ni thermal spray coatings as alternatives to hard chromium for erosion-corrosion resistance. *Surf. Coat. Technol.* **2008**, *202*, 1405-1417.
81. Fedrizzi, L.; Rossi, S.; Cristel, R.; Bonora, P.L. Corrosion and wear behaviour of HVOF cermet coatings used to replace hard chromium. *Electrochim. Acta* **2004**, *49*, 2803-2814.
82. Picas, J.A.; Fornand, A.; Matthäus, G. HVOF coatings as an alternative to hard chrome for pistons and valves. *Wear* **2006**, *261*, 477-484.
83. Bonora, R.G.; Voorwald, H.J.C.; Cioffi, M.O.H.; Junior, G.S.; Santos, L.F.V. Fatigue in AISI 4340 steel thermal spray coating by HVOF for aeronautic application. *Procedia Engin.* **2010**, *2*, 1617-1623.
84. Cherigui, M.; Fenineche, N.E.; Ji, G.; Grosdidier, T.; Coddet C. Microstructure and magnetic properties of Fe-Si-based coatings produced by HVOF thermal spraying process. *J. Alloys Compd.* **2007**, *427*, 281-290.
85. Gadow, R.; Killinger, A.; Stiegler, N. Hydroxyapatite coatings for biomedical applications deposited by different thermal spray techniques. *Surf. Coat. Technol.* **2010**, *205*, 1157-1164.
86. Lima, R.S.; Khor, K.A.; Li, H.; Cheang, P.; Marple, B.R. HVOF spraying of nanostructured hydroxyapatite for biomedical applications. *Mater. Sci. Eng. A* **2005**, *396*, 181-187.
87. Gaona, M.; Lima, R.S.; Marple, B.R. Influence of particle temperature and velocity on the microstructure and mechanical behaviour of high velocity oxy-fuel (HVOF)-sprayed nanostructured titania coatings. *J. Mater. Process. Technol*. **2008**, *198*, 426-435.

PUBLICATION II

Optimizing NiCr and FeCr HVOF coating structure for high temperature corrosion protection applications

In: Journal of Thermal Spray Technology (2014),
published online 20.11.2014.

PUBLICATION III

Thermal spray coatings for high temperature corrosion protection in biomass co-fired boilers

In: Journal of Thermal Spray Technology (2014),
published online 24.9.2014.

PUBLICATION IV

Nickel-based HVOF coatings promoting high temperature corrosion resistance of biomass-fired power plant boilers

In: Fuel Processing Technology 125 (2014) 236–245.

Fuel Processing Technology 125 (2014) 236–245

Contents lists available at ScienceDirect

Fuel Processing Technology

journal homepage: www.elsevier.com/locate/fuproc

Nickel-based HVOF coatings promoting high temperature corrosion resistance of biomass-fired power plant boilers

Maria Oksa *, Pertti Auerkari, Jorma Salonen, Tommi Varis

VTT Technical Research Centre of Finland, P.O. Box 1000, 02044 VTT Espoo, Finland

ARTICLE INFO

Article history:
Received 18 November 2013
Received in revised form 4 April 2014
Accepted 5 April 2014
Available online 3 May 2014

Keywords:
Thermal spray coating
HVOF
High temperature corrosion
Biomass combustion
Corrosion protection
Chlorine induced corrosion

ABSTRACT

There are over 1000 biomass boilers in Europe, and the number is increasing due to actions for reducing greenhouse gas emissions. Biomass boilers often experience strong corrosion due to harmful elements in fuels. In biomass burning, detrimental components include especially chlorine, potassium and heavy metals, which can cause chlorine-induced active oxidation or hot corrosion by molten phases even at fairly low temperatures. In order to increase the corrosion resistance of heat exchanger components, either more alloyed steels or protective coatings should be applied. High velocity oxy-fuel (HVOF) sprayed coatings may provide corrosion protection for low alloy tube materials. Three nickel based thermal spray coatings (Ni–24Cr–16.5Mo, Ni–22Cr<5Fe–9Mo–4Nb and Ni–22Cr–10Al–1Y) were tested for two years in a 40 MW circulating fluidized boiler (CFB), which had experienced severe corrosion and a tube failure. The coated tubes were installed to the cold and the hot economizer. After the exposure the coatings and the substrate materials were analyzed with SEM–EDX. The uncoated boiler tubes corroded strongly, whereas the thermal spray coatings exhibited excellent corrosion performance. This paper presents the tube failure at the cold economizer, exposure conditions, the analysis of the coated and uncoated samples, and the corrosion mechanisms of the steel tubes.

1. Introduction

Strong actions are needed to decrease the greenhouse gas emissions globally. To prevent severe impacts of climate change, the international community has agreed that global warming should be kept below 2 °C compared to the temperature in pre-industrial times, which means a temperature increase of maximum 1.2 °C above today's level. In Europe, there are several EU initiatives to reduce the emissions: the European Climate Change Programme (ECCP), which has led to the implementation of dozens of new policies and measures; the EU Emissions Trading System, which has become the EU's key tools for reducing the emissions from the industry cost-effectively; and legislation to raise the share of energy consumption produced by renewable energy sources, such as wind, solar and biomass, to 20% by 2020 [1].

There are over 1000 power plant boilers for biomass combustion in Europe, and the number is increasing [2]. Typical biomass fuels include wood, consisting of energy wood, forest residues and waste wood, black liquor, agricultural biomass such as energy plants, various types of grass or reeds, and residues/waste. Until today, wood is still the most important fuel for generating electricity from solid biomass. However, strong corrosion of boiler components can take place when burning biomass due to corrosive elements in fuels. These include alkali chlorides, KCl and NaCl, and elements forming low melting compounds e.g. zinc. Commonly, corrosion mechanisms occurring in biomass combustions are chlorine induced enhanced corrosion and hot corrosion by molten compounds [3,4]. The so-called active oxidation occurs in the presence of alkali chlorides as deposits and hydrogen chloride in the atmosphere [5]. Chlorine or chloride penetrates into the oxide–metal interface, where it reacts with the alloy components forming typically $FeCl_2$. The chloride evaporates and during its diffusion to the scale surface is oxidized in the area with higher oxygen vapor pressure forming a non-protective oxide scale. The chlorine is released in the reaction and is able to continue the enhanced corrosion reaction. Active oxidation induced by chlorine is presented in the reaction circuit, Fig. 1. The rate of $FeCl_2$ (g) outward diffusion through the oxide scale is rate controlling for the active oxidation process [5]. The reactions are similar for high chromium alloys. Chlorine reacts with $FeCr_2O_4$ or Cr_2O_3. However, mainly $FeCl_2$ is formed because of lower Gibbs free energy of $FeCl_2$ compared to $CrCl_2$ [5].

Molten phases in the deposits may result to oxide scale fluxing and hence strong corrosion, when the protective oxide scale is damaged and formation of the new scale is hindered. Elements in the combustion process forming low-melting phases include calcium-, potassium-, and sodium-sulfates and potassium- and sodium-chlorides containing heavy metals such as zinc and lead [6,7]. Copper in the presence of chlorine has also been reported to act detrimentally in boiler conditions accelerating corrosion of iron and nickel based alloys strongly [8]. Some

* Corresponding author. Tel.: +358 505365844; fax: +358 207227069.
E-mail addresses: maria.oksa@vtt.fi (M. Oksa), pertti.auerkari@vtt.fi (P. Auerkari), jorma.salonen@vtt.fi (J. Salonen), tommi.varis@vtt.fi (T. Varis).

http://dx.doi.org/10.1016/j.fuproc.2014.04.006
0378-3820/

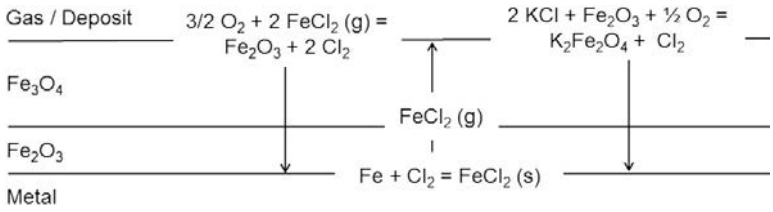

Fig. 1. A schematic illustration of the active oxidation reaction circuit caused by chlorine. The reactions are similar for NaCl. Adapted from [5].

reactions occurring in the presence of chlorine, heavy metals and sulfates are presented in Eqs. (1)–(3).

$$ZnCl_2\,(l) + 2Fe_2O_3 = (Zn, Fe)O + Fe_3O_4 + Cl_2 + ½O_2 \quad (1)$$

[6]

$$2CuCl_2 + O_2 \rightarrow 2CuO + 2Cl_2 \quad (2)$$

[8]

$$(Na, K)_2SO_4 + SO_2 + ½O_2 = (Na, K)_2S_2O_7 \quad (3)$$

[5]

In biomass combustion, protection of metallic boiler components, typically manufactured from carbon or low alloy steels, can be performed by applying high alloy materials or protective coatings. High-chromium alloy steels or nickel alloys have been tested in biomass boiler conditions [9–11]. Applicable coatings for corrosion protection in biomass boilers contain laser cladding [12], thermal spray coatings [13–16] and thermal spray coatings with sealing treatment [17,18]. Thermal spray methods have developed greatly during the last decades, and especially high velocity oxy-fuel method has improved to produce coatings with low porosity and high adhesion, which can be applied to severe high temperature corrosion applications [19].

Strong corrosion and a tube failure had occurred in economizers of a circulating fluidized bed boiler burning biofuel. To increase the corrosion resistance of the heat exchanger surfaces, thermal spray coatings were applied to the boiler tubes. The corrosion behavior of these nickel based coatings has not been reported in similar real biomass boiler conditions. The HVOF coatings with high chromium content were tested for two years in the power plant boiler.

2. Experimental

The tube failure occurred in the biomass boiler was analyzed. Three nickel based coatings with high amounts of chromium were thermally sprayed on short boiler tube sections, which were welded to actual tubes of a fluidized bed boiler. The duration of the exposure in boiler conditions was two years. The corrosion resistance of the coatings and the uncoated substrate material in the boiler conditions were characterized.

2.1. Tube failure

Severe corrosion, tube thinning and renewal of tubing even every second year had taken place in the circulating fluidized bed (CFB) power plant. A leakage also had occurred in the cold economizer of the boiler. The damaged tube, material St35.8, was removed from the boiler, photographed, and made into a cross-section, with subsequent analysis by an optical microscope, a scanning electron microscope, and an EDX analyzer.

2.2. Coating manufacturing and materials for boiler exposure

The coating materials were commercial powders Alloy 59 (NiCr16Mo), Inconel 625 (NiCr9Mo) and NiCrAlY (NiCr10Al). The HVOF spraying was performed with a Sulzer Metco Diamond Jet Hybrid 2701 spray gun. The coatings were applied on a carbon steel tube (St35.8, DIN 17175-79, size: 38 × 5.5 mm). The substrate material was grit blasted with alumina particles (500–700 μm) before the spraying. The goal was to produce sufficient corrosion and erosion resistance by dense and well adhered coatings. The powders are presented in Table 1. The two meter tube sections with coatings were welded to the actual tubes in the boiler in cold and hot economizers. Parameters for the spraying are presented in Table 2. Preheating of the substrate materials was performed up to about 100 °C.

2.3. The boiler exposure

The coating testing took place in a 40 MW circulating fluidized bed (CFB) boiler that burned solid biomass. The district heating power plant had encountered severe problems with corrosion, and the economizer tubes had to be replaced every two years. The test coatings were installed to the hot and the cold economizer, where strong corrosion and a tube failure had occurred. The design of the boiler and locations of the coatings are presented in Fig. 2. In this study, corrosion protection performance by thermal spray HVOF coatings was investigated in the real boiler conditions. The water in-let temperature to the economizers was about 102–115 °C, and the maximum water temperature in the hot economizer was about 200 °C. The temperature of the flue gas before the cold economizer was about 360–400 °C, and before the hot economizer about 520…800 °C. The coating testing in the boiler exposure was for two years. The boiler burned mainly wood-based fuels including recycled wood, mixed with small amounts of peat. The moisture content of the utilized wood was high, over 50%. Analyses of the dry ash are presented in Table 3.

Table 1
Chemical composition of the tested HVOF coating powders and the carbon steel tube material.

Code	Powder	Nominal composition
NiCr16Mo	Alloy 59	Ni–24 Cr–16.5 Mo–1.5 Fe–0.5 Al
NiCr9Mo	Inconel 625, AI-1625-TG	Ni–20…23 Cr –<5 Fe–8…10 Mo–3.15…4.15 Nb–Mn–Si–Ti–Al
NiCr10Al	NiCrAlY, Amperit 413.1	Ni–21…23 Cr–9…11 Al–0.8…1.2 Y
St35.8	Substrate	Fe – <0.17 C–0.10…0.35 Si–0.40…0.80 Mn – <0.040 P – <0.040 S

Table 2
HVOF spray parameters. The spray gun was DJ Hybrid, nozzle 2701.

C_3H_8 [l/min]	O_2 [l/min]	Air [l/min]	N_2 [l/min]	Ratio	Powder feed [g/min]	Stand-off [mm]
56	200	392	20	0.345	25	250

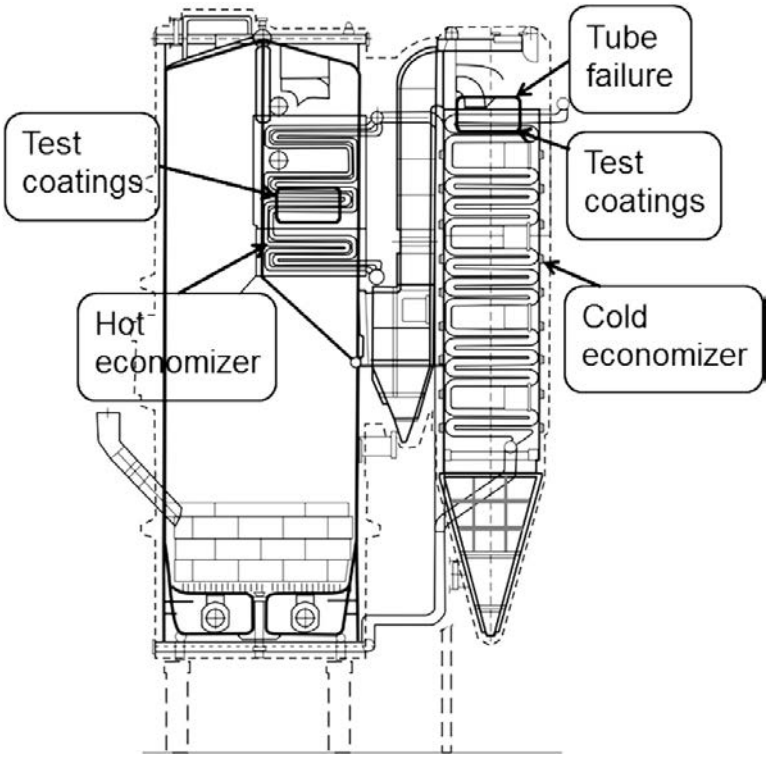

Fig. 2. Schematic image of the CFB boiler design. The locations of the test coatings in the economizers and the tube failure are presented in the figure.

2.4. Sample preparation and analysis

The coated tubes were removed from the boiler after two years and metallographic samples were prepared. The tubes were cut into thin rings, which were cast using epoxy. The coated specimens were cut into cross-sections with a wet cutter due to high hardness of the coatings. Grinding and polishing were performed with ethanol in order to prevent subsequent dissolution of water-soluble compounds. The specimens were studied with an optical microscope and a scanning electron microscope (SEM), and analyzed with an energy dispersive X-ray analyzer (EDX). Optical micrographs were taken from the as-coated specimens. The hardness of the coatings was tested with a Vickers hardness tester (HV0.3) prior the testing from separate samples as well.

3. Results and discussion

The coatings were covered partly with ash deposits, the thickest deposit being on the flue gas side. The endurance of the coatings NiCr16Mo, NiCr9Mo and NiCr10Al against corrosion in the biomass boiler exposure appeared superior compared to the uncoated tubes in the visual inspection of the samples. Thorough analysis of the coatings showed excellent corrosion resistance in the conditions. The carbon steel St35.8 tubes had experienced severe corrosion during the test period. Considerable material wastage had occurred and deep cavities had been formed during the two year usage in the biomass boiler.

Table 3
Elemental analysis of some of the components in the fly ash and the bottom ash (dry solid content).

	Element					
	Fluoride, F^-	Chloride, Cl^-	Sulfate, SO_4^{2-}	Copper, Cu	Lead, Pb	Zinc, Zn
Fly ash [mg/kg]	<100	4400	44,000	160	100	1500
Bottom ash [mg/kg]	<100	200	300	43	11	650

3.1. Tube failure in the cold economizer

A tube failure had occurred in the cold economizer of the biomass boiler. In the damaged tube local thinning was detected besides the leakage hole of about 5 mm in diameter, Fig. 3. The tube was covered with a thin light/brown deposit. The reason for the tube failure was severe corrosion with small erosion effect. The corrosion took place under a deposit on the fireside of the tube. The microstructure was typical for the St35.8 tube (ferrite–pearlite), so the overheating of the tube was ruled out. A high amount of chlorine was detected in the oxide–metal interface under the deposit in the corrosion pits, Fig. 4. Corrosion induced by chlorine was the main reason for severe material wastage of the tube. The chlorine from fuel and high amount of water vapor had probably enhanced the corrosion, which is discussed in Section 3.6 in more detail.

3.2. NiCr16Mo coating in the cold economizer

NiCr16Mo coating was dense with minor porosity. The coating had typical lamellar structure of thermal spraying. The coating was well adhered to the substrate, and only very little lamellar detachment was detected in the coating surface. The thickness of the NiCr16Mo coating was about 300 μm, and the hardness about 460 HV0.3. The cross-section of the NiCr16Mo coating before and after the exposure is presented in Fig. 5a) and d).

Fig. 3. Photograph of the tube failure, which had caused leakage in the cold economizer of a biomass boiler.

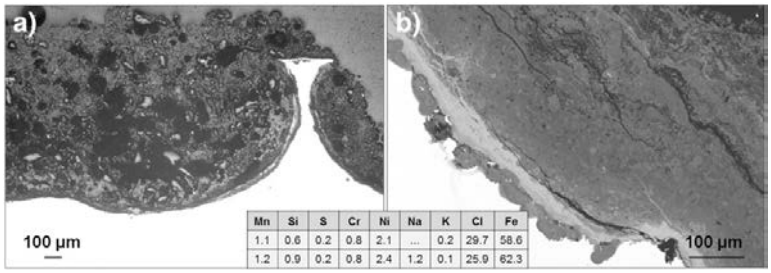

Mn	Si	S	Cr	Ni	Na	K	Cl	Fe
1.1	0.6	0.2	0.8	2.1	...	0.2	29.7	58.6
1.2	0.9	0.2	0.8	2.4	1.2	0.1	25.9	62.3

Fig. 4. a) Optical image and b) SEM image of the cross-section near the tube leakage area. EDX analyses of the corrosion product revealed high amount of chlorine at the metal–oxide interface [w. %].

The corrosion resistance of the NiCr16Mo coating was excellent in the two year biomass boiler testing. The coating showed no sign of corrosion, Fig. 6. The outer layer of the coating consisted of nickel, chromium, molybdenum, oxygen and a small amount of aluminum. Some detachment of the outer lamellas was found in the coating surface, but it had no effect on the corrosion performance. The thick deposit on the coating contained e.g. oxygen, calcium, sulfur, potassium, silicon, phosphorus, iron, aluminum and magnesium. Also manganese, zinc and chlorine were detected in small amounts. Sodium was not found in the deposit. EDX analyses of the deposits on the coatings and uncoated carbon steel are presented in Table 4. The share of the elements indicates that main components in the deposits were probably $CaSO_4$ and K_2SO_4.

3.3. NiCr9Mo coating in the cold economizer

NiCr9Mo coating had similar coating quality as NiCr16Mo with dense structure and sufficient adherence to the substrate with some

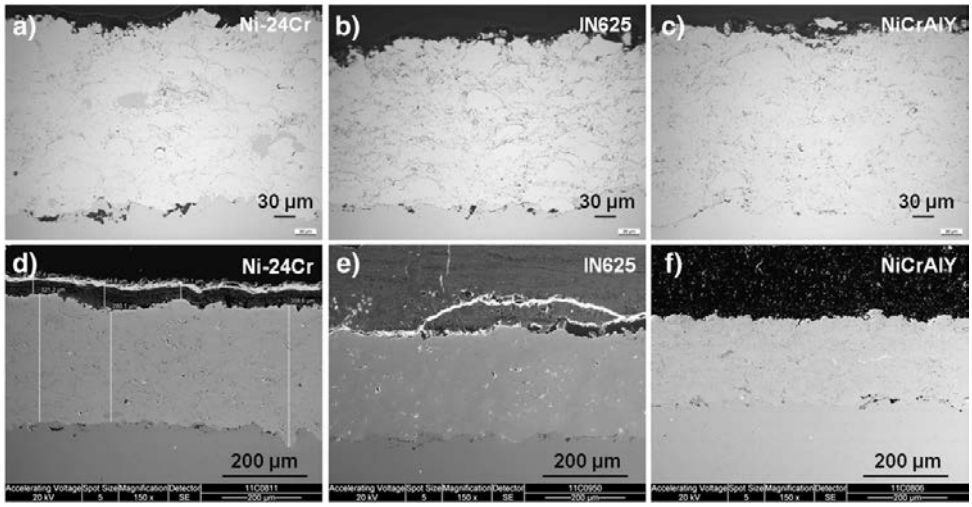

Fig. 5. Optical images of the coating cross-sections before the exposure: HVOF sprayed a) NiCr16Mo, b) NiCr16Mo, and c) NiCr16Mo. SEM images of the coating cross-sections after the two year exposure: d) NiCr16Mo, e) NiCr16Mo, and f) NiCr16Mo.

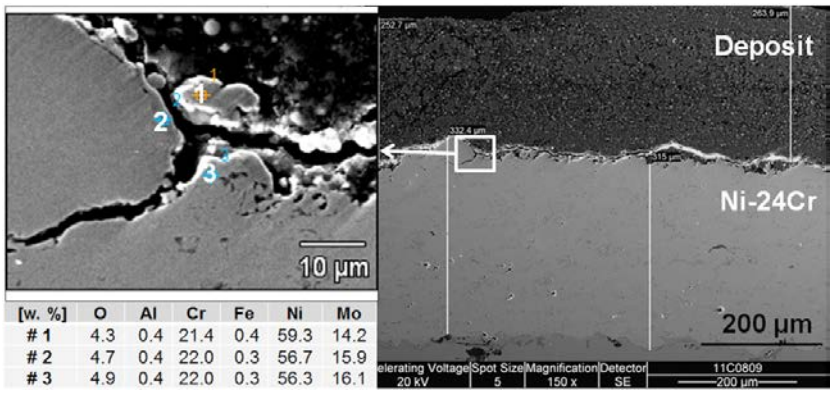

Fig. 6. SEM images of the outer surface of NiCr16Mo coating, which showed excellent corrosion resistance after the two year biomass boiler exposure. Some detachment of the outer lamellas was detected.

closed porosity. The average coating thickness was 300 µm, and the hardness of the NiCr9Mo coating was 506 HV0.3. The structure of the coating is presented in Fig. 5b) and e) before and after the exposure. The corrosion resistance of the NiCr9Mo coating was satisfactory. Only traces of chlorine and potassium were detected in the outer surface of the coating down to some tens of micrometers. There was a thick deposit on the flue gas side of the tube and a thinner one on the leeward side. The NiCr9Mo coating was intact and showed no signs of corrosion, Fig. 7. The thick deposit contained mainly oxygen, calcium, sulfur, potassium, silicon and iron. Corrosive elements such as potassium, chlorine, zinc and sodium were detected in the deposits, especially in the thin layer on the leeward side, Fig. 8.

3.4. NiCr10Al coating in the hot economizer

NiCr10Al coating had high corrosion performance in the biomass boiler conditions and protected the underlying carbon steel tube excellently. The coating was sufficiently dense with low porosity. The thickness of the coating was about 280 µm. The NiCr10Al coating had the highest hardness of these three coatings, about 530 HV0.3. The coating had also a thick deposit on the flue gas side. The composition of the deposit was similar to that of the other two coatings. The cross-section of the coating is presented in Fig. 9.

3.5. Carbon steel St35.8 in the cold and hot economizers

Severe deterioration of the uncoated carbon steel tubes had taken place in the biomass boiler in both the cold and the hot economizer. The tube leakage and stronger tube wall thinning had taken place in the cold economizer. A high amount of chlorine was detected at the metal–scale interface near the leakage. Similar corrosion morphologies have been presented by Spiegel [6] in experiments beneath heavy-metal rich sulfate melts and Montgomery et al. [11] in a reheater of a straw co-firing plant. Spiegel et al. [20] have also reported that the presence of eutectic melts on heat exchanger tubes, e.g. KCl-$ZnCl_2$ and $PbCl_2$, can lead to catastrophic corrosion rates even at relatively low temperatures of 250 °C. Due to low condensation temperature of zinc chlorine (144–302 °C), $ZnCl_2$ may have condensed on the tube surfaces in the upper part of the cold economizer, which has led to severe corrosion and further to leakage [21]. Several millimeters had been lost from the tube wall thickness of St35.8 tubes after the two-year exposure, the thinnest sections being only about 0.9 mm thick, Fig. 10. Thick deposits containing mainly oxygen, calcium, sulfur, potassium and silicon were formed on the tubes. Slightly more zinc was detected in the deposits of the cold economizer than of the hot economizer tubes. Both even and pitting types of corrosion were detected on the samples. Thick, multi-layered porous oxide scales were formed on the leeward side of the tubes. The oxide layers were composed mainly of iron oxide, with small amounts of sulfur, aluminum, manganese, silicon and calcium. Chlorine and potassium were detected in the oxide scale–metal interface. Thick deposits were detected in few locations of the carbon steel tube, mainly on the leeward side. A thin oxide layer was formed below the deposits. In those areas, tube wall had not thinned from the original wall thickness. Minimal corrosion with thin oxide scale on the metal surface observed below the thick deposits is presented in Fig. 11. In the deep corrosion cavities with loose oxide, chlorine was detected together with copper in the oxide–metal interface in the cold economizer, Fig. 12. Salmenoja and Mäkelä and Salmenoja et al. [22, 23] have reported serious corrosion that had occurred in a power boiler firing biofuels. Corrosion scales had layered structure and high chlorine concentrations were detected at the metal–scale interface, which corresponds to the findings in this study. The suggested corrosion mechanism in that case was related to the sulfation of alkali chloride containing deposits by gaseous SO_2. A similar mechanism due to high amounts of potassium and chlorine in the deposits may have enhanced corrosion in this studied case, even though the temperature in the economizer is much lower. Therefore a more apparent mechanism may be related to the presence of zinc and lead chlorides. Severe

Table 4
EDX analyses of the deposits on the coatings and carbon steel [w. %].

Element	O	Ca	S	K	Si	Fe	Mg	Al	P	Na	Mn	Zn	Cl	Ti	Pb
NiCr16Mo[a]	46.2	21.3	15.1	6.1	3.3	1.4	0.8	1.4	1.9	0.6	0.8	0.5	0.5	…	0.2
NiCr9Mo[a]	44.4	21.9	11.9	1.8	6.1	3.3	1.5	2.9	2.6	0.6	1.0	0.8	0.4	0.4	0.5
NiCr10Al[b]	36.2	25.1	13.6	8.5	4.9	1.9	2.1	1.8	2.3	0.6	1.3	0.7	0.5	0.3	0.3
St35.8[a]	36.5	24.6	8.3	7.3	4.5	4.2	4.3	2.4	3.3	0.7	1.9	1.0	0.5	0.4	0.2
St35.8[b]	40.2	20.8	6.3	3.9	8.1	6.2	3.5	4.5	3.0	0.8	1.5	0.4	0.4	0.3	0.2

[a] Cold economizer.
[b] Hot economizer.

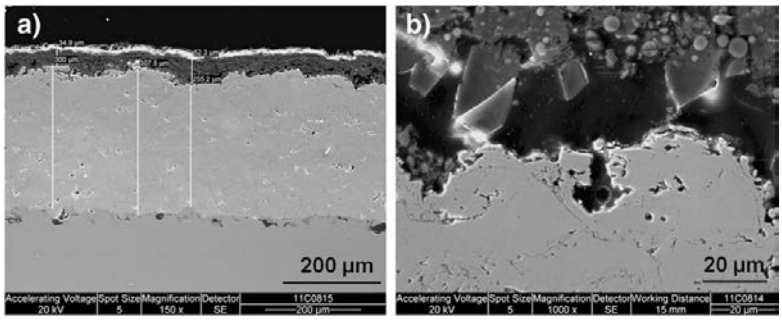

Fig. 7. SEM figures of a) the NiCr9Mo coating under the deposit on the leeward side, and b) outer surface of the NiCr9Mo coating under the thick deposit on the flue gas side of the tube.

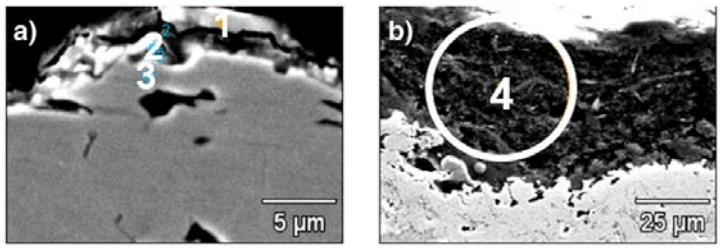

#	O	Na	Al	P	S	K	Ca	Cr	Fe	Ni	Zn	Nb	Mo
1	...	...	78.4	...	2.5	0.9	0.4	5.1	1.4	10.5	...	...	...
2	21.1	1.8	2.0	2.1	...	2.7	0.7	14.5	2.6	39.4	0.2	...	12.3
3	4.4	...	0.5	...	...	...	...	21.6	2.3	59.7	...	2.7	8.6

#	Ca	S	Fe	K	P	Si	Si	Ni	Al	Cl	Ba	Zn	Na	Mn
4	40.4	32.9	8.3	3.4	3.0	2.6	2.6	1.9	1.8	1.1	1.0	0.9	0.9	0.6

Fig. 8. EDX analyses of a) the coating surface of NiCr9Mo, and b) thin deposit on the coating on leeward side, which contained e.g. potassium, chlorine, zinc and sodium.

material wastage occurred especially on the windward side, which implies that alkali chloride–zinc/copper chloride condensation from flue gases on the tube surface may have been the probable cause for the enhanced corrosion. Thin layers containing e.g. sodium, sulfur, potassium and chlorine were present in the oxide–metal interface below the thick oxide scale, Fig. 13. In the hot economizer, similar damage had taken place with deep corrosion pits and loose oxide scales containing chlorine, Fig. 14. An enhanced amount of sulfur was also detected near the oxide–metal interface of the thick oxide layer, Fig. 15.

3.6. Corrosion mechanisms

Severe corrosion had taken place in the economizers of the fluidized bed boiler burning wood based biomass. A tube leakage had also occurred in the cold economizer. The carbon steel St35.8 tubes had thinned strongly up to 78% of the original tube wall thickness. However, only minor oxidation of the metal surface had taken place under the thick, solid deposits, Fig. 11. The boiler atmosphere contained sulfates, chlorides, zinc, copper, lead and fluorides, Table 3. Ash layers consisting

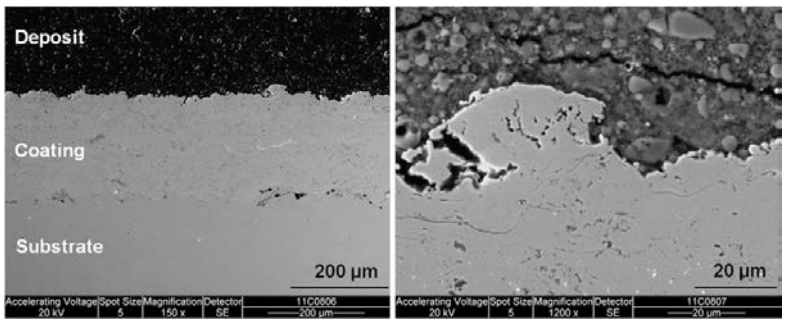

Fig. 9. SEM figures of the cross-section of the NiCr10Al coating below the thick deposit.

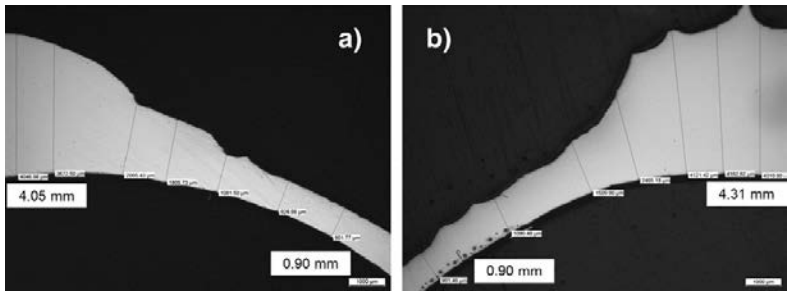

Fig. 10. Images of a cross-section of the St35.8 tube after the exposure in a) the hot economizer and b) the cold economizer. The extremely strong material wastage can clearly be detected in the figures, as the nominal thickness of the tube wall had been 5.5 mm.

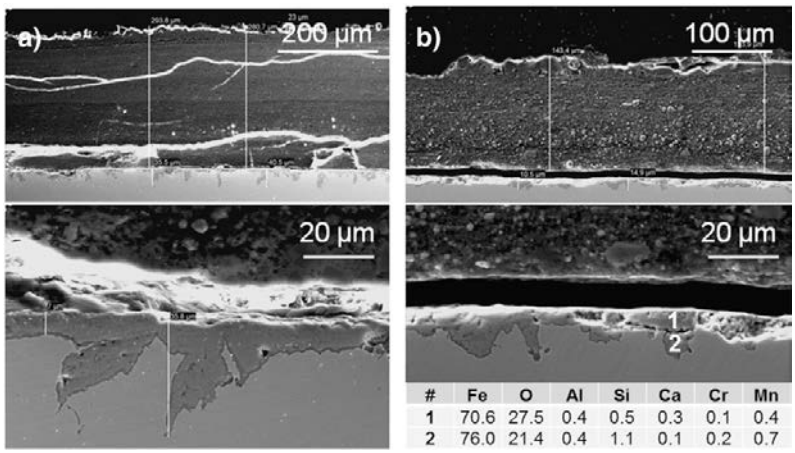

#	Fe	O	Al	Si	Ca	Cr	Mn
1	70.6	27.5	0.4	0.5	0.3	0.1	0.4
2	76.0	21.4	0.4	1.1	0.1	0.2	0.7

Fig. 11. a) Thin oxide layer penetrating into metal on the St35.8 tube below the thick deposit in the cold economizer. b) Composition of the thin oxide layer under the thick deposit in the hot economizer [w. %]. In both cases, corrosion is minimal under the thick solid deposit layer.

of elements forming low-melting compounds, such as alkali metals K and Na, zinc, chlorine and lead, were deposited on the tube surfaces, Table 4. Erosion caused by fly-ash and bed-ash had caused enhanced corrosion leaving the metal surface bare of oxide layer. Thick multi-layered oxide scales as well as deep corrosion pits were on the metal surface in other areas. Potassium, copper and chlorine were detected in the oxide–metal interface in the deep corrosion cavities below the porous oxide layers, Fig. 14. The appearance of the corrosion products next to the metal surface implies that molten phases may have been present during the corrosion process, Fig. 12.

The multi-layered non-protective oxide indicates the strong role of chlorine in the corrosion process, which produced loose and porous oxide scales unable to heal in the repeating corrosion circuit. Potassium, chlorine and copper were detected at the metal–scale interface and zinc

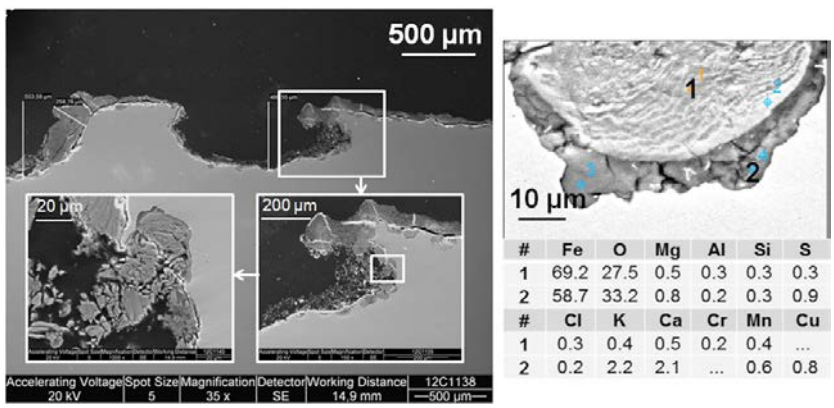

#	Fe	O	Mg	Al	Si	S
1	69.2	27.5	0.5	0.3	0.3	0.3
2	58.7	33.2	0.8	0.2	0.3	0.9
#	Cl	K	Ca	Cr	Mn	Cu
1	0.3	0.4	0.5	0.2	0.4	...
2	0.2	2.2	2.1	...	0.6	0.8

Fig. 12. Deep corrosion cavities on the St35.8 tube in the cold economizer. Both chlorine and copper were detected on oxide–metal interface in EDX analysis [w. %].

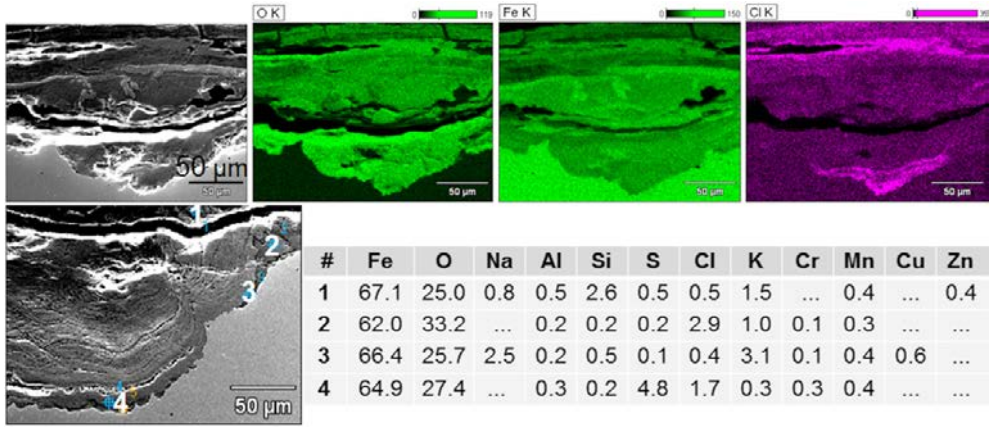

#	Fe	O	Na	Al	Si	S	Cl	K	Cr	Mn	Cu	Zn
1	67.1	25.0	0.8	0.5	2.6	0.5	0.5	1.5	...	0.4	...	0.4
2	62.0	33.2	...	0.2	0.2	0.2	2.9	1.0	0.1	0.3	...	...
3	66.4	25.7	2.5	0.2	0.5	0.1	0.4	3.1	0.1	0.4	0.6	...
4	64.9	27.4	...	0.3	0.2	4.8	1.7	0.3	0.3	0.4	...	...

Fig. 13. Thick oxide scales had formed on the St35.8 steel tube in the cold economizer. EDX analysis of the multi-layered oxide showed high amount of chlorine in the scales near the metal interface [w. %].

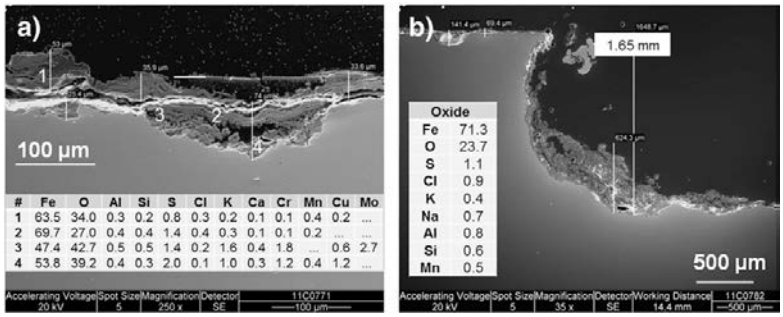

#	Fe	O	Al	Si	S	Cl	K	Ca	Cr	Mn	Cu	Mo
1	63.5	34.0	0.3	0.2	0.8	0.3	0.2	0.1	0.1	0.4	0.2	...
2	69.7	27.0	0.4	0.4	1.4	0.4	0.3	0.1	0.1	0.2	...	...
3	47.4	42.7	0.5	0.5	1.4	0.2	1.6	0.4	1.8	...	0.6	2.7
4	53.8	39.2	0.4	0.3	2.0	0.1	1.0	0.3	1.2	0.4	1.2	...

Fig. 14. a) Porous and loose multi-layered oxide scale on St35.8 material in the hot economizer. b) Strong corrosion of the carbon steel tube in the hot economizer. Chlorine was present in the oxide layers [w. %].

and lead in the deposits. Therefore it is suggested that in the relatively low material temperature of the economizer tubes, the extremely strong material wastage of the carbon steel tubes was caused by chlorine that formed corrosive compounds with potassium, copper, zinc and lead. Similar corrosion enhanced by volatile $FeCl_2$ (g) at around 400 °C in a boiler condition has been published by Persson et al. [10] and in laboratory tests under $ZnCl_2$–KCl mixture by Spiegel [6]. Copper oxide can be chlorinated to copper chloride by a reaction with HCl in the so-called Deacon reaction. Formation of metal chloride is exothermic and can take place in the temperature range 250–475 °C [24]. The forming

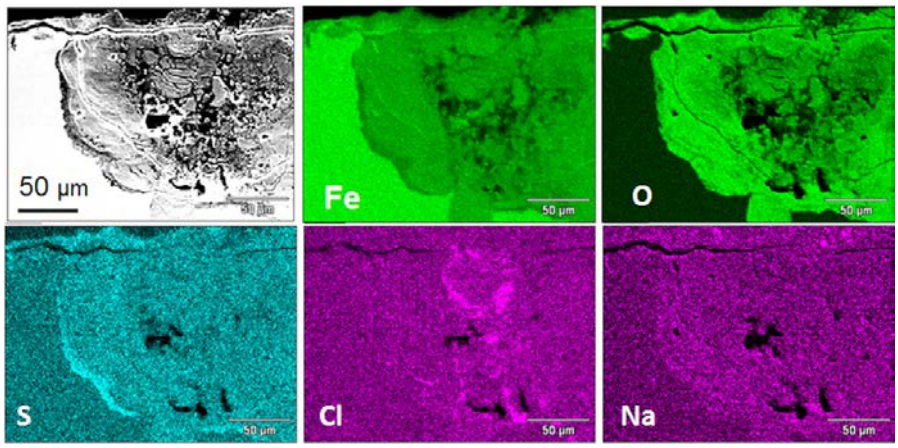

Fig. 15. EDX map analysis of a deep corrosion cavity on St35.8 steel tube in the hot economizer.

copper chloride melts are extremely corrosive, and might be one factor in the corrosion process.

The wood based fuel had high moisture content in the combustion. The high amount of water vapor in flue gases has been found to accelerate corrosion processes at elevated temperatures [25,26]. With carbon steel, water vapor has enhanced the iron oxide formation and detachment of the iron oxide layers. Breakaway oxidation has been reported on Fe–9Cr steel, with strong development of porous magnetite Fe_3O_4 scale and formation of extended gap in the scale [27].

The HVOF coatings NiCr16Mo, NiCr9Mo and NiCr10Al provided excellent protection for the carbon steel St35.8 in the fluidized bed biomass boiler conditions. After the two year exposure the coatings showed no corrosion. In the relatively low temperature with corrosive atmosphere the coatings were intact with some oxidation on the outer surface, Fig. 6. Small amounts of potassium, chlorine, zinc and sodium were observed on the coating–deposit interface. The deposit appears to have been melted next to the coating surface, Fig. 8. The composition of the coatings was nickel-base with high amounts of chromium alloying. NiCr16Mo contained also molybdenum, NiCr9Mo molybdenum and niobium, and NiCr10Al aluminum. The alloying of the coatings favors high corrosion performance even in an atmosphere with high chlorine and water vapor content and below the deposits containing chlorine, zinc and copper, which had caused severe corrosion to the St35.8 steel. Erosion by fly-ash and bed-ash had no effect on the coatings because of their high hardness and stable structure.

Iron and its oxides have been reported to be completely unable to withstand HCl attack, test conditions starting from 400 °C, whereas both chromium and nickel can resist corrosion against HCl [28]. The severe corrosion of carbon steel St35.8 compared to excellent performance of nickel-based coatings with high chromium content follows these findings. Severe corrosion of carbon steel compared to the coating materials can be explained also by higher solubility of iron chloride in the $ZnCl_2$–KCl melt than the solubility of nickel chloride and chromium (III) chlorine [29]. According to thermodynamic stability calculations, iron forms a liquid phase with chlorine at 310 °C, whereas reactions with chromium produce solid reaction products, Fig. 16a). Copper and zinc can form liquid phases at 430 °C and 320 °C, respectively, Fig. 16b).

3.7. Effect of protective coatings

The thermal spray coatings with high amounts of protective alloying elements showed excellent corrosion performance in the biomass boiler exposure. In the relatively low operation temperatures the iron based tube material corroded severely, whereas the e.g. chromium containing coatings outperformed in the conditions. The coatings had negligible reactions with the prevailing atmosphere due to their ability of forming protective oxide on the coating surface. The nickel-based coatings were sprayed with HVOF, which produced coatings with dense structure and good adherence to the substrate material. The coatings had lamellar structure with splats typical to thermally sprayed coatings. The NiCr10Al coating had the highest melting state, whereas some partly or un-molten particles were detected within the NiCr16Mo and NiCr9Mo coatings. Interconnecting porosity, which would allow the corrosive elements to diffuse into the coating and to the substrate material, was not detected. Corrosion attacks thermal spray coatings typically through oxidized lamellar boundaries and pores in the coating [13]. Therefore, in order to minimize porosity with sufficient melting of the powder particles and to produce excellent cohesion and minimized oxidation of the splats with satisfactory speed of the powder particles, optimization of the coating structure is extremely important.

4. Conclusions

A tube leakage had occurred in a cold economizer of a circulating fluidized bed (CFB) boiler burning mainly wood-based biomass. To increase the corrosion resistance of boiler components thermal spray coatings were tested in the boiler for two years. The coatings were high velocity oxy-fuel (HVOF) sprayed on carbon steel St35.8 tube sections which were welded to the boiler tubes in the cold and hot economizers. Despite the low temperatures of the economizers, severe corrosion took place on the St35.8 carbon steel tubes. However, the tested HVOF coatings had endured the boiler exposure well, and all the nickel based coatings offered excellent corrosion and erosion protection to the substrate material.

- The tube failure was caused by chlorine induced corrosion. Corrosion was probably enhanced by the presence of KCl–$ZnCl_2$ and high water vapor content of the fuel.
- The carbon steel tube St35.8 corroded strongly during the two year exposure in the biomass boiler burning mainly wood with high moisture content. Several millimeters of the tube wall thickness was consumed in two years with a maximum corrosion rate of 2.3 mm/year.
- Below the thick deposits, carbon steel St35.8 was relatively intact with a thin oxide layer on the metal surface.
- Cl, Cu, and K were detected below the thick, multi-layered, loose oxide scales at the metal–scale interface. Zn and Pb were identified in the deposits. It is suggested that the extremely severe corrosion of carbon steel was caused by chlorine induced corrosion together with the effect of potassium, copper, zinc and lead in the deposits.
- HVOF sprayed NiCr16Mo, NiCr9Mo and NiCr10Al coatings showed excellent corrosion resistance in the biomass boiler conditions during the two year exposure.

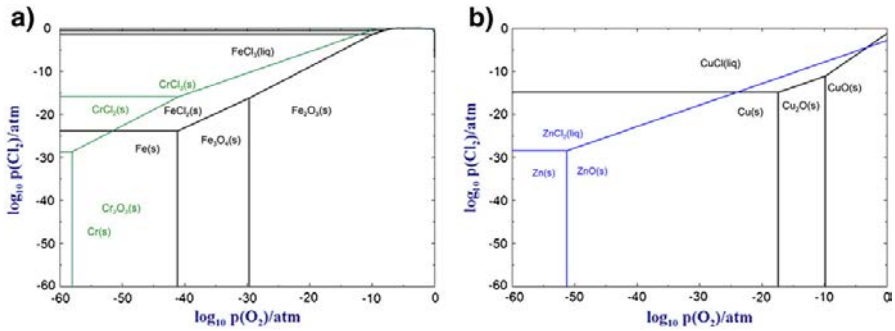

Fig. 16. a) Thermodynamic stability of iron and chromium at 310 °C in the presence of chlorine and oxygen. b) Phase diagram of Cu–Cl_2–O_2 and Zn–Cl_2–O_2 systems at 430 °C and at 320 °C, respectively. Calculated with FactSage 6.4.

Acknowledgments

Availability of the Turku Energia power plant boiler (Turku, Finland) for the coating testing is greatly appreciated. The authors would also like to thank J. Metsäjoki for thermodynamic calculations.

References

[1] http://ec.europa.eu/clima/policies/brief/eu/index_en.htm (Accessed 4.4.2014).
[2] Biomass to Energy, The World Market for Biomass Power Plants 2012/2013, EcoProg GmbH, Cologne, October 2012. (770 p.).
[3] H.P. Michelsen, F. Frandsen, K. Dam-Johansen, O.H. Larsen, Deposition and high temperature corrosion in a 10 MW straw fired boiler, Fuel Process. Technol. 54 (1998) 95–108.
[4] H.P. Nielsen, F.J. Frandsen, K. Dam-Johansen, L.L. Baxter, The implications of chlorine-associated corrosion on the operation of biomass-fired boilers, Prog. Energy Combust. Sci. 26 (2000) 283–298.
[5] H.J. Grabke, E. Reese, M. Spiegel, The effect of chlorides, hydrogen chloride and sulphur dioxide in the oxidation of steels below deposits, Corros. Sci. 37 (1995) 1023–1043.
[6] M. Spiegel, Salt melt induced corrosion of metallic materials in waste incineration plants, Mater. Corros. 50 (1999) 373–393.
[7] K. Nakagawa, Y. Matsunaga, The effect of chemical composition of ash deposit on the corrosion of boiler tubes in waste incinerators, Mater. Sci. Forum 251–254 (1997) 535–542.
[8] M.C. Galetz, J.T. Bauer, M. Schütze, M. Noguchi, C. Takato, H. Cho, The influence of copper in ash deposits on the corrosion of boiler tube alloys for waste-to-energy plants, Mater. Corros. 63 (2012) 1–8.
[9] P. Henderson, P. Szakálos, R. Pettersson, C. Andersson, J. Högberg, Reducing superheater corrosion in wood-fired boilers, Mater. Corros. 57 (2006) 128–134.
[10] K. Persson, M. Broström, J. Carlsson, A. Nordin, R. Backman, High temperature corrosion in a 65 MW waste to energy plant, Fuel Process. Technol. 88 (2007) 1178–1182.
[11] M. Montgomery, T. Vilhelmsen, S.A. Jensen, Potential high temperature corrosion problems due to co-firing of biomass and fossil fuels, Mater. Corros. 59 (2008) 783–793.
[12] R.F.A. Pettersson, J. Storesund, M. Nordling, Corrosion of overlay weld cladding in waterwalls of a waste-fired CFB boiler, In Proceedings: EUROCORR 2008 European Corrosion Congress — Managing Corrosion for Sustainability, 07–11 Sep 2008, Edinburgh, UK, 2008, p. 12.
[13] M.A. Uusitalo, P.M.J. Vuoristo, T.A. Mäntylä, High temperature corrosion of coatings and boiler steels below chlorine-containing salt deposits, Corros. Sci. 46 (2004) 1311–1331.
[14] T.S. Sidhu, R.D. Agrawal, S. Prakash, Hot corrosion of some superalloys and role of high-velocity oxy-fuel spray coatings—a review, Surf. Coat. Technol. 198 (2005) 441–446.
[15] M. Kaur, H. Singh, A survey of the literature on the use of high velocity oxy-fuel spray technology for high temperature corrosion and erosion–corrosion resistant coatings, Anti-Corrosion Methods Mater. 55 (2) (2008) 86–96.
[16] S. Tuurna, T. Varis, K. Ruusuvuori, S. Holmström, J. Salonen, P. Auerkari, T. Kinnunen, P. Yrjas, R. Finne, M. Nupponen, U. McNiven, H. Ahonen, A. Kapulainen, Managing corrosion in biomass boilers: benefits and limitations of coatings, In Proceedings: Baltica VIII Conference on Life Management and Maintenance for Power Plants, VTT, Espoo, Finland, vol. 2, 2010, pp. 22–36.
[17] B.S. Sidhu, D. Puri, S. Prakash, Mechanical and metallurgical properties of plasma sprayed and laser remelted Ni–20Cr and Stellite-6 coatings, J. Mater. Process. Technol. 159 (2005) 347–355.
[18] M. Oksa, E. Turunen, T. Varis, Sealing of thermally sprayed coatings, Surf. Eng. 20 (2004) 251–254.
[19] M. Oksa, S. Tuurna, T. Varis, Increased lifetime for biomass and waste to energy power plant boilers with HVOF coatings: high temperature corrosion testing under chlorine-containing molten salt, J. Therm. Spray Technol. 22 (2013) 783–796.
[20] M. Spiegel, A. Zahs, H.J. Grabke, Fundamental aspects of chlorine induced corrosion in power plants, Mater. High Temp. 20 (2003) 153–159.
[21] S. Enestam, Corrosivity of Hot Flue Gases in the Fluidized Bed Combustion of Recovered Waste Wood: Academic Dissertation, Åbo Akademi University, Åbo, Finland, 2011. 86.
[22] K. Salmenoja, K. Mäkelä, Relations between superheater corrosion conditions in a black liquor recovery boiler and a power boiler fired with biofuels, Nord. Pulp Pap. Res. J. 15 (2000) 24–28.
[23] K. Salmenoja, K. Mäkelä, M. Hupa, R. Backman, Superheater corrosion in environments containing potassium and chlorine, J. Inst. Energy 69 (1996) 155–162.
[24] U. Nieken, O. Watzenberger, Periodic operation of the Deacon process, Chem. Eng. Sci. 54 (1999) 2619–2626.
[25] P. Kofstad, High Temperature Corrosion, Elsevier Applied Science Publishers Ltd, Essex, England, 1988. 558.
[26] J. Pettersson, J.-E. Svensson, L.-G. Johansson, KCl-induced corrosion of a 304-type austenitic stainless steel in O_2 and in $O_2 + H_2O$ environment: the influence of temperature, Oxid. Met. 72 (2009) 159–177.
[27] J. Ehlers, D.J. Young, E.J. Smaardijk, A.K. Tyagi, H.J. Penkalla, L. Singheiser, W.J. Quadakkers, Enhanced oxidation of the 9%Cr steel P91 in water vapour containing environments, Corros. Sci. 48 (2006) 3428–3454.
[28] H. Asteman, M. Spiegel, Investigation of the HCl (g) attack on pre-oxidized pure Fe, Cr, Ni and commercial 304 steel at 400 °C, Corros. Sci. 49 (2007) 3626–3637.
[29] A. Ruh, M. Spiegel, Thermodynamic and kinetic consideration on the corrosion of Fe, Ni and Cr beneath a molten KCl–$ZnCl_2$ mixture, Corros. Sci. 48 (2006) 679–695.

PUBLICATION V

Performance testing of iron based thermally sprayed HVOF coatings in a biomass-fired fluidized bed boiler

In: Surface & Coatings Technology 251 (2014) 191–200.

Surface & Coatings Technology 251 (2014) 191–200

Contents lists available at ScienceDirect

Surface & Coatings Technology

journal homepage: www.elsevier.com/locate/surfcoat

Performance testing of iron based thermally sprayed HVOF coatings in a biomass-fired fluidised bed boiler

Maria Oksa [1], Tommi Varis, Kimmo Ruusuvuori

VTT Technical Research Centre of Finland, PO Box 1000, 02044 VTT Espoo, Finland

ARTICLE INFO

Article history:
Received 18 November 2013
Accepted in revised form 8 April 2014
Available online 24 April 2014

Keywords:
HVOF
Thermal spray coating
Corrosion protection
Biomass
High temperature corrosion
Chlorine corrosion

ABSTRACT

Managing high temperature corrosion problems in biomass firing boilers has been challenging especially due to high amounts of chemically active compounds, in particular alkali chlorides. Thermally sprayed coatings with high chromium content can offer a solution for protecting low alloyed substrate materials in locations prone to high temperature corrosion. Two thermally sprayed (HVOF — high velocity oxy-fuel) iron based coatings (Fe–27Cr–11Ni–4Mo and Fe–19Cr–9W–7Nb–4Mo) were exposed to biomass boiler conditions for two years. The fluidised bed boiler for district heating used mainly wood-based fuels mixed with small amounts of peat. The coated tubes were located at the hot economiser of the boiler, where the estimated material temperature was about 200 °C maximum. After the exposure the coatings and the carbon steel St35.8 substrate material were analysed with SEM–EDX. It was detected that corrosion due to elements such as chlorine, potassium, zinc, lead and copper had caused severe material wastage in the biomass boiler with relatively low heat exchanger surface temperatures. The low alloyed boiler tubes had suffered severely with a corrosion rate as high as 2 mm/year, whereas dense thermal spray coatings offered excellent protection during the exposure.

1. Introduction

Application of biomass as fuel for power production has been increasing due to legislation in Europe. To avoid severe impacts of climate change, the EU has committed to reduce its greenhouse gas (GHG) emissions to 20% below 1990 levels. Several initiatives to reduce greenhouse gas emissions are applied in the EU, including the European Climate Change Programme (ECCP), EU emission trading system and legislation to raise the share of energy consumption produced by renewable energy sources, such as biomass, to 20% by 2020. However, biomass can be very corrosive to boiler heat-exchanger components during combustion. Several corrosion mechanisms prevail in biomass combustion, including corrosion induced by chlorine as a major drawback to the exploitation of the technology [1]. Corrosion failures may lead to severe operational problems such as unexpected plant shutdowns, high maintenance costs and reduced availability of the plant. Wood derived fuels are the most utilised biomass type in Finland. Even though the Cl content in wood can be low, combustion of wood based fuel, markedly recycled wood, may accelerate corrosion rates in power plants [2].

High temperature corrosion is a severe problem in power plant boilers burning difficult biomass fuels with varying quality. Main components in ash of wood and woody biomass including bark are CaO, SiO_2, K_2O, MgO, Al_2O_3, P_2O_5, Fe_2O_3, MnO, SO_3 and Na_2O [3,4]. According to Obernberger and Thek [5], bark briquettes can contain 499 mg/kg sulphur, 375 mg/kg chlorine, 2410 mg/kg potassium, 10.1 mg/kg lead, 170 mg/kg zinc and 7.1 mg/kg copper, and the water content can be 9.6 wt.%. The water content has an influence on the combustion efficiency, the temperature of combustion and the corrosion mechanisms within the boiler. Typically fly ash and deposits in biomass combustion contain high amounts of potassium and chlorine. Corrosion mechanism in biomass firing or co-firing biomass include e.g. active oxidation by chlorine, selective chlorine corrosion, hot corrosion by eutectic melts and sulphidation [1,6,7]. A lot of emphasis has been laid to superheater area corrosion research at temperature ranges of 300…600 °C depending on the burnt fuel (waste–biomass-co-firing) [7–9], especially on corrosion caused by chlorine [6,7,10], but there are only few studies in biomass conditions at lower temperatures (<300 °C), where e.g. economisers operate [11].

During combustion, chlorine is typically released from the fuel almost completely. Also sulphur is readily released. In the fuel gases, chlorine is usually present as HCl, gaseous alkali metal chlorides (KCl, NaCl), or as fine alkali metal chloride particles. The main sulphur compound in the gas face is SO_2, and in the condensed phase it is typically found as alkali metal and calcium sulphates [12,13]. Fly ash may form detrimental ash deposits on tube surfaces in the economiser area of the flue gas duct, as well as condensing alkali vapours may enhance the fouling and corrosion of the cooled heat-exchanger surfaces [4]. Chlorine is especially detrimental to the heat exchanger surfaces because it forms compounds

E-mail addresses: maria.oksa@vtt.fi (M. Oksa), tommi.varis@vtt.fi (T. Varis), kimmo.ruusuvuori@vtt.fi (K. Ruusuvuori).
[1] Tel.: +358 505365844; fax +358 207227069.

http://dx.doi.org/10.1016/j.surfcoat.2014.04.025
0257-8972/

with a low melting point and a high volatility in the boiler conditions. Chlorine plays an important role in the fine particle and deposit formations. Alkali metal chlorides of biomass combustion have high vapour pressures and therefore they condensate at low temperatures in the flue gas. On the other hand, sulphur reacts with alkali metal (sodium or potassium) chlorides and hydroxides by sulphation reactions (Eqs. (1)–(2)) [14].

$$2\,(Na/K)OH + SO_2 + \frac{1}{2}\,O_2 \leftrightarrow (Na/K)_2SO_4 + H_2O \quad (1)$$

$$2\,(Na/K)Cl + H_2O + SO_2 + \frac{1}{2}\,O_2 \leftrightarrow (Na/K)_2SO_4 + 2\,HCl. \quad (2)$$

Bramhoff et al. [15] showed that an addition of 250–3000 vppm HCl (g) into oxidising atmosphere leads to accelerated catastrophic corrosion of a low alloy steel.

Zinc plays a detrimental role in particular when waste wood is used for combustion [6]. In biomass burning or waste incineration low melting compounds are for instance $ZnCl_2$, $FeCl_2$ and $FeCl_3$ with melting points of 318 °C, 676 °C and 303 °C, accordingly [16,17]. According to thermodynamic equilibrium calculations by Otsuka [18], vapour condensation of KCl, NaCl and $Na2_SO_4$, as well as lead and zinc salts takes place on the tube surfaces at a temperature lower than 350 °C. Pitting corrosion at low temperatures (300 °C) due to chlorides and sulphates that present as heavy metal salts in a melt or semi-melt phase has been reported by Montgomery [19]. Catastrophic corrosion rates can occur in the presence of molten chlorides on heat exchanger surfaces even at low temperatures of 250 °C [11]. Skrifvars has shown that enhanced corrosion can occur below the first melting point of alkali sulphate–alkali chloride salt [20]. It is assumed that water vapour accelerates the passive-layer breakdown. Chlorine, HCl and chlorides are especially detrimental on iron and low alloy steels as they prevent the formation of protective oxide layers [17]. Ehlers et al. [21] has shown that under the conditions of high $H_2O(g)/O_2$ ratios the penetration of water vapour molecules triggers the enhanced oxidation and sustains the high growth rates of the poorly protective Fe-rich oxide scale formed in the atmospheres. At very low temperatures, below 140 °C, condensing of flue gases containing H_2O, SO_3, NO_x or HCl can cause formation of acids either in small fog droplets or as a film on to the surface, which leads to dewpoint corrosion [22]. The dewpoint temperature of the specific compound depends on the pressures of the compound and water vapour. However, in typical economiser temperatures the dewpoint or downtime corrosion should not take place.

There is a need to tackle the corrosion problems in power plant boilers induced specially due to chlorine [2]. Efforts to limit corrosion caused by chlorine and alkali metals in boilers burning difficult fuels have led to the addition of sulphates into the boiler. The corrosion is reduced by capturing alkalis from their chlorides before deposition on the tube surfaces. The method is based on the reaction between sulphur trioxide and chlorides by sulphation of the alkali chlorides. Spraying of either ammonium sulphate solution or sewage sludge with iron and addition of aluminium sulphate into the boiler have been shown to decrease superheater corrosion both in wood and waste fired boilers [2,9,23]. The corrosion reduction of heat exchanger surfaces, e.g. economisers and superheaters that are exposed to the corrosive species has been performed by development of high alloyed steels and nickel alloys, but due to the high price of the materials, their use is limited. Coatings offer an option to prolong the lifetime of heat exchanger surfaces by corrosion protection of economical carbon or low alloy steels [24,25]. Present technological know-how on thermal spray techniques brings the coatings a promising solution for high temperature corrosion protection in the extreme conditions. Thermal spraying is a coating method, in which often metallic or ceramic raw material is heated up and sprayed in a molten or semi-molten form onto the substrate material. There are different spray methods, such as arc, plasma, and high velocity oxy-fuel (HVOF) spray, which all form a lamellar coating structure, the thickness of the coating being typically 200–500 μm, and coating density, lamellar structure and amount of oxidation varying dependently on the spray method, spray parameters and the raw material [26].

Thermal spray coatings, mainly metallic HVOF sprayed coatings can be applicable for high temperature erosion and corrosion protection applications, but performance of these coatings needs to be investigated in aggressive environments [27].

HVOF spraying is a suitable coating method for boiler applications, as it produces dense and well adhered protective coatings [28]. However, optimisation of the composition and the structure of thermal spray coating are especially important in the case of corrosion protection in extreme conditions, such as power plant boilers. Splat boundaries, interconnected voids and pores can act as a fast diffusion path to the corrosive species [29]. HVOF spraying can be performed in-situ in a boiler depending on the boiler design and arrangement of the tubes. However, due to the complex nature of thermal spraying, the best quality can be achieved in a workshop, with subsequent installation and welding of the coated tubes and local coating of the joint areas. Ceramic coatings are typically applied as TBCs (thermal barrier coatings) on gas turbines with a metallic bond coat, MCrAlY (M = Ni, Co) [30]. These mainly stabilised zirconium oxide ceramic coatings as an outer, porous layer, to protect blades from high temperature exposure and softening of the nickel superalloy. However, in boiler conditions, their application is not suitable due to differences in coefficient of thermal expansion (CTE) between the ceramic coating and a metallic boiler tube, as well as their harmful effect on thermal conductivity of heat exchanger surfaces due to their high thermal insulation properties.

Nickel based coatings have been reported to give satisfactory high temperature corrosion protection in biomass fuelled and waste to energy boiler [31,32], but iron based coatings can offer a more economical solution. Iron based thermal spray coatings with high chromium content were tested for two years in a power plant boiler, which had previously experienced heavy corrosion.

2. Materials and methods

Two iron based coating materials were thermally sprayed on boiler tube sections, which were welded into actual boiler tubes for two years of exposure in real boiler conditions. The power plant was a fluidised bed boiler burning mainly wood-based fuels. The district heating boiler did not include superheaters and the economisers were components with the shortest life in the boiler.

The tested HVOF coatings had high chromium content. The corrosion resistance of the coatings and the uncoated substrate material in the boiler conditions were analysed.

2.1. Coating manufacturing and materials for boiler exposure

The HVOF coating was performed with a Sulzer Metco Diamond Jet Hybrid 2700. The coating powders were an experimental Fe–27Cr (Fe–27Cr–11Ni–4Mo) and a commercial SHS9172HV1 (Fe–19Cr–9 W–7Nb–4Mo) from Nanosteel (The Nanosteel Company, Providence, RI, USA). The coatings were applied on a carbon steel tube (St35.8, DIN 17175-79, size 38 × 5.5 mm). Prior to the deposition, the base material was grit blasted with alumina particles (500–700 μm) to produce a surface with good adherence. The surface roughening is essential to guarantee good bonding between the base material and the coating. The aim was to manufacture dense and well adhered coatings, which could provide satisfactory protection to the base material against corrosion and erosion. The powder compositions are presented in Table 1. The coating was performed on short tube sections (about 2 m), which were welded to the actual tubes in the boiler. Spray parameters for the coatings are presented in Table 2, as well as the measured hardness.

Table 1
Chemical composition of the tested HVOF coatings and the carbon steel tube material.

Code	Particle size	Chemical composition
Fe–27Cr	−52 + 22 μm	Fe27.2Cr10.7Ni3.9Mo1.4Si2C
Fe–19Cr	−53 + 15 μm	Fe18.6Cr8.6W7.1Nb3.6Mo <5 B[a] 2.1C1.1Mn1.6Si
St35.8	Substrate	Fe 0.17 max. C 0.10–0.35 Si 0.40–0.80 Mn 0.040 max. P 0.040 max. S

[a] Could not be analysed with EDX.

2.2. The boiler exposure

The 40 MW fluidised bed boiler burned solid biomass, mainly wood-based fuels including recycled wood, mixed with small amounts of peat. The wood derived fuel consisted of 4–18% bark, 2–7% of recycled wood and 3–6% of peat. The main part of the fuel consisted of logging residue chips, sawdust, stump hog fuel and wood chips. Analysis of the fuel was not available. A schematic figure of the boiler design is presented in Fig. 1. The boiler produced hot water for district heating and hence contained only economisers, not superheaters. In the boiler, there had been serious problems with corrosion leading to tube leakage, and the economiser tubes had to be replaced every two years. By this study, feasibility of thermal spray coatings for corrosion protection instead of using higher alloyed boiler tubes was investigated.

The test coatings were installed to the hot counter-flow economiser, where severe corrosion had occurred. The goal was to investigate the possibility of corrosion protection by thermal spray coatings in the boiler. Temperature of the flue gas before the hot economiser was about 520…800 °C, water in-let temperature to the cold economiser was about 102–115 °C, and the maximum water temperature in the hot economiser was 200 °C. The boiler exposure duration for the coatings was two years. The moisture content of the utilised wood was high, over 50%. Analyses of detrimental elements in the dry ash are presented in Table 3. Other elements were not analysed. Sandberg et al. [33] have conducted a long-term measurement period analysing biomass fuels. Some of these results are presented in Table 3, as the wood derived fuels in Sweden are comparable to wood-based fuels in Finland.

2.3. Sample preparation and analysis

The tube sections with coatings were removed from the boiler after the two years of exposure and cut into rings, which were cast into epoxy. The specimens were prepared into metallographic cross-sections. The grinding and polishing were performed with ethanol in order to prevent subsequent dissolution of water-soluble compounds. The specimens were studied with an optical microscope and a scanning electron microscope (SEM), and analysed with an energy dispersive X-ray analyser (EDX). Separate samples were characterised in an as-coated state with an optical microscope and a Zwick ZHU 0.2 hardness tester using the cross-sections of the coating samples.

3. Results

3.1. The two-year biomass boiler exposure

The carbon steel St35.8 had experienced severe corrosion during the 2-year exposure in wood firing circulating fluidised bed boiler. Considerable material wastage had occurred and deep cavities had been formed in

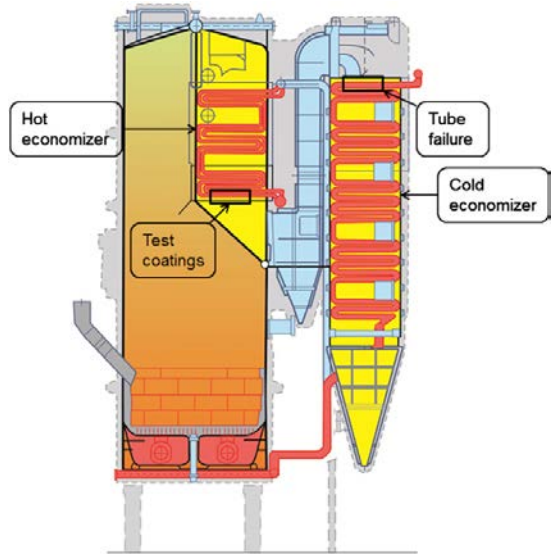

Fig. 1. Schematic drawing of the 40 MW circulating fluidised bed boiler and the location of the test coatings.

the biomass boiler conditions. The coatings Fe–27Cr and Fe–19Cr had endured very well under the boiler conditions. The coatings were covered mostly with ash deposit on the leeward side. In a visual inspection the coatings showed no sign of deterioration.

3.2. Carbon steel St35.8

The uncoated carbon steel tubes had suffered severe material wastage during the exposure. In worst cases, several millimetres had been corroded from the tube thickness, the thinnest sections being only about 1.5 mm thick. Both even and pitting types of corrosion were detected on the samples. Chlorine was detected on some of the corrosion layers, and hence the strong deterioration may have been induced by active oxidation. Uncoated tube samples are shown in Fig. 2. Strong orientation of the material wastage can be observed. The flue gas side, especially ±45°, had lost as much as two thirds of the nominal tube wall thickness. Because thick, porous, multi-layered oxide scales, which are often detected on low alloy steel in the case of chlorine corrosion, were not present in some areas, some erosion due to the fluidised bed sand may have occurred. In some areas a thick deposit was left on the carbon steel tubes. Below the deposit, only a very thin oxide layer was detected on the metal surface, including manganese, silicon and aluminium (Fig. 3). Thick deposit, thin oxide and low metal degradation rates were mainly present together. In certain areas deep corrosion cavities (up to 400 μm) were formed into the carbon steel tube (Fig. 4). Chlorine, sodium and sulphur were present in the corrosion products within the cavity. Severe pitting was detected principally in the side against the flue gas flow. Another example of strong material wastage of the carbon steel is presented in Fig. 5. Several hundred micrometre deep pits with partly detached oxide layers on the surface were formed on the tube surface. Below the oxide layer, smaller pits were detected, which contained e.g. potassium, sodium, copper and chlorine. Even

Table 2
HVOF spray parameters. The spray gun was DJ Hybrid, nozzle 2701.

Coating	C_3H_8 [l/min]	O_2 [l/min]	Air [l/min]	N_2 [l/min]	Fuel ratio	Sweeps	Powder feed [g/min]	Stand-off [mm]	IR [°C]
Fe–27Cr	56	200	392	20	0.345	20	25	250	160
Fe–19Cr	56	200	392	20	0.345	22	25	250	160

Table 3
Elemental analysis of detrimental elements in the fly ash and the bottom ash (dry solid content) and the wood derived fuels in [mg/kg] [33].

Element [mg/kg]	Fly ash	Bottom ash	Forest residue	Bark	Recycled wood
Organic carbon, TOC	21,000	<1000	51.7[a]	52.5[a]	49.4[a]
Fluoride, F^-	<100	<100	…	…	…
Chloride, Cl^-	4400	200	0.031[a]	0.019[a]	0.09[a]
Sulphate, SO_4^{2-}	44,000	300	0.01[b]	0.03[b]	0.07[b]
Arsenic, As	<15	<15	0.11	0.11	69
Barium, Ba	5300	3700	67	120	583
Cadmium, Cd	6.8	<0.1	0.26	0.38	1.8
Chromium, Cr	52	15	21	35	90
Copper, Cu	160	43	2.4	3.9	50
Mercury, Hg	0.47	<0.03	0.022	0.033	0.11
Molybdenum, Mo	6.9	2.7	0.74	1.3	0.41
Nickel, Ni	71	11	6	11	1.2
Lead, Pb	100	11	0.64	1	213
Antimony, Sb	<10	<10	…	…	…
Selenium, Se	17	<15	…	…	…
Zinc, Zn	1500	650	85	150	1950

[a] Percentage of dry fuel weight.
[b] Elemental S, percentage of dry fuel weight.

stronger corrosion pitting can be seen in Fig. 6, where almost a 2 mm wide and 1 mm deep pit with a porous multi-layered oxide scale is presented. Near the metal surface there was a corrosion product scale, which included sulphur, potassium, copper, chlorine and zinc.

3.3. Deposits on the coatings

Thick deposits had formed on the flue gas side of both coated tubes, shown in Fig. 7. Based on the EDX analysis, the deposits formed on hot economiser tubes consisted mainly of oxygen (O), calcium (Ca), sulphur (S), potassium (K), silicon (Si), iron (Fe), phosphorus (P), and aluminium (Al). Also smaller amounts of e.g. magnesium (Mg), manganese (Mn), zinc (Zn) and chlorine (Cl) were present. Main components of the deposits are presented in Fig. 7. Detailed EDX analyses of the deposits on both coatings are presented in Table 4. Similar results have been presented by Obernberger and Thek [5] and Åmand et al. [34] at biomass fired boilers, where main components in deposits have been K_2SO_4, $Ca_3(PO_4)_2$, NaCl, KCl, $CaSO_4$ and K_2CO_3.

3.4. Fe–27Cr and Fe–19Cr HVOF coatings

Fe–27Cr and Fe–19Cr coatings were sprayed with HVOF for high temperature corrosion protection of biomass fired boiler tubes. Thicknesses of the tested coatings were about 300 μm for Fe–27Cr and 375 μm for Fe–19Cr. Both coatings were dense and well adhered to the substrate. However, the outer surface of the coating showed weak cohesion and detachment of lamellas. Both coatings had a typical lamellar structure of thermally sprayed coatings with some porosity and non-molten particles in the structure, Fe–19Cr having a higher melting state. Hardness of the coatings was 658 HV0.3 for Fe–27Cr and 935 HV0.3 for Fe–19Cr, which is considerably higher than hardness of the carbon steel. Corrosion resistance of the coatings was excellent in the boiler exposure compared to the uncoated steel tubes (Fig. 8). SEM images of the coatings before and after the exposure are presented in Fig. 9.

Coating Fe–27Cr had endured the exposure well and showed excellent corrosion resistance in the boiler conditions. Corrosion products were not detected in the coating (Fig. 10). Fe–27Cr coating with alloying elements chromium (27%), molybdenum (4%) and silicon (1%) had high protection ability against high temperature corrosion induced by biomass burning. With sufficient oxygen partial pressures chromium can form a protective oxide layer on the coating surface, which prevents reaction with chlorine and hence the detrimental active oxidation [10]. Molybdenum has been shown to act favourable for the corrosion resistance in oxidising–chloridising environments by reacting slowly and behaving rather inertly [35]. Similar protective behaviour has been detected by alloying a small amount of silicon into steels [36].

Fe–19Cr coating had sufficient corrosion resistance in the boiler conditions. The overall corrosion performance was good and no severe corrosion was detected. Fe–19Cr powder has a nanoscale microstructure and the coating is partly amorphous, which have both been reported to act beneficially for corrosion resistance [24,37]. Only some thin surface areas, about 10 μm deep, of the Fe–19Cr coating had corrosion

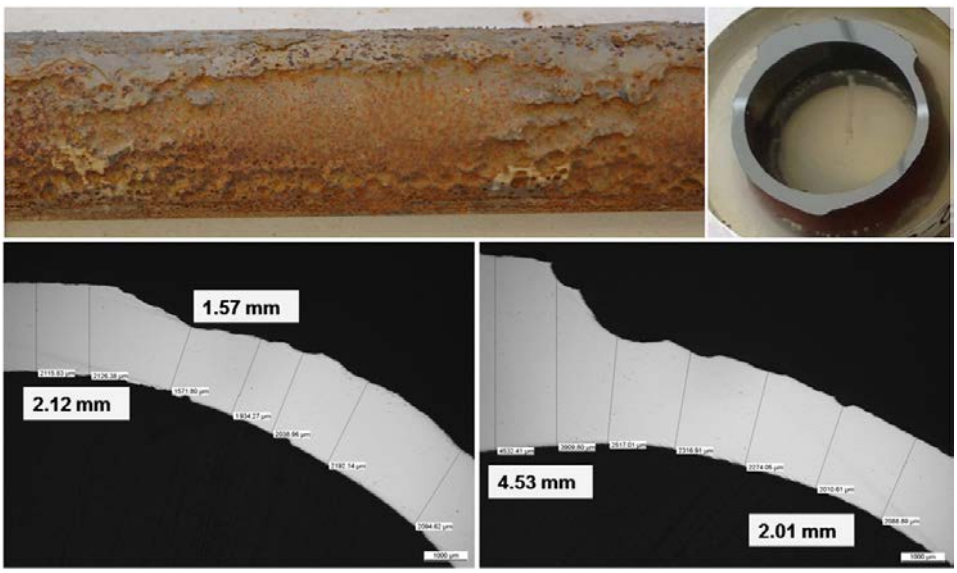

Fig. 2. Macroimage and cross-section of a St35.8 steel tube and optical microscope images of the cross-sections of the carbon steel tube after the exposure in hot economiser. Strong material wastage can clearly be seen in the tube samples mainly on the windward side.

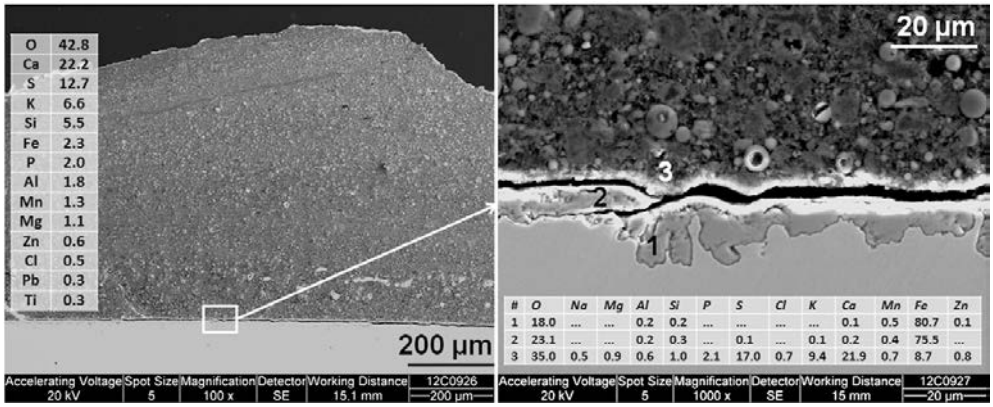

Fig. 3. Corrosion of St35.8 below the thick deposit in the hot economiser. The corrosion was minimal with thin oxide layers under the thick solid deposit layer. EDX analyses [wt.%] of the deposit and oxide layers are presented within the images.

products such as small amounts of chlorine and potassium (see Fig. 11a). However, there were few perpendicular cracks reaching down to the substrate material, which had led to some corrosion in the coating–substrate interface on these areas. Small amounts of sulphur and chlorine were detected under the coating near the crack (Fig. 11b).

4. Discussion

4.1. Corrosion mechanisms in biomass boiler exposure

4.1.1. Corrosion mechanisms of carbon steel

Carbon steel St35.8 had experience extremely strong corrosion in some parts of the hot economiser. Solid and thick deposit formed on the tube surface had protected the metal, and a thin iron oxide layer was present. However, some areas of the tubes had corroded severely and the tubes had thinned over 2/3 of the wall thickness. Erosion due to circulating bed sand (CFB boiler) may have increased the corrosion rate with uncoated carbon steel tubes in some areas, but mainly the material wastage was caused by corrosion. No erosion effect was seen in the coated tubes. The thick and dense deposit on the leeward side had remained intact only in a few areas. Especially on the windward side, the carbon steel tubes had deep corrosion cavities, which contained multi-layered, porous and poorly adherent iron oxide scale together with e.g. potassium, chlorine, sulphur, copper, sodium and zinc. In some cavities, the scale next to the metal surface had been molten (Fig. 6). Turbulence of the flue gases and local low melting compounds with chlorine have probably been the cause for the irregular material wastage in the tube circumference. Similar corrosion has been reported in biomass and waste boilers by e.g. [6–8]. Montgomery et al. [19,38] has reported pitting corrosion in the presence of heavy metal and chlorides/sulphates in melt or semi-melt phase at 300 °C, and the presence of Zn–K–Cl melt in waterwall at low water/steam temperature (285 °C) with high flue gas temperature, which support the findings in this study.

Chlorine corrosion mechanism is caused by the attack of gaseous chlorine, which reacts with iron and chromium forming volatile metal

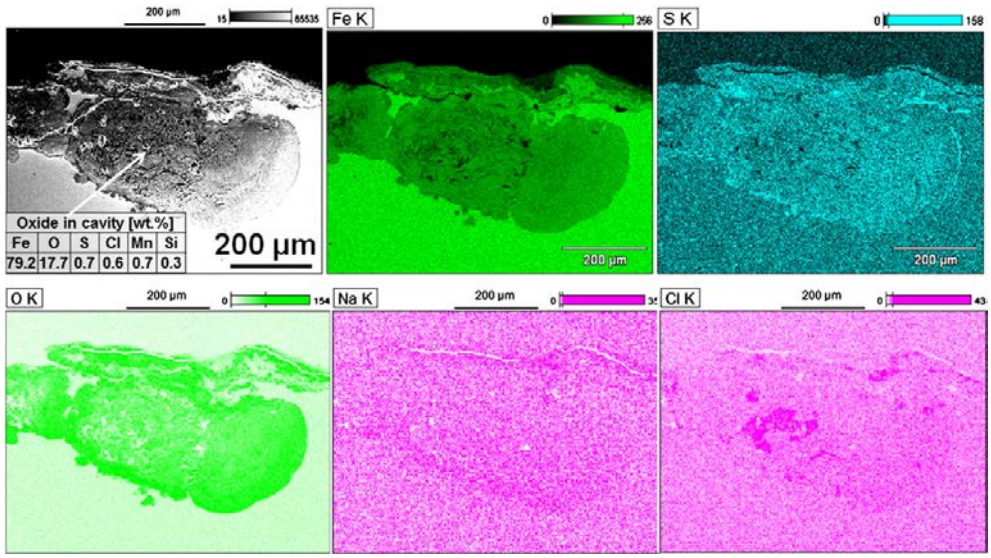

Fig. 4. Severe corrosion of the St35.8 steel tube in the hot economiser, EDX map analysis. Chlorine was found within the oxide of the corrosion cavity.

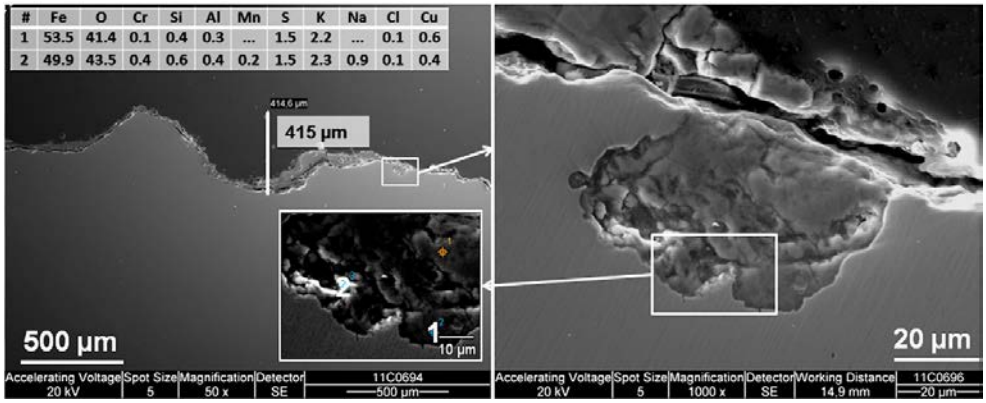

#	Fe	O	Cr	Si	Al	Mn	S	K	Na	Cl	Cu
1	53.5	41.4	0.1	0.4	0.3	...	1.5	2.2	...	0.1	0.6
2	49.9	43.5	0.4	0.6	0.4	0.2	1.5	2.3	0.9	0.1	0.4

Fig. 5. Severe corrosion of St35.8 carbon steel material. EDX point analyses 1–2 [wt.%] from the corrosion pit are presented in the small SEM image.

chlorides in the interface. It is proposed that high partial pressure of chlorine close to the metal is caused by a rapid sulphation of KCl to K_2SO_4 in a melt formed adjacent to the metal surface. When the KCl/K_2SO_4/Fe system becomes molten, the KCl sulphates quickly in the melt and generates a high partial pressure of Cl_2/HCl. This causes accelerated oxidation and can explain the internal corrosion of the metal, which is detected in Fig. 11. Chlorine induced corrosion has been suggested to occur in high temperatures, above 320…500 °C [8,16,17]. Therefore, the extremely severe corrosion must have been caused also by other elements. The material temperature in the hot economiser was estimated to be only about 10° higher than the water temperature due to the high cooling effect of the flowing water. Therefore, the maximum material temperature during operation was only about 210 °C, the flue gas temperatures being in the range of 520–800 °C.

Potassium, chlorine, sulphur, copper, sodium and zinc were detected in the corrosion products of carbon steel tubes. Enestam [39] has reported that the condensation temperature of $ZnCl_2$ is in the range 144–302 °C depending mainly on the chlorine content in the fuel, which can explain the presence of $ZnCl_2$ in the corrosion pits. Pb was not detected, but it was present in the boiler according to fly ash and the bottom ash analyses. Both zinc and copper have been shown to increase the corrosion rate of steels and nickel-based alloys in the presence of alkali chlorides. First melting point of a NaCl–KCl–CuO salt is already at 387 °C, and NaCl–KCl–ZnO at 400 °C, and for $ZnCl_2$–KCl eutectic it can be as low as 250 °C [16, 40]. Galetz [41] has also shown that the eutectic mixture of NaCl–KCl–Na_2SO_4–K_2SO_4 + addition of heavy metal heavy metal chlorides (Pb, Zn, Cu) can decrease the melting point below 300 °C. The chemical composition of the molten phases could not be fully revealed. The compounds for formation of the molten salt may have contained $FeCl_2$–KCl–CuCl–$ZnCl_2$ (Fig. 6).

The corrosion has probably been enhanced by water vapour, as a large amount of water vapour in flue gases has been reported to accelerate corrosion processes at elevated temperatures [42–44]. With Cr containing steels, the water vapour causes evaporation of chromium from the surface in the form of chromate $CrO_2(OH)_2$ (g) [45,46]. However, in the case of iron, the water vapour has increased the iron oxide formation, and cracking and spalling off the iron oxide layers. Ehlers [21] has reported breakaway oxidation of P91 steel (Fe–9Cr), associated with formation of large amounts of porous Fe_3O_4, and development of continuous gap in the scale. KCl has also been reported to be strongly corrosive towards

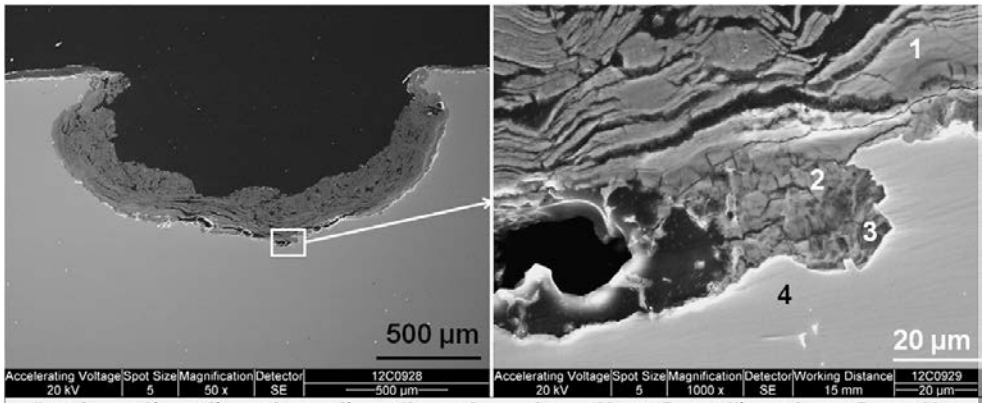

#	O	Al	Si	S	Cl	K	Ca	Cr	Mn	Fe	Ni	Cu	Zn	Mo
1	34.8	0.3	0.2	1.0	0.3	0.3	0.1	...	0.5	62.3	0.1	...	0.1	...
2	36.7	0.4	0.4	2.3	0.2	1.6	0.2	1.3	0.7	54.7	0.2	1.1	...	...
3	21.2	0.4	1.8	3.6	0.6	2.3	0.3	0.4	0.4	66.3	0.4	1.7	0.1	0.5
4	...	0.3	0.3	...	...	...	...	0.1	0.6	98.2	0.3	...	...	0.2

Fig. 6. Corrosion mechanism of St35.8 in the opposite side of the thick deposit in the hot economiser. Chlorine can be found in the oxide in the corrosion cavity according to EDX analyses [wt.%].

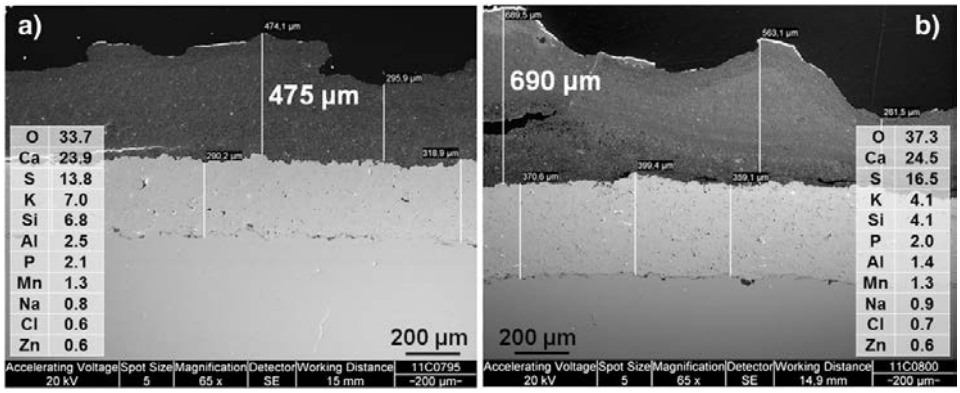

Fig. 7. SEM images of the thick deposits and their main chemical composition by EDX [wt.%] on the coated tubes: a) Fe–27Cr and b) Fe–19Cr.

stainless steel in environments containing O_2 and $O_2 + H_2O$. The sulphation reaction at the presence of water is presented in Eq. (3) [45]:

$$2\,KCl\ (s) + SO_2\ (g) + \frac{1}{2}O_2\ (g) + H_2O \rightarrow K_2SO_4\ (s) + 2\,HCl\ (g). \quad (3)$$

The high amount of water vapour may have played a strong role in the corrosion process, as after the test period the burnt wood was changed into fuel with lower moisture content (wood from the previous year), which lowered the corrosion damage of the tubes.

It is proposed that the corrosion of carbon steel has been chlorine induced corrosion, which has been enabled by low melting phases with chlorine, potassium, zinc and copper. A non-protective iron oxide layer formed on the metal surface has cracked due to reactions with water vapour and corrosive elements in the deposits. Chlorine and other elements have penetrated through the oxide layer into the oxide–metal interface, where suitable conditions with high chlorine vapour pressure have formed for active oxidation. Enhanced corrosion has led to the formation of porous oxide layers, which have spalled off from the metal and caused severe material wastage to the boiler tubes. The heavy metals present in the deposits have taken part into reactions with chlorine and in some places molten phases have formed.

4.1.2. Corrosion mechanisms of thermal spray coatings

Fe–27Cr and Fe–19Cr coatings showed no or negligible corrosion after the two years of exposure in a circulating fluidised bed boiler burning biomass. Both coatings were iron based with a high chromium content. Fe–27Cr coating contained also nickel, molybdenum and silicon. Coating Fe–19Cr contained alloying elements such as tungsten, niobium, molybdenum, boron, manganese and silicon. Both coatings were alloyed also with carbon for carbide formation to give resistance against fly-ash and bed-ash erosion in boiler conditions. The Fe–19Cr coating partly was amorphous and the powder contained a nanoscale microstructure according to the manufacturer. A prior tube failure in the boiler was caused by severe corrosion due to chlorine, which was detected in the metal–oxide interface of a 13CrMo44 boiler tube in the cold economiser. Analyses of the deposits demonstrated the presence of e.g. potassium, chlorine and zinc in the boiler surroundings. Chlorine was not detected on the Fe–27Cr coating, which was dense, well adhered to the substrate and did not contain open or interconnecting porosity and therefore was an excellent protection for carbon steel tube in the exposure. The metallic coating was partly oxidised (about 6 wt.%) during the coating process, and it was able to form sufficient protection against corrosion in the boiler conditions. Coating Fe–19Cr showed minor corrosion in the outer layer of the coating (20 µm), but was also dense and contained a small amount of porosity. However, the coating had few perpendicular cracks, which had allowed corrosion to proceed to the substrate. Iron oxide containing also sodium, sulphur, chlorine and small amounts of potassium and zinc was detected on the coating–substrate interface. The nature of the corrosion scale indicated that it had been molten during the exposure (Fig. 11).

4.2. Coating mechanical integration

Coating Fe–19Cr had about 20 perpendicular cracks around the perimeter of the studied cross-section (Fig. 12). This had led to corrosion in the substrate material under the coating near the crack. It is assumed that the cracks were formed during the coating process, as later studies have revealed the problem [28]. The cracking was probably due to a

Table 4
EDX analysis of the deposits on the Fe–27Cr and Fe–19Cr coatings [wt.%].

Element	O	Ca	S	K	Si	Fe	Mg	Al	P	Mn	Mo	Na	Cl	Zn	Ti	Ba	Pb
Fe–27Cr	33.7	23.9	13.8	7.0	6.8	2.8	2.2	2.5	2.1	1.3	1.0	0.8	0.6	0.6	0.4	0.3	0.3
Fe–19Cr	37.3	24.5	16.5	4.1	4.1	2.3	1.6	1.4	2.0	1.3	1.3	0.9	0.7	0.6	…	0.2	0.1

Fig. 8. A coated boiler tube after the exposure. Severe material wastage of the uncoated tube can be detected in the right side of the picture.

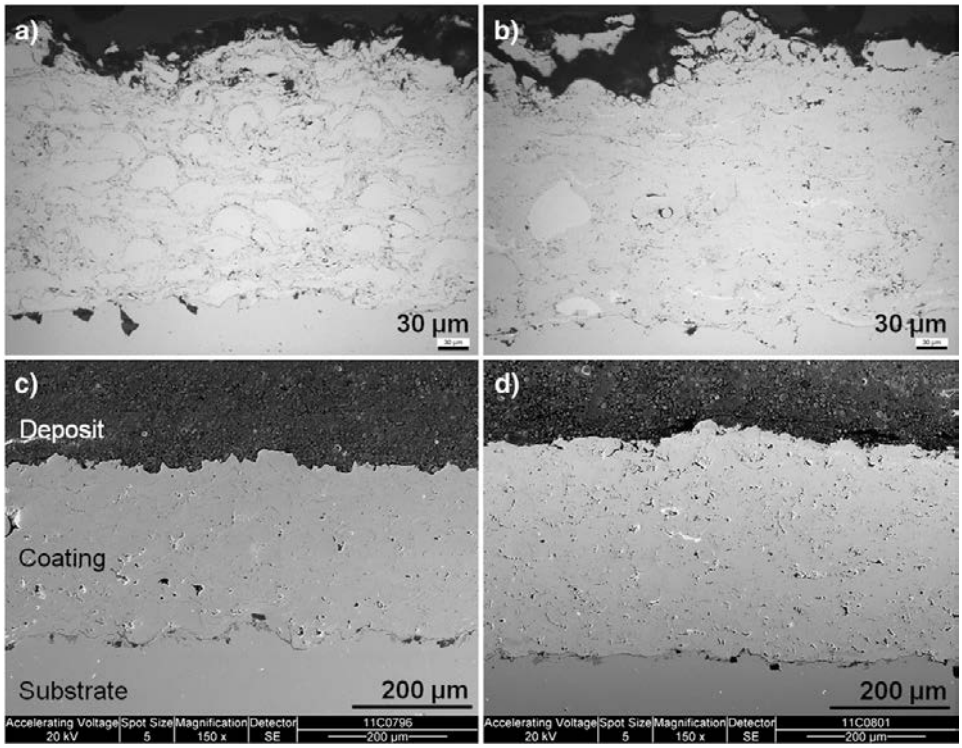

Fig. 9. Optical images of the coating cross-sections before the exposure: a) HVOF sprayed Fe–27Cr, and b) HVOF sprayed Fe–19Cr. SEM images of the coating cross-sections after the boiler exposure: c) Fe–27Cr, and d) Fe–19Cr.

thermal mismatch between the substrate and the coating, which had caused thermal stresses during the coating solidification. Either a bond coat to minimise the stresses due to the mismatch of CTEs between substrate and the Fe–19Cr coating should be applied, or the coating process should be optimised. Process parameter variation has a strong effect on the coating structure, e.g. residual stresses, density, porosity, melting state, cohesion and lamellar boundaries. Diagnostic tools, such as ICP, an in-situ coating property measurement device, and SprayWatch, a sensor for particle temperature and velocity, can be applied in process optimisation to measure the stresses formed during and after the coating, and spray jet properties.

5. Conclusions

Two iron-based thermally sprayed high velocity oxy-fuel (HVOF) coatings were exposed for two years in a circulating fluidised bed (CFB) biomass boiler, which used mainly wood as fuel. The coatings were sprayed on short tube sections, which were welded to the actual tubes in the boiler. The coatings were installed into the hot economiser. Even though the material temperatures on the boiler were low, the corrosion conditions caused severe damage to the carbon steel tubes. During the two years of exposure, the actual boiler tubes had lost even several millimetres of their thickness. Thick deposits with minor

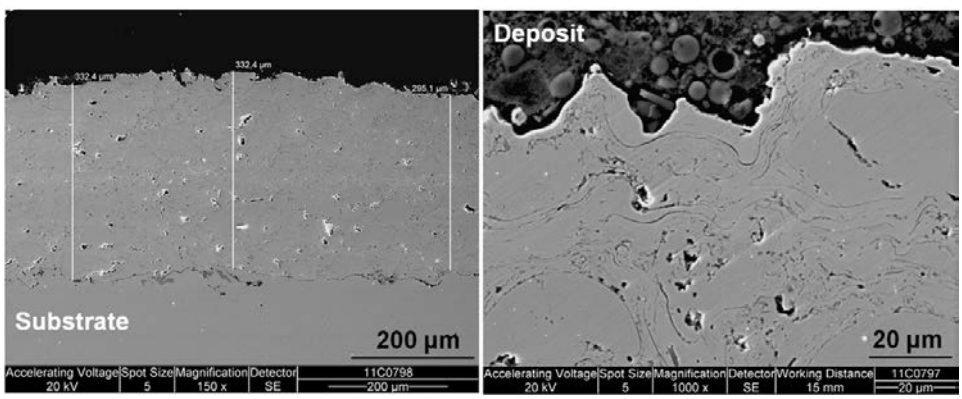

Fig. 10. SEM images of the Fe–27Cr coating. The coating showed no signs of corrosion.

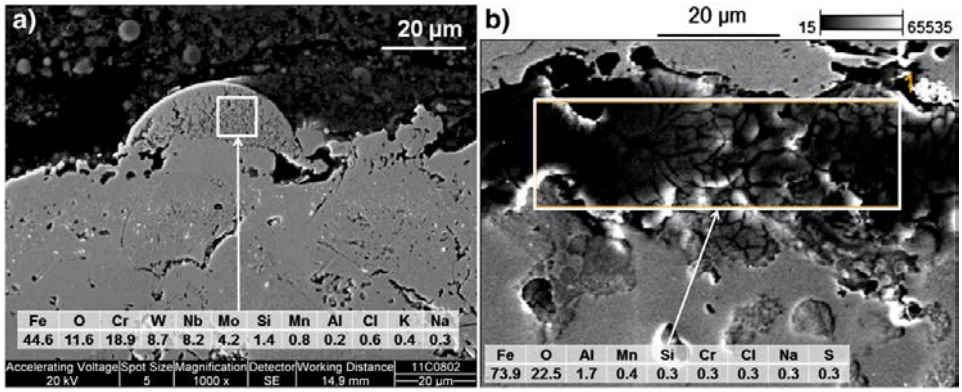

Fig. 11. SEM figures and EDX analyses [wt.%] of a) the coating surface showing corrosion on the outer lamella of the Fe–19Cr coating, and b) corrosion in the coating–substrate interface caused by cracking of the Fe–19Cr coating.

oxidation were mainly in the leeward side and severe pitting in the windward side. In comparison, the thermally sprayed coatings had endured in the boiler exposure well, and Fe–27Cr coating offered excellent protection to the substrate material. Fe–19Cr coating had sufficient corrosion resistance in the boiler conditions. However, the Fe–19Cr coating had few perpendicular cracks and hence the underlying material had corroded slightly.

- Wood based biomass with high moisture content had caused severe corrosion to the St35.8 carbon steel tubes in a circulating fluidised bed; several millimetres in two years.
- As there were corrosion products in the windward side pits, the effect of erosion has not been major in the material wastage. It is more probable that the formation of non-protective loose oxides has led to continuous spalling off the oxide layers and high corrosion rate.
- Corrosion mechanism of St35.8 carbon steel is proposed to have been corrosion induced by chlorine together with low melting phases of potassium, copper and zinc.
- Fe–27Cr HVOF coating had excellent corrosion resistance in the conditions and could be used to increase the lifetime of carbon steel or low alloy steel substrate material in biomass fired boilers.
- Fe–19Cr material showed sufficient corrosion resistance in the boiler conditions, but due to perpendicular cracks the coating did not protect the substrate material.

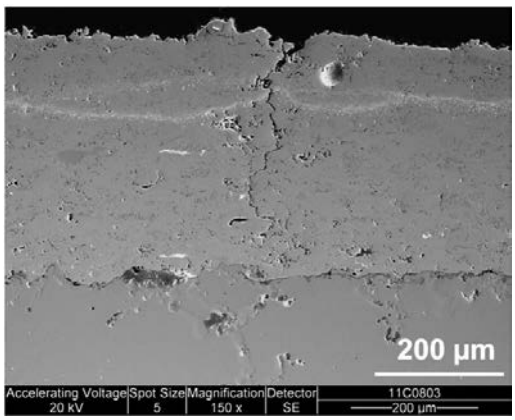

Fig. 12. SEM image of the Fe–19Cr coating cross-section showing the perpendicular cracking that propagates into the substrate.

- Structure and quality of the coating, such as adhesion, cohesion, density, interconnecting porosity and amorphous phases can be influenced by the optimisation of thermal spray process parameters. The coating structure is very important on corrosion resistance of thermal spray coatings in order to prevent the transport of corrosive elements towards the substrate.
- Thermal spray process parameters should be optimised for coating material Fe–19Cr to prevent the perpendicular cracking.

Conflict of interest

No conflict of interest.

Acknowledgements

The authors wish to acknowledge the valuable support of Turku Energia (Turku, Finland) during the course of this work.

References

[1] R.A. Antunes, M.C. Lopes de Oliveira, Corros. Sci. 76 (2013) 6–26.
[2] M. Aho, P. Yrjas, R. Taipale, M. Hupa, J. Silvennoinen, Fuel 89 (2010) 2376–2386.
[3] S.V. Vassilev, D. Baxter, C.G. Vassileva, Fuel 112 (2013) 391–449.
[4] M. Hupa, Energy Fuel 26 (2012) 4–14.
[5] I. Obernberger, G. Thek, Biomass Bioenergy 27 (2004) 653–669.
[6] F.J. Frandsen, Fuel 84 (2005) 1277–1294.
[7] M. Montgomery, T. Vilhelmsen, S.A. Jensen, Mater. Corros. 59 (2008) 783–793.
[8] K. Persson, M. Broström, J. Carlsson, A. Nordin, R. Backman, Fuel Process. Technol. 88 (2007) 1178–1182.
[9] P. Henderson, P. Szakálos, R. Pettersson, C. Andersson, J. Högberg, Mater. Corros. 57 (2006) 128–134.
[10] A. Zahs, M. Spiegel, H.J. Grabke, Corros. Sci. 42 (2000) 1093–1122.
[11] M. Spiegel, A. Zahs, H.J. Grabke, Mater. High Temp. 20 (2003) 153–159.
[12] L.A. Hansen, H.P. Nielsen, F.J. Frandsen, K. Dam-Johansen, S. Hørlyck, A. Karlsson, Fuel Process. Technol. 64 (2000) 189–209.
[13] T. Lind, E. Kauppinen, J. Hokkinen, J.K. Jokiniemi, M. Orjala, M. Aurela, R. Hillamo, Energy Fuel 20 (2006) 61–68.
[14] O. Sippula, T. Lind, J. Jokiniemi, Fuel 87 (2008) 2425–2436.
[15] D. Bramhoff, H.J. Grabke, E. Reese, H.P. Schmidt, (in German) Werkst. Korros. 41 (1990) 303–310.
[16] M. Spiegel, Mater. Corros. 50 (1999) 373–393.
[17] H.J. Grabke, Proceedings of the International Conference on Fireside Problems While Incinerating Municipal and Industrial Waste, 8–12.10.1989, Fla., USA, 1989, pp. 161–176.
[18] N. Otsuka, Corros. Sci. 50 (2008) 1627–1636.
[19] M. Montgomery, O. Biede, O.H. Larsen, Mater. Sci. Forum 522–523 (2006) 523–530.
[20] B.-J. Skrifvars, M. Westén-Karlsson, M. Hupa, K. Salmenoja, Corros. Sci. 52 (2010) 1011–1019.
[21] J. Ehlers, D.J. Young, E.J. Smaardijk, A.K. Tyagi, H.J. Penkalla, L. Singheiser, W.J. Quadakkers, Corros. Sci. 48 (2006) 3428–3454.
[22] W.M.M. Huijbregts, R. Leferink, Anti-Corros. Methods Mater. 51 (2004) 173–188.
[23] P. Viklund, R. Pettersson, A. Hjörnhede, P. Henderson, P. Sjövall, Corros. Eng. Sci. Technol. 44 (2009) 234–240.
[24] D.J. Branagan, Adv. Mater. Process. 169 (2011) 33–34.

[25] L. Paul, G. Clark, A. Ossenberg-Engels, T. Hansen, Power Eng. 111 (2007) 64–69.
[26] M. Oksa, E. Turunen, T. Suhonen, T. Varis, S.-P. Hannula, Coatings 1 (2011) 17–52.
[27] M. Kaur, H. Singh, S. Prakash, Anti-Corros. Methods Mater. 55 (2) (2008) 86–96.
[28] M. Oksa, S. Tuurna, T. Varis, J. Therm. Spray Technol. 22 (2013) 783–796.
[29] M.A. Uusitalo, P.M.J. Vuoristo, T.A. Mäntylä, Mater. Sci. Eng. A346 (2003) 168–177.
[30] J.R. Davis (Ed.), Handbook on Thermal Spray Technology, ASM International, Materials Park, Ohio, 2004.
[31] H.S. Sidhu, B.S. Sidhu, S. Prakash, Surf. Coat. Technol. 200 (2006) 5386–5394.
[32] T.S. Sidhu, S. Prakash, R.D. Agrawal, Scr. Mater. 55 (2006) 179–182.
[33] J. Sandberg, C. Karlsson, R. Bel Fdhila, Appl. Energy 88 (2011) 99–110.
[34] L.-E. Åmand, B. Leckner, D. Eskilsson, C. Tullin, Fuel 85 (2006) 1313–1322.
[35] H.J. Grabke, M. Spiegel, A. Zahs, Mater. Res. 7 (2004) 89–95.
[36] T. Ishitsuka, K. Nose, Corros. Sci. 44 (2002) 247–263.
[37] A. Inoue, Mater. Sci. Eng. A304–306 (2001) 1–10.
[38] M. Montgomery, A.N. Hansson, S.A. Jensen, T. Vilhelmsen, N.H. Nielsen, Mater. Corros. 64 (2013) 14–25.
[39] S. Enestam, Corrosivity of Hot Flue Gases in the Fluidized Bed Combustion of Recovered Waste Wood, 2011. (Academic Dissertation, Åbo, Finland).
[40] K. Nakagawa, Y. Matsunaga, Mater. Sci. Forum 251–254 (1997) 535–542.
[41] M.C. Galetz, J.T. Bauer, M. Schütze, M. Noguchi, C. Takato, H. Cho, Mater. Corros. 63 (2012) 1–8.
[42] P. Kofstad, High Temperature Corrosion, Elsevier Applied Science Publishers Ltd., Essex, England, 1988, p. 558.
[43] J.R. Regina, J.N. DuPont, A.R. Marder, Oxid. Met. 61 (2004) 69–90.
[44] H.P. Nielsen, F.J. Frandsen, K. Dam-Johansen, Energy Fuel 13 (1999) 1114–1121.
[45] H. Asteman, J.-E. Svensson, L.-G. Johansson, M. Norell, Oxid. Met. 52 (1999) 95–111.
[46] J. Pettersson, J.-E. Svensson, L.-G. Johansson, Oxid. Met. 72 (2009) 159–177.

PUBLICATION VI

Increased lifetime for biomass and waste to energy power plant boilers with HVOF coatings

High temperature corrosion testing under chlorine-containing molten salt

In: Journal of Thermal Spray Technology 22 (2013) 783–796.

Series title and number

VTT Science 74

Title	**Nickel- and iron-based HVOF thermal spray coatings for high temperature corrosion protection in biomass-fired power plant boilers**
Author(s)	Maria Oksa
Abstract	Biomass burning for production of electricity and heat has been increasing due to legislation in Europe. Growing awareness of environmental problems has led to strict restrictions on greenhouse emissions in the energy sector, and increased demand for higher use of renewable energy sources and carbon-neutral fuels, such as biomass. There are over 1000 biomass boilers in Europe, and the number is increasing. These plants often face serious problems due to high temperature corrosion. Fouling and corrosion in biomass boilers can lead to tube failure and leakage. In addition, demand for higher efficiency of electricity and heat generation requires an increase in steam temperatures, which raises the material temperatures of boiler tubes and may result in more severe corrosion problems. To overcome corrosion damages to boilers, commonly used low-alloyed steels are being replaced by higher-alloy tube materials. However, the high price and sometimes difficult machinability of these materials hinders their adoption. Thermal spray coatings can offer an attractive solution for corrosion protection of boiler tubing. The objective of this work was to determine the corrosion resistance of thermal spray coatings in biomass combustion conditions. The overall research aim was to enhance the lifetime of the heat exchanger surfaces of biomass power plant boilers. The research focused mainly on improving the high temperature corrosion resistance of thermal sprayed HVOF (high velocity oxy-fuel) coatings by optimizing their structure and verification of corrosion performance in biomass boiler conditions. Focus was also placed on determining the corrosion mechanisms of nickel- and iron-based coatings. The corrosion performance of the selected coatings was validated in both laboratory conditions and real biomass boiler conditions. According to this research, the tested HVOF sprayed nickel- and iron-based coatings can offer protection for low-alloy substrates in biomass boiler conditions. The results of the present study will help optimize the coating process for high temperature corrosion applications, and in adopting the use of thermal spray coatings for protection of the heat exchanger surfaces of biomass boilers.
ISBN, ISSN	ISBN 978-951-38-8206-8 (Soft back ed.) ISBN 978-951-38-8207-5 (URL: http://www.vtt.fi/publications/index.jsp) ISSN-L 2242-119X ISSN 2242-119X (Print) ISSN 2242-1203 (Online)
Date	January 2015
Language	English, Finnish abstract
Pages	87 p. + app. 112 p.
Name of the project	NextGenPower
Commissioned by	
Keywords	thermal spray, coating, process optimization, high temperature corrosion, biomass burning, corrosion protection
Publisher	VTT Technical Research Centre of Finland P.O. Box 1000, FI-02044 VTT, Finland, Tel. 020 722 111

Julkaisun sarja ja numero

VTT Science 74

Nimeke	**Termisesti ruiskutetut nikkeli- ja rautapohjaiset HVOF-pinnoitteet korkean lämpötilan korroosion suojaukseen biomassaa polttavissa voimalaitoksissa**
Tekijä(t)	Maria Oksa
Tiivistelmä	Eurooppalainen lainsäädäntö on lisännyt biomassan käyttöä polttoaineena sähkön ja lämmön tuotannossa. Lisääntynyt ympäristötietoisuus ja huoli maapallon tilasta ovat johtaneet tiukkoihin kasvihuonekaasujen päästörajoituksiin energiasektorilla ja lisänneet uusiutuvien energialähteiden ja hiilineutraalien polttoaineiden kysyntää. Euroopassa on yli 1000 biomassaa polttavaa voimalaitosta ja määrä on kasvamassa. Kuitenkin nämä polttolaitokset kärsivät usein vakavista korkean lämpötilan korroosio-ongelmista. Likaantuminen ja korroosio voivat aiheuttaa putkivaurioita ja pahimmassa tapauksessa putkivuotoja biomassaa polttavissa laitoksissa. Lisäksi energiatehokkuusvaatimukset sähkön ja lämmön tuotannossa johtavat höyryn lämpötilan nostamiseen, mikä aiheuttaa korkeammat materiaalilämpötilat ja mahdollisesti aikaisempaa vakavammat korroosio-ongelmat. Tyypillisesti korroosiota torjutaan vaihtamalla niukkaseosteiset teräkset enemmän seostettuihin putkimateriaaleihin. Nämä ovat kuitenkin kalliita ja niiden työstettävyys on joskus hankalaa, mikä hankaloittaa niiden käyttöönottoa. Termisesti ruiskutetut pinnoitteet voivat tarjota houkuttelevan ratkaisun kattilaputkien korroosionsuojaukseen. Tämä tutkimus tehtiin termisesti ruiskutettujen pinnoitteiden korroosionkestävyyden varmistamiseksi biomassapolton olosuhteissa. Tutkimuksen avulla pyritään nostamaan biomassaa polttavien voimalaitoskattiloiden lämmönvaihdinpintojen elinikää tulevaisuudessa. Työ kohdistui pääasiassa termisesti ruiskutettujen HVOF (suurnopeusruiskutus) -pinnoitteiden korkean lämpötilan korroosionkestävyyden parantamiseen optimoimalla pinnoitteiden rakennetta ja pinnoitteiden korroosionkestävyyden todentamiseen biomassapolton olosuhteissa. Tutkimuksessa tarkasteltiin myös nikkeli- ja rautapohjaisten pinnoitteiden korroosiomekanismeja. Valittujen pinnoitteiden korkean lämpötilan korroosionkestävyys testattiin laboratoriossa ja aidoissa biomassakattiloissa. Tutkimuksen perusteella testatut HVOF-ruiskutetut nikkeli- ja rautapohjaiset pinnoitteet tarjoavat suojan niukkaseosteisille putkimateriaaleille biomassapoltto-olosuhteissa. Tutkimuksen tulokset auttavat optimoimaan pinnoitusprosessia korkean lämpötilan korroosiosovelluksia varten ja mahdollistavat termisesti ruiskutettavien pinnoitteiden käyttöönottoa biomassaa polttavien voimaloiden lämmönvaihdinpintojen korroosion suojaukseen.
ISBN, ISSN	ISBN 978-951-38-8206-8 (nid.) ISBN 978-951-38-8207-5 (URL: http://www.vtt.fi/publications/index.jsp) ISSN-L 2242-119X ISSN 2242-119X (Painettu) ISSN 2242-1203 (Verkkojulkaisu)
Julkaisuaika	Tammikuu 2015
Kieli	Englanti, suomenkielinen tiivistelmä
Sivumäärä	87 s. + liitt. 112 s.
Projektin nimi	NextGenPower
Rahoittajat	
Avainsanat	terminen ruiskutus, pinnoite, prosessin optimointi, korkean lämpötilan korroosio, biopoltto, korroosiosuojaus
Julkaisija	VTT PL 1000, 02044 VTT, puh. 020 722 111

Nickel- and iron-based HVOF thermal spray coatings for high temperature corrosion protection in biomass-fired power plant boilers

Biomass burning for production of electricity and heat has been increasing due to legislation in Europe. Growing awareness of environmental problems has led to strict restrictions on greenhouse emissions in the energy sector, and increased demand for higher use of renewable energy sources and carbon-neutral fuels, such as biomass. There are over 1000 biomass boilers in Europe, and the number is increasing. These plants often face serious problems due to high temperature corrosion. Thermal spray coatings can offer an attractive solution for corrosion protection of boiler tubing. The objective of this work was to determine the corrosion resistance of thermal spray coatings in biomass combustion conditions.

The research focused mainly on improving the high temperature corrosion resistance of thermal sprayed HVOF (high velocity oxy-fuel) coatings by optimizing their structure and verification of corrosion performance in biomass boiler conditions, both in laboratory conditions and in real biomass boilers. According to this research, the tested HVOF sprayed nickel- and iron-based coatings can offer protection for low-alloy substrates in biomass boiler conditions. The results of the present study will help optimize the coating process for high temperature corrosion applications, and in adopting the use of thermal spray coatings for protection of the heat exchanger surfaces of biomass boilers.

ISBN 978-951-38-8206-8 (Soft back ed.)
ISBN 978-951-38-8207-5 (URL: http://www.vtt.fi/publications/index.jsp)
ISSN-L 2242-119X
ISSN 2242-119X (Print)
ISSN 2242-1203 (Online)